



Université  
de Lille

Université de Lille

Ecole Doctorale des Sciences de la Matière, du Rayonnement et de l'Environnement  
Unité de Catalyse et Chimie du Solide - UMR 8181

**Thèse de Doctorat**  
Mention: Molécules et Matière Condensée

**Jingpeng ZHAO**

**Oxydation catalytique sélective des alcools en composés  
carbonylés par des catalyseurs à base de Ru**

**Catalytic Selective Oxidation of Alcohols to  
Carbonyl Compounds by Ru-based Catalysts**

Soutenue le 18 Décembre 2019

Composition du Jury:

Gadi Rothenberg	Professeur des Universités	University of Amsterdam	Rapporteur
Karine Vigier	Professeur des Universités	Université de Poitiers	Rapporteur
Franck Dumeignil	Professeur des Universités	Université de Lille	Examineur & Jury président
Laurent Bonneviot	Professeur des Universités	ENS de Lyon	Examineur
Stéphane Streiff	Directeur	Solvay-E2P2L	Invité
Mickael CAPRON	Maître de Conférences	Université de Lille	Directeur de Thèse
Vitaly Ordonsky	Chargé de Recherches	Solvay-E2P2L	Directeur de Thèse



## Contents

<b>R ésum é.....</b>	<b>1</b>
<b>Abstract.....</b>	<b>3</b>
<b>CHAPTER 1 Literature Review.....</b>	<b>5</b>
1.1 Introduction.....	5
1.2 Metal-based selective oxidation of alcohols.....	6
1.2.1 Homogeneous oxidation of alcohols.....	7
1.2.2 Heterogeneous Oxidation of Alcohols - Liquid Phase.....	9
1.2.3 Heterogeneous oxidation of alcohols - gas phase.....	22
1.3 Metal-free selective oxidation of alcohols.....	25
1.3.1 Carbocatalysts for alcohols oxidation.....	26
1.3.2 Nitroxyl radical catalytic for alcohols oxidation.....	28
1.3.3 Quinones species for alcohols oxidation.....	31
1.4 Alcohol oxidation on electrocatalysts.....	34
1.5 Oxidants in alcohols oxidation.....	35
1.5.1 H <sub>2</sub> O <sub>2</sub> in homogeneous catalysis for alcohols oxidation.....	36
1.5.2 H <sub>2</sub> O <sub>2</sub> in heterogeneous catalysis for alcohols oxidation.....	37
1.5.3 O <sub>2</sub> in homogeneous catalysis for alcohols oxidation.....	38
1.5.4 O <sub>2</sub> in heterogeneous catalysis for alcohols oxidation.....	39
1.6 The objectives and outline of thesis.....	40
1.7 References.....	42
<b>Chapter 2. Experiments.....</b>	<b>54</b>
2.1 Materials and Chemicals.....	54
2.2 Catalysts Preparation.....	54
2.2.1 Synthesis of ruthenium nanoparticles (Ru NPs) catalysts.....	54
2.2.2 Synthesis of supported Ru/Al <sub>2</sub> O <sub>3</sub> catalyst.....	55
2.2.3 Synthesis of supported CQ/SiO <sub>2</sub> catalyst.....	55
2.2.4 Synthesis of core-shell Ru@quinones catalysts.....	56
2.2.5 Synthesis of Ru@MOFs catalysts.....	57
2.3 Catalyst Characterization.....	58
2.3.1 Transmission electron microscopy.....	58
2.3.2 X-ray diffraction.....	58
2.3.3 Temperature-programmed reduction.....	58

2.3.4 O <sub>2</sub> & CO chemisorption.....	59
2.3.5 Infrared spectroscopy analysis (FT-IR).....	59
2.3.6 Elemental analysis .....	60
2.3.7 Zeta Potentials.....	60
2.3.8 <i>In-situ</i> XPS.....	60
2.3.9 TGA Analysis.....	61
2.3.10 Solid NMR Analysis .....	61
2.3.11 High-resolution scanning electron microscope (HRSEM) .....	61
2.3.12 N <sub>2</sub> adsorption. ....	61
2.3.13 NH <sub>3</sub> -temperature programmed desorption (NH <sub>3</sub> -TPD).....	61
2.4 Catalysis.....	62
2.4.1 Liquid-phase catalytic oxidation of alcohols .....	62
2.4.2 Liquid-phase catalytic oxidation of aldehydes .....	62
2.4.3 Recyclability of catalysts .....	63
2.4.4 Analysis method.....	63
2.4.5 Calibration curves .....	63
2.4.6 Experimental error of autoclaves .....	64
2.4.7 Cyclic voltammetry.....	65
2.5 References.....	65
<b>CHAPTER 3 Selective Oxidation of Alcohols to Carbonyl Compounds over Small Size Colloidal Ru Nanoparticles .....</b>	<b>66</b>
3.1 Introduction.....	67
3.2 Results and Discussion .....	68
3.2.1 Synthesis and characterization of Ru NPs .....	68
3.2.2 Catalytic oxidation of alcohols .....	75
3.2.3 Mechanism study .....	80
3.3 Conclusion .....	85
3.4 References.....	86
<b>CHAPTER 4 Non-metallic Aerobic Oxidation of Alcohols over Anthraquinone Based Compounds.....</b>	<b>90</b>
4.1 Introduction.....	91
4.2 Results and discussion .....	92
4.2.1 Oxidation of alcohols over EQ .....	92

4.2.2 Effect of electrochemical potential of quinones on alcohol oxidation .	96
4.2.3 Supported anthraquinone for oxidation .....	100
4.2.4 Mechanism of the reaction.....	104
4.3 Conclusion .....	105
4.4 References.....	106
<b>CHAPTER 5 Nanocell Type Ru@quinone Core-shell Catalyst for Selective oxidation of alcohols to carbonyl compounds .....</b>	<b>109</b>
5.1 Introduction.....	110
5.2 Results and Discussion .....	111
5.2.1 Catalytic performance in oxidation of alcohols .....	111
5.2.2 Characterization of Ru@quinones Catalysts .....	117
5.2.3 Structure-catalytic performance relationship.....	120
5.2.4 Mechanism study .....	121
5.3 Conclusion .....	126
5.4 References.....	127
<b>CHAPTER 6 Direct Aerobic Oxidation of Mono-alcohols and Diols to Acetals Using Tandem Ru@MOF Catalysts.....</b>	<b>130</b>
6.1 Instruction .....	131
6.2 Results and Discussion .....	133
6.2.1 Synthesis and characterization of the catalysts.....	133
6.2.2 Direct Alcohol to Acetal Conversion .....	136
6.2.3 Mechanism study .....	142
6.3 Conclusion .....	145
6.4 References.....	146
<b>Chapter 7 General Conclusion and Perspectives.....</b>	<b>150</b>
7.1 General Conclusion.....	150
7.1.1 Selective conversion of alcohols to aldehydes/ketones over small Ru NPs.....	150
7.1.2 Oxidation of alcohols based on non-metal anthraquinone-based catalysts.....	151
7.1.3 Design nanocells Ru@SQ catalyst with core-shell structure.....	151
7.1.4 Oxidation of monoalcohols and polyols to acetals by Ru@MOF catalyst .....	152

7.2 Perspectives.....	152
7.2.1 Synthesis of subnanometric nanoparticles for selective oxidation of alcohols .....	152
7.2.2 Stable core-shell materials for oxidation of alcohols.....	153
7.2.3 Use of organic shell based on nitroxyl radicals .....	153
<b>Acknowledgement .....</b>	<b>156</b>

# Résumé

L'oxydation aérobie sélective des alcools en composés carbonylés est une transformation fondamentale et réalisable pour de nombreuses réactions biologiques et organiques fournissant des intermédiaires clés et des produits pharmaceutiques précieux. Les défis intrinsèques de réactivité et de sélectivité en chimie verte pour l'oxydation utilisant l'oxygène comme oxydant terminal limitent considérablement son application dans l'industrie. Les catalyseurs métalliques traditionnellement utilisés offrent une faible sélectivité due à la sur-oxydation des aldéhydes vers les acides correspondants. La combinaison récemment mise au point de piègeurs d'hydrogène organiques (*e.g.*, DDQ, TEMPO) et d'agents de régénération inorganiques ( $\text{Fe}^{3+}$ , NO) a été utilisée comme catalyseur pour une oxydation sélective des alcools en présence d'oxygène. Toutefois, la nature homogène du catalyseur et l'utilisation de produits chimiques toxiques et non respectueux de l'environnement nécessitent plus de développements de ce concept pour l'oxydation des alcools.

Pour résoudre ces problèmes, nous proposons l'application d'un concept hétérogène de nano-électrocells inspiré de l'électrocatalyse. Les catalyseurs contiennent des nano-anodes et des nano-cathodes disposées en structure noyau-coquille à l'échelle nanométrique. L'alcool est oxydé sur les sites non métalliques de la coquille, avec migration ultérieure de l'hydrogène vers le noyau métallique pour son oxydation en eau. Dans cette thèse, nous avons trouvé les matériaux "core" et "shell" appropriés, sur la base des espèces métalliques Ru et quinones non métalliques, respectivement, et nous les avons appliqués pour l'oxydation des alcools.

Tout d'abord, au chapitre 3, nous avons étudié l'effet de la taille des nanoparticules de Ru préparées par microémulsion pour l'oxydation des alcools; la plus grande sélectivité en aldéhydes a été obtenue sur les nanoparticules de Ru les plus petites (2 nm). Une diminution rapide de la sélectivité pour les nanoparticules non supportées et sur support de plus grandes tailles a été observée. Selon l'étude *in situ* du mécanisme de la réaction, la présence d'une couche d'oxyde de surface sur des nanoparticules de Ru de petite taille supprime la sur-oxydation non désirée des aldéhydes en acides.

Les performances catalytiques des matériaux «coquille » à base d'anthraquinones substituées ont été examinées pour l'oxydation catalytique d'alcools cycliques et activés en composés carbonylés correspondants dans le chapitre 4. La réactivité est sensible à la pression d'oxygène et le potentiel de réduction des espèces à base de quinone est d'une influence cruciale dans les réactions d'oxydation. En outre, le catalyseur à base de 2-carboxyanthraquinone greffée a démontré une performance catalytique comparable à celle de la molécule mère et pourrait agir comme catalyseur hétérogène. Le mécanisme a un caractère radical avec transfert d'hydrogène de l'alcool vers l'anthraquinone et oxydation subséquente de l'anthraquinone hydrogénée par l'oxygène.

Sur la base des recherches ci-dessus, les nanoparticules de Ru et les anthraquinones substituées ont été combinées pour établir des «nanocells » à structure noyau-coquille dans le chapitre suivant. Les nouveaux catalyseurs possèdent et combinent les propriétés des composants organiques et inorganiques qui offrent une performance supérieure en oxydation par rapport aux deux catalyseurs. La sélectivité des alcools aromatiques et aliphatiques augmente de façon spectaculaire pour atteindre plus de 90 % pour la plupart des alcools susmentionnés par rapport à leurs homologues pur Ru et anthraquinone. L'étude du mécanisme de la réaction à l'aide de différents outils physico-chimiques, y compris la voltampérométrie cyclique, indique le transfert d'hydrogène des alcools à l'anthraquinone et sa migration ultérieure vers le noyau Ru du catalyseur générant de l'eau. Il en résulte une séparation des processus d'oxydation et de réduction similaire à la performance des systèmes «electrocells » et conduit à la synthèse sélective de composés carbonylés.

L'oxydation des polyols est une tâche plus difficile et nécessite de nouvelles approches en termes de développement de catalyseurs. Dans le chapitre 6, nous proposons l'oxydation combinée à l'acétalisation à l'aide du catalyseur tandem Ru@MOF contenant des nanoparticules de Ru ultrafines (< 2 nm) dans la structure MOF. L'étude mécaniste révèle que la présence de sites d'acide de Lewis dans le MOF, de concert avec les sites actifs de Ru, convertit rapidement les aldéhydes en acétals, supprimant ainsi efficacement la formation de sous-produits d'oxydation excessive.

**Mots clés :** oxydation sélective, alcools, ruthénium, taille des particules, quinones, potentiels de réduction, nanocellules, déshydrogénation oxydative, réduction de l'oxygène, MOFs, core-shell.

# Abstract

Selective aerobic oxidation of alcohols to carbonyl compounds is a fundamental and practicable transformation for many biological and organic reactions providing key intermediates and valuable pharmaceuticals. The intrinsic reactivity and selectivity challenges in green chemistry for oxidation using oxygen as terminal oxidant significantly restrict its application in industry. Traditionally used metallic catalysts provide low selectivity due to over-oxidation of aldehydes further to acids. The recently developed combination of organic hydrogen scavengers (DDQ, TEMPO) and inorganic regeneration agents ( $\text{Fe}^{3+}$ , NO) have been used as a catalyst for mild selective oxidation of alcohols in the presence of oxygen. However, homogeneous nature of the catalyst and use of toxic and non-environmentally friendly chemicals require further development of this concept for oxidation of alcohols.

To solve these problems, we propose application of heterogeneous nano-electrocell concept inspired from electrocatalysis. The catalysts contain nano-anode and nano-cathode sites arranged in core-shell structure at nano-scale level. The alcohol is oxidized over the non-metallic shell sites, with subsequent migration of hydrogen to the metallic core for oxidation to water. In this thesis, we have found the appropriate “core” and “shell” materials, on the basis of metallic Ru and non-metallic quinones species, respectively, and applied it for oxidation of alcohols.

First of all, in Chapter 3 we investigated effect of the sizes of Ru nanoparticles prepared by microemulsion for oxidation of alcohols. The highest selectivity to aldehydes was obtained over the smallest Ru nanoparticles (2 nm) with rapid decrease of the selectivity for the larger Ru non-supported and supported nanoparticles. According to in-situ study of the mechanism of the reaction the presence of surface oxide layer over small size Ru nanoparticles suppresses over-oxidation of aldehydes to acids.

“Shell” catalytic performances of substituted anthraquinones were examined in catalytic oxidation of cyclic and activated alcohols to corresponding carbonyl compounds in the Chapter 4. The reactivity is sensitive to oxygen pressure and the reduction potential of quinone-species is of crucial influence in the oxidation reactions. In addition, grafted 2-carboxyanthraquinone catalyst has demonstrated

comparable catalytic performance to the parent molecule and could act as heterogeneous catalyst. The mechanism has radical character with transfer of hydrogen from alcohol to anthraquinone and subsequent oxidation of hydrogenated anthraquinone by oxygen.

Based on the research above, Ru nanoparticles and substituted anthraquinones were combined to establish the nanocells with core-shell structure in the next Chapter. The new catalysts possess and combine the properties of organic and inorganic components that provide superior performance in oxidation in comparison with both counterparts. The selectivity increases dramatically to > 90 % for most part of aromatic and aliphatic alcohols in comparison with pure Ru and anthraquinone counterparts. Investigation of the mechanism of the reaction using different physico-chemical tools including cyclic voltammetry indicates on hydrogen transfer from alcohols to anthraquinone with its subsequent migration to the Ru core of the catalyst generating water. It results in separation of oxidation and reduction processes similar to the performance of electrocell system and leads to selective synthesis of carbonyl compounds.

Oxidation of polyols is more challenging task and requires new approaches in terms of catalysts development. In the Chapter 6 we propose oxidation combined with acetalization using Ru@MOF tandem catalyst containing ultra-fine Ru nanoparticles (< 2 nm) in the MOF structure. Mechanistic study reveals that the presence of Lewis acid sites in the MOF work in concert with Ru active sites promptly converts aldehydes to acetals thereby effectively suppressing the formation of over-oxidation byproducts.

**Key words:** selective oxidation, alcohols, ruthenium, particle size, quinones, reduction potentials, nanocells, oxidative dehydrogenation, oxygen reduction, MOFs, core-shell

# CHAPTER 1 Literature Review

## 1.1 Introduction

“Green chemistry”, its core issues have focused on the new reaction system, including studying innovative synthetic methods and routes, seeking novel raw materials and exploring green reaction. To achieve that, it is necessary to control the chemical reaction and processes, which mainly contains the use of non-toxic and harmless materials and solvents, and the yield of the product; the employment of highly efficient and innocuous catalysts; no co-product or environmental by-products generated (water); mild reaction conditions with less waste and emissions; more green synthetic routes, such as bionics; the new equipment and technologies to improve productivity and reduce energy consumption.

**Table 1-1.** Several carbonyl compounds and applications<sup>1</sup>

Carbonyl compounds	Molecular formula	Applications
Acetaldehyde	CH <sub>3</sub> CHO	plastics\intermediate
Acetone	CH <sub>3</sub> COCH <sub>3</sub>	solvent\PMMA、intermediate
2-octanone	CH <sub>2</sub> (CH <sub>2</sub> ) <sub>5</sub> COCH <sub>3</sub>	spice
Glyoxal	HCOCOH	papermaking\spice e\pharmaceuticals
Cyclopentanone	C <sub>5</sub> H <sub>8</sub> O	pharmaceuticals\spice\rubber
Acetophenone	C <sub>6</sub> H <sub>5</sub> COCH <sub>3</sub>	solvent\spice
Glutaraldehyde	HCO(CH <sub>2</sub> ) <sub>3</sub> CHO	disinfection\tanning
Adipic aldehyde	HCO(CH <sub>2</sub> ) <sub>4</sub> CHO	crosslinker\disinfection
Acrolein	CH <sub>2</sub> =CHCHO	methionine
Benzaldehyde	C <sub>6</sub> H <sub>5</sub> CHO	spice\pharmaceuticals

In the industrial production and organic synthesis, the selective oxidation of alcohols to the corresponding carbonyl compounds is of vital importance. On the one hand, alcohols are synthetic simple, stable and plentiful and the introduction of carbonyl group to the molecule makes it "reactive". Therefore, carbonyl compounds,

as organic starting materials and crucial intermediates, are widely used in the fields of fuels, pharmaceuticals, spices, pesticides, fine chemicals, *etc.* For example (as shown in Table 1-1), the 37% formic acid solution, known as formalin, is generally applied in biological disinfection. Recently, the carbonylation of polyols has also attracted the attention of researchers. Glyoxal, a fine chemical product obtained by the selective oxidation of ethylene glycol, can be mainly used for coatings, medicine, metallurgy, textiles<sup>2</sup>. Similarly, the preparation of aromatic aldehyde is also of concern, of which the typical case is benzaldehyde. Consequently, a targeted transformation from alcohols to the aldehydes/ketones through a simple reaction has aroused great enthusiasm.

Reaction process of alcohols to aldehydes or ketones can be expressed by the following chemical equations (Figure 1-1). The significant influence of the number and position of hydroxyl groups relative to each other on catalytic selectivity pronounces the importance of catalysts. The product of oxidative reaction is an intermediate compound with unstable thermodynamics<sup>3</sup>, and its selectivity is always the most challenging problem.

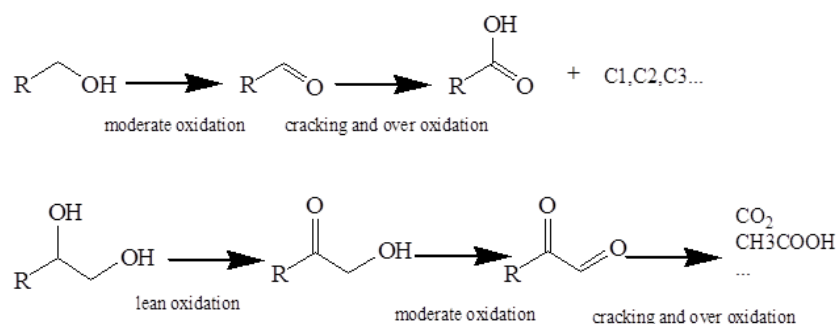


**Figure 1-1.** Reaction process of alcohols to aldehydes or ketones.

## 1.2 Metal-based selective oxidation of alcohols

Traditionally, the alcohols have been selectively oxidized into carbonyl compounds by using costly toxic heavy metal oxidants, such as chromium salt<sup>4-5</sup>, hypermanganate<sup>6-8</sup>, yielding large amounts of metal and organic solvent waste, which is extremely environmentally hazardous. To employ an appropriate catalyst and non-polluting oxidants turn into an intense research field. Studies have been carried out on the catalytic oxidation by means of homogeneous and heterogeneous routes, of which the later can be divided into liquid and gas phase catalysis based on the reaction conditions.

## 1.2.1 Homogeneous oxidation of alcohols

In homogeneous catalysis, the alcohol and the catalyst co-exist in the same phase, which can benefit the mass transfer and diffusion. Secondly, the metal like Ru, Pd, Cu, *etc.* can be properly liganded to improve the activity. It is particularly considerable for the conversion of the target molecules under mild conditions; while the homogeneous catalyst has an uniform active center and less side reactions<sup>9</sup>. However, the homogeneous catalyst synthesis is cumbersome and the complicated separation process of product and catalyst imposes restrictions on industrial application<sup>10</sup>. The homogeneous systems of alcohol catalytic oxidation mainly comprise Metal/TEMPO, Ru and Pd coordination complexes.

### 1.2.1.1 Metal/TEMPO systems for alcohols oxidation

TEMPO, (2,2,6,6-tetramethylpiperidin-1-yl)oxidanyl commonly is the chemical compound that known as a stable radical and employed in organic synthesis as a catalyst for the oxidation of alcohols to aldehydes. For Metal/TEMPO system, TEMPO will be reduced to TEMPOH and then re-oxidized by NaClO to TEMPO while the alcohol could be oxidized. In the past years, scientists have developed RuCl<sub>2</sub>(PPh<sub>3</sub>)<sub>3</sub>/TEMPO<sup>11</sup>, FeCl<sub>3</sub>/TEMPO/NaNO<sub>2</sub><sup>12</sup> (Figure 1-2), (bpy)CuI/TEMPO<sup>13</sup> and other functional catalysts<sup>14-15</sup>. However, the high cost and low utilization rate stifle the industrialization. Developing economical catalytic systems composed by transition metals becomes substantially essential.

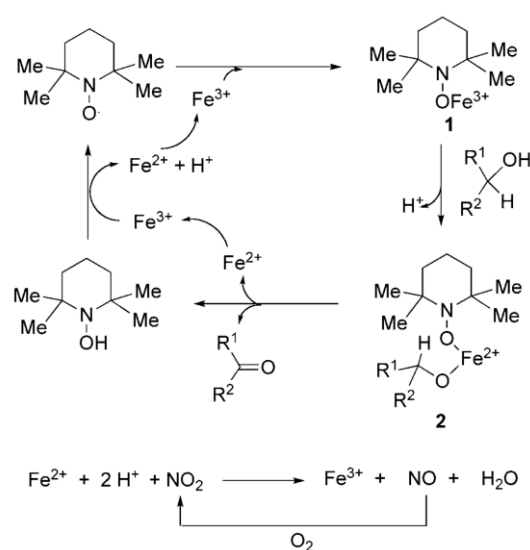


**Figure 1-2.** A proposed mechanism in FeCl<sub>3</sub>/TEMPO/NaNO<sub>2</sub><sup>12</sup>.

### 1.2.1.2 Ru coordination complex for alcohols oxidation

Among noble metal catalysts, Ru shows a strong ability to form complexes. In the homogeneous catalytic oxidation reaction, Ru compounds exhibit commendable activity for the primary alcohol and aliphatic alcohol, not excepting the unique selectivity for secondary alcohol. Perruthenate<sup>16</sup>, ruthenium complexes with phosphine<sup>17</sup> or Salen<sup>18</sup> have been successfully used in organic oxidation. Then the efficient compounds with good property, (n-Pr)<sub>4</sub>NRuO<sub>4</sub>(TPAP)<sup>19</sup>, tetra-n-propyl-ammoniumperruthenate<sup>20</sup>, RuO(O<sub>2</sub>CR)<sub>6</sub>L<sub>n</sub><sup>21</sup> and [(p-cymene)Ru-Cl<sub>2</sub>]<sub>2</sub>PPh<sub>3</sub><sup>22</sup>, were fabricated. However, the relatively complicated preparation process remains deficient in these systems.

### 1.2.1.3 Pd coordination complex for alcohols oxidation

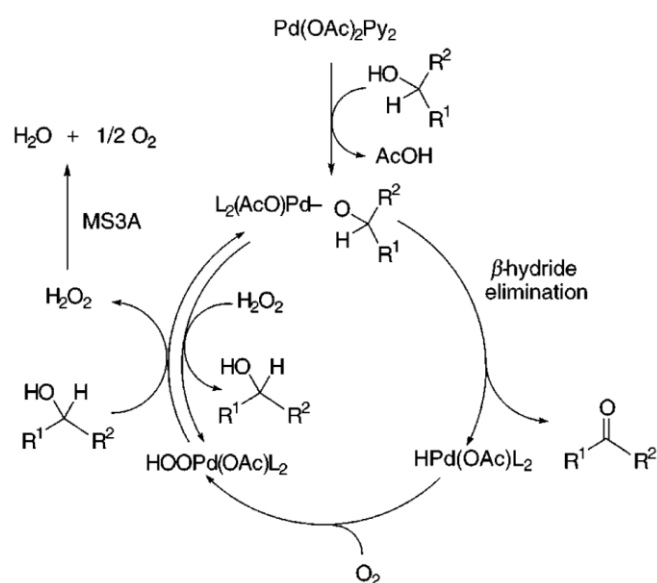


**Figure 1-3.** Mechanism for Pd(OAc)<sub>2</sub>/pyridine/MS3A catalyzed aerobic alcohol oxidation<sup>23</sup>.

Pd systems are the catalysts that assembling PdCl<sub>2</sub> or Pd(OAc)<sub>2</sub> with an inorganic or organic base, which are easily synthesized. Nishimura<sup>23</sup> *et al* reported Pd(OAc)<sub>2</sub>/pyridine/MS3A which could efficiently oxidize various alcohols at 80°C under atmospheric pressure and the possible mechanism was illustrated in Figure 1-3. The reaction proceeds *via* the production of a Pd(II)-alcoholate and a Pd(II)-pyridine complex followed by β-elimination of a Pd(II)-hydride which can react with O<sub>2</sub> to form a Pd(II)-hydroperoxide species, and this reactive species subsequently undergoes ligand exchange with alcohol to reproduce the Pd(II)-alcoholate and H<sub>2</sub>O<sub>2</sub>. The

valence of Pd remains unchanged in the cycle<sup>24</sup>. Active Pd(OAc)<sub>2</sub>(Et<sub>3</sub>N) was prepared by the reaction of Et<sub>3</sub>N and Pd(OAc)<sub>2</sub> by Sigman who designed and synthesized a Pd complex coordinate with carbyne ligand, whose TON was up to 1000<sup>25</sup>.

In 2000, Sheldon<sup>26</sup> *et al* described the water-soluble complex--palladium(II) bathophenanthroline in Figure 1-4, which is pH-sensitive. Higher pH could decrease both the conversion and reaction rate. The method is validated by the scope of the primary and secondary allylic, benzylic, and aliphatic alcohols that can be oxidized in both high activities and selectivities.

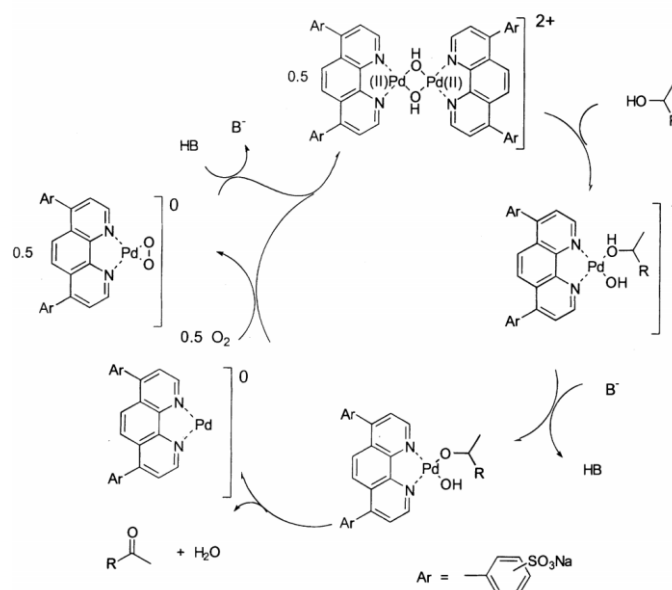


**Figure 1-4.** The catalytic cycle proposed for alcohol oxidation with the aqueous-soluble PhenS\*Pd(II) catalyst. Ar, aryl; B, base<sup>26</sup>.

#### 1.2.1.4 Other Metal Systems

Other precious metal, such as Au<sup>27</sup>, and the transition metals, Co<sup>28</sup>, Fe<sup>29</sup>, Cu<sup>30</sup>, V<sup>31-32</sup> *etc.* have been also applied to the selective catalytic oxidation of alcohols.

### 1.2.2 Heterogeneous Oxidation of Alcohols - Liquid Phase

Compared to the homogeneous catalysis, heterogeneous catalytic process has the advantages of relatively simple separation and cyclic utilization, which is a more efficient and environment-friendly technology.

#### 1.2.2.1 Platinum-group metals catalytic systems for alcohols oxidation

These catalysts are commonly Pt or Pd supported on Al<sub>2</sub>O<sub>3</sub> with the advantage

that the reaction conditions are very mild<sup>33-34</sup>. Researchers have found that adding a suitable adjuvant to a Pt-based catalyst can gain a binary or multicomponent catalyst which can significantly enhance the conversion of substrate and selectivity to the target molecule<sup>35-36</sup>. The doping agents generally adopted are Se<sup>37</sup>, Co<sup>38</sup>, Ce<sup>39</sup>, Ru<sup>40</sup>, Sn<sup>41</sup>. Mallat *et al* reported the supported catalysts in the selective monoalcohols oxidation by adding Bi<sup>42</sup>. The results showed that the activity was improved after a small amount of metal auxiliaries adding, and the yield registered a rapid growth from 1.5% to 99%. In 2004, Pillai<sup>43</sup> developed MgO supported Pd catalyst and compared its catalytic activity with the ones on hydrotalcite, Al<sub>2</sub>O<sub>3</sub>, SiO<sub>2</sub> and zeolite. The activity of Pd/MgO is attributed to the reducible nature of the support, which can be served as a ligand for the metal that helps transmission through the generation of a metal–alcoholate intermediate in the oxygen.

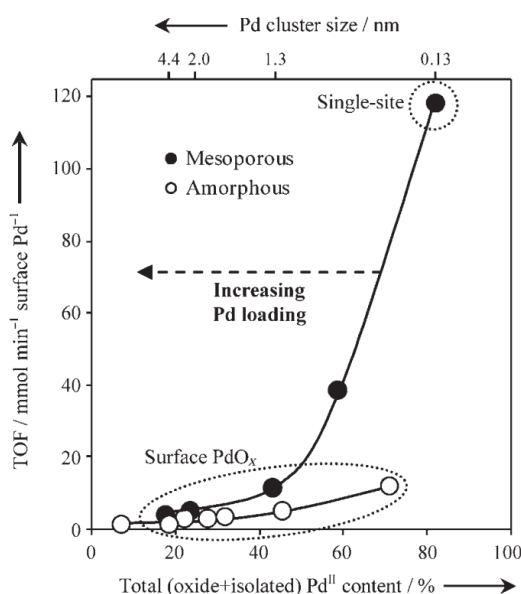


**Figure 1-5.** Catalytic performance of Pd clusters dispersed across conventional versus mesoporous alumina supports as a function of size and oxidation state in aerobic crotyl alcohol selox<sup>44</sup>.

A new mesoporous catalyst Pd/Al<sub>2</sub>O<sub>3</sub> was subsequently synthesized, which showed very high catalytic performance in the aerobic oxidation of allylic alcohols<sup>44</sup> (Figure 1-5). The higher specific surface area undoubtedly booms the dispersion of Pd, leading to the clusters for same loadings that are smaller than those achieved over the amorphous alumina. In addition, the higher defect density should be another key factor within the transitional support.

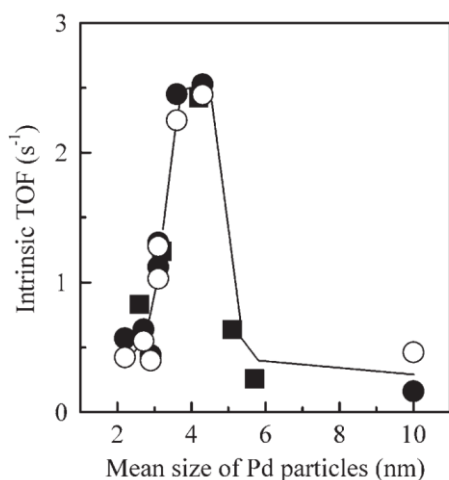


**Figure 1-6.** Dependence of the intrinsic turnover frequency on the mean size of Pd particles. Symbols: (■) catalysts reduced with hexanol; (●) catalysts reduced with H<sub>2</sub>, and TOF based on Pd dispersion estimated by mean size of Pd; (○) catalysts reduced with H<sub>2</sub>.<sup>45</sup>

SiO<sub>2</sub>-Al<sub>2</sub>O<sub>3</sub>-supported Pd catalysts<sup>45</sup> showed that the intrinsic TOF depended significantly on the size of Pd particles and showed a maximum at the mean size (3.6~4.3 nm), revealing that the selective oxidation based on Pd/SiO<sub>2</sub>-Al<sub>2</sub>O<sub>3</sub> was structure-sensitive (Figure 1-6).

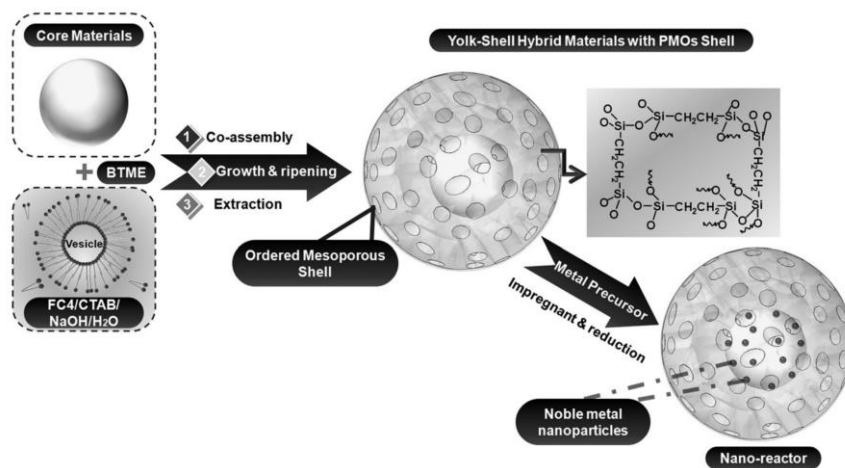


**Figure 1-7.** Synthesis procedure and proposed structure of yolk-shell hybrid materials with a PMO shell.<sup>46</sup>

Recently, Qiao demonstrated a good encapsulation of Pt, Pd nanoparticles into the structure of YS-PMO (periodic mesoporous organosilica) and obtained a yolk-shell hybrid (Pd/Pt-YS-PMO) with perpendicularly aligned mesoporous channels (Figure 1-7)<sup>46</sup>. The catalyst Pd/Pt-YS-PMO performed as a nanoreactor to selectively oxidize various alcohols into aldehydes. For the aliphatic alcohol 3-methyl-2-butanol, the catalyst showed a moderate activity with, nevertheless, a superior selectivity compared to conventional Pd/SiO<sub>2</sub> and Pd/C.

After treatment of hydroxyapatite (HAP), Kaneda constitutes a new type of Pd-grafted HAP<sup>47</sup>. Nanoclustered Pd<sup>0</sup> species can serviceably facilitate the reaction under an atmospheric O<sub>2</sub> pressure, offering a remarkable turnover number (TON) of up to 236000 with a good TOF of approximately 9800 h<sup>-1</sup> for the oxidation of 1-phenylethanol. Besides, Pd/MIL-101 catalyst was achieved with Pd nanoparticles deposited on an acidic MOF (MIL-101)<sup>48</sup>. It showed high activities in the liquid-phase oxidation over a variety of alcohols including benzyl, allylic, aliphatic and heterocyclic alcohols as well as diols, affording the target products in excellent yields.

**Table 1-2.** Benzyl alcohol oxidation with bi-metal catalysts<sup>49</sup>.

Catalyst	Benzaldehyde				Benzaldehyde	H <sub>2</sub> O <sub>2</sub>
	Conversion/%		Selectivity/%		Productivity	Productivity
	0.5h	8h	0.5h	8h	[mol/(hour/kg <sub>cat</sub> )]	[mol/(hour/kg <sub>cat</sub> )]
2.5% Au-2.5% Pd/Al <sub>2</sub> O <sub>3</sub>	2.6	83.3	90.5	86.6	174	23
2.5% Au-2.5% Pd/TiO <sub>2</sub>	3.7	74.5	95.2	91.6	165	64
2.5% Au-2.5% Pd/SiO <sub>2</sub>	3.6	35.7	97.2	88	76	80
2.5% Au-2.5% Pd/Fe <sub>2</sub> O <sub>3</sub>	3.6	63.4	74.9	66.4	102	16
2.5% Au-2.5% Pd/C	2.9	69.2	53.9	46.4	78	30
2.5% Au/TiO <sub>2</sub>	0.6	15.3	96.7	63.9	24	<2
2.5% Pd/TiO <sub>2</sub>	13.4	60.1	51.3	54.4	79	24

Additionally, bi-metal catalysts are also issued. Hutchings *et al* synthesized the catalytic Au-Pd/TiO<sub>2</sub> that gave a high TOF for the oxidation of alcohols<sup>49</sup>. The introduction of Au into Pd based material improved selectivity (Table 1-2). Here, Au acted as an electronic promoter for Pd and leads to an active catalyst what had a surface greatly enriched in Pd.

For the platinum-group metal catalyst, the mild reaction condition is exactly the preponderance, whereas the production cost is quite expensive. On the other hand, the selection of the appropriate additives also is in higher demand, thus its applications have mainly focus on the high value-added fine organic chemicals.

### 1.2.2.2 Ru-based catalytic systems for alcohols oxidation

Ru is shifted as means of highly efficient alcohol oxidation catalyst in heterogeneous system because of the cost and non-ideal reutilization in homogeneous catalysis. Yamaguchi *et al* firstly presented well-behaved Ru/Al<sub>2</sub>O<sub>3</sub> in oxidation of activated primary and secondary allylic alcohols which afforded the corresponding enals or enones without intramolecular hydrogen transfer or geometrical isomerization<sup>50</sup>. For non-activated 2-octanol, the ketone was achieved in 95% yield (Figure 1-8). Moreover, 1-octanol and 1-decanol were also oxidized with moderate conversions. However, increasing the reaction time did not improve the yields of the aldehydes due to the successive oxidation to acids.

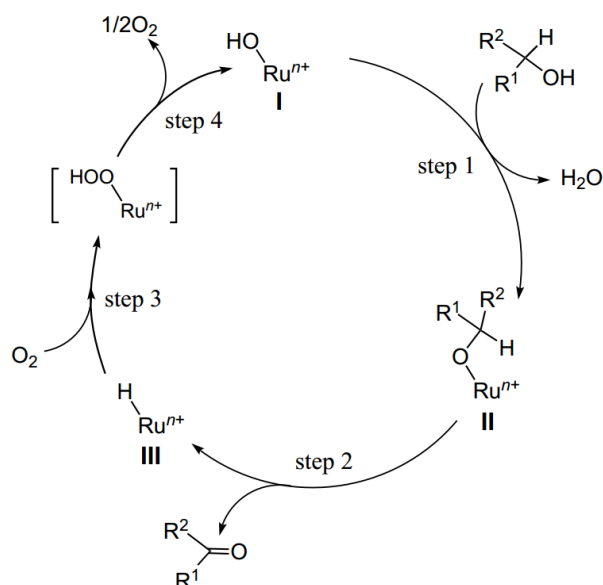


**Figure 1-8.** Possible mechanism for selective oxidation of primary hydroxy groups with Ru/Al<sub>2</sub>O<sub>3</sub><sup>50</sup>.

Apart from Al<sub>2</sub>O<sub>3</sub> as a carrier, inorganic oxide CeO<sub>2</sub><sup>51-53</sup>, ZrO<sub>2</sub><sup>54-55</sup>, SiO<sub>2</sub><sup>56-57</sup> were also employed into the supported catalysts but pessimistic in the oxidation of aliphatic alcohols. Recently, the magnetic catalyst Ru/HAP- $\gamma$ -Fe<sub>2</sub>O<sub>3</sub><sup>58</sup> with  $\gamma$ -Fe<sub>2</sub>O<sub>3</sub> nanocrystal dispersed in hydrotalcite and Ru uniformly distributed on the outer surface has been reported (Figure 1-9), which is effective under atmospheric pressure<sup>59</sup>.

Ru compounds represent a versatile group of catalysts that are crucial in plenty of organic transformations. Recently, Carson *et al* loaded a ruthenium complex into an aluminum metal-organic framework (MOF) (Figure 1-10) and established a new catalytic system with PhI(OAc)<sub>2</sub> as the oxidant under very mild reaction conditions<sup>60</sup>. Samples with low Ru grafting and higher surface areas were much more active since

the bpydc ligands immobilized to the MOF avoided the deactivation of the catalyst *via* creation of inactive species.

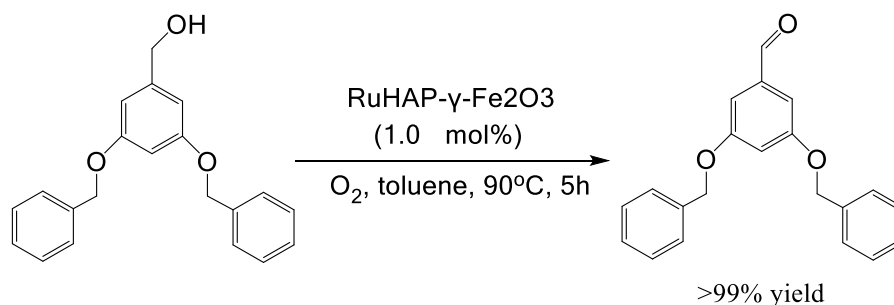


**Figure 1-9.** Oxidation of 3,5-dibenzoyloxybenzyl alcohol with  $\text{Ru/HAP-}\gamma\text{-Fe}_2\text{O}_3$ .<sup>58</sup>

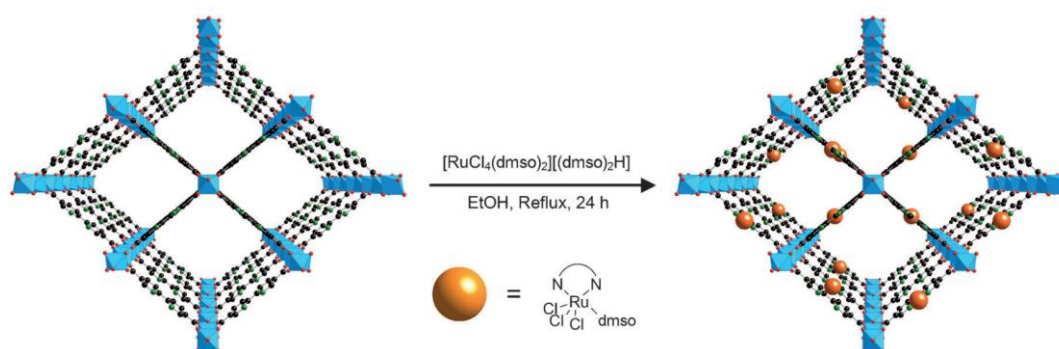


**Figure 1-10.** Representative structure and post-synthetic modification of MOF-253. Blue octahedra represent Al atoms; grey, red and green spheres represent C, O and N atoms, respectively; orange spheres represent the Ru complex,  $[\text{RuCl}_3(\text{dmsO})]$ .<sup>60</sup>

Compared with the widespread use of inorganic materials as catalyst supports, fewer reports are concerned on the application of polymer in catalytic alcohols oxidation. Kobayshi<sup>61</sup> *et al* developed the cross-linked polystyrene-microencapsulated  $\text{RuCl}_2$  that based on electronic interactions between metals and benzene rings of polystyrene derivatives as the catalyst for oxidation of alcohols to aldehydes and ketones. The catalyst synthesized shows higher activity than the non-immobilized catalyst, which is available and reusable for both flow and batch reaction systems.

Specially, element additive showed an unexpected effect.  $\text{Ru}^{\text{IV}}\text{-Co}^{\text{III}}$  (1 : 1.5) binary oxide<sup>62</sup> was obtained (Figure 1-11) and more efficient than  $\text{RuO}_2$  in the alcohol oxidation reaction with air. The mechanism on the hydrous  $\text{Ru-Co}$  oxide deemed to be as an oxidative dehydrogenation containing the generation of a Ru alkoxide intermediate, followed by  $\beta$ -elimination to form the aldehyde and a Ru hydride species, while cobalt could activate  $\text{O}_2$  in catalyst re-oxidation. Additionally, metalloprotein inspired self-assembled Ru catalyst by molecular convolution was investigated in selective alcohol oxidation with thermal stability<sup>63</sup>. The TON and TOF

of the catalyst arrived at 1031 and 516 h<sup>-1</sup>, respectively.

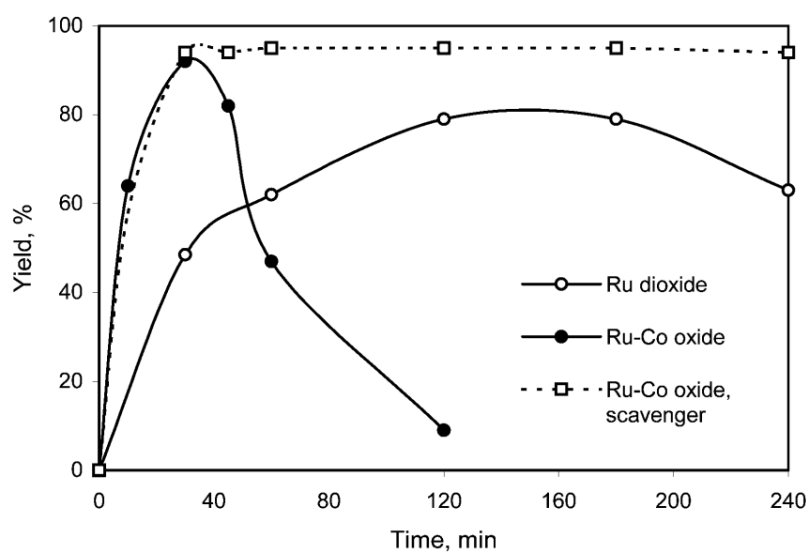


**Figure 1-11.** Yield of cinnamaldehyde vs. time for the aerobic oxidation of cinnamyl alcohol (2.5 mmol) catalysed by RuO<sub>2</sub> or by Ru–Co (1 : 1.5) oxide with and without radical scavenger (0.11 mmol) in toluene (10 ml) at 110 °C (alcohol : Ru = 10:1)<sup>62</sup>.

### 1.2.2.3 Au-based catalytic systems for alcohols oxidation

The activity of Au is largely structure-sensitive<sup>64</sup>. Small-crystal-size Au loaded on oxides or active carbon had attracted considerable attention. Prati proposed a new liquid-phase system with Au dispersed on the carbon surface for oxidation of diols<sup>65</sup>. In comparison with Pd/C and Pt/C catalysis<sup>66</sup> (Table 1-3), nano-Au expressed better catalytic efficiency and recyclability. The study found that, as well as a dominating impact from the particle size, the support material also has a strong effect on the catalytic activity. Analogously, Kumar<sup>67</sup> *et al* studied Au/CNT for the oxidation of aromatic alcohols that exhibited benign performance, but not for aliphatic alcohol.

**Table 1-3.** Oxidation of propene-1,2-diol at pH 8.<sup>66</sup>

Catalyst	t/h	T/K	PYR/mol%	HYDR/mol%	Conv./%	Selec./%
1% Au/C	10	363	--	--	30	100
5% Pd/C	5	343	8	13	46	11
5% Pt/C	5	343	4	24	56	32

Hutchings<sup>68</sup> *et al* proposed supported catalyst Au/CeO<sub>2</sub> for the oxidation of primary alcohols under base-free condition. The research revealed the mechanism of ester generation. It could consist of hemiacetal formation between the aldehyde and residual alcohol, followed by direct oxidation to the observed ester. Corma<sup>69</sup> *et al*

modified nanocrystalline CeO<sub>2</sub> from a stoichiometric oxidant into a catalytic carrier material and the Au nanoparticles could interact with the catalyst surface that stabilizes the positive oxidation states of gold by creating Ce<sup>3+</sup> and oxygen deficient sites in the ceria (Figure 1-12). In solvent-free and non-alkaline environment, Au/CeO<sub>2</sub> could oxidize benzyl alcohol and aliphatic secondary alcohol to the corresponding aldehydes and ketones products with high TOFs and selectivities; while in the alkaline environment, the primary alcohol was converted into the carboxylic acid.

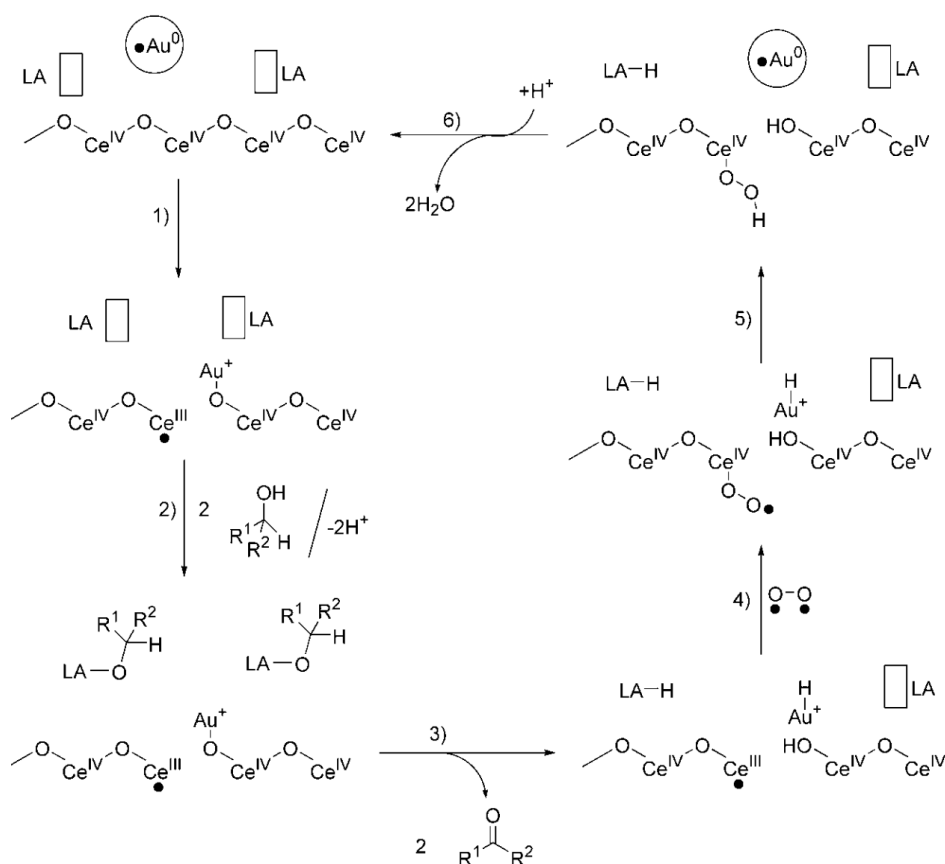


**Figure 1-12.** Proposed mechanism for the oxidation of alcohols in the presence of Au/CeO<sub>2</sub> as the catalyst. LA= Lewis acid.<sup>69</sup>

By using the multi-step photodeposition and single-step photo deposition methods, Au/CeO<sub>2</sub> samples with various Au contents were prepared and exhibited high selectivity in oxidation of benzyl alcohol to aldehyde under visible light irradiation from a green LED<sup>70</sup>, as Figure 1-13 showed.

Oxidation by oxygen of 1,4- butanediol to  $\gamma$ -butyrolactone with high selectivity has been reported over Au catalysts at 1.25 MPa air pressure in organic solvent tributylphosphate<sup>71</sup> (Figure 1-14). However, the role of solvent is not very clear in this work.

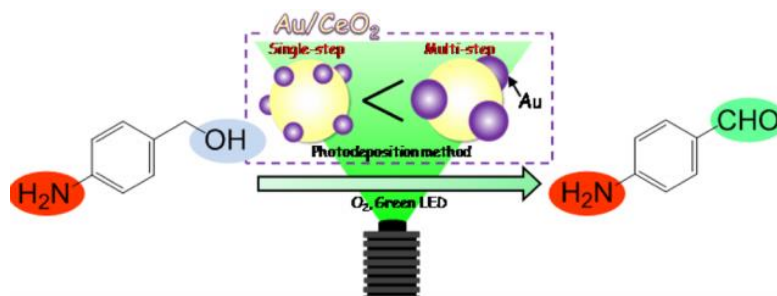


**Figure 1-13.**  $Au/CeO_2$  for selective oxidation in aqueous suspensions under irradiation by visible light from a green LED.<sup>70</sup>

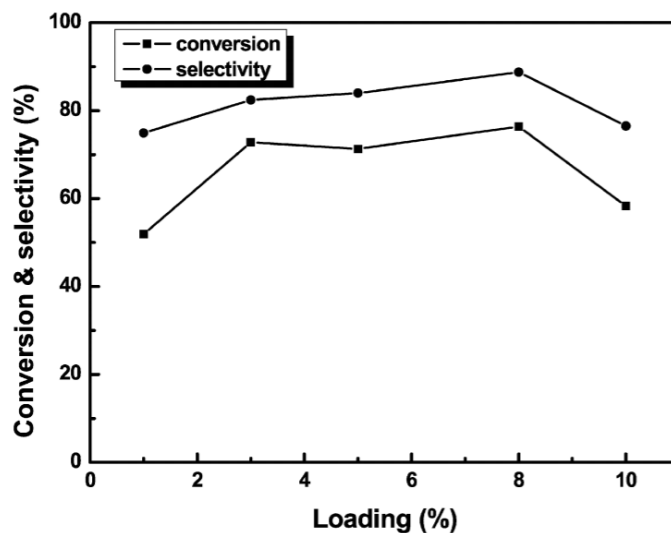


**Figure 1-14.** Dependence of gold loadings of  $Au/TiO_2$  catalysts calcined at 673 K and 1,4-butanediol conversion and  $\gamma$ -butyrolactone selectivity. Reaction was carried out at 393 K for 8 h.<sup>71</sup>

Cao<sup>72</sup> *et al* demonstrated the meso-structured catalyst  $Au/Ga_3Al_3O_9$ . Under mild condition, these catalysts can even efficiently catalyze the aromatic aerobic oxidation of several alcohols in the absence of water or base. However, oxidation of aliphatic 1-octanol is less selective.

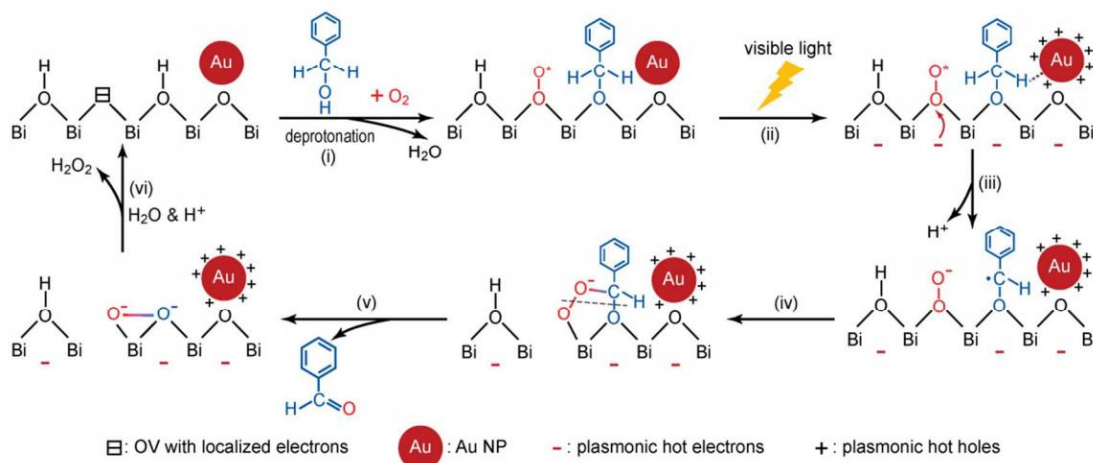


**Figure 1-15.** Proposed mechanism of selective BO oxidation over  $Au-BiOCl-OV$ .<sup>73</sup>

In 2017, a new plasmonic catalyst of Au supported on BiOCl was reported<sup>73</sup>. Through synergistic effect of plasmonic hot electrons and holes, it could photocatalyze benzyl alcohol oxidation with O<sub>2</sub> under visible light. Oxygen vacancies inside BiOCl accelerated the trapping and producing O<sup>-</sup> radicals (Figure 1-15), while plasmonic hot holes oxidize alcohol to corresponding carbon-centered radicals.

#### 1.2.2.4 Molecular sieves catalysts for alcohols oxidation

Microporous materials with high specific surface area, excellent pore structure, strong ion exchange, have been widely used in the industry, such as the materials with titanium-silicon, vanadium-silicon, boron-silicon, chromium-silicon. Zhan *et al* synthesized the catalyst that RuO<sub>2</sub> nanoparticles were encapsulated into faujasite in the absence of organic template<sup>74</sup>, which could be applied in selective catalytic oxidation of alcohols, which showed green and efficient catalytic performance.

MCM-41 mesoporous molecular sieves containing Cu were synthesized by the method of direct insertion of metal ions<sup>75</sup>. The partial oxidation of methanol and ethanol over this material to formaldehyde and acetaldehyde resulted in good conversion (~90%). It found that Cu determined the catalytic activity. In addition, octahedral molecular sieve K-OMS-2 with MnO<sub>6</sub> as a structural unit was obtained and then modified to H-K-OMS-2 by Suib group<sup>76</sup> (Figure 1-16). For benzyl alcohol, the good conversion and selectivity were indicated, and the acidification treatment strengthened the catalytic performance for other alcohols.

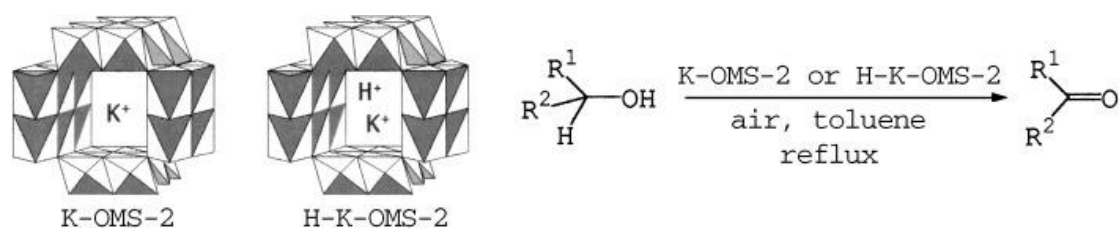


**Figure 1-16.** K-OMS-2 and H-K-OMS-2 for oxidation of alcohols.<sup>76</sup>

#### 1.2.2.5 Hydrotalcites catalysts for alcohols oxidation

Hydrotalcites ("HT"), with the formula M<sub>6</sub>Al<sub>2</sub>(OH)<sub>6</sub>CO<sub>3</sub>·4H<sub>2</sub>O, can treat as a good catalyst because of its unique layered structure and anion exchangeability<sup>77-78</sup>. Kaneda *et al* investigated the substituted hydrotalcite in the selective aerobic oxidation of alcohols<sup>79</sup>. It found that M<sub>6</sub>Al<sub>2</sub>Ru<sub>0.5</sub>(OH)<sub>6</sub>CO<sub>3</sub>, M = Mg, Co, Mn, Fe, Zn could catalyze the oxidation of allyl alcohol, benzyl alcohol and heterocyclic alcohol

to the corresponding aldehydes and ketones, of which the optimum was Co. However, only Ru-Co-Al-CO<sub>3</sub> can catalyze the oxidation of aliphatic secondary alcohols, nevertheless, not for primary alcohols. Similarly, MgMnTi hydrotalcite-like layered double hydroxides (LDHs) catalyst was found to efficiently oxidize the various alcohols, except for the saturated alcohols<sup>80</sup>.

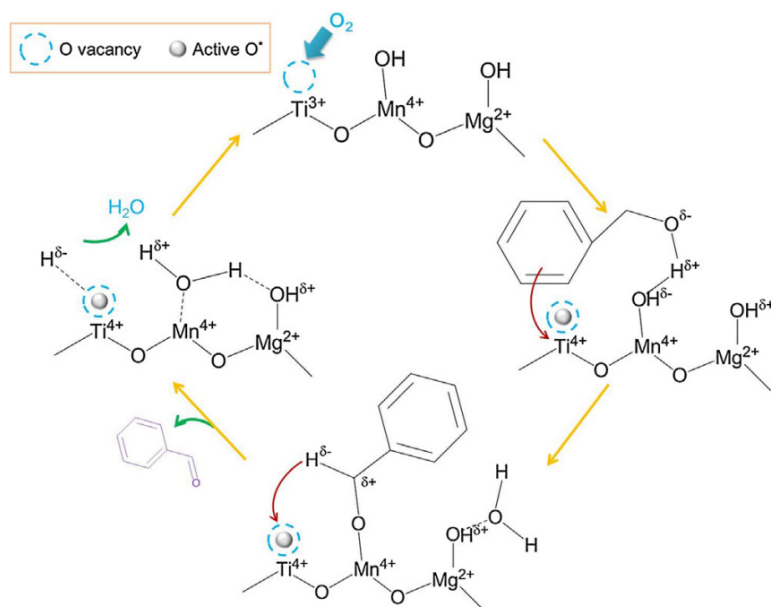


**Figure 1-17.** Possible reaction pathway of the oxidation of benzyl alcohol over Mg<sub>4</sub>Mn<sub>2</sub>Ti<sub>1.0</sub>-LDH catalyst.<sup>81</sup>

Through a co-precipitation method, Zhou *et al* modified hydrotalcite and metalloporphyrin intercalated materials as efficient catalysts<sup>81</sup>. The hybrid material, MTSPP-Zn<sub>2</sub>Al LDHs (Figure 1-17) can heterogenize the metalloporphyrins and stabilize the molecule; while the surface basicity of the layered double hydroxides has a positive impact on the catalytic performance.

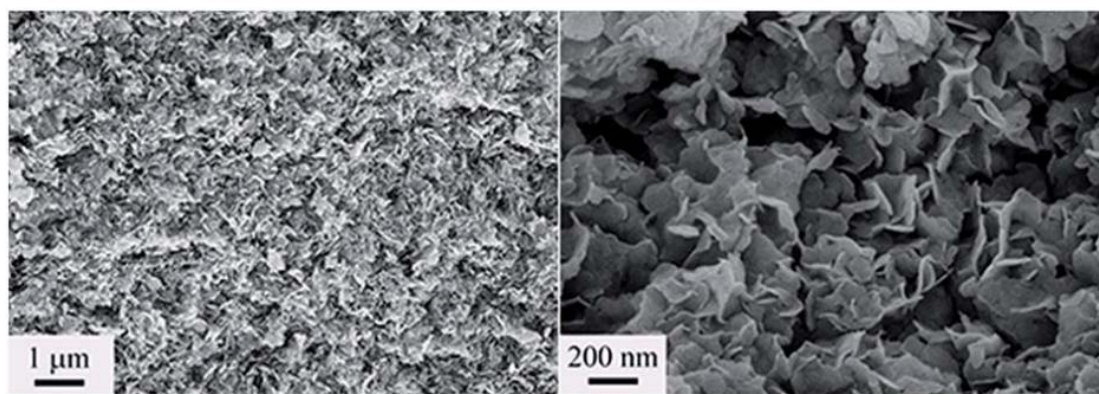


**Figure 1-18.** SEM images of CO<sub>3</sub><sup>2-</sup>-Co<sub>x</sub>Fe-LDH.<sup>82</sup>

In addition, CoAl-HT-Si with higher surface and pore volume was reported and showed good conversion (90%) and selectivity (97%) for decanol<sup>83</sup>. Recently, CO<sub>3</sub><sup>2-</sup>

-Co<sub>x</sub>Fe-LDHs (x= 2, 3, 4 and 5) compounds (Figure 1-18) have been produced with different Co/Fe ratios and recommend into the selective oxidation of alcohols by tertbutylhydroperoxide<sup>82</sup>, by which pentan-2-ol could be oxidized with >90% yields to 2-pentanone.

### 1.2.2.6 Heteropolyacid catalysts for alcohols oxidation

On account of economic, environmental and oxidizability, heteropolyacid compounds gain researchers' attention. However, they also have weaknesses of overdependence on external conditions<sup>84</sup>. Figure 1-19 states the schematic diagrams of phosphotungstic acid with a typical Keggin structure, which has coordination ability to the substrates and affect the activity and selectivity. Keggin heteropolyacids can be substantially dissociated in aqueous solutions/organic media<sup>85</sup> and the acidity of the heteropoly acid (H<sub>a</sub>XW<sub>12</sub>O<sub>40</sub>) is positively correlated to the increase of the oxidation state of the central element<sup>86</sup>.

The phosphotungstic acid, SiO<sub>2</sub> supported H<sub>3</sub>PW<sub>12</sub>O<sub>40</sub> catalyst (HPA) targeted to achieve the selective oxidation of aromatic alcohol with O<sub>2</sub> as oxidant. The study found that loading HPA greatly improved reactivity of the catalyst, which stemmed from the high specific surface of the support and the more effective contact<sup>87</sup>.

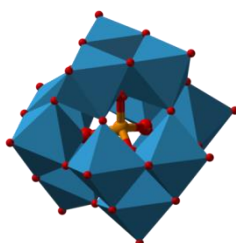


**Figure 1-19.** *The structure of typical Keggin.*

Oxidation of diols by hydrogen peroxide over dissolved heteropolyacids in biphasic system has been reported<sup>88</sup>. In the case of 1,4-BDO the main product was  $\gamma$ -butyrolactone (Table 1-4). Noyori presented a reaction that carried out in organic-water system with H<sub>2</sub>O<sub>2</sub> concentration of 3%~30%<sup>89</sup>, in which secondary alcohol was oxidized to ketone and could reach impressive yield of 83%~96% by using sodium tungstate dihydrate as catalyst.

The Nb<sub>2</sub>O<sub>5</sub>-supported heteropolyacid catalyst was proposed by Lingaiah<sup>90</sup>. In the organic-water system, the conversion of benzyl alcohol and the selectivity to benzoic acid were 50% and 90%, respectively, and the catalytic performance was affected by

the loading of heteropolyacids at 250~310 °C. Afterwards, Parida<sup>91</sup> *et al* reported a novel PMA/ZrO<sub>2</sub>-CeO<sub>2</sub> catalyst worked at 80 °C and the molar ratio of H<sub>2</sub>O<sub>2</sub>/substrate was 1:1. The conversion of benzyl alcohol and its selectivity to benzaldehyde were improved to 85% and 96%, respectively (Figure 1-20).

**Table 1-4.** Oxidation of diols with [WZnMn(II),(ZnW<sub>9</sub>O<sub>34</sub>)<sub>2</sub>]<sup>12-</sup> in a biphasic medium.<sup>88</sup>

Substrate	Products	Conversion/mol%
1,2-butanediol	2-keto-1-butanol	34
2,3-butanediol	2-keto-3-butanol	41
1,3-butanediol	3-keto-1-butanol	26
2,4-pentanediol	2-keto-4-pentanol	35
1-phenyl-1,2-ethanediol	2-hydroxyacetophenone	50
	benzaldehyde	
1,4-butanediol	γ-butyrolactone	17

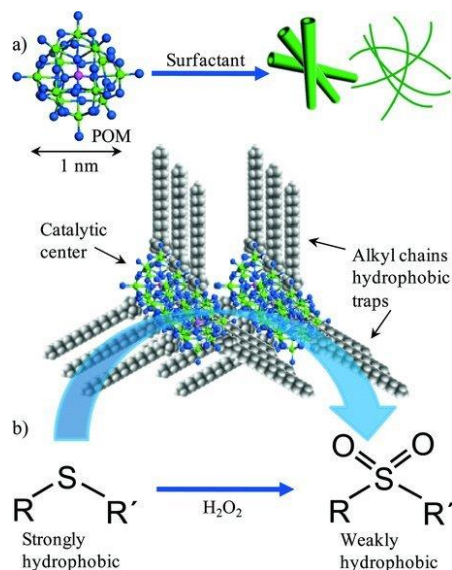


**Figure 1-20.** Schematic illustrations of a) preparation of POM semitube and wire assemblies (top) and b) the oxidation of sulfides to sulfones (bottom). Center: Illustration of the catalytic center (POM) and hydrophobic traps (alkyl chains) in amphiphilic POM mesostructures.<sup>92</sup>

Phosphotungstic acid was firstly combined with single-alkyl-chain surfactant molecules to form templates and assembled into amphiphilic nanotubes and linear structures<sup>92</sup>. This is a bifunctional catalyst that simultaneously activates both substrates and oxidants. The hydrophobic group of the mesoporous catalyst attracted the substrate to react, while hydrophilic groups were synergistic with H<sub>2</sub>O<sub>2</sub> as oxidant. The polyoxometalate catalyst Zn/Sb-polyoxotungstate (Figure 1-21),  $\alpha$ -NH<sub>4</sub>-[Zn<sub>2</sub>Sb<sub>2</sub>]

(1a) and  $\beta$ -Na-[Zn<sub>2</sub>Sb<sub>2</sub>] (2a) were developed by Patzke to oxidize alcohols. For 2-ethyl-1,3-hexanediol, both catalysts perform 99% conversion and 99% selectivity to 2-ethyl-3-oxo-1-hexanol<sup>93</sup>.

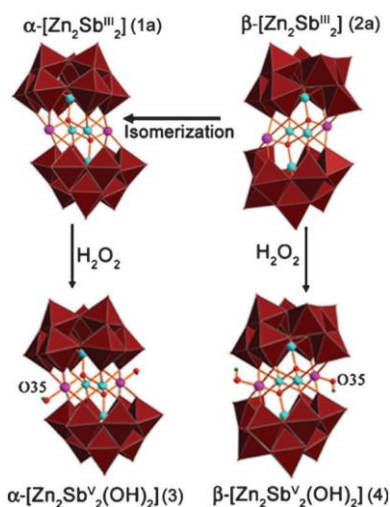


**Figure 1-21.** Combined polyhedral/ball-and-stick representations of  $\alpha/\beta$ -[Zn<sub>2</sub>Sb<sup>III</sup><sub>2</sub>(ZnW<sub>9</sub>O<sub>34</sub>)<sub>2</sub>]<sup>14-</sup> and their corresponding high-valent species  $\alpha/\beta$ -[Zn<sub>2</sub>Sb<sup>V</sup><sub>2</sub>(OH)<sub>2</sub>(ZnW<sub>9</sub>O<sub>34</sub>)<sub>2</sub>]<sup>12-</sup>.<sup>93</sup>



**Figure 1-22.** Selective oxidation of alcohols with hydrogen peroxide catalyzed by [PEOdidodecylimidazolium]<sub>3</sub>[PW<sub>12</sub>O<sub>40</sub>]<sub>2</sub>.<sup>94</sup>

In 2015, Wang *et al* employed [PEOdidodecylimidazolium]<sub>3</sub>[PW<sub>12</sub>O<sub>40</sub>]<sub>2</sub>, a polyethylene oxide-supported long-chain imidazolium polyoxometalate hybrid catalyst for dodecanol oxidation with H<sub>2</sub>O<sub>2</sub> at room temperature<sup>94</sup>. It obviously found that the advantage effect appeared with the carbon length increased, which may attribute to stronger lipophilic ability and better surface-active performance.

### 1.2.3 Heterogeneous oxidation of alcohols - gas phase

The heterogeneous catalytic oxidation in liquid phase is commonly performed in mild conditions and is suitable for high-boiling and labile alcohols. However, there are also problems in the separation of the solvent, product and catalyst; while low

production efficiency makes it difficult to be applied to the industrial production.

The gas phase oxidation with oxygen as oxidant avoids the solvent minimizes the harmful material and is in line with the advocacy of the "green chemistry". However, the temperature in gas-phase reaction is higher than liquid-phase. The instantaneous heat cannot be removed timely, which generally leads to a decreased of selectivity to the target molecule. Moreover, long-chain alcohols are harder to be oxidized at high temperature. As a result, seeking for a rational catalyst at low-temperature is on demand.

### 1.2.3.1 IB-group metals catalysts for alcohols oxidation in gas phase

IB-group metals containing Cu, Ag, Au, are widely used in the selective catalytic oxidation of alcohols<sup>95-96</sup>, of which crystalline Ag and supported Ag are exhaustively studied. Knyazev<sup>97</sup> studied the selective oxidation process of glycol with electrolytic Ag. It suggested that the adsorbed oxygen arose on Ag surface during the reaction, which was beneficial for the reactive sites. However, for the polyols and aromatic alcohols it is inadaptable, requiring a high temperature of 500~600 °C which can easily inactivated the catalyst.

**Table 1-5** Effect of DEP on the catalyst composition.<sup>98</sup>

Catalyst	Reaction	Ag (wt%)	
		before reaction	after reaction
8% Ag/SiC	100h without DEP	8.4	8.0
8% Ag/SiC	120h with 20ppm DEP	8.2	6.2
5% Ag/SiC	96h with 20ppm	5.6	4.8

In 1993, Ag/SiC<sup>98</sup> was studied for the oxidative dehydrogenation of ethylene glycol into glyoxal and got a breakthrough progress with 98% conversion and 73% selectivity, while the phosphite compounds DEP was needed to keep a high selectivity (Table 1-5). For electrolytic Ag catalysts, it is generally desirable to exhibit good activity above 500 °C; while for the supported Ag, poor thermal conductivity and un-reuse limit its industrial application.

Besides Ag, Au and Cu also have good performances. Rossi introduced Au/SiO<sub>2</sub> into the gas-phase alcohol-catalyzed oxidation<sup>99</sup> (Table 1-6). Subsequently, bimetallic Au/Ni-fiber<sup>100</sup> was selectively oxidized cyclohexanol to cyclohexanone at a conversion of 73% with the selectivity of 99% at 340 °C. Cu catalysts indicated

outstanding capability in the transformation of cyclohexanol to cyclohexanone. Gyung *et al* declared Cu/SiO<sub>2</sub> catalyst with Mn added could greatly improve the conversion and selectivity<sup>101</sup>. Fan *et al* proved that mesoporous K-Cu-TiO<sub>2</sub> with stable copper(I) could accomplish the gas-phase oxidation with the yield of > 99% for the benzyl alcohol to benzaldehyde at low temperatures and a high TOF (up to 108 h<sup>-1</sup>)<sup>102</sup>. The composites AuCu(alloy)-Cu<sub>2</sub>O shaped during reaction and their cooperative effect contributed to encourage the low-temperature activity. The conversion of 1-octanol was 65% and the selectivity was 93% with air as oxidant at 380 °C<sup>103</sup>.

**Table 1-6.** Gas-phase alcohol-catalyzed oxidation with Au/SiO<sub>2</sub>.<sup>99</sup>

Entry	Catalyst	Reagent	T/K	Conv./%	Selec./%
1	1% Au/SiO <sub>2</sub>	1-propanol	523	27	100
			573	44	100
2	1% Au/SiO <sub>2</sub>	1-butanol	523	51	100
			573	63	94
3	1% Au/SiO <sub>2</sub>	1-propanol	523	23	100
			573	29	100
4	1% Au/SiO <sub>2</sub>	phenylcarbinol	523	50	100
			553	75	98
5	1% Au/SiO <sub>2</sub>	prop-2-en-1-ol	523	42	97
			373	69	100
6	1% Au/SiO <sub>2</sub>	2-propanol	423	100	100
			393	34	100
7	1% Au/SiO <sub>2</sub>	2-butanol	423	64	100
			393	72	87
8	1% Au/SiO <sub>2</sub>	2-pentanol	423	85	84
			393	85	100
9	1% Au/SiO <sub>2</sub>	3-pentanol	423	97	100

### 1.2.3.2 Fe/Mo catalysts for alcohols oxidation in gas phase

Fe<sub>2</sub>O<sub>3</sub>, MoO<sub>3</sub> could be treated as the catalyst with the addition of P and Co, which was synthesized by Awasarkar<sup>104</sup>. The addition of phosphorus element formed a new phase, which favored in glyoxal selectivity in avoidance of deep oxidation.

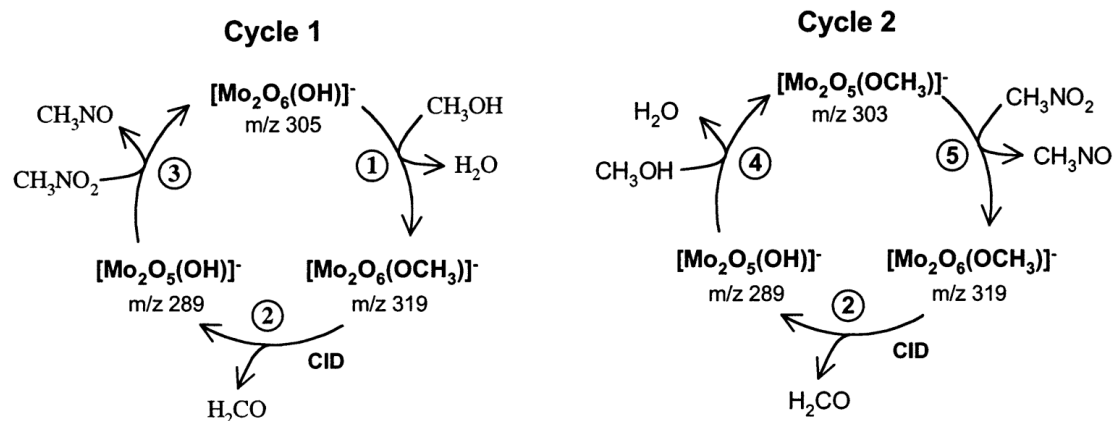


**Figure 1-23.** Gas-phase catalytic cycles for the oxidation of methanol to formaldehyde.<sup>105</sup>

In 2002, two gas-phase catalytic cycles (Figure 1-23) for the two-electron oxidation of primary and secondary alcohols were detected by Richard<sup>105</sup>. Here, a binuclear dimolybdate center  $[\text{M}_2\text{O}_6(\text{OCHR}_2)]^-$  (M= Cr, Mo, W) served as the catalyst in the oxidation of methanol to formaldehyde at 300~400 °C, which was in accordance with the expected order of basicity of the hydroxo ligand.

### 1.2.3.3 Heteropolyacid catalysts for alcohols oxidation in gas phase

Mahoru adopted  $\text{H}_3\text{PMo}_{12}\text{O}_{40}$ /zeolite as catalyst for the catalytic oxidation of hydroxyacetone with the 76.8% yield; while the conversion was 96% with  $\text{FePO}_4$  as catalyst, and yield of hydroxyacetone was 88% respectively<sup>106</sup>. Song *et al* proposed  $\text{H}_3\text{PMo}_{12}\text{O}_{40}$ /SM-CMK-3, a catalyst supported on a carbon material<sup>107</sup>. After activation in  $\text{N}_2$  and  $\text{O}_2$  atmosphere, the reaction was carried out with  $\text{O}_2$  at 260 °C, the conversion of benzyl alcohol and the selectivity towards benzaldehyde were 98% and 96%, respectively.

### 1.3 Metal-free selective oxidation of alcohols

The use of metal-based catalysts that present good activity triggers questions of sustainability. Transition metal ions were not easily removed and could generate toxic wastes which are referred as being not green. Recently, the recyclable non-metal analogues are explored as the promising and environment-friendly catalytic technology in the oxidation processes.

### 1.3.1 Carbocatalysts for alcohols oxidation

Compared to traditional metal based catalysts, carbon-based materials afford additional advantages due to the giant  $\pi$  structures that favor strong interactions with diverse substrates. And its physicochemical and electronic properties that in principle determine the catalysis processes, can be tailored and fine-tuned by molecular engineering and/or heteroatomic doping. A plenty of studies have reported that doping of heteroatoms into graphene and other carbon based materials gives rise to enhanced performance with undoped one as a control<sup>108</sup>.

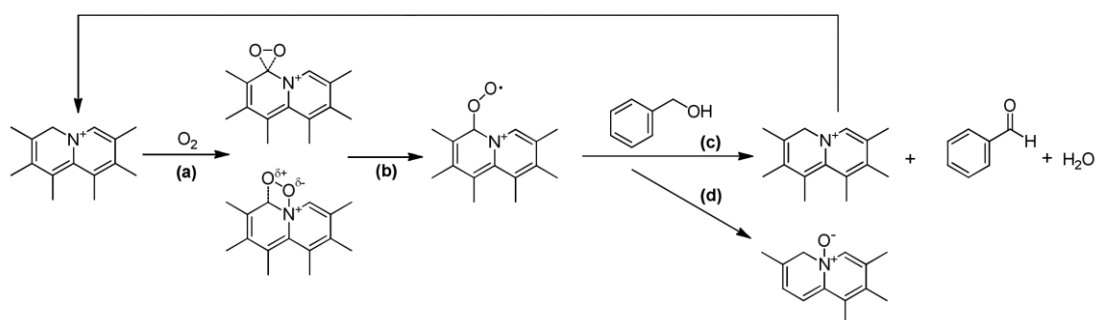


**Figure 1-24.** Possible reaction pathways for aerobic oxidation of benzyl alcohol over nitrogen-doped activated carbon catalyst<sup>113</sup>.

Bielawski took the lead in harnessing the inherent reactivity of graphene oxide (GO) and other graphene-based materials to facilitate useful synthetic transformations<sup>109</sup>. The molecular engineering of active sites on a graphene scaffold was reported by Wang<sup>110</sup>. Among three types of nitrogen species doped into the graphene lattice-pyridinic N, pyrrolic N, and graphitic N-the graphitic  $sp^2$  N species were established to be catalytically active centers in aerobic alcohol oxidation. Kinetic analysis showed the possible formation of a  $sp^2$  N-O<sub>2</sub> adduct transition state, which can oxidize alcohols directly to aldehydes without any byproduct, might be a pivotal element step. Other cases of nitrogen-doped annealed nanodiamonds<sup>111</sup> and nitrogen rich carbon nanotubes in the conversion of glycerol into dihydroxyacetone by using tert-butyl hydroperoxide as an oxidant<sup>112</sup> embedded pyridine nitrogen groups in a carbon matrix that are believed to be involved as active sites. However, the nitrogen-doped activated carbon catalyst was announced inactive for the oxidation of 3-phenyl-1-propanol, 1-heptanol and cyclohexylmethanol<sup>113</sup>. In other words, the alcohols in which the carbon bonding to hydroxyl group may be activated by its adjacent conjugated system can be oxidized by the nitrogen-doped catalysts (Figure

1-24). In direct contrast to N-doped graphene, the work function of P-doped carbon materials connected to the P bond configuration<sup>114</sup>, and nitrogen, phosphorus, and sulfur co-doped hollow carbon shells<sup>115</sup> that improves the hydrophilicity of the catalysts are studied and established.

Besides, mesoporous carbon nitride polymer (mpg-C<sub>3</sub>N<sub>4</sub>) can perform as a metal-free photocatalyst to activate O<sub>2</sub> with visible light, avoiding the cost, toxicity, and purification problems associated with corresponding transition-metal systems<sup>116</sup>. By combining the surface basicity and semiconductor functions, the photocatalytic system can realize a high catalytic selectivity to generate benzaldehyde as shown in Figure 1-25. Another recent novel protocol: N-, O-, and S-tridoped, polypyrrole derived nanoporous carbons that can serve as metal-free, selective electrocatalysts and catalysts for oxygen reduction reaction and alcohol oxidation reaction, respectively<sup>117</sup>.

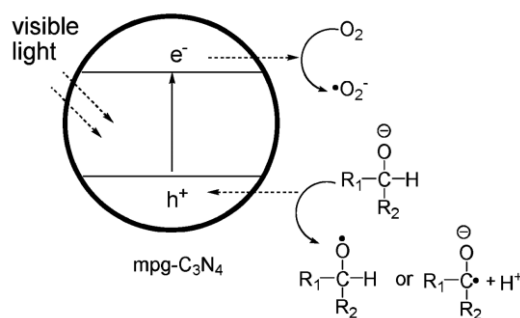


**Figure 1-25.** *Electron Transfer Reactions with mpg-C<sub>3</sub>N<sub>4</sub>.*<sup>116</sup>

Rothenberg combined such a carbon with metal-oxide catalysts to yield cooperative catalysts. These simple materials boost the catalytic oxidation of several alcohols, using molecular oxygen at atmospheric pressure and low temperature (80oC). Cobalt and copper oxide demonstrate the highest activities. It propose that the reaction should not be viewed as occurring at an ‘active site’, but rather at an ‘active doughnut’--the volume surrounding the base of a carbon-supported metal-oxide particle<sup>118</sup>. Subsequently, they proved that when both the particle and substrate are catalytically active, there exists a defined “active doughnut” volume, where most of the catalytic action takes place. Its size and shape can be estimated from the particles’ size and their spatial distribution, as well as from the lifetime, absorption, and diffusivity of the reaction intermediates. The active doughnut concept offers a useful framework for planning and analysing the optimal size of catalytically active particles, and their distribution on the surface<sup>119</sup>.

### 1.3.2 Nitroxyl radical catalytic for alcohols oxidation

The mechanism of TEMPO-based selective alcohols oxidation is basically on account of the *in-situ* generation of N-oxoammonium cations with the assistance of terminal oxidants or acid induced disproportionation. Often only 1 mol % or even less of the nitroxyl radical is required as the catalyst, which is definitely competitive with the pre-existing metal-based systems. The relevant features determine the pH-dependent different behaviors with regard to the mechanism: whereas hydride-transfer processes preferably occur in acidic medium (Figure 1-26, left), while the adduct formation and subsequent Cope-type elimination pathways are dominant under basic conditions<sup>120</sup>.

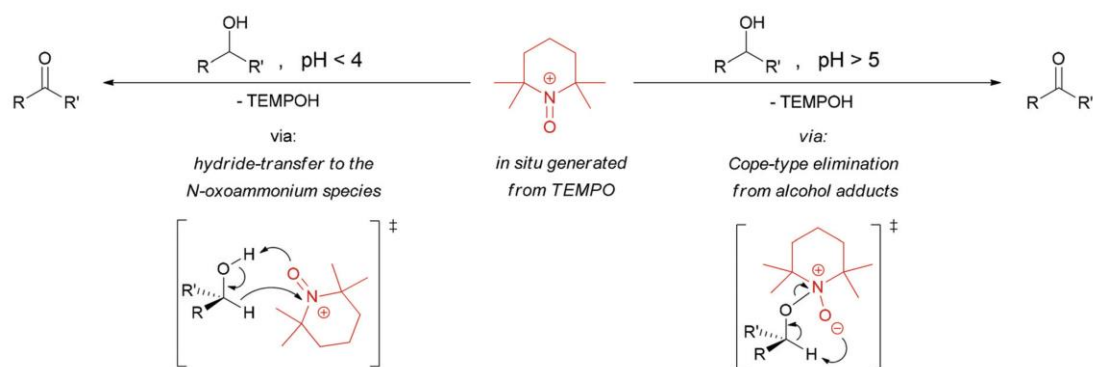


**Figure 1-26.** Mechanisms of N-oxoammonium cation mediated oxidation of alcohols in acidic (left) and basic media (right).<sup>120</sup>

The inexpensive and readily available sodium hypochlorite (“Anelli conditions”)<sup>121</sup> or  $\text{PhI}(\text{OAc})_2$  (“Margarita conditions”)<sup>122</sup> are commonly used as terminal oxidants for the aldehyde or ketone synthesis. Since secondary alcohols are better hydride donors and sterically less bulky, primary alcohols are preferably oxidized than former<sup>123</sup>. Generally, the mild alkaline conditions, *e.g.*  $\text{NaHCO}_3$  buffer, improve the activity and selectivity for primary alcohols that could be oxidized to the corresponding carbonyl compounds with slightly excessive sodium hypochlorite.

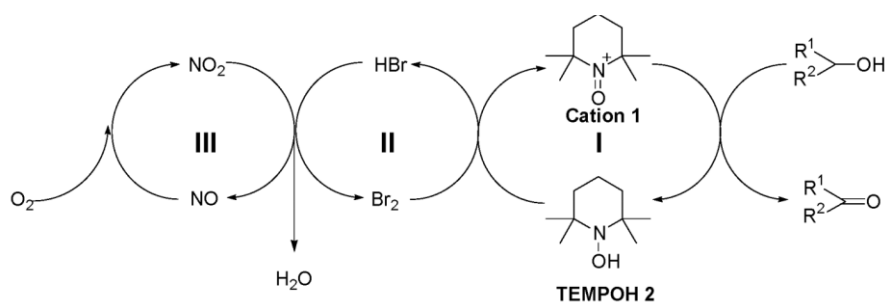


**Figure 1-27.** Overall catalytic mechanism of TEMPO/ $\text{Br}_2$ / $\text{NaNO}_2$ .<sup>124</sup>

In 2004, Hu firstly explored an aerobic metal-free alcohol oxidation with a catalyst system consisting of TEMPO/Br<sub>2</sub>/NaNO<sub>2</sub> under air (Figure 1-27), where the Br<sub>2</sub>/Br<sup>-</sup> redox pair has to be replaced with HOBr/Br<sup>-</sup> and water formation takes place during the N-oxoammonium salt generation<sup>124</sup>. Aromatic and aliphatic primary and secondary alcohols were efficiently and selectively oxidized to the corresponding aldehydes or ketones.

In addition to Br-based systems, hydrochloric acid has been found to cooperate exquisitely with NaNO<sub>2</sub>/TEMPO in catalyzing the molecular-oxygen-driven oxidation of a broad range of alcohol substrates (Figure 1-28)<sup>125</sup>. A hydride transfer process seems to be operative since a higher catalyst loading was necessary to oxidize primary aliphatic alcohols with equal levels of efficiency.

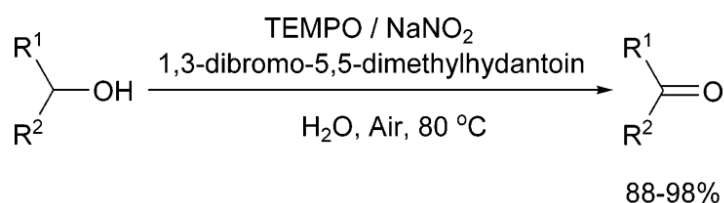


**Figure 1-28.** TEMPO-catalyzed aerobic oxidation of alcohols.

Very recently, extension to selective oxidation in natural lignins were accomplished with an optimal co-catalyst system composed of 4-acetamido-TEMPO in combination with HNO<sub>3</sub> and HCl<sup>126</sup>. Moreover, the use of N-chlorosuccinimide as primary oxidant also gives carbonyl compounds selectively without over-oxidation to the respective carboxylic acids<sup>127-129</sup>. In addition, the TEMPO-catalyzed procedure is also an option for the oxidation of primary hydroxyl groups in carbohydrates in high yields<sup>130-132</sup>. The oxidation of sucrose gave sucrose tricarboxylate in good yields, when an excess of sodium hypochlorite was employed.

TEMPO immobilization on polymer or inorganic support affords heterogeneous catalysts, which is in favor of facile separation after the reaction, which could efficiently and selectively oxidizes primary and secondary alcohols to their carbonyl compounds with aqueous NaOCl<sup>133-134</sup>. The reactions terminated within 1 h and requires bromides as co-catalyst. Methyl tert-butyl ether (MTBE) that could not dissolve the catalysts was added as a co-solvent in the oxidation of 1-octanol and 1-hexanol, which prevented the deeper oxidation.

Another sample supported on the mesoporous MCM-41 zeolite<sup>135</sup> was shown to catalyze the hypochlorite oxidation of R-methyl glucoside selectively to 1-O-methyl

glucuronate (Figure 1-29). However, the partial catalyst degradation was observed. It was assumed that the high density of active sites on the silica surface led to interactions between neighboring functional groups which then resulted in an oxoammonium ion-mediated cleavage of amino-bonds and partial destruction of the supported catalyst.

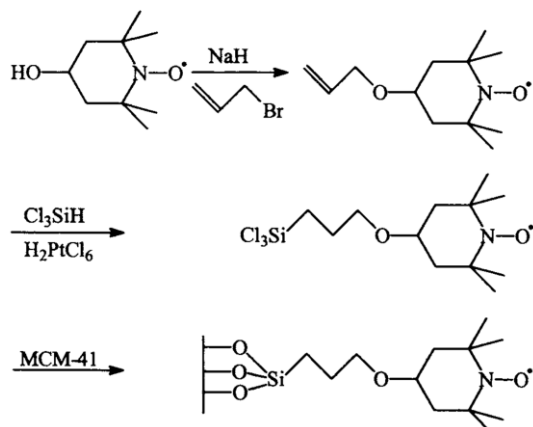


**Figure 1-29.** Synthesis of MCM-41/TEMPO.<sup>136</sup>

Circulatory problems were subsequently improved. TEMPO covalently attached via orthosilicate linkers to hydroxyl-groups at the SBA-15 surface with well-defined pore size and shape has been studied<sup>137</sup>. The resulting catalyst was reusable for 14 consecutive runs and quantitative oxidation of benzylic alcohol under relatively mild conditions was achieved.

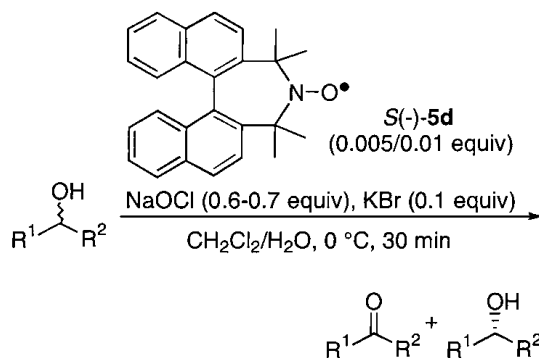


**Figure 1-30.** Active binaphthyl-based nitroxyl radical *S*-(-)-5d -catalyzed aerobic oxidation of alcohols.<sup>138</sup>

Besides TEMPO, the optically active binaphthyl-based nitroxyl radical *S*-(-)-5d was employed as the catalyst for the kinetic resolution of racemic secondary alcohols (Figure 1-30)<sup>138</sup>.

### 1.3.3 Quinones species for alcohols oxidation

Quinones are important redox highly active materials that can be used in a variety of redox processes, including the manufacture of industrial chemicals, the oxidation of organic molecules<sup>139-140</sup>. Analogous to TEMPO, quinones feature three readily accessible oxidation states, namely, fully oxidized quinone, one-electron-reduced semiquinone, and two-electron-reduced hydroquinone as Figure 1-31 shown<sup>141</sup>, which are capable of mediating redox processes.

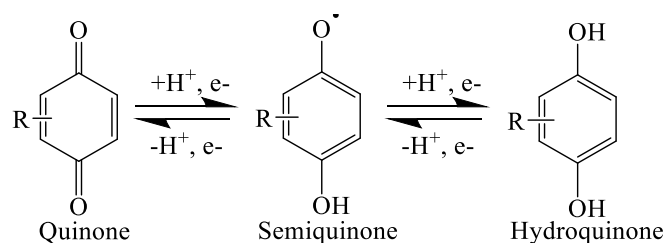


**Figure 1-31.** Quinones feature three readily accessible oxidation states.<sup>141</sup>

However, quinones are more generally applied as stoichiometric and less-extensive catalysts for the oxidation of organic molecules. Redox cycling between oxidized and hydrogenated quinone species facilitates the anthraquinone-mediated industrial synthesis of hydrogen peroxide<sup>142</sup>. The incongruity between oxidation and reduction steps requires sequential operation of the two stoichiometric half reactions in the cycle, the use of a quinone mediator common to both half reactions demonstrates the prospects for engaging quinones as catalysts in redox reactions.

2,3-dichloro-5,6-dicyano-1,4-benzoquinone (DDQ) and chloranil with a high reduction potential are recognized as a strong oxidant and commonly mediate hydride abstraction from a substrate<sup>143</sup> and forms an ion-pair product<sup>144</sup>. The mechanism might proceed through the formation of a quinone–substrate charge-transfer complex<sup>145-146</sup>. DDQ has important application as an oxidant in the functionalization of activated C-H bonds, including in several process-scale pharmaceutical syntheses<sup>147</sup>. Deprotonation of the substrate by DDQH<sup>-</sup> can afford the corresponding dehydrogenated product<sup>148</sup>, as featured in the formation of aldehydes and ketones from activated alcohols<sup>149</sup>. However, the direct hydride abstraction limits dehydrogenation process of substrates containing quite activated C-H bonds (*e.g.* benzylic, allylic), which has provided the motivation to develop methods capable of using catalytic amounts of DDQ or chloranil in quinone-mediated reactions.

In 1978, the first DDQ-catalyzed reaction was reported, and showed that the transformation of allylic alcohols to  $\alpha,\beta$ -unsaturated ketones could be achieved by 10 mol% DDQ in the presence of 30 mol% periodic acid under biphasic conditions at room temperature<sup>150</sup>. Helquist subsequently illustrated similar reactivity with  $\text{Mn}(\text{OAc})_3$  as the stoichiometric oxidant. By using 20 mol% DDQ and 6.0 equiv  $\text{Mn}(\text{OAc})_3$ , allylic alcohols over benzylic alcohols are observed to be oxidized to the corresponding aldehydes and ketones under mild conditions (Figure 1-32)<sup>151</sup> with good chemoselectivity. However, the use of excess amounts of  $\text{Mn}(\text{OAc})_3$  made this protocol environmentally unfriendly.

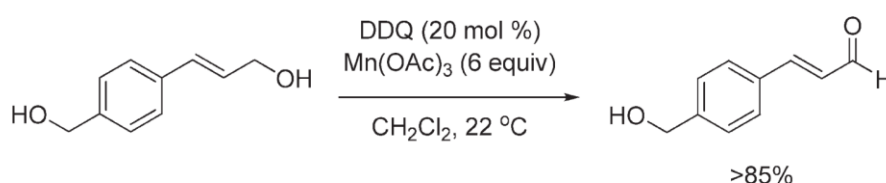


**Figure 1-32.** Chemoselective oxidation of alcohols employing catalytic quantities of DDQ as the oxidant and  $\text{Mn}(\text{OAc})_3$  as the co-oxidant.<sup>151</sup>

A lower catalytic amount of DDQ-catalyzed (1~20 mol%) method reported requires  $\text{NaNO}_2$  as a co-catalyst and  $\text{O}_2$  as terminal oxidant in the presence of AcOH (Figure 1-33)<sup>152</sup>. And the practical utility of this catalytic system has been demonstrated in the gram-scale oxidation of cinnamyl alcohol. Innovatively, Moody disclosed a similar catalyst system with catalytic amount of DDQ and  $\text{NaNO}_2$  or tert-butyl nitrite under visible light irradiation<sup>153</sup>.

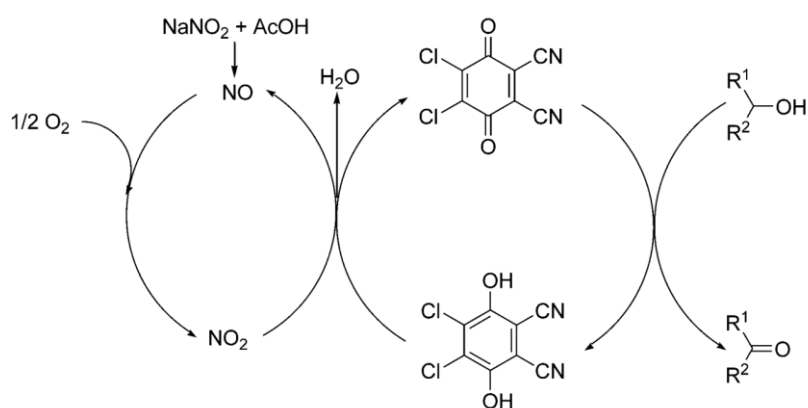


**Figure 1-33.** Proposed catalytic cycle for the aerobic oxidation by DDQ/  $\text{NaNO}_2$ / AcOH.<sup>152</sup>

The development of an efficient and inexpensive co-catalyst in combination with catalytic amount of DDQ for the aerobic oxidation of alcohols is still highly desired. Very recently, Li found a  $\text{Fe}(\text{NO}_3)_3$ /DDQ catalyzed system with air serving as the

terminal oxidant, which exhibits excellent substrate tolerance and a variety of benzylic, heterocyclic, allylic and propargylic alcohols are selectively transformed to the corresponding aldehydes and ketones in good yields<sup>154</sup>. The DDQ-catalyzed systems applied to other aerobic alcohol oxidation reactions have been announced in which additional co-catalysts, such as 2,2,6,6-tetramethylpiperidinyloxy<sup>155</sup> or N-bromosuccinimide<sup>156</sup>, are used in combination with DDQ and NO<sub>x</sub>.

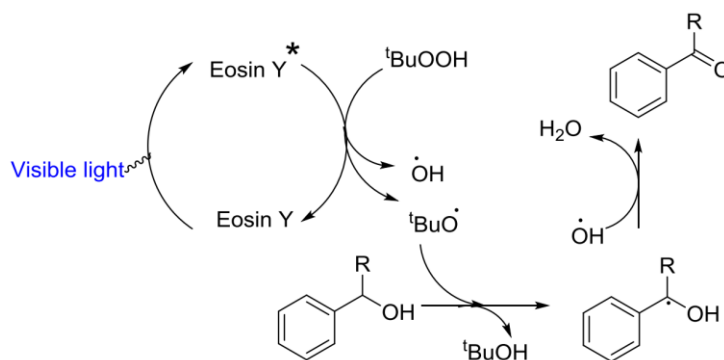


**Figure 1-34.** Plausible mechanism by Eosin Y/TBHP.<sup>157</sup>

Another low-cost, easily available and highly chemoselective visible-light mediated strategy comprising of Eosin Y and TBHP has been developed (Figure 1-34)<sup>157</sup>. The method not only obviates the use of toxic metal catalysts, but also high energy light sources. The reaction is easily extendable to primary as well as secondary benzyl alcohols having diverse set of electron withdrawing as well as donating functions at room temperature maintaining high selectivity.

Besides, the possibility of quinones as being this active promoter has been discussed, which could be assembled as heterogeneous catalyst with activated carbon was used as a support, consists of PV<sub>2</sub>Mo<sub>10</sub>O<sub>40</sub><sup>5-</sup> and quinone together are active for the alcohols oxidation<sup>158</sup>. The presence of a sufficient concentration of p-chloranil is required so as to allow the formation of the proposed polyoxometalate-semiquinone complex that, in a two electron oxidation, dehydrogenates the benzylic alcohol to yield the benzaldehyde.

Briefly, catalytic quantities of DDQ in combination with FeCl<sub>3</sub>, Mn(OAc)<sub>3</sub>, or MnO<sub>2</sub> as the terminal oxidant remain rather high (10~20 mol%), and a large excess of the terminal oxidant is typically employed. Issues include its relatively high toxicity and high cost, environmental hazards associated with water-mediated liberation of HCN. In addition, the stoichiometric use of DDQ produces equimolar quantities of the corresponding hydroquinone by-product, which makes purification difficulties on the



presenting excellent electrocatalytic performance including high electrocatalytic activity and high poison tolerance toward methanol electro-oxidation. In particular, the platinum-decorated graphene aerogel microspheres exhibit an extremely high mass activity of 1098.9 mA mg<sup>-1</sup> toward methanol oxidation as well as excellent antipoisoning ability, which are dramatically enhanced compared with Pt particles dispersed on graphene oxide and commercial carbon black supports<sup>164</sup>.

The oxidation of glycerol is more complex than that of ethanol, in accord with the presence of two and three hydroxyl groups, respectively. Figure 1-36 illustrates the general reaction schemes proposed for the oxidation of EG and glycerol on metal electrocatalysts. Like ethanol, polyalcohols are prevalently converted to alkali metal (poly)carboxylates on Pd-based electrocatalysts in alkaline media<sup>165</sup>. found that the activity of Pt<sub>p</sub> increases by about 5-fold when the optimal quantity of Bi ions is added to the solution. Besides, the adatom strongly impacts the reaction products by suppressing the pathways with C–C bond breaking, hindering the formation of CO (and other unknown intermediates) and enhancing the production of glycerate. Different from the results in acid media for Pt<sub>p</sub>-Bi systems where Bi blocks the oxidation pathway through the primary carbon, glycerate is the main product in alkaline media, and dihydroxyacetone is either produced in extremely low quantities or not produced<sup>166</sup>.

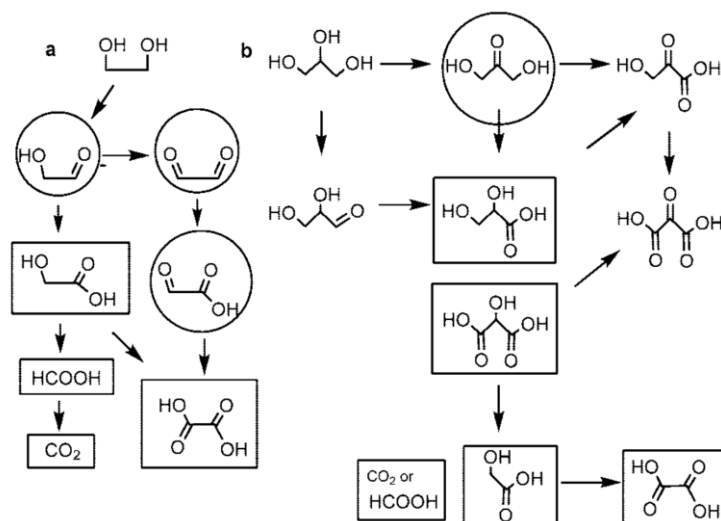


**Figure 1-36.** General schemes for EG and glycerol oxidation on metal catalysts and electrocatalysts in either acidic or basic media.

## 1.5 Oxidants in alcohols oxidation

Many oxidizing reagents containing permanganate and dichromate have been

previously used to implement oxidation reactions. However, these are all hazardous processes and produce a wide variety of toxic products. Thus, the catalytic selective oxidation with H<sub>2</sub>O<sub>2</sub> or O<sub>2</sub> as the oxidant becomes a promising direction.

### 1.5.1 H<sub>2</sub>O<sub>2</sub> in homogeneous catalysis for alcohols oxidation

As-mentioned above, the most effective catalysts are the transition elements Ru and Pd that perform *via* oxometal or hydridometal mechanisms. In comparison, the most effective catalysts with H<sub>2</sub>O<sub>2</sub> as the oxidant are Mo(VI)<sup>167</sup>, W(VI)<sup>168</sup> with a d<sup>0</sup> configuration, that operate *via* a peroxometal mechanism. The reason could be that ruthenium species catalyze rapid decomposition of H<sub>2</sub>O<sub>2</sub> and become less feasible, while early transition metal in high oxidation states are less active materials for H<sub>2</sub>O<sub>2</sub> decomposition<sup>169</sup>.

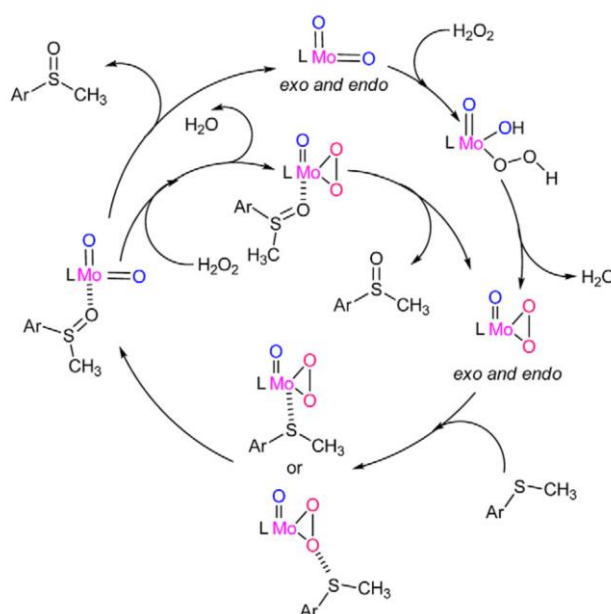


**Figure 1-37.** Proposed pathway for the formation of sulfoxide in the case of chiral molybdenum complex.<sup>170</sup>

The peroxo catalysts of Mo-<sup>170-171</sup> (Figure 1-37) and W-<sup>172-173</sup> were reported to be effective in the oxidation of alcohols with H<sub>2</sub>O<sub>2</sub>. Furthermore, molybdenum- and tungsten-containing heteropolyanions are also selective catalysts for alcohol oxidations with H<sub>2</sub>O<sub>2</sub><sup>174-175</sup>. Transition metal mono-substituted Keggin-type heteropolyacids, [XW<sub>11</sub>MO<sub>39</sub>]<sup>(n-m)-</sup> (X = P, Si, B), in which a transition metal cation, M<sup>m+</sup>, is coordinated to the binding sites of lacunary heteropolyanions [XW<sub>11</sub>O<sub>39</sub>]<sup>n-</sup>, could be as oxidative catalysts due to their thermal and chemical stability and redox

and acidic properties<sup>176</sup>. Methyltrioxorhenium catalyzed the oxidation of alcohols with H<sub>2</sub>O<sub>2</sub> via a peroxometal mechanism and primary benzylic and secondary aliphatic alcohols afforded the corresponding aldehydes and ketones, respectively, using two equivalents of H<sub>2</sub>O<sub>2</sub><sup>177</sup>. The addition of a catalytic quantity of bromide ions could greatly enhance the rate by a factor of 1000.

### 1.5.2 H<sub>2</sub>O<sub>2</sub> in heterogeneous catalysis for alcohols oxidation

In contrast with Mo- and W- homogeneous catalysis that is susceptible to leaching, one of the major discoveries in heterogeneous oxidations using H<sub>2</sub>O<sub>2</sub> as the oxidant in the last decade was the discovery of titanium-based catalysts<sup>178-179</sup>. The finding of commendable oxidation activity with 30% aqueous H<sub>2</sub>O<sub>2</sub> as the oxidant, stimulated the extensive studies of redox molecular sieves as heterogeneous catalysts for liquid phase oxidations. The elevated activity of titanium-silicate may be due to the hydrophobicity of the framework that stimulates the adsorption of the hydrophobic substrates and H<sub>2</sub>O<sub>2</sub><sup>180</sup>. The scope of alcoholic substrates is although restricted due to the limited size of the pores in titanium-silicate of 5.4 × 5.6 Å. The development of Ti-molecular sieves with larger pores as Ti-beta<sup>181</sup> and mesoporous materials as Ti-MCM-41<sup>182</sup> could solve these issues. Remarkably with allylic alcohols reaction in H<sub>2</sub>O<sub>2</sub>, in presence of Ti-silicate or Ti-beta, generally provides high selectivities for epoxidation<sup>183</sup>, rather than oxidation of the alcohol.

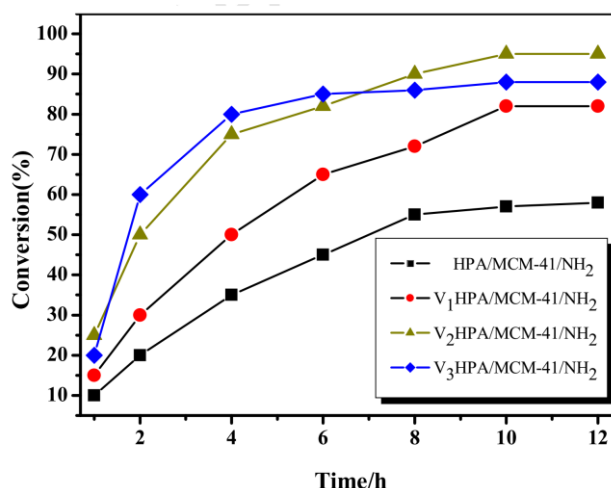


**Figure 1-38.** Time profiles of benzyl alcohol oxidation over four VHPW/MCM-41/NH<sub>2</sub> catalysts.<sup>184</sup>

Additionally, vanadium-substituted phosphotungstates (VHPW) immobilized on amine-functionalized mesoporous MCM-41 and their catalysis in selective oxidation

of various alcohols with H<sub>2</sub>O<sub>2</sub> were compared. Among the catalysts, the divanadium-substituted V<sub>2</sub>HPW/MCM-41/NH<sub>2</sub> is proved to be a highly efficient solid catalyst for aromatic alcohols oxidation to the aldehydes (Figure 1-38)<sup>184</sup>.

### 1.5.3 O<sub>2</sub> in homogeneous catalysis for alcohols oxidation

Ruthenium, due to the ability to hydrogen transfer, can be introduced to the aerobic oxidation of alcohols by employing O<sub>2</sub> and hydrogen acceptor in a multistep electron-transfer process. Trinuclear ruthenium carboxylates<sup>185</sup> are effective catalysts for the aerobic oxidation of short-chain aliphatic alcohols with activities approximately 10 times higher than those of RuCl<sub>3</sub> and RuCl<sub>2</sub>(PPh<sub>3</sub>)<sub>3</sub>. RuCl(OAc)(PPh<sub>3</sub>)<sub>3</sub>/hydroquinone/Co(salophen)(PPh<sub>3</sub>) system and a modified Ru/quinone/Co were reported, which catalyzed the aerobic oxidation of aromatic and secondary aliphatic alcohols<sup>186-187</sup>. The similar transformations can be accomplished using PdCl<sub>2</sub>/Na<sub>2</sub>CO<sub>3</sub> and Adogen 464 as phase transfer catalyst<sup>188</sup>. The oxidation of vicinal diols is faster and more selective than the oxidation of primary and secondary alcohols; vicinal 1,2-diols are oxidized selectively to hydroxy ketones, whereas primary alcohols are oxidized in preference to secondary alcohols (Figure 1-39)<sup>189</sup>. A primary disadvantage of these Pd-based systems is the relatively low activity and the reactions normally require > 12 h for completion with at least 5 mol% loading.

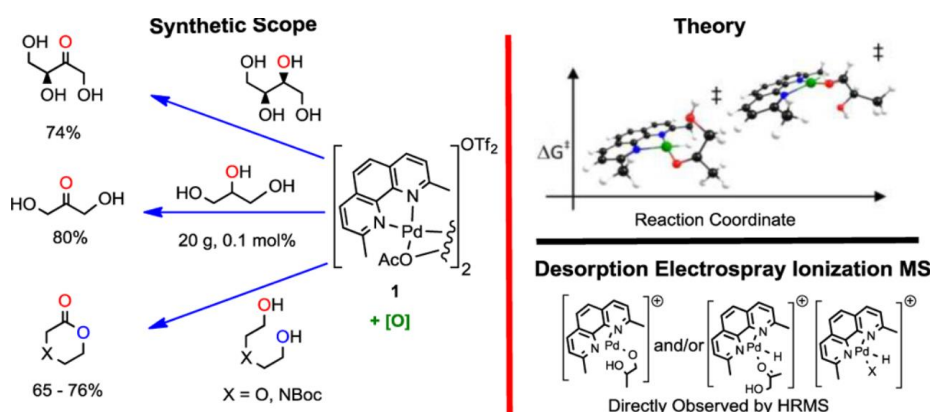


**Figure 1-39.** The regio- and chemoselective oxidation of unprotected vicinal polyols with [(neocuproine)Pd(OAc)<sub>2</sub>(OTf)<sub>2</sub>]<sup>189</sup>.

In addition to Ru and Pd, co(acac)<sub>3</sub>/N-hydroxyphthalimide as co-catalyst catalyzes the aerobic oxidation of primary and secondary alcohols<sup>190</sup>, which probably refers to a free radical mechanism. However, the material is more likely to leaching.

### 1.5.4 O<sub>2</sub> in heterogeneous catalysis for alcohols oxidation

Similar to the homogeneous systems, many heterogeneous catalysts are on account of ruthenium and oxoruthenium species capable of catalyzing aerobic oxidation of alcohols. For example, both RuO<sub>2</sub><sup>74</sup> and Ru/Al<sub>2</sub>O<sub>3</sub><sup>191</sup> (5 wt.% loading) catalyze the aerobic oxidation of activated alcohols such as allylic alcohols and  $\alpha$ -ketols. Besides, 1,2-cyclohexanediol undergoes aerobic oxidative cleavage forming dicarboxylic acids when heated together with a ruthenium pyrochlore oxide catalyst, [A<sub>2+x</sub>Ru<sub>2-x</sub>O<sub>7-y</sub>] (A= Pb, Bi; 0<x<1;0<y<0.5), under high oxygen pressure in water at alkaline pH<sup>192</sup>.

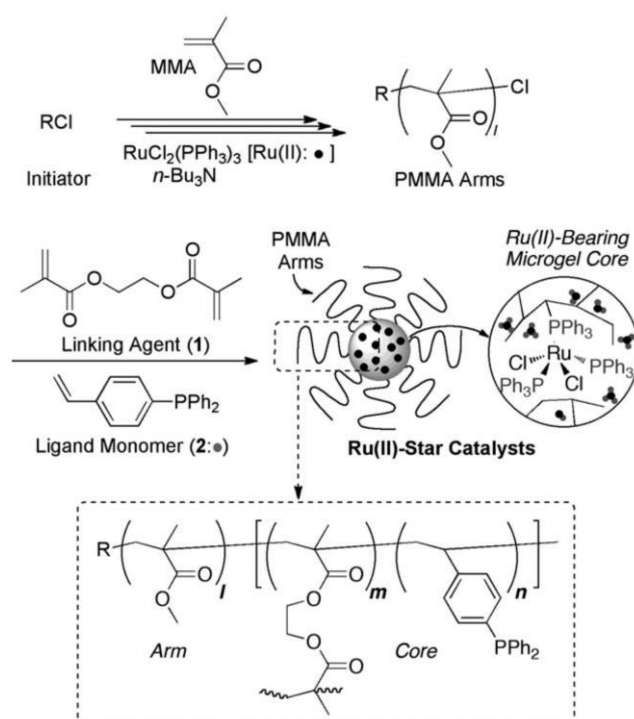


**Figure 1-40.** Synthesis of Ru(II)-bearing microgel star polymer catalysts via Ru(II)-catalyzed living radical polymerization.<sup>193</sup>

Ruthenium hydrotalcites form a second group of mixed oxide catalysts. A robust heterotrimetallic RuMnMn species coordinated to a hydrotalcite surface as a macroligand facilitates the highly efficient aerobic oxidation of alcohols<sup>194</sup>. Different metals embedded in the Brucite layer and the hydrotalcites having Ru in the Brucite layer-with the general formula M<sub>6</sub>Al<sub>2</sub>Ru<sub>0.5</sub>(OH)<sub>16</sub>CO<sub>3</sub> (M=Mg, Co, Mn, Fe, Zn)-have been reported<sup>195-196</sup>. Nonetheless, primary aliphatic alcohols are barely oxidized to aldehydes using the ruthenium-hydrotalcites.

An alternative approach is immobilizing homogeneous catalysts by grafting to a support. The polymer Amberlyst A-26 supported perruthenate (PSP)<sup>197</sup> could be a

good example, which is capable of oxidizing 2,3-epoxy-1-octanol. However, the activity is at least four times lower than that of the homogeneous analogue. Similarly, ruthenium-bearing microgel core star polymer catalysts were directly synthesized *via*  $\text{RuCl}_2(\text{PPh}_3)_3$ -catalyzed living radical polymerization of methyl methacrylate (MMA), followed by the arm-linking reaction with ethylene glycol dimethacrylate (Figure 1-40)<sup>193</sup>, which held catalytic activity after three times recovery under air-exposure.

In summary, molecular oxygen with low cost and nontoxic by-products make it a highly appealing oxidant that can address key “green chemistry” priorities in the industrial aerobic oxidation reactions.

## 1.6 The objectives and outline of thesis

Even if a lot of progress has been reported recently in oxidation of alcohols this is still a challenging task. The main problems in the existing processes of alcohols oxidation to corresponding aldehydes or ketones are:

- 1) The promising results have been obtained in the oxidation of activated aromatic and allylic alcohols, the selective transformation of long-chain aliphatic alcohols and diol-type molecules is still a challenging topic when heterogeneous catalysts are used;
- 2) The most efficient processes for oxidation of alcohols are based on homogeneous catalysts;
- 3) Low selectivity due to over-oxidation of aldehydes further to acids and esters;
- 4) Low activity in oxidation of polyols due to electro-deficiency of the molecule after oxidation of one hydroxyl group.

The target of this research was development of heterogeneous catalytic system able to selectively oxidize different alcohols including aliphatic to carbonyl compounds.

Thus, an attempt has been made to design a new efficient catalyst in this thesis to combine advantages of both metal-based (high activity) and non-metallic catalysts (high selectivity) by splitting the reaction into two half-reactions (Figure 1-39). The principle is to divide the labor between two remote active sites, one of them (at surfaces) being able to activate the organic (reactant to be transformed) while the other site (a metal) is kept protected in a core-shell structure where it can activate only the co-reactant ( $\text{O}_2$ ) due to higher permeation rate of these gases through the porous

membrane in comparison with organic molecules. The protons are formed at the non-metallic surface nano-anode together with formation of the aldehyde, and they are consumed at the internal metal nano-cathode after their transport through conductive shell due to potential difference between active sites.

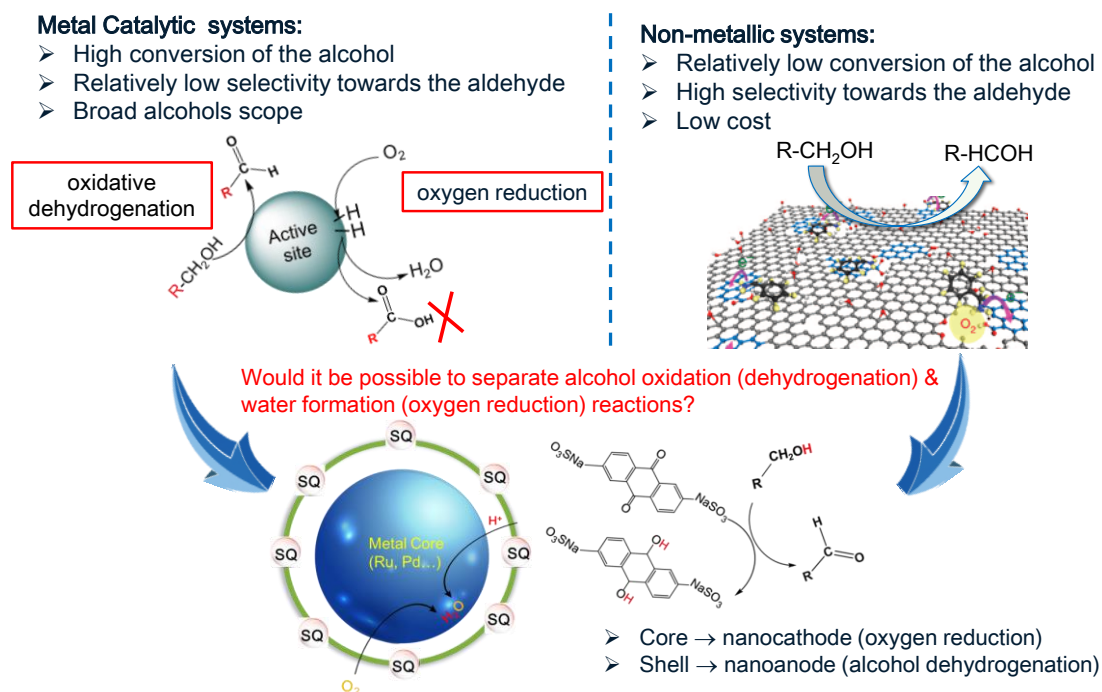


**Figure 1-39.** Scheme of “nanocells” catalyst with core-shell structure.

The main objectives of this work were:

- ✓ identification of the best components for the fabrication of the nano-electrocells;
- ✓ synthesis of the core-shell nano-electrocells based on the selected compounds;
- ✓ deep characterization of the nano-electrocells using model electrochemical cell;
- ✓ catalytic testing for the validation of performances in oxidation of alcohols.

The results of this PhD Thesis have been arranged in 4 Chapters. First of all, in Chapter 3 we investigated effect of the sizes of Ru nanoparticles as a “core” prepared by microemulsion for oxidation of alcohols. “Shell” catalytic performances of substituted anthraquinones were examined in catalytic oxidation of cyclic and activated alcohols to corresponding carbonyl compounds in the Chapter 4. Based on the research above, Ru nanoparticles and substituted anthraquinones were combined to establish the nanocells with core-shell structure in the Chapter 5. In the Chapter 6 we propose oxidation of polyols combined with acetalization using Ru@MOF tandem catalyst containing ultra-fine Ru nanoparticles (< 2 nm) in the MOF structure.

## 1.7 References

1. Abel, E. W., *Comprehensive Organometallic Chemistry II: A Review of the Literature. Cumulative Indexes* **1982**, 14.
2. Yakovleva, E. Y.; Belotserkovskaya, V. Y., Gas-chromatographic determination of the components of the catalytic oxidation of ethylene glycol to glyoxal. *J. Anal. Chem.* **2010**, 65 (8), 833-837.
3. Ryland, B. L.; Stahl, S. S., Practical Aerobic Oxidations of Alcohols and Amines with Homogeneous Copper/TEMPO and Related Catalyst Systems. *Angew. Chem. Int. Ed.* **2014**, 53 (34), 8824-8838.
4. LEE, D.; SPITZE, U. A., The Aqueous Dichromate Oxidation of Primary Alcohols. *J. Org. Chem.* **1970**, 35 (10), 3589-3590.
5. MUZART, J., Chromium-Catalyzed Oxidations in Organic Synthesis. *Chem. Rev.* **1992**, 92 (1), 113-140.
6. PERREE-FAUVET, M.; GAUDEMER, A., Manganese Porphyrin-catalysed Oxidation of Olefins to Ketones by Molecular Oxygen. *J. Am. Chem. Soc., Chem. Commun.* **1981**, 1 (17), 874-875.
7. Regen, S. L.; Koteel, C., Activation through impregnation. Permanganate-coated solid supports. *J. Am. Chem. Soc.* **1977**, 99 (11), 3837-3838.
8. Satoshi, I.; Koji, K.; Shigeru, I.; Teruaki, M., A New and Facile Method for the Direct Preparation of  $\alpha$ -Hydroxycarboxylic Acid Esters from  $\alpha,\beta$ -Unsaturated Carboxylic Acid Esters with Molecular Oxygen and Phenylsilane. *Chem. Lett.* **1990**, 19 (10), 1869-1872.
9. Semmelhack, M. F.; Schmid, C. R.; CortCs., D. A.; Chou, C. S., Oxidation of alcohols to aldehydes with oxygen an cupic ion, mediated by nitronium ion. *J. Am. Chem. Soc.* **1984**, 106, 3374-3376.
10. Arends, I. W. C. E.; Li, Y.-X.; Ausan, R.; Sheldon, R. A., Comparison of TEMPO and its derivatives as mediators in laccase catalysed oxidation of alcohols. *Tetrahedron* **2006**, 62 (28), 6659-6665.
11. Dijkman, A.; Marino-Gonza Iez, A.; Payeras, A. M. i.; Arends, I. W. C. E.; Sheldon, R. A., Efficient and Selective Aerobic Oxidation of Alcohols into Aldehydes. *J. Am. Chem. Soc.* **2001**, 123, 6826-6833.
12. Ma, S.; Liu, J.; Li, S.; Chen, B.; Cheng, J.; Kuang, J.; Liu, Y.; Wan, B.; Wang, Y.; Ye, J.; Yu, Q.; Yuan, W.; Yu, S., Development of a General and Practical Iron Nitrate/TEMPO-Catalyzed Aerobic Oxidation of Alcohols to Aldehydes/Ketones: Catalysis with Table Salt. *Adv. Synth. Catal.* **2011**, 353 (6), 1005-1017.
13. Hoover, J. M.; Stahl, S. S., Highly Practical Copper(I)/TEMPO Catalyst System for Chemoselective Aerobic Oxidation of Primary Alcohols. *J. Am. Chem. Soc.* **2011**, 133 (42), 16901-16910.
14. Dobereiner, G. E.; Crabtree, R. H., Dehydrogenation as a Substrate-Activating Strategy in Homogeneous Transition-Metal Catalysis. *Chem. Rev.* **2010**, 110, 681-703.
15. Zhu, Y.; Zhao, B.; Shi, Y., Highly Efficient Cu(I)-Catalyzed Oxidation of Alcohols to Ketones and Aldehydes with Diaziridinone. *Org. Lett.* **2013**, 15 992-995.
16. Punniyamurthy, T.; Velusamy, S.; Iqbal, J., Recent Advances in Transition Metal Catalyzed Oxidation of Organic Substrates with Molecular Oxygen. *Chem. Rev.* **2005**, 105, 2329-2363.
17. Hongbing, J.; Tomoo, M.; Kohki, E., Highly Efficient Oxidation of Alcohols to Carbonyl Compounds in the Presence of Molecular Oxygen Using a Novel Heterogeneous Ruthenium Catalyst. *Tetrahedron Lett.* **2002**, 43, 7179-7183.

18. Miyata, A.; Furukawa, M.; Irie, R.; Katsuki, T., Catalytic aerobic oxidation of diols under photo-irradiation: highly efficient synthesis of lactols. *Tetrahedron Lett.* **2002**, *43*, 3481–3484.
19. Schmidt, A.-K. C.; Stark, C. B. W., TPAP-Catalyzed Direct Oxidation of Primary Alcohols to Carboxylic Acids through Stabilized Aldehyde Hydrates. *Org. Lett.* **2011**, *13*, 4164–4167.
20. Hasan, M.; Musawir, M.; Davey, P. N.; Kozhevnikov, I. V., Oxidation of primary alcohols to aldehydes with oxygen catalysed by tetra-n-propylammonium perruthenate. *J. Mol. Catal. A: Chem.* **2002**, *180*, 77–84.
21. Bilgrien, C.; Davis, S.; Drago, R. S., The Selective Oxidation of Primary Alcohols to Aldehydes by O<sub>2</sub> Employing a Trinuclear Ruthenium Carboxylate Catalyst. *J. Am. Chem. Soc.* **1987**, *109*, 3786-3787.
22. Adair, G. R. A.; Williams, J. M. J., Oxidant-free oxidation: ruthenium catalysed dehydrogenation of alcohols. *Tetrahedron Lett.* **2005**, *46* (47), 8233-8235.
23. Nishimura, T.; Onoue, T.; Ohe, K.; Uemura, S., Palladium(II)-Catalyzed Oxidation of Alcohols to Aldehydes and Ketones by Molecular Oxygen. *J. Org. Chem.* **1999**, *64*, 6750-6755.
24. CHULTZ, M. J.; PARK, C. C.; SIGMAN, M. S., A Convenient Palladium-Catalyzed Aerobic Oxidation of Alcohols at Room Temperature. *Chem. Commun.* **2002**, *24*, 3034-3035.
25. Jensen, D. R.; Schultz, M. J.; Mueller, J. A.; Sigman, M. S., A Well-Defined Complex for Palladium-Catalyzed Aerobic Oxidation of Alcohols: Design, Synthesis, and Mechanistic Considerations. *Angew. Chem. Int. Ed.* **2003**, *115* (32), 3940-3943.
26. Brink, G.-J. t.; Arends, I. W. C. E.; Sheldon, R. A., Green, catalytic oxidation of alcohols in water. *Science* **2000**, *287*, 1636-1639.
27. Guan, B.; Dong Xing; Cai, G.; Wan, X.; Yu, N.; Fang, Z.; Liping Yang; Shi, Z., Highly Selective Aerobic Oxidation of Alcohol Catalyzed by a Gold(I) Complex with an Anionic Ligand. *J. Am. Chem. Soc.* **2005**, *127*, 18004-18005.
28. Iwahama, T.; Yoshino, Y.; Keitoku, T.; Sakaguchi, S.; Ishii, Y., Efficient Oxidation of Alcohols to Carbonyl Compounds with Molecular Oxygen Catalyzed by N-Hydroxyphthalimide Combined with a Co Species. *J. Org. Chem.* **2000**, *65*, 6502-6507.
29. n, S. E. M.; Sua rez, D. o. F., Catalytic aerobic oxidation of alcohols by Fe(NO<sub>3</sub>)<sub>3</sub>-FeBr<sub>3</sub>. *Tetrahedron Lett.* **2002**, *43*, 4475–4479.
30. MARKO, I. E.; GAUTIER, A.; DUMEUNIER, R.; DODA, K.; PHILLIPART, F.; BROWN, S. M.; URCH, C. J., Efficient, Copper-Catalyzed, Aerobic Oxidation of Primary Alcohols. *Angew. Chem. Int. Ed.* **2004**, *43*, 1588-1591.
31. VELUSAMY, S.; T., P., Novel Vanadium-Catalyzed Oxidation of Alcohols to Aldehydes and Ketones under Atmospheric Oxygen. *Org. Lett.* **2004**, *6*, 217-219.
32. Hanson, S. K.; Wu, R.; Silks, L. A. P., Mild and Selective Vanadium-Catalyzed Oxidation of Benzylic, Allylic, and Propargylic Alcohols Using Air. *Org. Lett.* **2011**, *8*, 1908–1911.
33. Wu, H.; Zhang, Q.; Wang, Y., Solvent-Free Aerobic Oxidation of Alcohols Catalyzed by an Efficient and Recyclable Palladium Heterogeneous Catalyst. *Adv. Synth. Catal.* **2005**, *347* (10), 1356-1360.
34. Alardin, F.; Delmon, B.; Ruiz, P.; Devillers, M., Stability of bimetallic Bi–Pd and Pb–Pd carbon-supported catalysts during their use in glyoxal oxidation. *Catal. Today* **2000**, *61*, 255-262.
35. Besson, M.; Gallezot, P., Selective oxidation of alcohols and aldehydes on metal catalysts. *Catal. Today* **2000**, *57*, 127-141.

36. Kluytmans, J. H. J.; Markusse, A. P.; Kuster, B. F. M.; Marin, G. B.; Schouten, J. C., Engineering aspects of the aqueous noble metal catalysed alcohol oxidation. *Catal. Today* **2000**, *57*, 143-155.
37. Kimura, H.; Kimura, A.; Kokubo, I.; Wakisaka, T.; Mitsuda, Y., Palladium based multi-component catalytic systems for the alcohol to carboxylate oxidation reaction. *Appl. Catal. A: Gen.* **1993**, *95*, 143-169.
38. Hronec, M.; Cvengro, Z.; Kizlink, J., Competitive oxidation of alcohols in aqueous phase using Pd/C catalyst. *J. Mol. Catal.* **1993**, *83*, 75-82.
39. OI, R.; TAKENAKA, S., Selective Conversion of m-Hydroxybenzyl Alcohol to m-Hydroxybenzaldehyde. *Chem. Lett.* **1988**, *1*, 1115-1116.
40. Deffernez, A.; Hermans, S.; Devillers, M., Bimetallic Bi-Pt, Ru-Pt and Ru-Pd and trimetallic catalysts for the selective oxidation of glyoxal into glyoxalic acid in aqueous phase. *Appl. Catal. A: Gen.* **2005**, *282* (1-2), 303-313.
41. Pinxt, H. H. C. M.; Kuster, B. F. M.; Marin, G. B., Promoter effects in the Pt-catalysed oxidation of propylene glycol. *Appl. Catal. A: Gen.* **2000**, *191*, 45-54.
42. Mallat T.; Bodnar Z.; Baiker A.; Greis O. Strubig H.; Reller A., Preparation of promoted platinum catalysts of designed geometry and the role of promoters in the liquid-phase oxidation of 1-methoxy-2-propanol. *J. Catal.* **1993**, *142*, 237-253.
43. Pillai, U. R.; Sahle-Demessie, E., Selective oxidation of alcohols by molecular oxygen over a Pd/MgO catalyst in the absence of any additives. *Green Chem.* **2004**, *6* (3), 161.
44. Hackett, S. F. J.; Brydson, R. M.; Gass, M. H.; Harvey, I.; Newman, A. D.; Wilson, K.; Lee, A. F., High-Activity, Single-Site Mesoporous Pd/Al<sub>2</sub>O<sub>3</sub> Catalysts for Selective Aerobic Oxidation of Allylic Alcohols. *Angew. Chem. Int. Ed.* **2007**, *46* (45), 8593-8596.
45. Chen, J.; Zhang, Q.; Wang, Y.; Wan, H., Size-Dependent Catalytic Activity of Supported Palladium Nanoparticles for Aerobic Oxidation of Alcohols. *Adv. Synth. Catal.* **2008**, *350* (3), 453-464.
46. Liu, J.; Yang, H. Q.; Kleitz, F.; Chen, Z. G.; Yang, T.; Strounina, E.; Lu, G. Q. M.; Qiao, S. Z., Yolk-Shell Hybrid Materials with a Periodic Mesoporous Organosilica Shell: Ideal Nanoreactors for Selective Alcohol Oxidation. *Adv. Funct. Mater.* **2012**, *22* (3), 591-599.
47. Mori, K.; Hara, T.; Mizugaki, T.; Ebitani, K.; Kaneda, K., Hydroxyapatite-Supported Palladium Nanoclusters: A Highly Active Heterogeneous Catalyst for Selective Oxidation of Alcohols by Use of Molecular Oxygen. *J. Am. Chem. Soc.* **2004**, *126*, 10657-10666.
48. Chen, G.; Wu, S.; Liu, H.; Jiang, H.; Li, Y., Palladium supported on an acidic metal-organic framework as an efficient catalyst in selective aerobic oxidation of alcohols. *Green Chem.* **2013**, *15* (1), 230-235.
49. Enache, D. I.; Edwards, J. K.; Hutchings, G. J., Solvent-free oxidation of primary alcohols to aldehydes using Au-Pd/TiO<sub>2</sub> catalysts. *Science* **2006**, *311*, 362-365.
50. Yamaguchi, K.; Mizuno, N., Supported ruthenium catalyst for the heterogeneous oxidation of alcohols with molecular oxygen. *Angew. Chem. Int. Ed.* **2002**, *23*, 4538-4541.
51. Ebitani, K.; Ji, H.-B.; Mizugaki, T.; Kaneda, K., Highly Active Trimetallic Ru/CeO<sub>2</sub>/CoO(OH) Catalyst for Oxidation of Alcohols in the Presence of Molecular Oxygen. *J. Mol. Catal. A: Chem.* **2004**, *212* (1-2), 161-170.
52. Hosokawa, S.; Hayashi, Y.; Imamura, S.; Wada, K.; Inoue, M., Effect of the Preparation Conditions of Ru/CeO<sub>2</sub> Catalysts for the Liquid Phase Oxidation of Benzyl Alcohol. *Catal. Lett.* **2009**, *129* (3-4), 394-399.

53. Sato, T.; Komanoya, T., Selective Oxidation of Alcohols with Molecular Oxygen Catalyzed by Ru/MnOx/CeO<sub>2</sub> under Mild Conditions. *Catal. Commun.* **2009**, *10* (7), 1095-1098.
54. Yasu-eda, T.; Kitamura, S.; Ikenaga, N.; Miyake, T.; Suzuki, T., Selective Oxidation of Alcohols with Molecular Oxygen over Ru/CaO–ZrO<sub>2</sub> Catalyst. *J. Mol. Catal. A: Chem.* **2010**, *323* (1-2), 7-15.
55. Kim, Y. H.; Hwang, S. K.; Kim, J. W.; Lee, Y. S., Zirconia-Supported Ruthenium Catalyst for Efficient Aerobic Oxidation of Alcohols to Aldehydes. *Ind. Eng. Chem. Res.* **2014**, *53* (31), 12548-12552.
56. Dulie`re, E.; Devillers, M.; Marchand-Brynaert, J., Novel Phosphinite–Ruthenium(II) Complexes Covalently Bound on Silica Synthesis, Characterization, and Catalytic Behavior versus Oxidation Reactions of Alcohols into Aldehydes. *Organometallics* **2003**, *22*, 804-811.
57. Clerick, S.; De Canck, E.; Hendrickx, K.; Van Speybroeck, V.; Van Der Voort, P., Heterogeneous Ru(III) Oxidation Catalysts via ‘click’ Bidentate Ligands on a Periodic Mesoporous Organosilica Support. *Green Chem.* **2016**, *18* (22), 6035-6045.
58. Mori, K.; Satoko, K.; Takayoshi, H.; Tomoo, M.; Kohki, E.; Koichiro, J.; Kiyotomi, K., Development of Ruthenium-Hydroxyapatite-Encapsulated Superparamagnetic  $\gamma$ -Fe<sub>2</sub>O<sub>3</sub> Nanocrystallites as an Efficient Oxidation Catalyst by Molecular Oxygen. *Chem. Lett.* **2007**, *19*, 1249-1256.
59. Opre, Z.; Grunwaldt, J.; Maciejewski, M.; Ferri, D.; Mallat, T.; Baiker, A., Promoted Ru-hydroxyapatite: Designed Structure for Fast and Highly Selective Oxidation of Alcohols with Oxygen. *J. Catal.* **2005**, *230* (2), 406-419.
60. Carson, F.; Agrawal, S.; Gustafsson, M.; Bartoszewicz, A.; Moraga, F.; Zou, X.; Mart ń-Matute, B., Ruthenium Complexation in an Aluminium Metal-Organic Framework and Its Application in Alcohol Oxidation Catalysis. *Chem. Eur. J.* **2012**, *18* (48), 15337-15344.
61. Kobayashi, S.; Miyamura, H.; Akiyama, R.; Ishida, T., Highly Active, Immobilized Ruthenium Catalysts for Oxidation of Alcohols to Aldehydes and Ketones. Preparation and Use in Both Batch and Flow Systems. *J. Am. Chem. Soc.* **2005**, *127*, 9251-9254
62. Musawir, M.; Davey, P. N.; Kelly, G.; Kozhevnikov, I. V., Highly Efficient Liquid-phase Oxidation of Primary Alcohols to Aldehydes with Oxygen Catalysed by Ru–Co Oxide. *Chem. Commun.* **2003**, *12*, 1414-1415.
63. Jamatia, R.; Gupta, A.; Mahato, M.; Patil, R. A.; Ma, Y.-R.; Pal, A. K., A Metalloprotein Inspired Ruthenium Complex as an Efficient and Reusable Catalyst for Selective Oxidation of Alcohols to their Corresponding Carbonyl Compounds. *ChemistrySelect* **2016**, *1* (18), 5929-5935.
64. Liu, Y.; Zhao, G.; Wang, D.; Li, Y., Heterogeneous catalysis for green chemistry based on nanocrystals. *Nati. Sci. Rev.* **2015**, *2* (2), 150-166.
65. Prati, L.; Rossi, M., Gold on Carbon as a New Catalyst for Selective Liquid Phase Oxidation of Diols. *J. Catal.* **1998**, *176*, 552–560.
66. Zhang, X.; Shi, H.; Xu, B.-Q., Catalysis by Gold: Isolated Surface Au<sup>3+</sup> Ions are Active Sites for Selective Hydrogenation of 1,3-Butadiene over Au/ZrO<sub>2</sub> Catalysts. *Angew. Chem. Int. Ed.* **2005**, *44* (43), 7132-7135.
67. Kumar, R.; Gravel, E.; Hag ège, A.; Li, H.; Jawale, D. V.; Verma, D.; Namboothiri, I. N. N.; Doris, E., Carbon nanotube–gold nanohybrids for selective catalytic oxidation of alcohols. *Nanoscale* **2013**, *5* (14), 6491.
68. Enache, D. I.; Knight, D. W.; Hutchings, G. J., Solvent-free Oxidation of Primary Alcohols to Aldehydes using Supported Gold Catalysts. *Catal. Lett.* **2005**, *103* (1-2),

43-52.

69. Abad, A.; Concepción, P.; Corma, A.; García, H., A Collaborative Effect between Gold and a Support Induces the Selective Oxidation of Alcohols. *Angew. Chem. Int. Ed.* **2005**, *117* (26), 4134-4137.
70. Tanaka, A.; Hashimoto, K.; Kominami, H., Preparation of Au/CeO<sub>2</sub> Exhibiting Strong Surface Plasmon Resonance Effective for Selective or Chemoselective Oxidation of Alcohols to Aldehydes or Ketones in Aqueous Suspensions under Irradiation by Green Light. *J. Am. Chem. Soc.* **2012**, *134* (35), 14526-14533.
71. Huang, J.; Dai, W.; Li, H.; Fan, K., Au/TiO<sub>2</sub> as high efficient catalyst for the selective oxidative cyclization of 1,4-butanediol to  $\gamma$ -butyrolactone. *J. Catal.* **2007**, *252* (1), 69-76.
72. Huang, J.; Dai, W.-L.; Fan, K., Remarkable support crystal phase effect in Au/FeO<sub>x</sub> catalyzed oxidation of 1,4-butanediol to  $\gamma$ -butyrolactone. *J. Catal.* **2009**, *266* (2), 228-235.
73. Li, H.; Qin, F.; Yang, Z.; Cui, X.; Wang, J.; Zhang, L., New Reaction Pathway Induced by Plasmon for Selective Benzyl Alcohol Oxidation on BiOCl Possessing Oxygen Vacancies. *J. Am. Chem. Soc.* **2017**, *139* (9), 3513-3521.
74. ZHAN, B.-Z.; WHITE, M. A.; SHAM, T.-K.; PINCOCK, J. A.; DOUCET, R. J.; RAO, K. V. R.; ROBERTSON, K. N.; CAMERON, T. S., Zeolite-Confined Nano-RuO<sub>2</sub>: A Green, Selective, and Efficient Catalyst for Aerobic Alcohol Oxidation. *J. Am. Chem. Soc.* **2003**, *125*, 2195-2199.
75. Velu, S.; Wang, L.; Okazaki, M.; Suzuki, K.; Tomura, S., Characterization of MCM-41 mesoporous molecular sieves containing copper and zinc and their catalytic performance in the selective oxidation of alcohols to aldehydes. *Micropor. Mesopor. Mat.* **2002**, *54*, 113-126.
76. ON, Y.-C.; MAKWANA, V. D.; HOWELL, A. R.; SUIB, S. L., Efficient, Catalytic, Aerobic Oxidation of Alcohols with Octahedral Molecular Sieves. *Angew. Chem. Int. Ed.* **2001**, *40*, 4280-4283.
77. Mobley, J. K.; Crocker, M., Catalytic oxidation of alcohols to carbonyl compounds over hydrotalcite and hydrotalcite-supported catalysts. *RSC Adv.* **2015**, *5* (81), 65780-65797.
78. Nishimura, S.; Takagaki, A.; Ebitani, K., Characterization, synthesis and catalysis of hydrotalcite-related materials for highly efficient materials transformations. *Green Chem.* **2013**, *15* (8), 2026.
79. Matsushita, T.; Ebitani, K.; Kaneda, K., Highly efficient oxidation of alcohols and aromatic compounds catalysed by the Ru-Co-Al hydrotalcite in the presence of molecular oxygen. *Chem. Commun.* **1999**, *8*, 265-266.
80. Du, Y.; Wang, Q.; Liang, X.; He, Y.; Feng, J.; Li, D., Hydrotalcite-like MgMnTi non-precious-metal catalyst for solvent-free selective oxidation of alcohols. *J. Catal.* **2015**, *331*, 154-161.
81. Zhou, W.-Y.; Tian, P.; Sun, F. a.; He, M.-Y.; Chen, Q., Highly efficient transformation of alcohol to carbonyl compounds under a hybrid bifunctional catalyst originated from metalloporphyrins and hydrotalcite. *J. Catal.* **2016**, *335*, 105-116.
82. Zhou, W. Y.; Pan, J. G.; Wu, Z.; Qian, J. F.; He, M. Y.; Chen, Q., Efficient catalytic oxidation of alcohol to carbonyl compounds over CoFe hydrotalcites. *RSC Adv.* **2016**, *6* (87), 84106-84112.
83. Baskaran, T.; Kumaravel, R.; Christopher, J.; Sakthivel, A., Silicate anion intercalated cobalt-aluminium hydrotalcite (CoAl-HT-Si): a potential catalyst for alcohol oxidation. *RSC Adv.* **2014**, *4* (22), 11188.
84. Ren, Y.; Yue, B.; Gu, M.; He, H., Progress of the Application of Mesoporous

Silica-Supported Heteropolyacids in Heterogeneous Catalysis and Preparation of Nanostructured Metal Oxides. *Materials* **2010**, *3* (2), 764-785.

85. Y. Izumi, K. U.; Onaka, M., Book Review: Zeolite, Clay and Heteropoly Acid in Organic Reactions. *Angew. Chem. Int. Ed.* **1994**, *33*, 1893-1893.

86. Barcza, L.; Pope, M., Heteroconjugation of Inorganic Anions in Nonaqueous Solvents. III. Complexes of Polymolybdates and -tungstates with Chloral Hydrate. *J. Phys. Chem* **1975**, *79*, 92-93.

87. Farhadi, S.; Afshari, M.; Maleki, M.; Babazadeh, Z., Photocatalytic oxidation of primary and secondary benzylic alcohols to carbonyl compounds catalyzed by H<sub>3</sub>PW<sub>12</sub>O<sub>40</sub>/SiO<sub>2</sub> under an O<sub>2</sub> atmosphere. *Tetrahedron Lett.* **2005**, *46* (49), 8483-8486.

88. Neumann, R.; Khenkin, A. M.; Juwiler, D.; Hagit Miller; Gara, M., Catalytic oxidation with hydrogen peroxide catalyzed by 'sandwich' type transition metal substituted polyoxometalates. *J. Mol. Catal. A: Chem.* **1997**, *17*, 169-183.

89. Kazuhiko Sato; Masao Aoki; Junko Takagi; Noyori, R., Organic Solvent- and Halide-Free Oxidation of Alcohols with Aqueous Hydrogen Peroxide. *J. Am. Chem. Soc.* **1997**, *119*, 12386-12387.

90. Rao, P. S. N.; Venkateswara Rao, K. T.; Sai Prasad, P. S.; Lingaiah, N., The role of vanadium in ammonium salt of heteropoly molybdate supported on niobia for selective oxidation of benzyl alcohol. *Catal. Commun.* **2010**, *11* (6), 547-550.

91. Mallick, S.; Rana, S.; Parida, K., Facile Method for the Synthesis of Phosphomolybdic Acid Supported on Zirconia-Ceria Mixed Oxide and Its Catalytic Evaluation in the Solvent-Free Oxidation of Benzyl Alcohol. *Ind. Eng. Chem. Res.* **2012**, *51* (23), 7859-7866.

92. Nisar, A.; Zhuang, J.; Wang, X., Construction of Amphiphilic Polyoxometalate Mesostructures as a Highly Efficient Desulfurization Catalyst. *Adv. Mater.* **2011**, *23* (9), 1130-1135.

93. Ni, L.; Patscheider, J.; Baldrige, K. K.; Patzke, G. R., New Perspectives on Polyoxometalate Catalysts: Alcohol Oxidation with Zn/Sb-Polyoxotungstates. *Chem. Eur. J.* **2012**, *18* (42), 13293-13298.

94. Wang, Z.-g.; Yang, Y.; Cao, X.-h.; Lu, M., Highly selective oxidation of alcohols with hydrogen peroxide and polyethylene oxide-supported long-chain imidazolium polyoxometalate hybrid catalyst. *J. Iran. Chem. Soc.* **2015**, *12* (10), 1765-1770.

95. Shen, J.; Shan, W.; Zhang, Y.; Du, J.; Xu, H.; Fan, K.; Shen, W.; Tang, Y., A novel catalyst with high activity for polyhydric alcohol oxidation: nanosilver/zeolite film. *Chem. Commun.* **2004**, (24), 2880.

96. Davis, S. E.; Ide, M. S.; Davis, R. J., Selective Oxidation of Alcohols and Aldehydes over Supported Metal Nanoparticles. *Green Chem.* **2013**, *15* (1), 17-45.

97. A. S. Knyazev; O. V. Vodyankina; L. N. Kurina; Koshcheev, S. V.; Boronin, A. I., Cleaning of the Surface of Silver Crystals Used as Catalysts of Gas-Phase Oxidation of Ethylene Glycol to Glyoxal. *Russ. J. Appl. Chem.* **2004**, *77*, 41-45.

98. P., G.; S., T.; Y., C.; G., M.; A., S., Oxidative Dehydrogenation of Ethylene Glycol into Glyoxal Effect of Diethylphosphite on SiC-Supported Silver Catalysts. *J. Catal.* **1993**, *142*, 729-734.

99. Biella, S.; Rossi, M., Gas phase oxidation of alcohols to aldehydes or ketones catalysed by supported gold. *Chem. Commun.* **2003**, (3), 378-379.

100. Zhao, G.; Deng, M.; Jiang, Y.; Hu, H.; Huang, J.; Lu, Y., Microstructured Au/Ni-fiber catalyst: Galvanic reaction preparation and catalytic performance for low-temperature gas-phase alcohol oxidation. *J. Catal.* **2013**, *301*, 46-53.

101. Jeon, G. S.; Chung, J. S., Effect of iron on Cu-SiO<sub>2</sub> catalysts for the

- dehydrogenation of cyclohexanol to cyclohexanone. *Korean J. Chem. Eng.* **1997**, *14*, 49-5.
102. Jie Fan; Yihu Dai; Yunlong Li; Nanfeng Zheng; Guo, J.; Yan, X.; Stucky, G. D., Low-temperature, highly selective, gas-phase oxidation of benzyl alcohol over mesoporous K-Cu-TiO<sub>2</sub> with stable copper (I) oxidation state. *J. Am. Chem. Soc.* **2009**, *131*, 15568–15569.
103. Zhao, G.; Hu, H.; Deng, M.; Ling, M.; Lu, Y., Au/Cu-fiber catalyst with enhanced low-temperature activity and heat transfer for the gas-phase oxidation of alcohols. *Green Chem.* **2011**, *13* (1), 55-58.
104. V.R. Chumbhale; Awasarkar, P. A., Oxidative dehydrogenation of ethylene glycol into glyoxal over phosphorus-doped ferric molybdate catalyst. *Appl. Catal. A-Gen.* **2001**, *205*, 109–115.
105. Tom Waters; O’Hair, R. A. J.; Wedd, A. G., Catalytic Gas Phase Oxidation of Methanol to Formaldehyde. *J. Am. Chem. Soc.* **2003**, *125*, 3384-3396.
106. Aia, M.; Ohdan, K., Effects of the method of preparing iron orthophosphate catalyst on the structure and the catalytic activity. *Appl. Catal. A-Gen.* **1999**, *180*, 47–52.
107. Kim, H.; Kim, P.; Lee, K.-Y.; Yeom, S. H.; Yi, J.; Song, I. K., Preparation and characterization of heteropolyacid/mesoporous carbon catalyst for the vapor-phase 2-propanol conversion reaction. *Catal. Today* **2006**, *111* (3-4), 361-365.
108. Su, C.; Loh, K. P., Carbocatalysts: graphene oxide and its derivatives. *Accounts Chem. Res.* **2012**, *46* (10), 2275-2285.
109. Dreyer, D. R.; Jia, H. P.; Bielawski, C. W., Graphene oxide: a convenient carbocatalyst for facilitating oxidation and hydration reactions. *Angew. Chem. Int. Ed.* **2010**, *49* (38), 6813-6816.
110. Long, J.; Xie, X.; Xu, J.; Gu, Q.; Chen, L.; Wang, X., Nitrogen-doped graphene nanosheets as metal-free catalysts for aerobic selective oxidation of benzylic alcohols. *ACS Catal.* **2012**, *2* (4), 622-631.
111. Lin, Y.; Su, D., Fabrication of nitrogen-modified annealed nanodiamond with improved catalytic activity. *ACS Nano* **2014**, *8* (8), 7823-7833.
112. Gupta, N.; Khavryuchenko, O.; Villa, A.; Su, D., Metal-Free Oxidation of Glycerol over Nitrogen-Containing Carbon Nanotubes. *ChemSusChem* **2017**, *10* (15), 3030-3034.
113. Watanabe, H.; Asano, S.; Fujita, S.-i.; Yoshida, H.; Arai, M., Nitrogen-doped, metal-free activated carbon catalysts for aerobic oxidation of alcohols. *ACS Catal.* **2015**, *5* (5), 2886-2894.
114. Patel, M. A.; Luo, F.; Khoshi, M. R.; Rabie, E.; Zhang, Q.; Flach, C. R.; Mendelsohn, R.; Garfunkel, E.; Szostak, M.; He, H., P-doped porous carbon as metal free catalysts for selective aerobic oxidation with an unexpected mechanism. *ACS Nano* **2016**, *10* (2), 2305-2315.
115. Yang, S.; Peng, L.; Huang, P.; Wang, X.; Sun, Y.; Cao, C.; Song, W., Nitrogen, Phosphorus, and Sulfur Co-Doped Hollow Carbon Shell as Superior Metal-Free Catalyst for Selective Oxidation of Aromatic Alkanes. *Angew. Chem. Int. Ed.* **2016**, *55* (12), 4016-4020.
116. Su, F.; Mathew, S. C.; Lipner, G.; Fu, X.; Antonietti, M.; Blechert, S.; Wang, X., mpg-C<sub>3</sub>N<sub>4</sub>-catalyzed selective oxidation of alcohols using O<sub>2</sub> and visible light. *J. Am. Chem. Soc.* **2010**, *132* (46), 16299-16301.
117. Meng, Y.; Voiry, D.; Goswami, A.; Zou, X.; Huang, X.; Chhowalla, M.; Liu, Z.; Asefa, T., N<sup>-</sup>, O<sup>-</sup>, and S<sup>-</sup> tridoped nanoporous carbons as selective catalysts for oxygen reduction and alcohol oxidation reactions. *J. Am. Chem. Soc.* **2014**, *136* (39),

13554-13557.

118. Slot, T. K.; Eisenberg, D.; van Noordenne, D.; Jungbacker, P.; Rothenberg, G., Cooperative catalysis for selective alcohol oxidation with molecular oxygen. *Chem. Eur. J.* **2016**, *22* (35), 12307-12311.

119. Slot, T. K.; Eisenberg, D.; Rothenberg, G., Cooperative Surface-Particle Catalysis: The Role of the "Active Doughnut" in Catalytic Oxidation. *ChemCatChem* **2018**, *10* (10), 2119-2124.

120. Wertz, S.; Studer, A., Nitroxide-catalyzed transition-metal-free aerobic oxidation processes. *Green Chem.* **2013**, *15* (11), 3116-3134.

121. Lucio Anelli, P.; Biffi, C.; Montanari, F.; Quici, S., Fast and selective oxidation of primary alcohols to aldehydes or to carboxylic acids and of secondary alcohols to ketones mediated by oxoammonium salts under two-phase conditions. *J. Org. Chem.* **1987**, *52* (12), 2559-2562.

122. De Mico, A.; Margarita, R.; Parlanti, L.; Vescovi, A.; Piancatelli, G., A versatile and highly selective hypervalent iodine (III)/2, 2, 6, 6-tetramethyl-1-piperidinyloxy-mediated oxidation of alcohols to carbonyl compounds. *J. Org. Chem.* **1997**, *62* (20), 6974-6977.

123. Tebben, L.; Studer, A., Nitroxides: applications in synthesis and in polymer chemistry. *Angew. Chem. Int. Ed.* **2011**, *50* (22), 5034-5068.

124. Liu, R.; Liang, X.; Dong, C.; Hu, X., Transition-metal-free: A highly efficient catalytic aerobic alcohol oxidation process. *J. Am. Chem. Soc.* **2004**, *126* (13), 4112-4113.

125. Wang, X.; Liu, R.; Jin, Y.; Liang, X., TEMPO/HCl/NaNO<sub>2</sub> Catalyst: A Transition-Metal-Free Approach to Efficient Aerobic Oxidation of Alcohols to Aldehydes and Ketones Under Mild Conditions. *Chem. Eur. J.* **2008**, *14* (9), 2679-2685.

126. Rahimi, A.; Azarpira, A.; Kim, H.; Ralph, J.; Stahl, S. S., Chemoselective metal-free aerobic alcohol oxidation in lignin. *J. Am. Chem. Soc.* **2013**, *135* (17), 6415-6418.

127. Cleve, A.; Fritzeimer, K.-H.; Heinrich, N.; Klar, U.; Müller-Fahrnow, A.; Neef, G.; Ottow, E.; Schwede, W., 11 $\beta$ -Aryl steroids in the androstene series. The role of the 11 $\beta$ -region in steroid progesterone receptor interaction. *Tetrahedron* **1996**, *52* (5), 1529-1542.

128. Neimann, K.; Neumann, R., A new non-metal heterogeneous catalyst for the activation of hydrogen peroxide: a perfluorinated ketone attached to silica for oxidation of aromatic amines and alkenes. *Chem. Commun.* **2001**, (5), 487-488.

129. Van Vliet, M. C.; Arends, I. W.; Sheldon, R. A., Perfluoroheptadecan-9-one: a selective and reusable catalyst for epoxidations with hydrogen peroxide. *Chem. Commun.* **1999**, (3), 263-264.

130. Lemoine, S.; Thomazeau, C.; Joannard, D.; Trombotto, S.; Descotes, G.; Bouchu, A.; Queneau, Y., Sucrose tricarboxylate by sonocatalysed TEMPO-mediated oxidation. *Carbohydr. Res.* **2000**, *326* (3), 176-184.

131. Heeres, A.; Van Doren, H. A.; Gotlieb, K. F.; Bleeker, I. P., Synthesis of  $\alpha$ - and  $\beta$ -D-glucopyranuronate 1-phosphate and  $\alpha$ -D-glucopyranuronate 1-fluoride: Intermediates in the synthesis of D-glucuronic acid from starch. *Carbohydr. Res.* **1997**, *299* (4), 221-227.

132. Medgyes, A.; Farkas, E.; Lipták, A.; Pozsgay, V., Synthesis of the monosaccharide units of the O-specific polysaccharide of *Shigella sonnei*. *Tetrahedron* **1997**, *53* (12), 4159-4178.

133. Tahiri, C.; Vignon, M. R., TEMPO-oxidation of cellulose: Synthesis and

- characterisation of polyglucuronans. *Cellulose* **2000**, *7* (2), 177-188.
134. Dijkman, A.; Arends, I. W.; Sheldon, R. A., Polymer immobilised TEMPO (PIPO): an efficient catalyst for the chlorinated hydrocarbon solvent-free and bromide-free oxidation of alcohols with hypochlorite. *Chem. Commun.* **2000**, (4), 271-272.
135. Verhoef, M. J.; Peters, J. A.; van Bekkum, H., MCM-41 supported TEMPO as an environmentally friendly catalyst in alcohol oxidation. *Stud. Surf. Sci. Catal.* **1999**, *125*, 465-472.
136. Verhoef, M. J.; Peters, J. A.; van Bekkum, H., MCM-41 supported TEMPO as an environmentally friendly catalyst in alcohol oxidation. In *Stud. Surf. Sci. Catal.*, 1999; Vol. 125, pp 465-472.
137. Wan, Y.; Zhao, D., On the controllable soft-templating approach to mesoporous silicates. *Chem. Rev.* **2007**, *107* (7), 2821-2860.
138. Rychnovsky, S. D.; McLernon, T. L.; Rajapakse, H., Enantioselective oxidation of secondary alcohols using a chiral nitroxyl (N-oxoammonium salt) catalyst. *J. Org. Chem.* **1996**, *61* (4), 1194-1195.
139. Song, C.; Dong, X.; Yi, H.; Chiang, C.-W.; Lei, A., DDQ-catalyzed direct C(sp<sup>3</sup>)-H amination of alkylheteroarenes: synthesis of biheteroarenes under aerobic and metal-free conditions. *ACS Catal.* **2018**, *8* (3), 2195-2199.
140. Buckle, D. R.; Collier, S. J.; McLaws, M. D., 2,3-Dichloro-5,6-dicyano-1,4-benzo-quinone. *Encyclopedia of Reagents for Organic Synthesis* **2001**, DOI: 10.1002/047084289X.
141. Wendlandt, A. E.; Stahl, S. S., Quinone-Catalyzed Selective Oxidation of Organic Molecules. *Angew. Chem. Int. Ed.* **2015**, *54*, 14638 – 14658.
142. Dewkar, G. K.; Shaikh, T. M.; Pardhy, S.; Kulkarni, S. S.; Sudalai, A., Titanium superoxide catalyzed selective oxidation of phenols to p-quinones with aq. H<sub>2</sub>O<sub>2</sub>. **2005**.
143. Smith, J. R. L.; Calvin, M., Studies on the Chemical and Photochemical Oxidation of Bacteriochlorophyll1. *J. Am. Chem. Soc.* **1966**, *88* (19), 4500-4506.
144. Lemaire, M.; Guy, A.; Imbert, D.; Guetté J.-P., Asymmetric control of oxidation of aromatic substrates using a donor-acceptor interaction. *J. Chem. Soc. Chem. Commun.* **1986**, (10), 741-742.
145. Hans-Dieter Becker; Anders Bjork; Adler, E., Quinone Dehydrogenation. Oxidation of Benzylic Alcohols with 2,3-Dichloro-5,6-dicyanobenzoquinone. *J. Org. Chem.* **1980**, *45*, 1596-1600.
146. Luca, O. R.; Wang, T.; Konezny, S. J.; Batista, V. S.; Crabtree, R. H., DDQ as an electrocatalyst for amine dehydrogenation, a model system for virtual hydrogen storage. *New J. Chem.* **2011**, *35* (5), 998-999.
147. Sharma, P. K.; Kolchinski, A.; Shea, H. A.; Nair, J. J.; Gou, Y.; Romanczyk, L. J.; Schmitz, H. H., Scale-up syntheses of two naturally occurring procyanidins:(-)-epicatechin-(4β, 8)-(+)-catechin and (-)-epicatechin-3-O-galloyl-(4β, 8)-(-)-epicatechin-3-O-gallate. *Org. Process Res. Dev.* **2007**, *11* (3), 422-430.
148. Paukstat, R.; Brock, M.; Heesing, A., Dehydrierungen von 1, 2-Dihydroarenen mit Chinonen: Regio-und Stereoselektivität der Teilschritte. *Chem. Ber.* **1985**, *118* (7), 2579-2592.
149. Peng, K.; Chen, F.; She, X.; Yang, C.; Cui, Y.; Pan, X., Selective oxidation of benzylic or allylic hydroxyl group of sec-1, 2-diols. *Tetrahedron Lett.* **2005**, *46* (7), 1217-1220.
150. Scott, J. W.; Parrish, D. R.; Bizzarro, F. T., A Rapid and Mild Process for the Oxidation of 2, 3-Dichloro-5, 6-dicyanobenzoquinone (DDQ) from 2, 3-Dichloro-5,

- 6-dicyanohydroquinone (DDHQ). *Org. Prep. Proced. Int.* **1977**, *9* (2), 91-94.
151. Cosner, C. C.; Cabrera, P. J.; Byrd, K. M.; Thomas, A. M. A.; Helquist, P., Selective Oxidation of Benzylic and Allylic Alcohols Using Mn(OAc)<sub>3</sub>/Catalytic 2, 3-Dichloro-5, 6-dicyano-1, 4-benzoquinone. *Org. Lett.* **2011**, *13* (8), 2071-2073.
152. Wang, L.; Li, J.; Yang, H.; Lv, Y.; Gao, S., Selective oxidation of unsaturated alcohols catalyzed by sodium nitrite and 2, 3-dichloro-5, 6-dicyano-1, 4-benzoquinone with molecular oxygen under mild conditions. *J. Org. Chem.* **2011**, *77* (1), 790-794.
153. Walsh, K.; Sneddon, H. F.; Moody, C. J., Solar photochemical oxidations of benzylic and allylic alcohols using catalytic organo-oxidation with DDQ: Application to lignin models. *Org. Lett.* **2014**, *16* (19), 5224-5227.
154. Hu, Y.; Chen, L.; Li, B., Fe (NO<sub>3</sub>)<sub>3</sub>/2, 3-dichloro-5, 6-dicyano-1, 4-benzoquinone (DDQ): An efficient catalyst system for selective oxidation of alcohols under aerobic conditions. *Catal. Commun.* **2018**, *103*, 42-46.
155. Qiu, C.; Jin, L.; Huang, Z.; Tang, Z.; Lei, A.; Shen, Z.; Sun, N.; Mo, W.; Hu, B.; Hu, X., Symbiotic catalysis relay: molecular oxygen activation catalyzed by multiple small molecules at ambient temperature and its mechanism. *ChemCatChem* **2012**, *4* (1), 76-80.
156. Tong, X.; Sun, Y.; Yan, Y.; Luo, X.; Liu, J.; Wu, Z., Transition metal-free catalytic oxidation of aromatic alcohols with molecular oxygen in the presence of a catalytic amount of N-bromosuccinimide. *J. Mol. Catal. A: Chem.* **2014**, *391*, 1-6.
157. Devari, S.; Rizvi, M. A.; Shah, B. A., Visible light mediated chemo-selective oxidation of benzylic alcohols. *Tetrahedron Lett.* **2016**, *57* (30), 3294-3297.
158. Neumann, R.; Khenkin, A. M.; Vigdergauz, I., Quinones as Co-Catalysts and Models for the Surface of Active Carbon in the Phosphovanadomolybdate-Catalyzed Aerobic Oxidation of Benzylic and Allylic Alcohols: Synthetic, Kinetic, and Mechanistic Aspects. *Chem. Eur. J.* **2000**, *6* (5), 875-882.
159. Bhattacharya, A.; DiMichele, L. M.; Dolling, U. H.; Douglas, A. W.; Grabowski, E. J., Silylation-mediated oxidation of 4-aza-3-ketosteroids with DDQ proceeds via DDQ-substrate adducts. *J. Am. Chem. Soc.* **1988**, *110* (10), 3318-3319.
160. Simões, F.; Dos Anjos, D.; Vigier, F.; Léger, J.-M.; Hahn, F.; Coutanceau, C.; Gonzalez, E. R.; Tremiliosi-Filho, G.; De Andrade, A.; Olivi, P., Electroactivity of tin modified platinum electrodes for ethanol electrooxidation. *J. Power Sources* **2007**, *167* (1), 1-10.
161. Tian, N.; Zhou, Z.-Y.; Yu, N.-F.; Wang, L.-Y.; Sun, S.-G., Direct electrodeposition of tetrahedral Pd nanocrystals with high-index facets and high catalytic activity for ethanol electrooxidation. *J. Am. Chem. Soc.* **2010**, *132* (22), 7580-7581.
162. Spendelow, J. S.; Wieckowski, A., Electrocatalysis of oxygen reduction and small alcohol oxidation in alkaline media. *Phys. Chem. Chem. Phys.* **2007**, *9* (21), 2654-2675.
163. Xia, X.; Iwasita, T.; Ge, F.; Vielstich, W., Structural effects and reactivity in methanol oxidation on polycrystalline and single crystal platinum. *Electrochim. Acta* **1996**, *41* (5), 711-718.
164. He, M.; Fei, G.; Zheng, Z.; Cheng, Z.; Wang, Z.; Xia, H., Pt Nanoparticle-Loaded Graphene Aerogel Microspheres with Excellent Methanol Electro-Oxidation Performance. *Langmuir* **2019**, *35* (10), 3694-3700.
165. Shen, P. K.; Xu, C., Alcohol oxidation on nanocrystalline oxide Pd/C promoted electrocatalysts. *Electrochem. Commun.* **2006**, *8* (1), 184-188.
166. de Souza, M. B.; Vicente, R. A.; Yukuhiro, V. Y.; VMT Pires, C. o. T.;

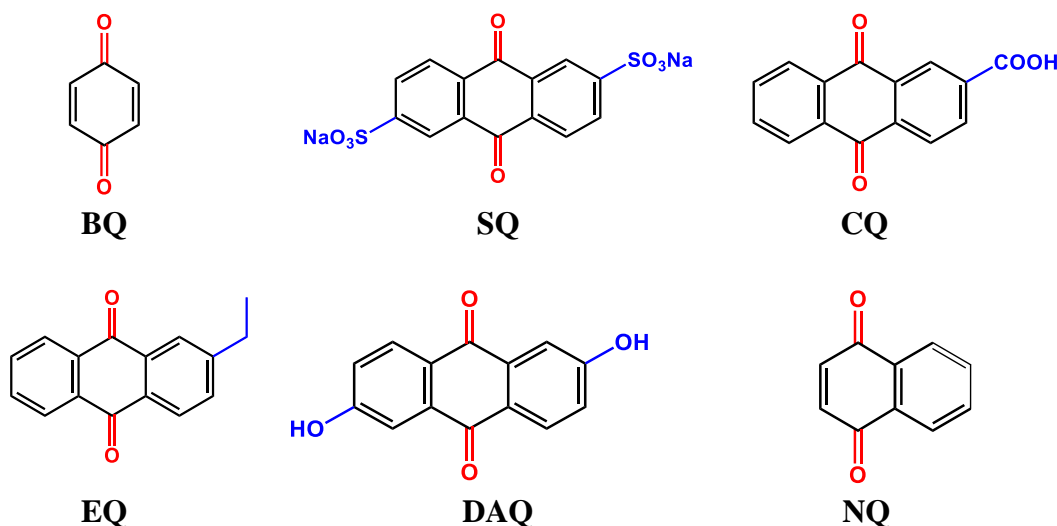
- Cheuquepán, W.; Bott-Neto, J. L.; Solla-Gullón, J.; Fernández, P. S., Bi-modified Pt Electrodes toward Glycerol Electrooxidation in Alkaline Solution: Effects on Activity and Selectivity. *ACS Catal.* **2019**, *9* (6), 5104-5110.
167. Kawamura, K.; Yasuda, T.; Hatanaka, T.; Hamahiga, K.; Matsuda, N.; Ueshima, M.; Nakai, K., Oxidation of aliphatic alcohols and benzyl alcohol by H<sub>2</sub>O<sub>2</sub> under the hydrothermal conditions in the presence of solid-state catalysts using batch and flow reactors. *Chem. Eng. J.* **2016**, *285*, 49-56.
168. Hida, T.; Nogusa, H., Practical and versatile oxidation of alcohol using novel Na<sub>2</sub>WO<sub>4</sub>-H<sub>2</sub>O<sub>2</sub> system under neutral conditions. *Tetrahedron* **2009**, *65* (1), 270-274.
169. Barak, G.; Dakka, J.; Sasson, Y., Selective oxidation of alcohols by a H<sub>2</sub>O<sub>2</sub>-RuCl<sub>3</sub> system under phase-transfer conditions. *J. Org. Chem.* **1988**, *53* (15), 3553-3555.
170. Chakravarthy, R. D.; Suresh, K.; Ramkumar, V.; Chand, D. K., New chiral molybdenum complex catalyzed sulfide oxidation with hydrogen peroxide. *Inorg. Chim. Acta* **2011**, *376* (1), 57-63.
171. Luan, Y.; Wang, G.; Luck, R. L.; Yang, M.; Han, X., Oxidation of Alcohols with Hydrogen Peroxide Catalyzed by Molybdenum (VI)-Peroxo Complex under Solvent-free Conditions. *Chem. Lett.* **2007**, *36* (10), 1236-1237.
172. Ballistreri, F. P.; Tomaselli, G. A.; Toscano, R. M.; Conte, V.; Di Furia, F., Spectroscopic and structural properties of some molybdenum and tungsten polyoxoperoxo complexes. A comparison with mononuclear complexes. *J. Mol. Catal.* **1994**, *89* (3), 295-301.
173. Maiti, S. K.; Banerjee, S.; Mukherjee, A. K.; Malik, K. A.; Bhattacharyya, R., Oxoperoxo molybdenum (VI) and tungsten (VI) and oxodiperoxo molybdate (VI) and tungstate (VI) complexes with 8-quinolinol: Synthesis, structure and catalytic activity. *New J. Chem.* **2005**, *29* (4), 554-563.
174. Neumann, R.; Levin, M., Selective aerobic oxidative dehydrogenation of alcohols and amines catalyzed by a supported molybdenum-vanadium heteropolyanion salt Na<sub>5</sub>PMo<sub>2</sub>V<sub>2</sub>O<sub>40</sub>. *J. Org. Chem.* **1991**, *56* (19), 5707-5710.
175. Zhao, W.; Zhang, Y.; Ma, B.; Ding, Y.; Qiu, W., Oxidation of alcohols with hydrogen peroxide in water catalyzed by recyclable kegglin-type tungstoborate catalyst. *Catal. Commun.* **2010**, *11* (6), 527-531.
176. Pope, M. T.; Müller, A., Polyoxometalate chemistry: an old field with new dimensions in several disciplines. *Angew. Chem. Int. Ed. Engl.* **1991**, *30* (1), 34-48.
177. Espenson, J. H.; Zhu, Z.; Zauche, T. H., Bromide ions and methyltrioxorhenium as cocatalysts for hydrogen peroxide oxidations and brominations. *J. Org. Chem.* **1999**, *64* (4), 1191-1196.
178. Arends, I. W.; Sheldon, R. A.; Wallau, M.; Schuchardt, U., Oxidative transformations of organic compounds mediated by redox molecular sieves. *Angew. Chem. Int. Ed. Engl.* **1997**, *36* (11), 1144-1163.
179. Maspero, F.; Romano, U., Oxidation of alcohols with H<sub>2</sub>O<sub>2</sub> catalyzed by Titanium Silicalite-1. *J. Catal.* **1994**, *146* (2), 476-482.
180. Sheldon, R. A.; Wallau, M.; Arends, I. W.; Schuchardt, U., Heterogeneous catalysts for liquid-phase oxidations: philosophers' stones or Trojan horses? *Accounts Chem. Res.* **1998**, *31* (8), 485-493.
181. Jappar, N.; Xia, Q.; Tatsumi, T., Oxidation activity of Ti-beta synthesized by a dry-gel conversion method. *J. Catal.* **1998**, *180* (2), 132-141.
182. Davies, L. J.; McMorn, P.; Bethell, D.; Page, P. C. B.; King, F.; Hancock, F. E.; Hutchings, G. J., Oxidation of crotyl alcohol using Ti-β and Ti-MCM-41 catalysts. *J. Mol. Catal. A: Chem.* **2001**, *165* (1-2), 243-247.

183. Adam, W.; Corma, A.; Reddy, T. I.; Renz, M., Diastereoselective catalytic epoxidation of chiral allylic alcohols by the TS-1 and Ti- $\beta$  zeolites: evidence for a hydrogen-bonded, peroxy-type loaded complex as oxidizing species. *J. Org. Chem.* **1997**, *62* (11), 3631-3637.
184. Dong, X.; Wang, D.; Li, K.; Zhen, Y.; Hu, H.; Xue, G., Vanadium-substituted heteropolyacids immobilized on amine-functionalized mesoporous MCM-41: A recyclable catalyst for selective oxidation of alcohols with H<sub>2</sub>O<sub>2</sub>. *Mater. Res. Bull.* **2014**, *57*, 210-220.
185. Bilgrien, C.; Davis, S.; Drago, R. S., The selective oxidation of primary alcohols to aldehydes by oxygen employing a trinuclear ruthenium carboxylate catalyst. *J. Am. Chem. Soc.* **1987**, *109* (12), 3786-3787.
186. Wang, G.-Z.; Andreasson, U.; Bäckvall, J.-E., Aerobic oxidation of secondary alcohols via ruthenium-catalysed hydrogen transfer involving a new triple catalytic system. *J. Am. Chem. Soc., Chem. Commun.* **1994**, (9), 1037-1038.
187. Bäckvall, J.-E.; Chowdhury, R. L.; Karlsson, U., Ruthenium-catalysed aerobic oxidation of alcohols via multistep electron transfer. *J. Am. Chem. Soc., Chem. Commun.* **1991**, (7), 473-475.
188. A ĩ-Mohand, S.; H énin, F.; Muzart, J., Palladium (II)-mediated oxidation of alcohols using 1, 2-dichloroethane as Pd (O) reoxidant. *Tetrahedron Lett.* **1995**, *36* (14), 2473-2476.
189. Chung, K.; Banik, S. M.; De Crisci, A. G.; Pearson, D. M.; Blake, T. R.; Olsson, J. V.; Ingram, A. J.; Zare, R. N.; Waymouth, R. M., Chemoselective Pd-catalyzed oxidation of polyols: synthetic scope and mechanistic studies. *J. Am. Chem. Soc.* **2013**, *135* (20), 7593-7602.
190. Iwahama, T.; Sakaguchi, S.; Nishiyama, Y.; Ishii, Y., Aerobic oxidation of alcohols to carbonyl compounds catalyzed by N-hydroxyphthalimide (NHPI) combined with Co (acac) 3. *Tetrahedron Lett.* **1995**, *36* (38), 6923-6926.
191. Antonyraj, C. A.; Jeong, J.; Kim, B.; Shin, S.; Kim, S.; Lee, K.-Y.; Cho, J. K., Selective oxidation of HMF to DFF using Ru/ $\gamma$ -alumina catalyst in moderate boiling solvents toward industrial production. *J. Ind. Eng. Chem.* **2013**, *19* (3), 1056-1059.
192. Felthouse, T. R., Catalytic oxidative cleavage of vicinal diols and related oxidations by ruthenium pyrochlore oxides: new catalysts for low-temperature oxidations with molecular oxygen. *J. Am. Chem. Soc.* **1987**, *109* (24), 7566-7568.
193. Terashima, T.; Ouchi, M.; Ando, T.; Sawamoto, M., Oxidation of sec-alcohols with Ru (II)-bearing microgel star polymer catalysts via hydrogen transfer reaction: Unique microgel-core catalysis. *J. Polym. Sci. Polym. Chem.* **2011**, *49* (5), 1061-1069.
194. Ebitani, K.; Motokura, K.; Mizugaki, T.; Kaneda, K., Heterotrimetallic RuMnMn Species on a hydrotalcite surface as highly efficient heterogeneous catalysts for liquid-phase oxidation of alcohols with molecular oxygen. *Angew. Chem. Int. Ed.* **2005**, *44* (22), 3423-3426.
195. Matsushita, T.; Ebitani, K.; Kaneda, K., Highly efficient oxidation of alcohols and aromatic compounds catalysed by the Ru-Co-Al hydrotalcite in the presence of molecular oxygen. *Chem. Commun.* **1999**, (3), 265-266.
196. Friedrich, H. B.; Khan, F.; Singh, N.; van Staden, M., The Ru-Cu-Al-hydrotalcite-catalysed oxidation of alcohols to aldehydes or ketones. *Synlett* **2001**, *2001* (06), 0869-0871.
197. Hinzen, B.; Lenz, R.; Ley, S. V., Polymer supported perruthenate (PSP): Clean oxidation of primary alcohols to carbonyl compounds using oxygen as cooxidant. *Synthesis* **1998**, *1998* (07), 977-979.

# Chapter 2. Experiments

## 2.1 Materials and Chemicals

The chemicals  $\text{RuCl}_3 \cdot \text{H}_2\text{O}$ ,  $\gamma\text{-Al}_2\text{O}_3$ , CTAB,  $\text{NaBH}_4$ , biphenyl, toluene, benzyl alcohol, 4-chlorobenzyl alcohol, 4-methylbenzyl alcohol, cinnamyl alcohol, 1,2-hexanediol, furfuryl alcohol, HMF, 1-octanol, 2-octanol, 2-hexanol, cyclohexanol, 1,4-benzoquinone(BQ), 2-ethylanthraquinone (EQ), 1,4-naphthoquinone (NQ), anthraquinone-2-carboxylic acid (CQ), 2,6-dihydroxyanthraquinone (DAQ), disodium anthraquinone-2,6-disulfonate (SQ) are purchased from J&K Scientific Ltd. The chemical structure was shown in **Scheme 2-1**. All commercially available alcohols and solvents used were purified by standard procedures<sup>1</sup>.



**Scheme 2-1.** Chemical structure of quinones.

## 2.2 Catalysts Preparation

### 2.2.1 Synthesis of ruthenium nanoparticles (Ru NPs) catalysts

Four reverse micellar microemulsions with different ratios of CTAB/1-hexanol/water (as shown in Table 2-1) were prepared.

As the procedures in Figure 2-1, 20 g microemulsion A comprising 0.22 g  $\text{RuCl}_3$ , and 20 g microemulsion B comprising 0.13 g  $\text{NaBH}_4$  were prepared. The two

microemulsions were mixed by adding microemulsion B into microemulsion A drop by drop for 1 h under vigorous stirring. After that, Ru nanoparticles with uniform particle size distribution were formed inside the micelles. The microemulsion was broken by centrifugation, and the precipitate was washed 3 times with hot water, and dried at 80 °C for 12 h. The synthesized samples were denoted according to the m-Ru NP-X, where X is the water content in the composition.

**Table 2-1.** Different emulsion ratios to prepare metallic Ru nanoparticles (m-Ru NPs) catalysts

CTAB, g	Hexanol, g	Water, g	Catalysts
5	4.5	0.5	m-Ru-5
4.7	4.3	1	m-Ru-10
4.2	3.8	2	m-Ru-20
2.9	2.6	4.5	m-Ru-45

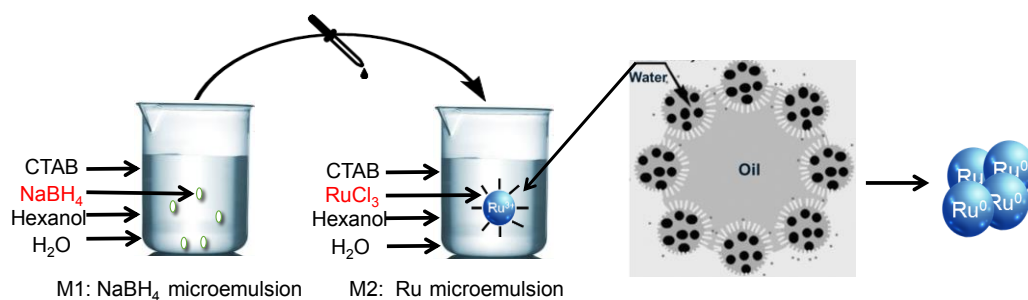


**Figure 2-1.** Preparation of Ru nanoparticles by micro-emulsion method.

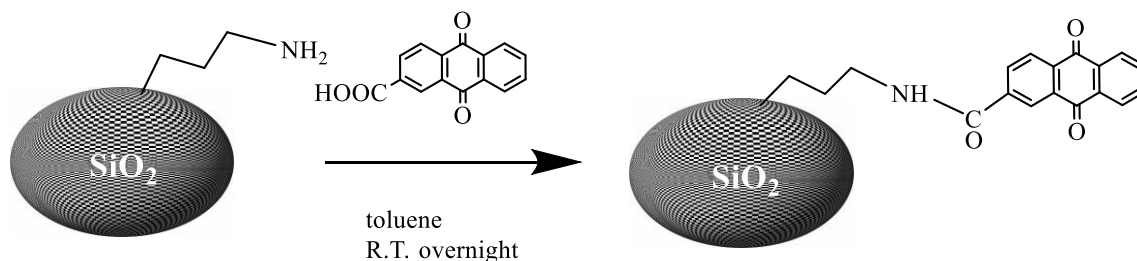
### 2.2.2 Synthesis of supported Ru/Al<sub>2</sub>O<sub>3</sub> catalyst

The conventional reference Ru/Al<sub>2</sub>O<sub>3</sub> with 5 wt% of metal loading was prepared by incipient wetness impregnation of  $\gamma$ -Al<sub>2</sub>O<sub>3</sub> with an aqueous RuCl<sub>3</sub> solution as described before<sup>2</sup>. The resulting solid was dried at 80 °C overnight. Then, the powder was calcined in air at 400 °C for 4 h with a heating rate of 1 °C min<sup>-1</sup>. The catalyst has been reduced in the reactor prior the test at 200 °C for 1 h in a flow of H<sub>2</sub>/Ar (5 vol. % H<sub>2</sub>). Another reference catalyst m-Ru-5/Al<sub>2</sub>O<sub>3</sub> has been prepared by impregnation of prepared m-Ru-5 nanoparticles in aqueous solution over  $\gamma$ -Al<sub>2</sub>O<sub>3</sub> support to provide 5 wt% of Ru. The catalyst has been dried in vacuum oven at 80 °C overnight.

### 2.2.3 Synthesis of supported CQ/SiO<sub>2</sub> catalyst

The supported quinone catalyst (CQ/SiO<sub>2</sub>) was prepared by a grafting method. 1 g of commercially available aminopropyl-functionalized silica having approximately 1 mmol/g amino groups was placed in the vessel together with 50 mg of

anthraquinone-2-carboxylic acid dissolved in 15 mL of toluene (Scheme 2-2). The mixture obtained was stirred overnight at ambient temperature. The catalyst has been separated by centrifugation, washed with toluene and ethanol to remove traces of anthraquinone-2-carboxylic acid and dried at 80 °C. The procedure is standard for the synthesis amide bond over silica surface<sup>3</sup>.



**Scheme 2-2.** Synthesis of supported CQ/SiO<sub>2</sub> catalyst.

#### 2.2.4 Synthesis of core-shell Ru@quinones catalysts

Reverse micellar microemulsions of CTAB/1-hexanol/water (as shown in **Table 2-2**) have been prepared. The details of preparation are as described in 2.2.1 section. The synthesized samples were denoted to the Ru NPs.

**Table 2-2.** Different emulsion ratios to prepare Ru nanoparticles.

CTAB, g	Hexanol, g	Water, g	$n_{CTAB}/n_{hexanol}$ , molar ratio	Catalysts
5	4.5	0.5	0.31	Ru NPs

The catalysts Ru@SQ with varied shell thickness were obtained by incipient wetness impregnation of Ru NPs with SQ aqueous solution. Briefly, different amounts of SQ have been ultrasonically dissolved in 3 mL H<sub>2</sub>O, which are subsequently impregnated on 100 mg Ru NPs. The resulting slurry were evaporated by rotary evaporator and consequently dried at 60 °C in vacuum oven overnight. A series of samples Ru@SQ-X % (X = 10, 25, 50 and 80) were obtained, where X was the weight percentage of SQ. The black samples have been grinded prior the test.

Other catalysts containing 80 wt. % of quinones have been prepared using the same procedure and different type of quinones: benzoquinone (Ru@BQ), naphthaquinone (Ru@NQ), 2-ethylanthraquinone (Ru@EQ) and 2-carboxyanthraquinone (Ru@CQ).

## 2.2.5 Synthesis of Ru@MOFs catalysts

**MIL-101(Cr):** Cr(NO<sub>3</sub>)<sub>3</sub> 9H<sub>2</sub>O (1 g, 2.5 mmol) and 1,4-dicarboxybenzene (H<sub>2</sub>BDC) (415 mg, 2.5 mmol) were dispersed in 10 mL distilled water at room temperature. The mixture was then transferred to a 25 mL Teflon-lined autoclave and heated in a 200 °C oven for 7 h. After cooling down to room temperature, the product was collected by centrifugation and washed with DMF and methanol multiple times. The collected green powder was dispersed in methanol for later use.

**MOF-808(Zr):** Trimesic acid (H<sub>3</sub>BTC, 3.75 mmol, 0.786 g) and ZrOCl<sub>2</sub> 8H<sub>2</sub>O (3.75 mmol, 1.209 g) were mixed in DMF (150 mL) and formic acid (150 mL). The mixture was placed in a closed 1 L Schott DURAN bottle and heated at 130 °C for 7 h. After cooling down, the obtained white powder was washed by DMF (3X), methanol (3X) and collected by centrifugation. The MOF-808(Zr) was activated at 150 °C for 20 h before performing experiments.

**MIL-100(Al):** Aluminum nitrate nonahydrate (Al(NO<sub>3</sub>)<sub>3</sub> 9H<sub>2</sub>O) 2.25 g and H<sub>3</sub>BTC 1.11g (metal/linker ratio = 1: 0.875) were mixed in H<sub>2</sub>O (30 mL) and DMF (1.2 mL). The pH of the solution was adjusted to 1.6 using HNO<sub>3</sub>. Then the mixture was placed in a 50 ml Teflon-lined autoclave and heated in a 200 °C oven for 4 h. After cooling down to room temperature, the product was collected by centrifugation and washed with DMF (3X) and methanol (3X). The methanol dispersion of the MIL-100(Al) was kept for later use.

**Ru@MIL-101(Cr):** 200 mg of MIL-101(Cr) was placed into a 250 ml round bottom flask. Ruthenium(III) chloride hydrate (RuCl<sub>3</sub>•xH<sub>2</sub>O, 49.5 mg) was dissolved in a DI water/ethanol (200 µl : 2 ml) mixed solvent and added to the flask. Dichloromethane (DCM, 10 mL) was added to the mixture and sonicated for 5 min to achieve a clear solution. After adding 20 ml petroleum ether, black precipitate was formed leaving a colorless transparent supernatant. After drying the precipitate in a 70 °C oven, the solid was reduced into a U-shaped glass tube under atmospheric hydrogen atmosphere (H<sub>2</sub>, 200 °C) overnight.

**MIL-101(Cr)@Ru:** 200 mg MIL-101(Cr) powder was placed into a 50 mL centrifuge tube. Then RuCl<sub>3</sub> xH<sub>2</sub>O (49.5 mg) was added along with 5 mL methanol. The product was dry in a 70 °C oven. Then the samples were reduced under a continuously flowing H<sub>2</sub> atmosphere (1 atm) in a U-shaped glass tube at 200 °C overnight.

**Ru@MOF-808(Zr)** and **Ru@MIL-100(Al)** were prepared similarly to Ru@MIL-101(Cr).

## 2.3 Catalyst Characterization

### 2.3.1 Transmission electron microscopy

The TEM (Transmission Electron Microscopy) analyses were carried out on a Jeol 2100F (field emission gun) microscope operating at 200 kV equipped with a probe corrector for the spherical aberrations. The point-to-point resolution reached was on the order of 2 Å under the parallel TEM mode and 1 Å under the STEM (Scanning TEM) mode. High angle annular dark field (HAADF)-scanning transmission electron microscopy (STEM) imaging, and energy dispersive X-ray spectroscopy (EDX) of the calcined analysis were performed on a double corrected CFEG Jeol-ARM200 transmission electron microscope, operated at 200 kV and by using scanning speed 20 μs/px for imaging and 0.05 μs/px for EDX for a with a 0.1 nm probe size and a current of 120pA. More than 100 particles were counted to estimate the average Ru particles size and standard deviation from TEM images.

### 2.3.2 X-ray diffraction.

X-ray diffraction (XRD) was recorded on a PANalytical Empyrean X-ray diffractometer in Bragg-Brentano configuration with the 0.02° step size and 1 s step time. The Cu Kα radiation (40 kV and 30 mA) was used as the X-ray source. The crystalline phases were identified by comparing the diffraction patterns with those of the standard powder XRD files (JCPDS). Crystal grain size was calculated using the Scherrer equation:

$$D = \frac{K\lambda}{\beta \cos \theta}$$

Here, K=0.89, λ =1,54056 Å , β=full width at half maximum (rad), θ=angle(rad).

### 2.3.3 Temperature-programmed reduction

The H<sub>2</sub> temperature-programmed reduction (H<sub>2</sub>-TPR) experiments were carried out by the AutoChem II 2920 apparatus (Micromeritics Figure 2-2) using 0.05 g of the sample in a flow of H<sub>2</sub>/Ar (5 vol. % H<sub>2</sub>). The temperature was increased from room temperature to 200 °C at a rate of 10 °C/min and hold for 30 min at 200 °C.

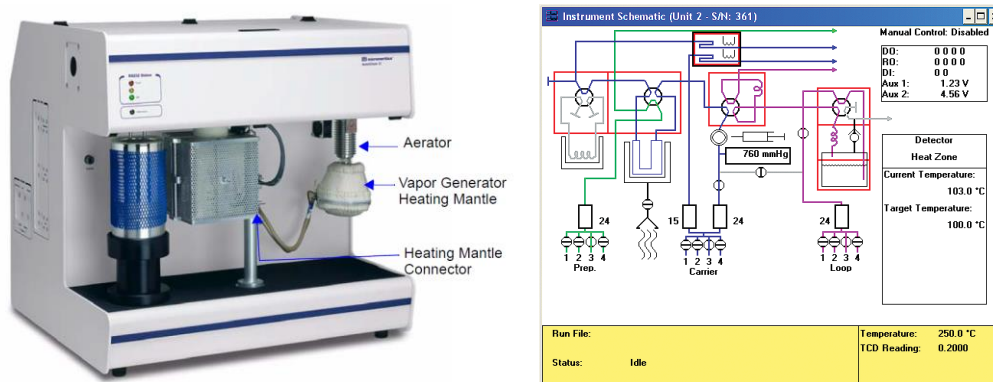


**Figure 2-2.** Micromeritics AutoChem II 2920 apparatus.

### 2.3.4 O<sub>2</sub> & CO chemisorption

The Ru NPs active site has been measured by O<sub>2</sub> pulse chemisorption on the same instrument. The catalyst has been cooled down to 0 °C followed by pulses of 3% O<sub>2</sub>/He till saturation of oxygen signal. O<sub>2</sub> adsorption amount was calculated as the difference between the total O<sub>2</sub> injected and the amount measured at the outlet with a stoichiometry of one O<sub>2</sub> per ruthenium surface atom.

CO pulse adsorption was performed using a Micromeritics Autochem II 2920 instrument. The sample was reduced at 200 °C by 10 % H<sub>2</sub>/He and then cooled down to 45 °C in a helium flow. CO pulses were injected at that temperature in the flow of 5% CO/He until the adsorption reached saturation. CO adsorption amount was calculated as the difference between the total CO injected and the amount measured at the outlet with a stoichiometry of one O<sub>2</sub> per ruthenium surface atom.

### 2.3.5 Infrared spectroscopy analysis (FT-IR)

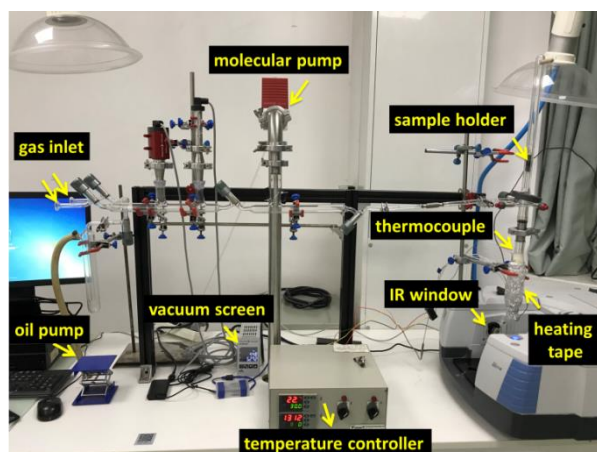


**Figure 2-3.** Picture of fourier transform infrared (FT-IR) setup with homemade vacuum system.

Infrared spectra have been observed using Thermo Fisher Scientific Nicolet 6700 FTIR with  $4\text{ cm}^{-1}$  optical resolution (Figure 2-3) with a MCT detector, equipped with high-vacuum system and heating zone. Prior to the analysis, the catalysts were pressed into discs.

### 2.3.6 Elemental analysis

Quantitative elemental analyses were performed by inductively coupled plasma optic emission spectroscopy 720-ES ICP-OES (Agilent) with axially viewing and simultaneous CCD detection. The quantitative determination of metal content in the catalysts was made based on the analysis of certificated standard solution. The ICP Expert™ software (version 2.0.4) provided metal concentration in the samples allowing estimating the weight percentage of components. The minimum detection limitation is 0.1 ppm and the accuracy is better than 5%.

### 2.3.7 Zeta Potentials

The zeta potential of the particles was measured at ambient temperature by the Zetasizer from Malvern Instruments and the software Dispersion Technology Software (DTS). Water was used as the dispersant with a concentration of catalyst 1 wt. % at  $\text{pH} = 7$ . The analysis was performed with 12 zeta runs and 2 mm measurement position at a scattering angle of  $90^\circ$ .

### 2.3.8 *In-situ* XPS

X-ray photoelectron spectroscopy (XPS) spectra were acquired using a Thermo Scientific ESCALAB 250Xi X-ray Photoelectron Spectrometer equipped with a 150 mm hemispherical electron energy analyzer. The monochromatic Al  $K\alpha$  (1486.6 eV) X-ray source was used at 225 W (15 kV, 15 mA). All processing and spectra deconvolution was performed in Thermo Scientific Avantage Software. The binding energy (BE) scale was calibrated to external standard of Al 2p peak (*i.e.*, 74.5 eV) of  $\text{Al}_2\text{O}_3$  added to the samples before *ex-situ* analysis. In the *in-situ* experiments the BE scale was calibrated to Na 1s (*i.e.*, 1072.4 eV) of sodium detected in the samples as minor contamination. *In-situ* ethanol treatment was performed in high pressure gas cell (HPGC 300, Fermi Instruments) of XPS spectrometer at 60 mbar of ethanol vapor,  $100^\circ\text{C}$  for 20 min.

### **2.3.9 TGA Analysis**

TGA was carried out by SDT Q600 at heating rate of 10 °C/min in the temperature range of 25~800 °C under air/N<sub>2</sub> condition.

### **2.3.10 Solid NMR Analysis**

Solid State MAS NMR was recorded on a Bruker Avance 400 spectrometer. For <sup>1</sup>H NMR spectrum, one pulse sequence has been applied, for <sup>13</sup>C, we used CP MAS sequence. Chemical shifts are given in ppm with respect to TMS as external reference for <sup>1</sup>H and <sup>13</sup>C NMR.

### **2.3.11 High-resolution scanning electron microscope (HRSEM)**

Images were obtained using a JSM-7800F Prime Scanning Electron Microscopy at 5 kV. The samples were pre-coated with Au for 10 seconds using an SBC-12 sputter coater.

### **2.3.12 N<sub>2</sub> adsorption.**

N<sub>2</sub> adsorption isotherms were collected by a volumetric gas adsorption analyzer (Quantachrome Instruments Autosorb-iQ-MP-AG). Typically, 50-80 mg powder sample was loaded in a 6 mm large bulb sample cell and degassed under vacuum at 120 °C for 8 h. The BET surface area was determined using the data points in the pressure range of 0.01-0.1 P/P<sub>0</sub> from the N<sub>2</sub> adsorption isotherms at 77 K.

### **2.3.13 NH<sub>3</sub>-temperature programmed desorption (NH<sub>3</sub>-TPD)**

The Ru@MOF catalysts were pre-reduced at 473 K for 10 min in a flow of 10% H<sub>2</sub>/Ar using an AUTOCHEM II (Micromeritics), and cool down at 318 K under Ar before the NH<sub>3</sub>-TPD test. Then the sample was subjected to a flow of diluted NH<sub>3</sub> for 30 min at 373 K. Excess NH<sub>3</sub> was desorbed in a flow of dry He at 373 K for 1 h. Typical TPD experiments were carried out by increasing temperature from 373 K to 573 K in a flow of dry He. The rate of heating was 9 K min<sup>-1</sup>.

## 2.4 Catalysis

### 2.4.1 Liquid-phase catalytic oxidation of alcohols

The liquid-phase oxidations of different alcohols in O<sub>2</sub> or inert N<sub>2</sub> atmosphere were conducted in a 30-mL stainless steel autoclave geared with a pressure gauge and a safety rupture disc (TVS-N2-30, Taiatsu Techno Corporation, Japan, **Figure 2-4**). In a typical experiment, the reactor was charged with 3.0 g of alcohol and catalyst (~50 mg). The proper solvents/solvent-free were used in the test. Then, the reactor was sealed and evacuated by applying vacuum followed by charging 10 bar O<sub>2</sub> or N<sub>2</sub> into the reactor. Finally, the reactor was placed on a heating plate equipped with an aluminum heating block and a magnetic stirrer (500 rpm) at 80~150 °C for 1~48 h. After reaction, the reactor was cooled down to room temperature, and the mixture was filtrated and analyzed on a gas chromatography (Agilent 7890B) equipped with a HP-5 capillary column (length 30 m, diameter 320 μm, film thickness 0.32 μm) using biphenyl as the internal standard.

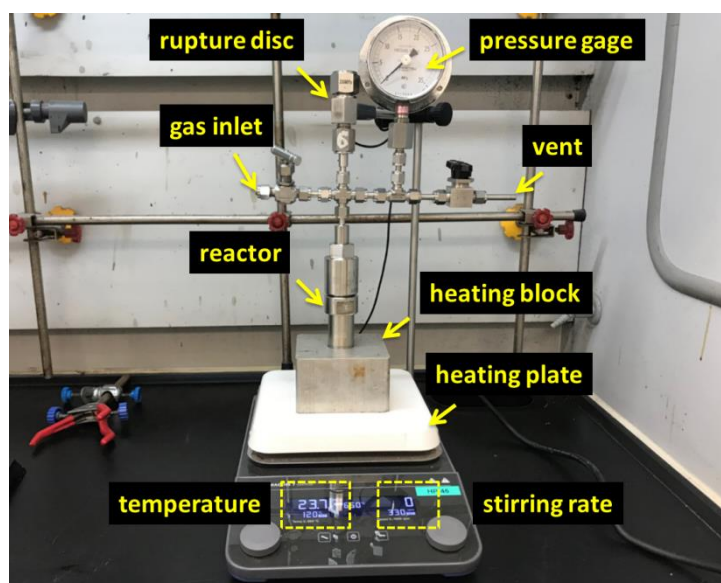


**Figure 2-4.** *Taiatsu autoclave for liquid-phase oxidation of alcohols.*

### 2.4.2 Liquid-phase catalytic oxidation of aldehydes

The catalytic oxidation of aldehydes was also tested in the same autoclave. Typically, 30 mg of catalyst or without catalyst in blank experiment and 0.5 g of octanal were placed into a reactor with air as oxidant at atmospheric pressure under solvent free conditions. The mixture was stirred at 60 °C and reaction time was 0.25~3 h.

### 2.4.3 Recyclability of catalysts

The stability of the heterogeneous catalyst has been tested for 3 times by filtering of the catalyst after each cycle with subsequent addition to the fresh alcohol mixture for the next oxidation test as described above.

### 2.4.4 Analysis method

The alcohol conversions and products selectivity are based on gas chromatograph (GC). The  $A$  appearing in the following calculation method indicates the peak area of substances in the GC,  $f_i$  indicates the calibration coefficient,  $n$  means moles of products (in terms of carbon atom moles),  $C_i$  is the number of carbon atoms, and  $M_i$  is molecular weight of products.

The alcohol conversion rate is calculated using biphenyl as an internal standard:

$$\text{Conversion} = \left(1 - \frac{n(\text{alcohol unreacted})}{n(\text{alcohol initial})}\right) * 100\% ;$$

$$\text{Selectivity} = \frac{n(\text{product})}{n(\text{alcohol initial}) - n(\text{alcohol unreacted})} * 100\% ;$$
$$n(\text{alcohol unreacted}/\text{products}) = f_i * \frac{A_i * m_s}{A_s * M_i} * C_i .$$

Here,  $m_s$  and  $A_s$  are mass and GC peak area of standard biphenyl, respectively.

The carbon balance is calculated by the total amount of carbon actually detected (the sum of all carbon-containing compounds detected by the FID) divided by the total amount of carbon consumed in the reaction.

### 2.4.5 Calibration curves

The calibration curves are calculated according to internal standard method, which is to add biphenyl as an internal standard to a certain amount of sample mixture to be analyzed.  $f_i$  indicates the calibration coefficient which is obtained according to the mass ratio of the sample and biphenyl vs. the ratio of the corresponding chromatographic peak area as follow:

$$f = \frac{A_s/A_i}{M_s/M_i}$$

Here,  $A_s$  and  $A_i$  are the GC peak areas of biphenyl and samples, respectively; while  $m_s$  and  $m_i$  are the mass of biphenyl and samples, respectively.

Four levels of concentration were tested in duplicate and regression lines were calculated for each compound. In the case of model 1-octanol oxidation, calibration data are shown in Figure 2-5.

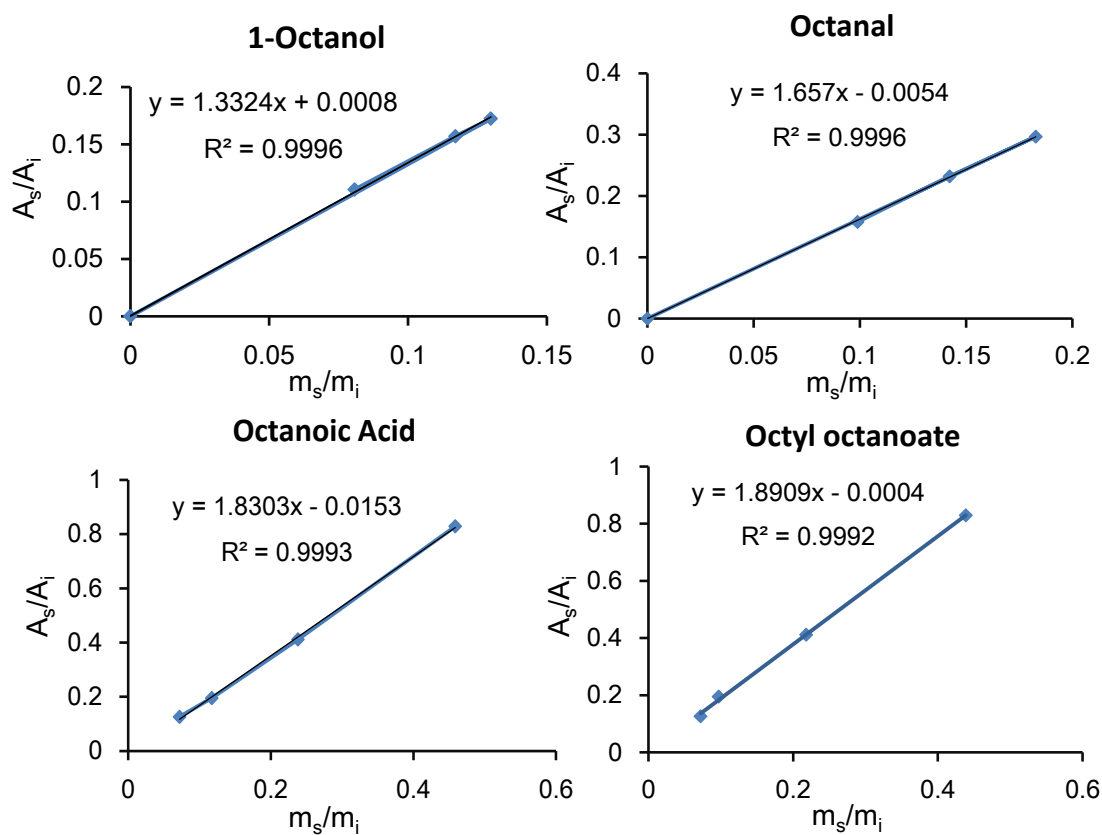


**Figure 2-5.** Calibration curves of 1-octanol, octanal, octanoic acid, octyl octanoate.

#### 2.4.6 Experimental error of autoclaves

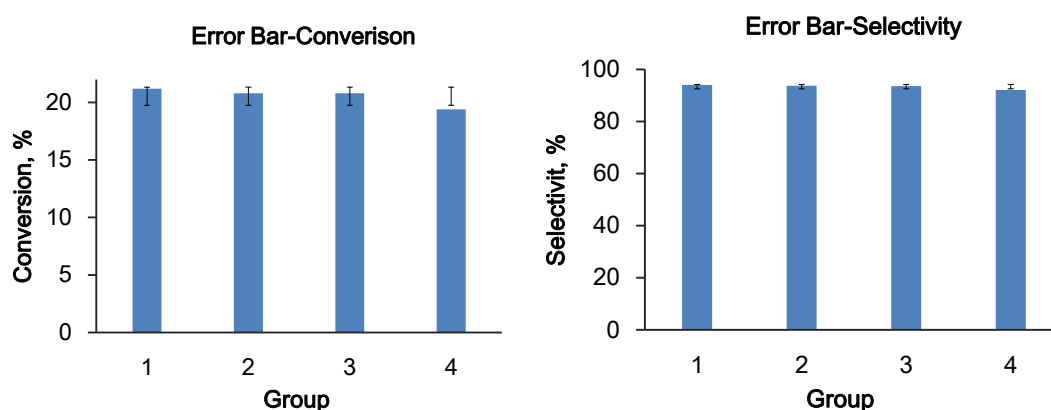


**Figure 2-6.** Conversion of benzyl alcohol and selectivity to benzaldehyde in four parallel experiments.

In order to exclude the error of the reactor, commercial 5 wt% Ru/Al<sub>2</sub>O<sub>3</sub> was used to catalyze oxidation of benzyl alcohol with four parallel experiments under same reaction conditions, and the data as Figure 2-6 shows. Reaction conditions: 50 mg supported catalyst, 2.0 g benzyl alcohol and solvent-free with 10 bar O<sub>2</sub> at 100 °C for 4h.

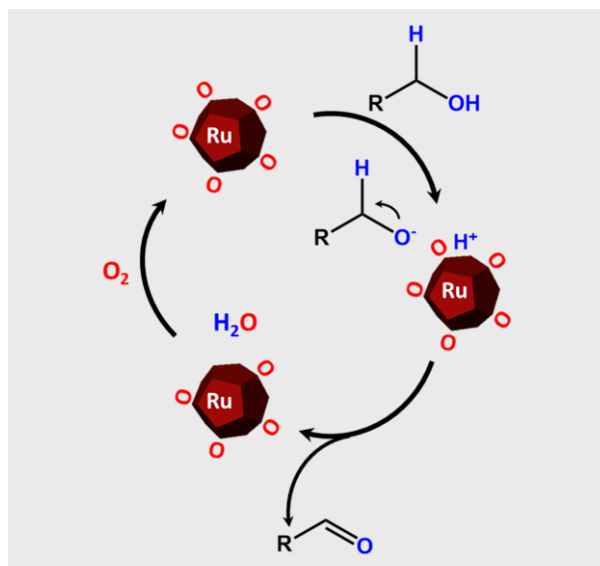
#### 2.4.7 Cyclic voltammetry

Cyclic voltammetry (CV) was performed with a three-electrode setup controlled by a potentiostat (Reference 3000, Gamry Instruments Inc.). The synthesized catalysts, including Ru-S NPs and SQ, were dispersed in ethanol by ultrasonication to form a well-dispersed ink (10 mg/ml) by using Nafion 117 solution (5 wt%) as a binder. 100 µL of the ink was deposited onto a polished and pre-cleaned glassy-carbon electrode with a working area of 0.1256 cm<sup>2</sup>. For 80% Ru-S@SQ, the working electrode was composed of glassy carbon (GC) electrode surface orderly coated by 80 µL SQ ink after solvent extraction of the 20 µL Ru-S NPs slurry. Ag/Ag<sup>+</sup> was used as the reference electrode in all measurements while Pt wire as counter electrode. Typically, cyclic voltammetry was carried out at 25 °C in 8 mL solution of 0.1 M LiClO<sub>4</sub> in DMSO saturated with Ar, at a constant sweep rate of 100 mV/s.

#### 2.5 References

1. Perrin, D. D.; Armarego, W. L. F., Purification of Laboratory Chemicals 3th Edition. . Pergamon Press: Oxford, U.K. **1988**.
2. Yamaguchi, K.; Mizuno, N., Supported ruthenium catalyst for the heterogeneous oxidation of alcohols with molecular oxygen. *Angew. Chem. Int. Ed.* **2002**, *23*, 4538-4541.
3. Ronzani, F.; Costarramone, N.; Blanc, S.; Benabbou, A. K.; Bechec, M. L.; Pigot, T.; Oelgemöller, M.; Lacombe, S., Visible-light photosensitized oxidation of α-terpinene using novel silica-supported sensitizers: Photooxygenation vs. photodehydrogenation. *J. Catal.* **2013**, *303*, 164-174.

# CHAPTER 3 Selective Oxidation of Alcohols to Carbonyl Compounds over Small Size Colloidal Ru Nanoparticles



---

## ABSTRACT:

The selective oxidation of alcohols to corresponding aldehydes is one of the most challenging problems in modern chemistry due to over-oxidation of these products further into corresponding acids and esters. Herein, we report an efficient and eco-friendly method for selective oxidation of aliphatic, unsaturated and aromatic alcohols to aldehydes (> 90 %) using small size (2 nm) non-supported colloidal Ru nanoparticles. The selectivity rapidly decreases with increase of the size of nanoparticles (from 2 to 10 nm) or after their deposition over support. X-ray photoelectron spectroscopy suggests that this catalytic performance can be attributed to high content Ru-O species on the surface of small size Ru nanoparticles, which undergo reduction with formation of water and aldehyde and easy oxidation cycles during the reaction according to the Mars–van Krevelen mechanism. The presence of surface oxide layer over small size Ru nanoparticles suppresses over-oxidation of aldehydes to acids.

---

This chapter is based on the following publication:

*J.P. Zhao, W.Y. Hernández, W.J. Zhou, Y. Yang, E. I. Vovk, M. Capron\*, V. Ordonsky\*, ChemCatChem, 2019. [doi.org/10.1002/cctc.201901249](https://doi.org/10.1002/cctc.201901249)*

### 3.1 Introduction

The selective conversion of alcohols to carbonyl compounds is one of the most important processes in organic chemistry <sup>1</sup>. Traditionally, alcohols have been selectively oxidized into aldehydes or ketones by the use of costly and highly toxic stoichiometric reagents such as iodine <sup>2</sup>, manganese <sup>3-4</sup> or chromium oxide <sup>5</sup>, generating high amount of environmentally hazardous metal and organic solvent waste. As continuation of this strategy, several organic molecules such as TEMPO and DDQ have been implemented for selective oxidation of alcohols <sup>6-7</sup>. However, the process is not catalytic and requires regeneration of these molecules for further use in oxidation. Additional problem is recovery of dissolved oxidant from the product solution.

In order to solve these problems, different heterogeneous catalytic systems based on metal catalysts using Pt <sup>8-9</sup>, Pd <sup>10-11</sup>, Au <sup>12-13</sup> have been proposed for selective oxidation of alcohols. These catalytic systems are usually efficient in the selective oxidation of aromatic and activated allylic alcohols but less active and selective for oxidation of aliphatic and especially primary alcohols. In solvent free conditions the selectivity to aldehyde during oxidation of primary alcohols, e.g. 1-octanol, usually has not exceed 40 % at about 50 % of alcohol conversion <sup>14</sup>.

Among metallic catalyst Ru has been shown to be quite efficient in oxidation reactions <sup>15</sup>. However, the selective oxidation of aliphatic alcohols to aldehyde or ketone over heterogeneous systems is still a challenging problem due to formation of corresponding acids and esters <sup>16-17</sup>. Different types of supports such as Al<sub>2</sub>O<sub>3</sub> <sup>18</sup>, CeO<sub>2</sub> <sup>19-20</sup>, ZrO<sub>2</sub> <sup>21-22</sup> and SiO<sub>2</sub> <sup>23</sup> have been used for the preparation of the catalysts by incipient wetness impregnation for oxidation of aliphatic alcohols. Kaneda proposed the Ru hydrotalcite catalysts <sup>24</sup> in the selective oxidation of activated aromatic and allylic alcohols to aldehydes and ketones under atmospheric pressure. However, oxidation of aliphatic alcohols resulted in the synthesis of corresponding acids. Mixed Ru–Co binary oxides prepared by co-precipitation have been reported for selective oxidation of primary alcohols to corresponding aldehydes with 83 % selectivity at 52 % conversion. Nevertheless, the reaction was conducted in large excess of toluene as a solvent, low TOF numbers (1.4 h<sup>-1</sup>) and in the presence of 2,6-di-tert-butyl-p-cresol as a radical scavenger <sup>25</sup>. Prati <sup>26</sup> discovered that bimetallic Au-Ru catalysts supported on activated carbon showed a higher activity with respect to the monometallic

counterparts. Both monometallic Ru and bimetallic Ru-Au catalysts demonstrated high selectivity to aldehyde during oxidation of octanol; however, the reaction has been performed at very mild conditions (80 °C), using a toluene/octanol ratio equal to 10. The high selectivity in oxidation of aliphatic alcohols to aldehydes at similar conditions with a high excess of toluene has been attained over monomeric Ru<sup>3+</sup> cation coordinated with 4 oxygen atoms and 1 chlorine<sup>27</sup>. Comparable catalytic performances have been found on the zeolite supported nano-sized RuO<sub>2</sub><sup>28</sup>.

The application of different alcohols and oxidation conditions for Ru based catalysts makes difficult the identification of the key factors affecting the catalytic performance of the selective oxidation process. Size and support effects have been identified as the main parameters affecting activities and selectivities in different reactions, such as oxidation of CO<sup>29</sup>.

In this work, we have studied particle size and support effect on alcohols oxidation over Ru NP-based catalysts. Uniform non supported Ru NPs with a controlled size from 2 to 9 nm were synthesized by microemulsion method. The NPs have been systematically studied by different physicochemical methods with subsequent analysis of the catalytic performance in oxidation of primary and secondary alcohols. The high selectivity to carbonyl compounds has been attained over small size non-supported Ru nanoparticles. The effect has been assigned to high content RuO<sub>x</sub> species on the surface of small size Ru nanoparticles oxidizing alcohols according to Mars–van Krevelen mechanism.

## 3.2 Results and Discussion

### 3.2.1 Synthesis and characterization of Ru NPs

Water-in-oil microemulsions with water droplets formed by reverse micelles dispersed in continuous hexanol phase have been used for the synthesis of metal nanoparticles. The hexanol-CTAB-water phase diagram shows that microemulsion exists in a certain compositional range (**Figure 3-1**). The reverse micelle sizes have been controlled by amount of water with dissolved Ru salt in a certain compositional range of hexanol-CTAB-water phase diagram. This method was used earlier for the synthesis of different size metal nanoparticles of Pt, Pd and Ni<sup>30-32</sup>. **Table 3-1** demonstrates the compositions with different water content for the synthesis of metal

nanoparticles.

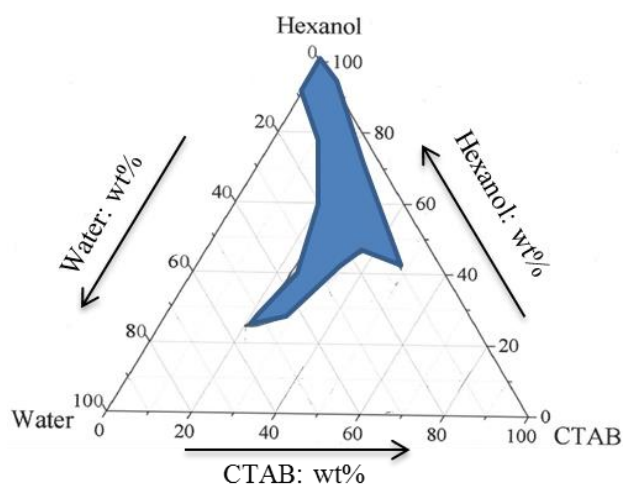
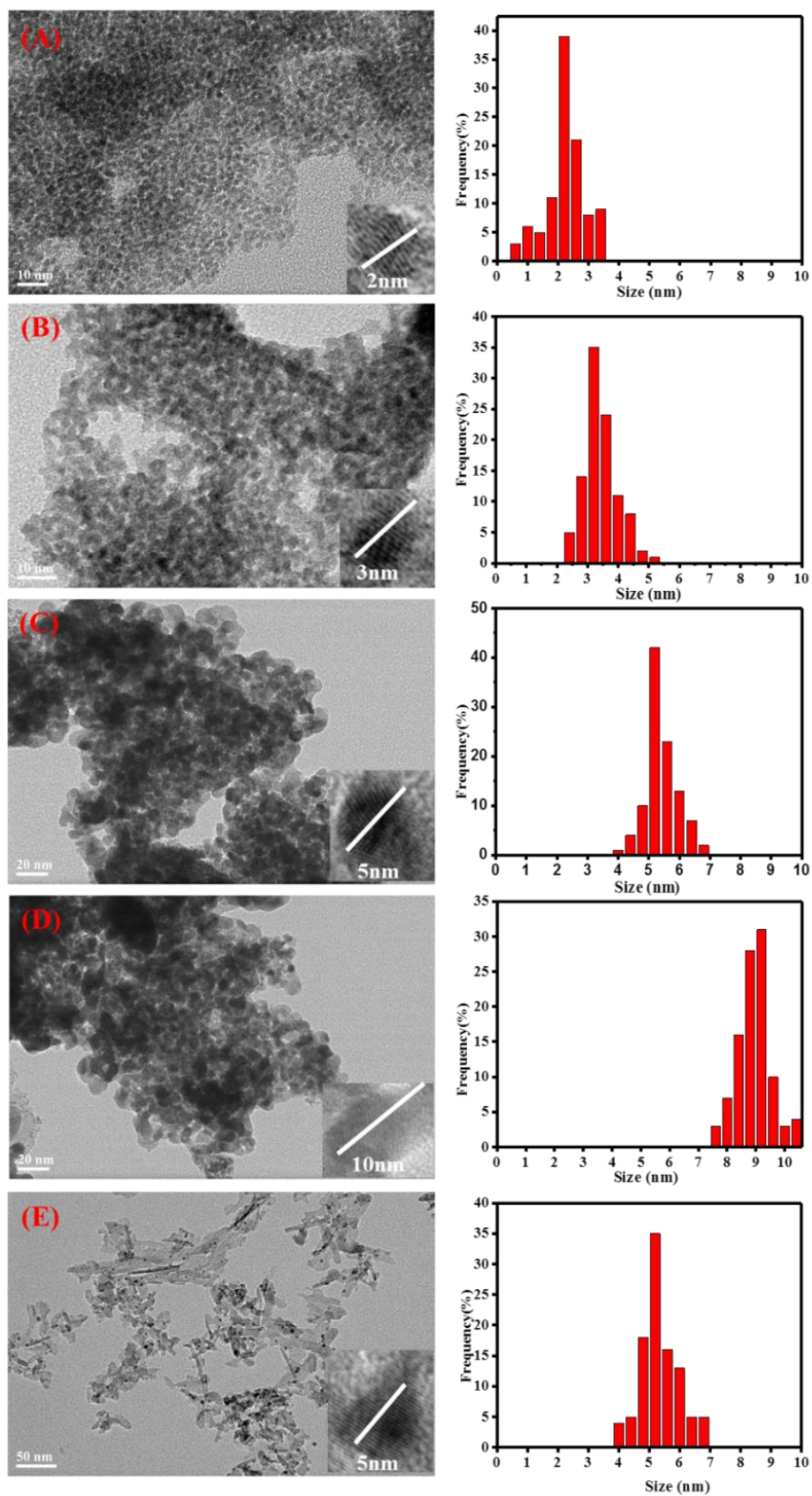


**Figure 3-1.** Phase diagram for CTAB/Hexanol/Water systems with blue zone of microemulsion composition.

**Table 3-1.** Different emulsion ratios to prepare m-Ru catalysts

CTAB, g	Hexanol, g	Water, g	$n_{CTAB}/n_{hexanol}$ , molar ratio	Concentration of water, %	Catalysts
5	4.5	0.5	0.31	5	m-Ru-5
4.7	4.3	1		10	m-Ru-10
4.2	3.8	2		20	m-Ru-20
2.9	2.6	4.5		45	m-Ru-45

The TEM images and histograms shown in **Figure 3-2** indicate uniform spherically shape aggregated nanoparticles in all the synthesized Ru NPs. A series of Ru NPs with the diameter of 2, 3, 5 and 9 nm were synthesized with water contents of 5, 10, 20 and 45 % in microemulsion, respectively. The average particle size is displayed in **Table 3-2**. Synthesis of smaller size Ru nanoparticles ( $\approx 1$ nm) requires organic ligands with N and S as stabilizers as has been demonstrated by the group of Chaudret <sup>33</sup>. The reference catalyst Ru/Al<sub>2</sub>O<sub>3</sub> contains Ru nanoparticles with the sizes about 5 nm (**Figure 3-2**).

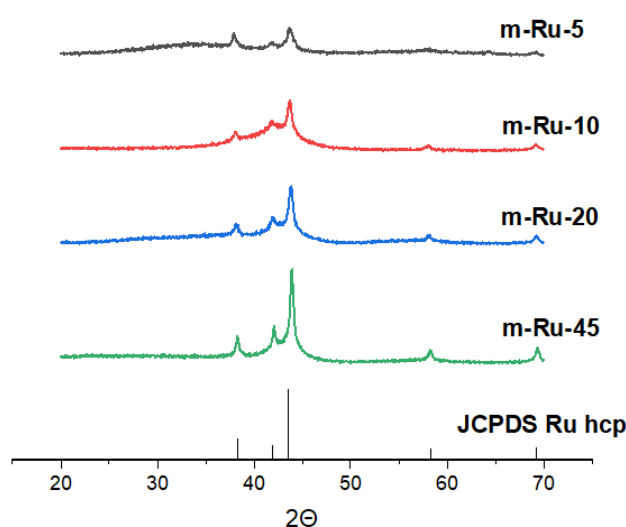


**Figure 3-2.** TEM images of Ru nanoparticles: *m*-Ru-5 (A), *m*-Ru-10 (B), *m*-Ru-20 (C), *m*-Ru-45 (D) and Ru/Al<sub>2</sub>O<sub>3</sub> (E)

**Table 3-2.** Characterization of metal nanoparticles

Samples	TEM	XRD		Pulse adsorption, mmol/g <sub>Ru</sub>		Surface area m <sup>2</sup> /g	XPS Binding energy (eV)			Zeta potential (mV)
		<i>D</i> (nm)	<i>I</i> <sub>(100)/<i>I</i><sub>(101)</sub></sub>	<i>O</i> <sub>2</sub>	<i>CO</i>		<i>Ru</i> <sup>0</sup> 3 <i>p</i> <sub>3/2</sub>	<i>RuO</i> <sub>x</sub> 3 <i>p</i> <sub>3/2</sub>	<i>I</i> <sub><i>RuO</i><sub>x</sub>/<i>Ru</i></sub>	
<b>m-Ru-5</b>	2.2	0.64	1.104	0.045	81	462.3	464.9	0.46	-37	
<b>m-Ru-10</b>	3.2	0.36	0.989	0.046	73	462.1	464.8	0.38	-32	
<b>m-Ru-20</b>	5.2	0.27	0.597	0.067	44	461.8	464.6	0.27	-19	
<b>m-Ru-45</b>	8.8	0.26	0.359	0.085	26	461.2	464.1	0.21	-3	
<b>Ru/Al<sub>2</sub>O<sub>3</sub></b>	5.2	-	0.67	0.117	49	461.8	464.4	0.25	-13	

XRD patterns of the prepared Ru NPs are displayed in **Figure 3-3**. All the materials were characterized by the presence of diffraction peaks at 38.4 °, 42.2 °, 43.8 °, 58.2 ° and 69.4 2θ, corresponding to the diffraction of (100), (002), (101), (102) and (110) planes of the hexagonal close-packed (hcp) Ru metal, respectively (ICDD-JCPDS card No. 06-0663).

**Figure 3-3.** Powder XRD patterns of different sizes of *m*-Ru catalysts

Despite the structural similarities of the studied materials, there is a clear difference in the relative intensity of the (100) crystallographic plane in *m*-Ru-5 nanoparticles, as well as its position. As can be seen in **Figure 3-3** and **Table 3-2**, the relative intensity of the (100) plane in *m*-Ru-5 is much higher than that observed in the other materials. In fact, the favored exposure of this crystallographic plane decreases with increase of the size of nanoparticles reaching minimal  $I_{(100)}/I_{(101)}$  ratio

for m-Ru-45 material. Besides, the (100) pattern shifts to lower angles as the particle size decreases from 38.4 ° for m-Ru-45 to 37.9 ° for m-Ru-5. These variations in intensity and position of the (100) plane could be related to the distortion of the crystallographic structure of metallic ruthenium, as a consequence, of the decreased particle size. Higher contribution of low-index (100) surface in small nanoparticles is the result of its low surface energy in comparison with other planes<sup>34</sup>.

In addition, external surface of metal nanoparticles has been studied by O<sub>2</sub> chemisorption experiments. The surface area of Ru nanoparticles defined by chemisorbed O<sub>2</sub> according to the method described earlier<sup>35</sup> with an average Ru/O chemisorption stoichiometry 1 is reported the **Table 3-2**. The results show full correlation of adsorbed O<sub>2</sub> amount with sizes of metal nanoparticles measured by TEM.

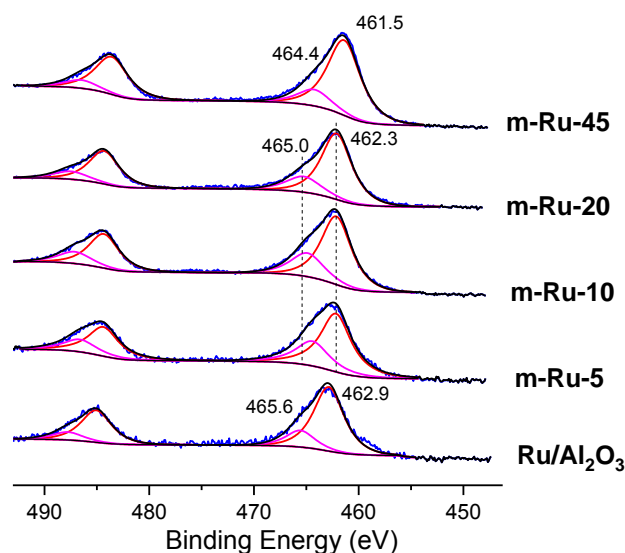


**Figure 3-4.** Ru 3p XPS spectra of the catalysts

Ex-situ XPS Ru 3p analysis was performed to further investigate the electronic state of the ruthenium species in the samples (**Figure 3-4**). Morgan in his work<sup>36</sup> has analyzed various Ru species including metallic Ru, RuO<sub>2</sub> and Ru(OH)<sub>3</sub> demonstrating different Ru 3p<sub>3/2</sub> BEs. Ru 3p<sub>3/2</sub> with BE 461 – 462 eV peak is associated with metallic state while Ru<sup>n+</sup> species demonstrate a 462.5 – 465 eV peak<sup>37</sup>. Shen with coauthors have reported the Ru 3p spectra during direct oxidation of metallic Ru: the oxide related 3p doublet appears at about 3 eV higher BE<sup>38</sup>. XPS spectra in **Figure 3-4** also show presence of ruthenium in two oxidation states: metallic Ru (Ru 3p<sub>3/2</sub> BE 461.5 – 462.9 eV) and species with lower electronic density, oxidized Ru<sup>n+</sup> (Ru 3p<sub>3/2</sub>

BE 464.4 – 465.6 eV). Taking into account that XRD shows the contribution of only metallic Ru phase this signal might be assigned to oxide/hydroxide dispersed over the surface of ruthenium nanoparticles. The contribution of ruthenium oxide/hydroxide species increases from 0.21 to 0.46 with decrease of the size of Ru nanoparticles (**Table 3-2**) most probably due to higher contribution of defected sites and easier oxidation of small size defected nanoparticles. The metallic Ru 3p doublet shifts to higher binding energy values with the decrease of the size of Ru nanoparticles (**Figure 3-4, Table 3-2**). The m-Ru-45 sample shows a Ru 3p doublet with  $3p_{3/2}$  peak binding energy 461.5 eV and the m-Ru-5 sample - 462.8 eV. This shift could be caused by final state effect coming from difference in atomic relaxation between bulk metals and metallic nanoparticles. The emitted photoelectrons are not immediately replaced for small size metal nanoparticles which leads to a net positive charge in the photoemission final state<sup>39</sup>. Similar behavior has been also reported for Pd and Pt nanoparticles<sup>40</sup>. In the case of the Ru supported catalyst (Ru/Al<sub>2</sub>O<sub>3</sub>), the Ru 3p doublet show the highest BE which could be explained by interaction of Ru nanoparticles with Lewis acid sites of alumina.

XPS analysis defines the metal electronic state under ultra-high vacuum conditions, however, the catalytic tests have been conducted in liquid medium. The charge of metal nanoparticles in liquid phase might affect the catalytic performance. Charge of metal nanoparticles affects their distribution in the reactor initiating its agglomeration. The zeta potential is widely used for quantification of the magnitude of the charge. The zeta potential is caused by the net electrical charge at the slipping plane. **Table 3-2** demonstrates zeta potentials for different size Ru nanoparticles and Ru/Al<sub>2</sub>O<sub>3</sub>. Small size nanoparticles have high negative charge potential (-37 mV for m-Ru-5) which decrease with increase of the size of metal nanoparticles till almost neutral for m-Ru-45. The presence of surface oxidized species for small size nanoparticles in agreement with XPS should lead to charging of metal nanoparticles by dissociation of Ru-O<sup>-</sup>H<sup>+</sup> species. Small metal nanoparticles with high surface area and surface energy have a tendency to aggregate with each other spontaneously<sup>41</sup> which may be prevented due to their charge repulsion<sup>42</sup>.

Low electronic density over small size Ru nanoparticles caused by Ru-O species should lead to changes in adsorption properties for the molecules sensitive to electronic density of the metal. In order to support this assumption, the pulse adsorption (**Table 3-2**) of CO has been studied over Ru nanoparticles and alumina

supported Ru catalyst. CO adsorption was low over smallest nanoparticles and increased for larger nanoparticles, which is totally reverse to adsorption of oxygen over metal nanoparticles (**Table 3-2**). The highest adsorption of CO was demonstrated over Ru supported over alumina. Low adsorption of CO over small size non supported Ru nanoparticles might be explained by presence of hydroxyl groups on defect sites which leads to lower electronic density over metal sites and also lower accessibility for CO.

The thermal stability of the m-Ru catalysts have been investigated by TGA (**Figure 3-5**). To confirm the impurity, Figure 3-5A compared fresh m-Ru-45 catalyst washed by 1 time (line a), by 3 times (line b), and the one after reaction (line c). The data shows weight losses in roughly two steps. Within the scope of 25~100 °C, the weight losses (5 wt%) are ascribed to the adsorbed water. The major weight loss was observed between 200 °C and 300 °C that could correspond to desorption or decomposition of the organic phases. The additive washing leads to a decreased weight loss with 70 wt% losses after one cycle washing and only 35 wt% after 3 cycles. Especially, it was found that line b and c manifested disparate weight losses in the range of 150~220 °C and line c presented a higher initial temperature for losses, which could be separately interpreted by the diverse capping, 1-hexanol (boiling point ~157 °C) and mixed octanol & octanal (boiling point ~180 °C). Meanwhile, **Figure 3-5B** revealed the heat flow changes in the process, representing the characteristics of desorption transition. The curves showed that the endothermic peaks at 180 °C and 210 °C which illustrated that the cappings of Ru NPs are mostly 1-hexanol (boiling point ~157 °C) and little amount of CTAB (melting point ~240 °C). **Figure 3-5C** declared that the catalyst after calcination in inert atmosphere could remove the impurity completely so that no weight losses came up. And metallic Ru Nps was oxidized above 300 °C under air with an increase weight of ~22% to gain RuO<sub>2</sub>. It can be seen that smaller particles m-Ru-5 were much easier to be oxidized by initial surface oxidation at 300 °C and then faster increasing weight after 400 °C than m-Ru-45 at 600 °C, which coincides with the high surface energy and activity.

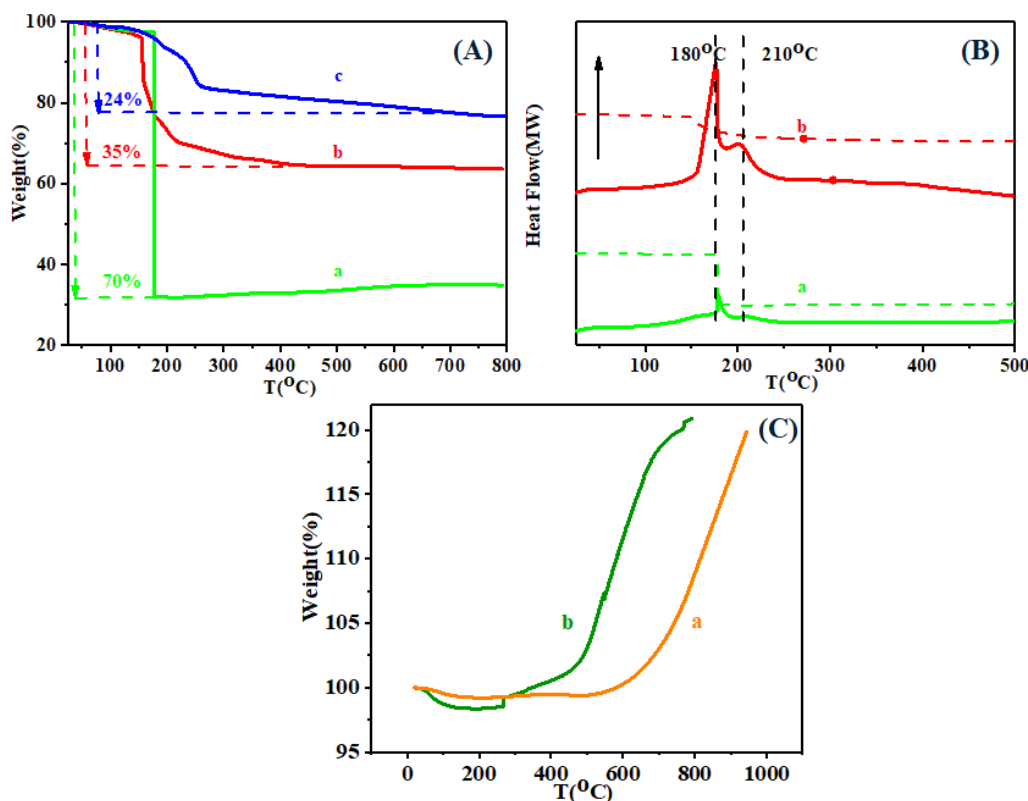


**Figure 3-5.** DSC-TGA spectra. (A) a: *m*-Ru-45 catalyst after washing by 1 time; b: *m*-Ru-45 catalyst after washing by 3 times; c: *m*-Ru-45 catalysts after reaction; and all samples are tested in  $N_2$  atmosphere; (B) the heat flows of *m*-Ru-45 washed by 1 time (line a) and 3 times (line b) in  $N_2$  atmosphere; (C) *m*-Ru-45 (line a) and *m*-Ru-5 (line b) catalysts after calcination are tested in air.

### 3.2.2 Catalytic oxidation of alcohols

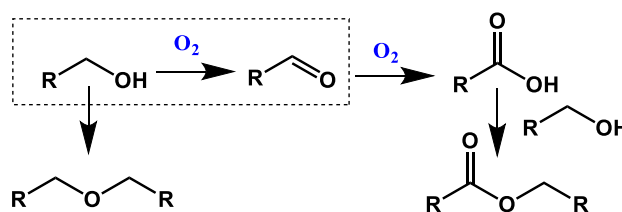


**Figure 3-6.** Scheme of the reaction of alcohols oxidation. Reaction conditions: 3.0 g 1-octanol, 50.0 mg catalysts, 10 bar  $O_2$ , 100 °C and solvent-free.

1-octanol has been commonly used as a model aliphatic alcohol for oxidation reactions. The catalytic performance of 1-octanol to 1-octanal oxidation was investigated using pure oxygen as an oxidant, at 100 °C. The main products of the reaction besides oxidation of alcohol to aldehyde involve deeper oxidation of aldehyde to octanoic acid with subsequent esterification to octyl octanoate (**Figure 3-6, 3-7**). Alcohol in the presence of acid also participates in etherification to dioctyl

ether.

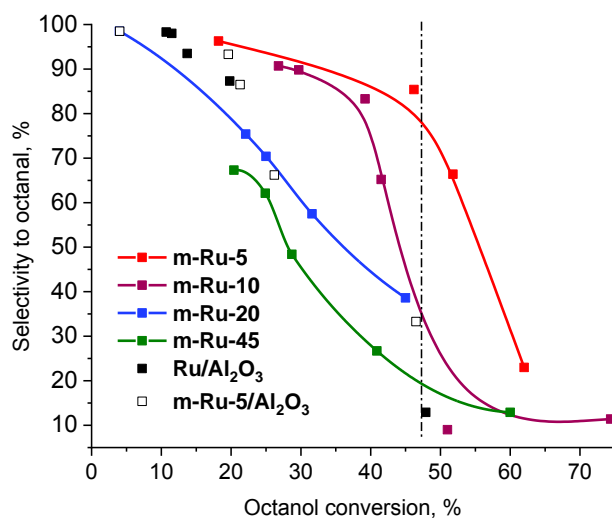


**Figure 3-7.** Selectivity to octanal versus octanol conversion for different size Ru nanoparticles and alumina supported catalysts (3.0 g 1-octanol, 30 mg catalysts, 10 bar O<sub>2</sub>, 100 °C and solvent-free).

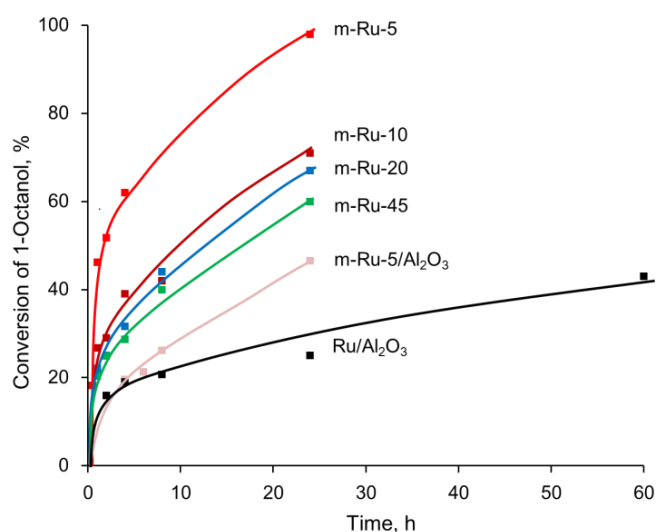


**Figure 3-8.** Activity comparison of different Ru nanoparticles and Ru/Al<sub>2</sub>O<sub>3</sub>.

**Figure 3-8** shows the activity comparison of different Ru nanoparticles and Ru/Al<sub>2</sub>O<sub>3</sub>. Smallest Ru nanoparticles m-Ru-5 demonstrates the highest activity in oxidation of octanol, which decreases significantly for larger metal nanoparticles. Normalization of initial activity by metal surface area defined by O<sub>2</sub> adsorption shows that TOF numbers are comparable for all catalysts and have value about 60 h<sup>-1</sup> (**Figure 3-9**) which demonstrates superiority in comparison with Ru-Co-hydroxyapatite<sup>43</sup> (TOF = 20 h<sup>-1</sup>), Ru<sub>0.35</sub>MnFe<sub>1.65</sub>O<sub>4</sub> (0.2 h<sup>-1</sup>)<sup>44</sup>,

$\text{RuO}_4^-/\text{polymer}$  ( $1.1 \text{ h}^{-1}$ )<sup>45</sup>,  $\text{Ru}_{0.3}\text{Co}_2\text{CeO}_x$  ( $2.5 \text{ h}^{-1}$ )<sup>44</sup>. It has to be noted that reference  $\text{Ru}/\text{Al}_2\text{O}_3$  and  $\text{m-Ru-5}/\text{Al}_2\text{O}_3$  catalyst have similar intrinsic activity. Thus, size of Ru nanoparticles does not demonstrate strong effect on TOF numbers of octanol oxidation to aldehyde.

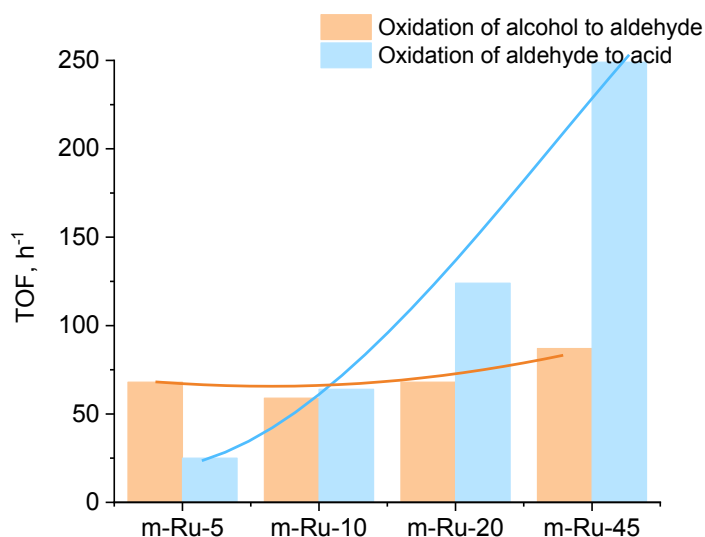


**Figure 3-9.** TOF numbers of octanol (3.0 g 1-octanol, 30 mg catalyst, 10 bar  $\text{O}_2$ , 100 °C) and octanal (0.5 g 1-octanal, 30 mg catalyst; air, 60 °C) oxidation over different size Ru nanoparticles.

The selectivity to 1-octanal decreases fast with increase of octanol conversion due to acid and ester formation (**Figure 3-7**, **Table 3-3**). The reference catalyst provides selectivity about 30 % to 1-octanal at 46 % conversion of octanol in solvent-free oxidation conditions, in a good agreement with previous literature reports<sup>46</sup>. Ru nanoparticles having similar particle size to  $\text{Ru}/\text{Al}_2\text{O}_3$  catalyst, i.e.  $\text{m-Ru-20}$ , provides higher selectivity to the target product at lower octanoic acid formation. In addition, the size decrease of Ru nanoparticles leads to gradual increase of the selectivity to octanal. For the smallest Ru nanoparticles, oxidation of octanol results in 85 % selectivity at 47 % conversion, which is 5-7 times higher in comparison with the largest metal nanoparticles and reference  $\text{Ru}/\text{Al}_2\text{O}_3$  catalyst. This selectivity is one of the best in comparison with solvent-free aliphatic alcohols oxidation<sup>47-48</sup>. In addition, it could be confirmed that the small Ru NPs has a good ability of recyclability in **Figure 3-10**.

Further selective oxidation of 1-octanol under these reaction conditions is hard to perform due to non-catalytic autoxidation of octanal by oxygen<sup>49</sup>. It is interesting to

note that impregnation of m-Ru-5 nanoparticles over alumina support leads to significant decrease of the selectivity in comparison with pure m-Ru-5, which makes it comparable with reference Ru/Al<sub>2</sub>O<sub>3</sub> catalyst. Thus, the properties of Ru metal nanoparticles are significantly changing in the presence of support.

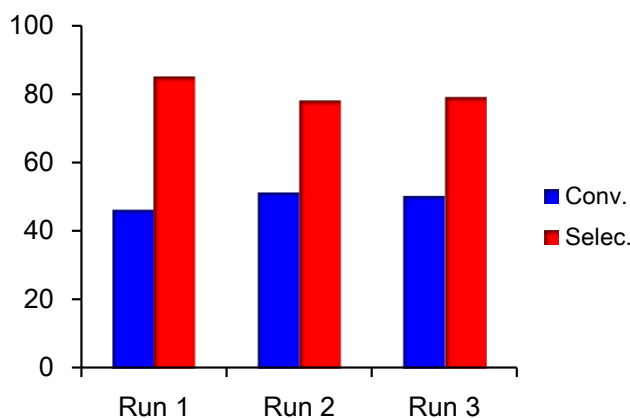


**Figure 3-10.** Recyclability of m-Ru-5 in oxidation of 1-octanol. Reaction conditions: 3.0 g 1-octanol, 50.0 mg catalysts, 10 bar O<sub>2</sub>, 100 °C and solvent-free.

**Table 3-3.** Catalytic performance in oxidation of 1-octanol (3.0 g 1-octanol, 30 mg catalysts, 10 bar O<sub>2</sub>, 100 °C and solvent-free, time 1-25 h)

Catalyst	Conv./%	Selec. / mol.%				TOF/h <sup>-1a</sup>
		1-Octanal	Octanoic acid	Octyl octanoate	Ether	
m-Ru-5	46	85	11	2	0	68
m-Ru-10	41	65	23	4	4	49
m-Ru-20	45	38	25	26	6	68
m-Ru-45	40	26	25	26	21	87
m-Ru-5/Al <sub>2</sub> O <sub>3</sub>	46	33	36	5	22	69
Ru/Al <sub>2</sub> O <sub>3</sub>	43	12	29	54	2	33

<sup>a</sup> The turnover frequency was calculated by the moles of 1-octanol converted per mole of Ru in the whole catalyst per hour, TOFs calculated was the point when reached for 2h.

From the results presented before, one could say that small size non-supported Ru nanoparticles suppress (or slow down) the deep oxidation of the formed aldehydes

towards carboxylic acid. In order to support this assumption we have performed octanal oxidation as model reaction. Mild reaction conditions were used in order to avoid non-catalytic oxidation (**Table 3-4**). In the absence of catalyst, almost no conversion of octanal was observed at 60 °C and air (instead of oxygen). The presence of Ru nanoparticles leads to fast conversion of octanal mainly to octanoic acid. Our results show significant increase of intrinsic activity in oxidation to acid with increase of the particle size. Thus, the TOF numbers increase 10 times from 25 to 249 h<sup>-1</sup> with increase of the particles sizes from m-Ru-5 to m-Ru-45, respectively (**Figure 3-9**). The ratio of TOF for oxidation of octanol to aldehyde to TOF for oxidation of octanal to acid decreases from 2.7 for m-Ru-5 to 0.3 for m-Ru-45.

**Table 3-4.** Oxidation of 1-octanal with different size m-Ru (1-octanal, 0.5 g; m-Ru, 30mg; solvent-free and air as oxidant at atmospheric pressure)

Catalysts	Aldehyde	Gas	T /°C	Time /h	Conv. /% 1-octanal to octanoic acid	TOF /h <sup>-1</sup> <sub>a</sub>
NA	1-octanal	Air	60	0.25	2	-
NA	1-octanal	Air	60	0.5	3	-
m-Ru-5	1-octanal	Air	60	0.5	22	25
m-Ru-10	1-octanal	Air	60	0.5	25	64
m-Ru-20	1-octanal	Air	60	0.5	29	124
m-Ru-45	1-octanal	Air	60	0.5	35	249
Ru/Al <sub>2</sub> O <sub>3</sub>	1-octanal	Air	60	3	24	77

As seen in **Figure 3-11**, the catalysts after reduction showed a better performance than the calcined and the blank ones at the same conversion. The possible reason could be that the reduction process effectually deoxygenized fractional RuO<sub>2</sub> to metallic Ru and then improve the activity and selectivity; while the calcination treatment gave rise to the agglomeration of particles to some extent which had a negative effect.

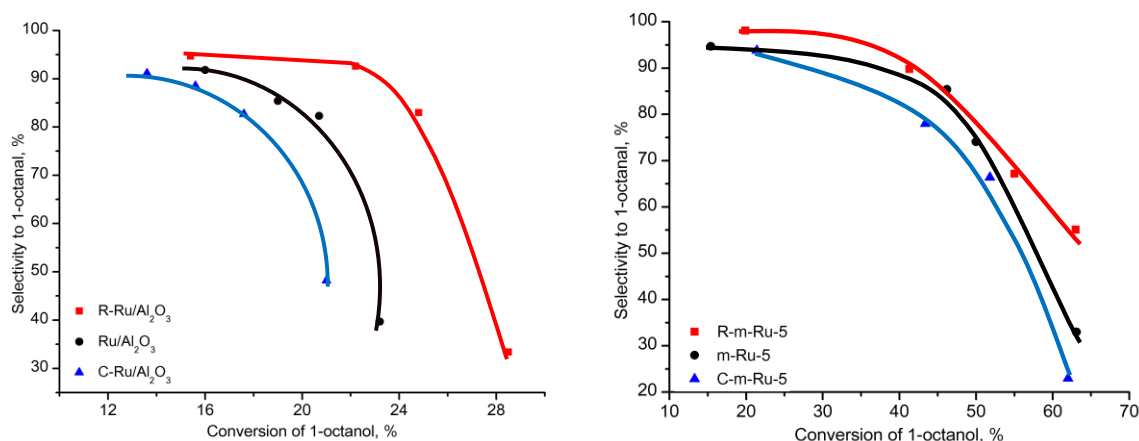


**Figure 3-11.** Reduction and calcination effects of catalysts in catalytic selective oxidation of 1-octanol. Reaction conditions: 3.0 g 1-octanol, 50.0 mg catalysts, 10 bar O<sub>2</sub>, 100 °C and solvent-free.

### 3.2.3 Mechanism study

The presence of oxygen species on the surface of small-size Ru nanoparticles could be responsible for the improved selectivity observed in the oxidation of alcohols to carbonyls. In order to verify if this oxygen could be involved in oxidation of alcohols we have performed catalytic test using Ru nanoparticles with different sizes under inert atmosphere. **Figure 3-12** demonstrates the results of these tests for several cycles over m-Ru-5 and m-Ru-45. The first cycle leads to appearance of octanal as the only product of the reaction. The amount of the product is the highest for m-Ru-5 nanoparticles and decreases for m-Ru-45. The amount of product corresponds well to the surface content of oxygen species determined by XPS analysis. The second cycle after filtration of the catalyst at room temperature does not show any production of aldehyde over large and small nanoparticles (**Figure 3-12**).

Analysis of XPS spectra after reaction shows strong increase of the contribution of metallic phase, which clearly indicates on the oxidation of alcohol by surface oxygen species located on the smallest Ru nanoparticles. This corresponds to a “low temperature” probably favored by the lability of the surface oxygen species in m-Ru-5 catalyst (**Figure 3-12**). Bulk RuO<sub>2</sub> and Ru(OH)<sub>3</sub> have been also tested in oxygen-free conversion of octanol; however, the amount of product was several orders of magnitude lower than amount of oxygen in the material (**Table 3-5**).

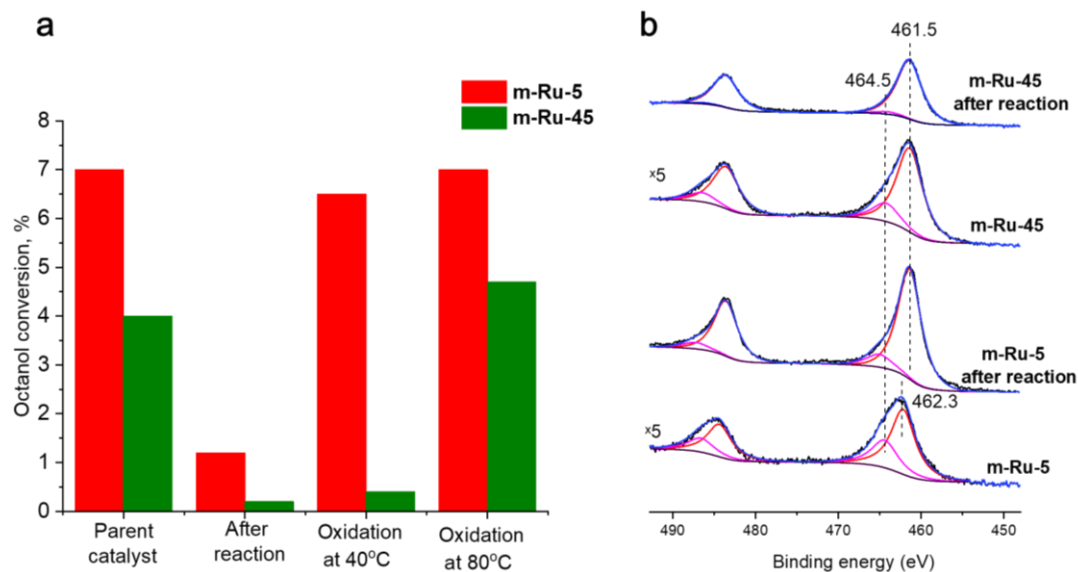


**Figure 3-12.** Conversion of octanol after cycles in inert atmosphere (0.3 g 1-octanol, 2 g toluene, 150 mg catalyst, 10 bar  $N_2$ , 100 °C, 4 h) using parent catalyst, catalyst after reaction and catalyst after reaction treated for 4 h at 40 and 80 °C (a) and Ru 3p XPS analysis of the parent catalysts and catalysts after reaction (b)

**Table 3-5.** Oxidation of 1-octanol in  $N_2$  atmosphere with different size m-Ru (1-octanol, 0.3 g; solvent toluene, 2 g; catalyst, 150 mg;  $N_2$  10 bar, 4 h, 100 °C)

Cycle number	Catalysts	Pretreatment / °C	Conv. /%	Amount of aldehyde / mmol <sup>a</sup>	Amount of $RuO_x$ / mmol <sup>b</sup>
1		-	7	0.161	
2	m-Ru-5	r.t.	1.2	0.027	0.683
3		40	6.5	0.15	
4		80	7.3	0.168	
1		m-Ru-45	-		
2	m-Ru-45	r.t.		0.005	0.312
3		40		0.009	
4		80		0.102	
1		$Ru(OH)_3$	-	3.8	
1	$RuO_2$	-	2.3	0.053	1.12

<sup>a</sup> The amount of aldehyde in the reactor has been calculated as amount of octanol (0.3 g) multiplied by conversion to aldehyde;

<sup>b</sup> The amount of  $RuO_x$  in the reactor has been calculated as amount of catalyst divided by atomic-weight and multiplied by  $I_{RuO_x/Ru}$  defined by XPS.

The mobility of oxygen in different materials has been studied using electrolysis for oxygen evolution reaction (OER), which is used for water electrolysis and metal

electro winning processes<sup>50</sup>. RuO<sub>2</sub> OER kinetic has demonstrated the highest activity of (100) and (110) orientation in comparison with (101) and (111) orientations. DFT calculations suggest under-coordinated Ru atoms on crystallized facets are active sites for the OER, the density of which correlates with activity on the four RuO<sub>2</sub> orientations. A Ru–O bond strength in under-coordinated RuO<sub>2</sub> of about 100 kJ/mol is much smaller than that of terminal O on other transition metal oxide<sup>51</sup>. It explains the ability of surface oxygen species over small size Ru nanoparticles with high contribution of (100) plane (**Figure 3-3**) to be easily reduced and oxidized in comparison with bulk RuO<sub>2</sub> and Ru(OH)<sub>3</sub>. The oxidation of alcohol in this case can be considered as reverse OER reaction where 2 -Ru-OH sites are oxidized to 2-RuO(OH) complex, which can be reduced afterwards by alcohol and dehydrated to 2 -Ru-OH.

Heating of m-Ru-5 to 40 °C for 4 h leads to recover of activity with production of comparable amount of aldehyde for subsequent cycles (**Figure 3-12**). The re-oxidation of metal surface has been supported by XPS analysis. However, treatment of m-Ru-45 at the same conditions does not show production of aldehyde for the second cycle, which indicates on less efficient re-oxidation in comparison with small size nanoparticles. Treatment in air at 80 °C leads to recover of catalytic activity for both small and large metal nanoparticles. Large size Ru nanoparticles require higher oxidation temperature. It means that re-oxidation of small size Ru nanoparticles is more efficient in comparison with large nanoparticles.

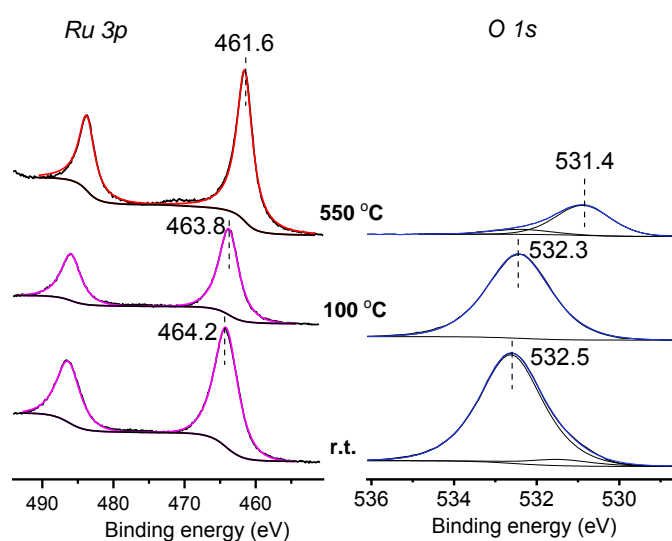


**Figure 3-13.** In-situ XPS Ru 3p and O 1s analysis of m-Ru-5 parent catalyst, after contact with ethanol and TPD.

The role of oxygen species over the surface of small size non-supported Ru nanoparticles has been additionally studied using in-situ XPS technique and ethanol as model alcohol compound. In this case, m-Ru-5 sample was placed on stainless steel sample holder, dried at room temperature and inserted in the spectrometer avoiding long interaction with atmosphere. **Figure 3-13** shows Ru 3p and O 1s spectra of m-Ru-5 nanoparticles after interaction with ethanol within spectrometer and after heating in vacuum. Ru 3p spectrum shows presence of RuO<sub>x</sub> species without metallic Ru which could be explained by deeper oxidation of Ru nanoparticles in contact with alcohol. O 1s spectrum of the sample demonstrates presence of the peak at 532.5 eV which is associated with oxygen in RuO<sub>2</sub> · xH<sub>2</sub>O and/or Ru(OH)<sub>3</sub><sup>37</sup>. The atomic O:Ru ratio calculated from O 1s and Ru 3p spectra for this sample is 4:1; it points on high concentration of H<sub>2</sub>O/OH<sup>-</sup> species on ruthenium surface. The in-situ treatment of the sample in ethanol vapor at 100 °C does not affect the O 1s spectrum sufficiently (it becomes more symmetric and slightly shifts to lower BE). At the same time, Ru 3p is shifted to lower BE by 0.6 eV still demonstrating the one state of ruthenium. This behavior can be associated with interaction of oxidized ruthenium and ethanol with the formation of surface intermediates. The subsequent heating to 550 °C shows significant shift in Ru 3p to 461.6 eV due to transformation of Ru<sup>n+</sup> to metallic Ru. At the same time, oxygen species disappear from the O 1s spectrum indicating strong reduction of Ru nanoparticles during thermo-desorption. The additional small peak at 531.4 eV is related to iron oxide from sample holder.

Simultaneous analysis of the desorbing species by mass-spectrometer during thermo-desorption shows several types of products besides desorption of ethanol (m/z=31) at the temperatures 250-300 °C. The signals of acetic acid (m/z=60) and acetaldehyde (m/z=29 and 15) prove oxidation of ethanol by surface oxide species during desorption from the surface of Ru nanoparticles. Additionally, CO (m/z=28) and CO<sub>2</sub> (m/z=44) signals indicates secondary decarbonylation and decarboxylation processes (**Figure 3-14**).

Traditionally oxidation of alcohols over noble metal catalyst proceed through formation of metal alkoxides and a metal hydride with subsequent desorption of aldehyde and regeneration of metal sites by oxidation of adsorbed hydrogen (oxidative dehydrogenation mechanism)<sup>52-53</sup>. On the other hand, Mars–van Krevelen mechanism has been proposed for nonprecious transition metal oxide catalysts (MnO<sub>x</sub>,

VO<sub>x</sub>) occurring at relatively high reaction temperatures (> 200 °C). In this case, reaction proceed also by formation of alkoxide with β-hydride elimination subtracted by the terminal oxygen group adjacent to the adsorbed alkoxy group with formation of water<sup>54-55</sup>. The lattice oxygen is subsequently substituted by aerobic oxygen.

The similar mechanism has been observed by Over in CO oxidation using RuO<sub>2</sub> (110) surface<sup>56</sup>. The authors observed high reactivity of the "O-rich" Ru surface in CO oxidation to CO<sub>2</sub> by presence of both metallic Ru and Ru covered by O for efficient adsorption of CO and reaction with nearby O to form CO<sub>2</sub>. The metallic sites are re-oxidized back to Ru-O species. It is interesting to note that in the group of Chaudret CO oxidation at room temperature over small size Ru NPs was suppressed due to over-oxidation to RuO<sub>2</sub><sup>57</sup>. The organic ligands have been used to protect metal surface from oxidation to RuO<sub>2</sub>. In our case, presence of alcohols in the liquid phase during oxidation could play the role of ligands protecting metal from full oxidation to oxide.

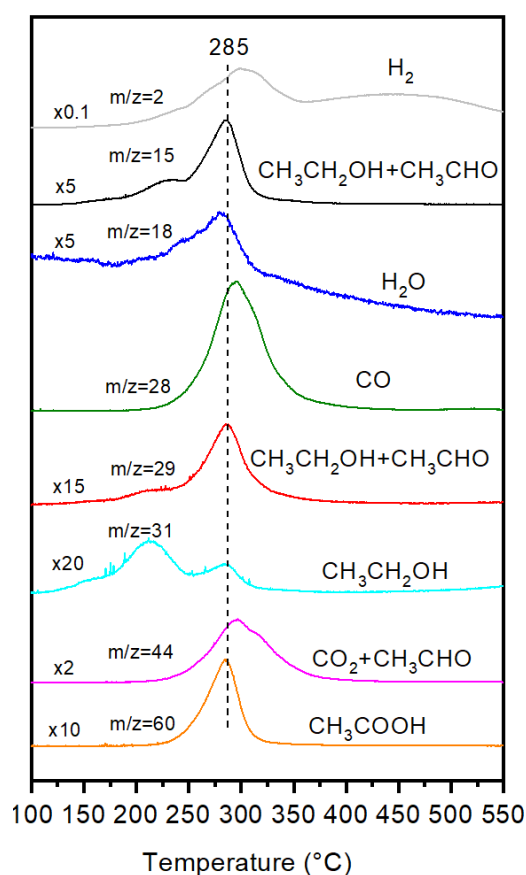


**Figure 3-14.** MS analysis of the products during TPD.

The similar mechanism could be proposed for oxidation of alcohols over small size Ru nanoparticles with formation of alkoxides over metal sites with subsequent

$\beta$ -hydride abstraction to nearby  $\text{RuO}_x$  species and elimination of water (**Figure 3-15**). The presence of both metallic Ru and  $\text{RuO}_x$  species in close proximity is important for this reaction. Pure  $\text{Ru}(\text{OH})_3$  or  $\text{RuO}_2$  could not provide oxidation of alcohols (**Table 3-5**). The high deficiency of surface Ru sites provides fast re-oxidation of the surface in comparison with large and supported nanoparticles (**Figure 3-15**). The presence of high content oxygen species on the surface of small size Ru nanoparticles confirmed by XPS (**Figure 3-4**) and Zeta potential (**Table 3-2**) protect them from adsorption and further oxidation of aldehydes and could be the main reason for high selectivity of alcohols oxidation to aldehydes over these catalysts (**Figure 3-15**).

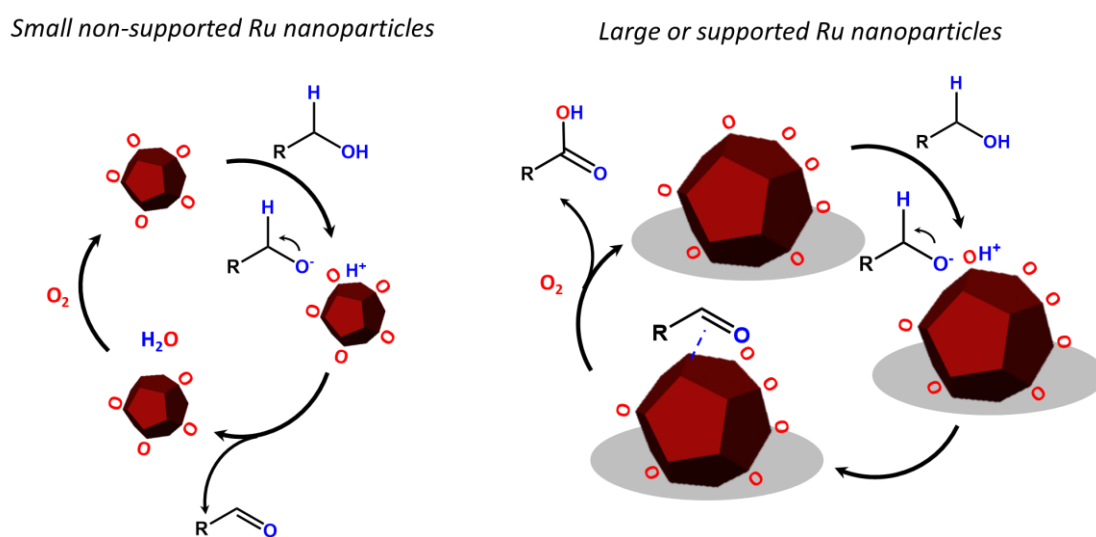


**Figure 3-15.** Mechanism of oxidation of alcohol over small size and large size supported Ru nanoparticles

### 3.3 Conclusion

In summary, we have developed a highly efficient method for oxidation of alcohols to aldehydes and ketones using small size non-supported Ru nanoparticles. A series of Ru nanoparticles with sizes in the range 2 to 9 nm have been prepared using microemulsion method and studied in oxidation of alcohols. Decrease of the particle sizes results in gradual increase of the selectivity of alcohols oxidation to aldehydes with the highest selectivity for the smallest 2 nm non-supported Ru nanoparticles. The small size Ru nanoparticles exhibit excellent selectivity (> 90 %) and activity for a wide range of different alcohols (aliphatic, aromatic and unsaturated) in the catalytic oxidation to aldehydes. The oxidation reaction is carried out under mild reaction conditions without solvent or using ethanol to dissolve solid substrate.

This effect is the result of high content of RuO<sub>x</sub> species on the surface of small Ru nanoparticles with fast re-oxidation of surface Ru atoms after oxidation of alcohols according to Mars–van Krevelen mechanism. Besides it, surface RuO<sub>x</sub> protects small size Ru nanoparticles from adsorption and deeper oxidation of aldehydes further to acids and concomitant ester formation.

### 3.4 References

1. D. I. Enache; J. K. Edwards; P. Landon; B. S. Espriu; A. F. Carley; A. A. Herzing; M. Watanabe; C. J. Kiely; D. W. Knight; Hutchings, G. J., Solvent-Free Oxidation of Primary Alcohols to Aldehydes Using Au-Pd/TiO<sub>2</sub> Catalysts. *Science* **2006**, *311* (5759), 362-365.
2. M. Uyanik; Ishihara, K., Hypervalent Iodine-mediated Oxidation of Alcohols. *Chem. Commun.* **2009**, *1*, 2086-2099.
3. Satoshi, I.; Koji, K.; Shigeru, I.; Teruaki, M., A New and Facile Method for the Direct Preparation of  $\alpha$ -Hydroxycarboxylic Acid Esters from  $\alpha,\beta$ -Unsaturated Carboxylic Acid Esters with Molecular Oxygen and Phenylsilane. *Chem. Lett.* **1990**, *19* (10), 1869-1872.
4. M. PERREE-FAUVET; GAUDEMER, A., Manganese Porphyrin-catalysed Oxidation of Olefins to Ketones by Molecular Oxygen. *J. Chem. Soc. Chem. Commun.* **1981**, *1282*, 874-875.
5. Muzart, J., Chromium-Catalyzed Oxidations in Organic Synthesis. *Chem. Rev.* **1992**, *92*, 113-140.
6. S. Ma; J. Liu; S. Li; B. Chen; J. Cheng; J. Kuang; Y. Liu, B. W.; Y. Wang; J. Ye; Q. Yu; W. Yuan; S. Yu, Development of a General and Practical Iron Nitrate/TEMPO-Catalyzed Aerobic Oxidation of Alcohols to Aldehydes/Ketones: Catalysis with Table Salt. *Adv. Synth. Catal.* **2011**, *353*, 1005 – 1017.
7. H. D. Becker; A. Bjork; Adler, E., Quinone Dehydrogenation. Oxidation of Benzylic Alcohols with 2,3-Dichloro-5,6-dicyanobenzoquinone. *J. Org. Chem.* **1980**, *45*, 1596-1601.
8. Jinho, O.; Saswati, D.; Hyunjoo, L., Selective Conversion of Glycerol to 1,3-Propanediol Using Pt-sulfated Zirconia. *Green Chem.* **2011**, *13* (8), 2004.
9. Zhai, W.; Xue, S.; Zhu, A.; Luo, Y.; Tian, Y., Plasmon-Driven Selective Oxidation of Aromatic Alcohols to Aldehydes in Water with Recyclable Pt/TiO<sub>2</sub> Nanocomposites. *ChemCatChem* **2011**, *3* (1), 127-130.
10. Parlett, C. M. A.; Bruce, D. W.; Hondow, N. S.; Lee, A. F.; Wilson, K., Support-Enhanced Selective Aerobic Alcohol Oxidation over Pd/Mesoporous Silicas. *ACS Catal.* **2011**, *1* (6), 636-640.
11. Hackett, S. F. J.; Brydson, R. M.; Gass, M. H.; Harvey, I.; Newman, A. D.; Wilson, K.; Lee, A. F., High-Activity, Single-Site Mesoporous Pd/Al<sub>2</sub>O<sub>3</sub> Catalysts for Selective Aerobic Oxidation of Allylic Alcohols. *Angew. Chem. Int. Ed.* **2007**, *46* (45), 8593-8596.
12. Tanaka, A.; Hashimoto, K.; Kominami, H., Preparation of Au/CeO<sub>2</sub> Exhibiting Strong Surface Plasmon Resonance Effective for Selective or Chemoselective Oxidation of Alcohols to Aldehydes or Ketones in Aqueous Suspensions under Irradiation by Green Light. *J. Am. Chem. Soc.* **2012**, *134* (35), 14526-14533.
13. Su, F. Z.; Liu, Y. M.; Wang, L. C.; Cao, Y.; He, H. Y.; Fan, K. N., Ga-Al

- Mixed-Oxide-Supported Gold Nanoparticles with Enhanced Activity for Aerobic Alcohol Oxidation. *Angew. Chem. Int. Ed.* **2008**, *120*, 340–343.
14. He, Y.; Feng, J.; Brett, G. L.; Liu, Y.; Miedziak, P. J.; Edwards, J. K.; Knight, D. W.; Li, D.; Hutchings, G. J., Oxidation of Aliphatic Alcohols by Using Precious Metals Supported on Hydrotalcite under Solvent- and Base-Free Conditions. *ChemSusChem* **2015**, *8* (19), 3314-3322.
  15. Davis, S. E.; Ide, M. S.; Davis, R. J., Selective Oxidation of Alcohols and Aldehydes over Supported Metal Nanoparticles. *Green Chem.* **2013**, *15* (1), 17-45.
  16. Schmidt, A. C.; Stark, C. B. W., TPAP-Catalyzed Direct Oxidation of Primary Alcohols to Carboxylic Acids through Stabilized Aldehyde Hydrates. *Org. Lett.* **2011**, *13*, 4164-4167.
  17. Gunanathan, C.; Milstein, D., Applications of Acceptorless Dehydrogenation and Related Transformations in Chemical Synthesis. *Science* **2013**, *341* (6143), 250-263.
  18. Zhao, G.; Ling, M.; Hu, H.; Deng, M.; Xue, Q.; Lu, Y., An Excellent Au/meso- $\gamma$ -Al<sub>2</sub>O<sub>3</sub> Catalyst for the Aerobic Selective Oxidation of Alcohols. *Green Chem.* **2011**, *13* (11), 3088.
  19. Ebitani, K.; Ji, H.-B.; Mizugaki, T.; Kaneda, K., Highly Active Trimetallic Ru/CeO<sub>2</sub>/CoO(OH) Catalyst for Oxidation of Alcohols in the Presence of Molecular Oxygen. *J. Mol. Catal. A: Chem.* **2004**, *212* (1-2), 161-170.
  20. Hosokawa, S.; Hayashi, Y.; Imamura, S.; Wada, K.; Inoue, M., Effect of the Preparation Conditions of Ru/CeO<sub>2</sub> Catalysts for the Liquid Phase Oxidation of Benzyl Alcohol. *Catal. Lett.* **2009**, *129* (3-4), 394-399.
  21. Kim, Y. H.; Hwang, S. K.; Kim, J. W.; Lee, Y. S., Zirconia-Supported Ruthenium Catalyst for Efficient Aerobic Oxidation of Alcohols to Aldehydes. *Ind. Eng. Chem. Res.* **2014**, *53* (31), 12548-12552.
  22. Yasu-eda, T.; Kitamura, S.; Ikenaga, N.; Miyake, T.; Suzuki, T., Selective Oxidation of Alcohols with Molecular Oxygen over Ru/CaO–ZrO<sub>2</sub> Catalyst. *J. Mol. Catal. A: Chem.* **2010**, *323* (1-2), 7-15.
  23. Clerick, S.; De Canck, E.; Hendrickx, K.; Van Speybroeck, V.; Van Der Voort, P., Heterogeneous Ru(III) Oxidation Catalysts via ‘click’ Bidentate Ligands on a Periodic Mesoporous Organosilica Support. *Green Chem.* **2016**, *18* (22), 6035-6045.
  24. Mori, K.; Satoko, K.; Takayoshi, H.; Tomoo, M.; Kohki, E.; Koichiro, J.; Kiyotomi, K., Development of Ruthenium-Hydroxyapatite-Encapsulated Superparamagnetic  $\gamma$ -Fe<sub>2</sub>O<sub>3</sub> Nanocrystallites as an Efficient Oxidation Catalyst by Molecular Oxygen. *Chem. Lett.* **2007**, *19*, 1249-1256.
  25. Musawir, M.; Davey, P. N.; Kelly, G.; Kozhevnikov, I. V., Highly Efficient Liquid-phase Oxidation of Primary Alcohols to Aldehydes with Oxygen Catalysed by Ru–Co Oxide. *Chem. Commun.* **2003**, *12*, 1414-1415.
  26. Prati, L.; F. Porta; Wang, D.; Villa, A., Ru Modified Au Catalysts for the Selective Oxidation of Aliphatic Alcohols. *Catal. Sci. Technol.* **2011**, *1* (9), 1624-1629.
  27. Yamaguchi, K.; Mori, K.; Mizugaki, T.; Ebitani, K.; Kaneda, K., Creation of a monomeric Ru species on the surface of hydroxyapatite as an efficient heterogeneous catalyst for aerobic alcohol oxidation. *J. Am. Chem. Soc.* **2000**, *122* (29), 7144-7145.
  28. ZHAN, B.-Z.; WHITE, M. A.; SHAM, T.-K.; PINCOCK, J. A.; DOUCET, R. J.; RAO, K. V. R.; ROBERTSON, K. N.; CAMERON, T. S., Zeolite-Confined Nano-RuO<sub>2</sub>: A Green, Selective, and Efficient Catalyst for Aerobic Alcohol Oxidation. *J. Am. Chem. Soc.* **2003**, *125*, 2195-2199.
  29. Joo, S. H.; Park, J. Y.; Renzas, J. R.; Butcher, D. R.; Huang, W.; Somorjai, G. A., Size Effect of Ruthenium Nanoparticles in Catalytic Carbon Monoxide Oxidation. *Nano Lett.* **2010**, *10* (7), 2709-2713.

30. Christophe, C.; Patrick, U.; Sylvain, B.; Stève, B., Colloidal Syntheses of Shape- and Size-Controlled Pt Nanoparticles for Electrocatalysis. *Electrocatalysis* **2012**, *3* (2), 75-87.
31. Chen, D.; Wu, S., Nanoparticle Size Control in Microemulsion Synthesis. *Chem. Mater.* **2000**, *12*, 1354-1360.
32. Chen, J.; Zhang, Q.; Wang, Y.; Wan, H., Size-Dependent Catalytic Activity of Supported Palladium Nanoparticles for Aerobic Oxidation of Alcohols. *Adv. Synth. Catal.* **2008**, *350* (3), 453-464.
33. Amiens, C.; Chaudret, B.; Ciuculescu-Pradines, D.; Colliere, V.; Fajerweg, K.; Fau, P.; Kahn, M.; Maisonnat, A.; Soulantica, K.; Philippot, K., Organometallic approach for the synthesis of nanostructures. *New J. Chem.* **2013**, *37* (11), 3374-3401.
34. Shen, X.; Garces, L. J.; Ding, Y.; Laubernds, K.; Zerger, R. P.; Aindow, M.; Neth, E. J.; Suib, S. L., Behavior of H<sub>2</sub> Chemisorption on Ru/TiO<sub>2</sub> Surface and its Application in Evaluation of Ru Particle Sizes Compared with TEM and XRD Analyses. *Appl. Catal. A: Gen.* **2008**, *335* (2), 187-195.
35. Rossetti, I.; Pernicone, N.; Forni, L., Characterisation of Ru/C Catalysts for Ammonia Synthesis by Oxygen Chemisorption. *Appl. Catal. A: Gen.* **2003**, *248* (1-2), 97-103.
36. Morgan, D. J., Resolving ruthenium: XPS studies of common ruthenium materials. *Surf. Interface Anal.* **2015**, *47* (11), 1072-1079.
37. Jamatia, R.; Gupta, A.; Mahato, M.; Patil, R. A.; Ma, Y.-R.; Pal, A. K., A Metalloprotein Inspired Ruthenium Complex as an Efficient and Reusable Catalyst for Selective Oxidation of Alcohols to their Corresponding Carbonyl Compounds. *ChemistrySelect* **2016**, *1* (18), 5929-5935.
38. J.Y. Shen; A. Adnot; Kaliaguine, S., An ESCA Study of the Interaction of Oxygen with the Surface of Ruthenium. *Appl. Surf. Sci.* **1991**, *51*, 47-60.
39. Roberts, F. S.; Anderson, S. L.; Reber, A. C.; Khanna, S. N., Initial and Final State Effects in the Ultraviolet and X-ray Photoelectron Spectroscopy (UPS and XPS) of Size-Selected Pd<sub>n</sub> Clusters Supported on TiO<sub>2</sub>(110). *J. Phys. Chem. C* **2015**, *119* (11), 6033-6046.
40. Felten, A.; Ghijsen, J.; Pireaux, J. J.; Drube, W.; Johnson, R. L.; Liang, D.; Hecq, M.; Van Tendeloo, G.; Bittencourt, C., Electronic Structure of Pd Nanoparticles on Carbon Nanotubes. *Micron* **2009**, *40* (1), 74-79.
41. T. López-Leoń; J. L. Ortega-Vinuesa; D. Bastos-González; Elaissari, A., Cationic and Anionic Poly(N-isopropylacrylamide) Based Submicron Gel Particles-Electrokinetic Properties and Colloidal Stability. *J. Phys. Chem. B* **2006**, *110*, 4629-4636.
42. Viau, G.; Brayner, R.; Poul, L.; Chakroune, N.; Fievet, F., Ruthenium Nanoparticles Size, Shape and Self-Assemblies. *Chem. Mater.* **2003**, *15*, 486-494.
43. Opre, Z.; Grunwaldt, J.; Maciejewski, M.; Ferri, D.; Mallat, T.; Baiker, A., Promoted Ru-hydroxyapatite: Designed Structure for Fast and Highly Selective Oxidation of Alcohols with Oxygen. *J. Catal.* **2005**, *230* (2), 406-419.
44. H. Ji; K.Ebitani; T. Mizugaki; Kaneda, K., Environmentally Friendly Alcohol Oxidation Using Heterogeneous Catalyst in the Presence of Air at Room Temperature. *Catal. Commun.* **2002**, *3*, 511-517.
45. B. Hinzen; R. Lenz; Ley, S. V., Polymer Supported Perruthenate (PSP) Clean Oxidation of Primary Alcohols to Carbonyl Compounds Using Oxygen as Cooxidant. *Synthesis* **1999**, *1*, 977-979.
46. Yamaguchi, K.; Mizuno, N., Scope, Kinetics, and Mechanistic Aspects of Aerobic Oxidations Catalyzed by Ruthenium Supported on Alumina. *Chem. Eur. J.* **2003**, *9*

(18), 4353-4361.

47. Sato, T.; Komanoya, T., Selective Oxidation of Alcohols with Molecular Oxygen Catalyzed by Ru/MnO<sub>x</sub>/CeO<sub>2</sub> under Mild Conditions. *Catal. Commun.* **2009**, *10* (7), 1095-1098.

48. Dulière, E.; Devillers, M.; Marchand-Brynaert, J., Novel Phosphinite–Ruthenium(II) Complexes Covalently Bound on Silica Synthesis, Characterization, and Catalytic Behavior versus Oxidation Reactions of Alcohols into Aldehydes. *Organometallics* **2003**, *22*, 804-811.

49. Sankar, M.; Nowicka, E.; Carter, E.; Murphy, D. M.; Knight, D. W.; Bethell, D.; Hutchings, G. J., The Benzaldehyde Oxidation Paradox Explained by the Interception of Peroxy Radical by Benzyl Alcohol. *Nat. Commun.* **2014**, *5*, 3332-3338.

50. Stoerzinger, K. A.; Diaz-Morales, O.; Kolb, M.; Rao, R. R.; Frydendal, R.; Qiao, L.; Wang, X. R.; Halck, N. B.; Rossmeisl, J.; Hansen, H. A., Orientation-dependent oxygen evolution on RuO<sub>2</sub> without lattice exchange. *ACS Energy Lett.* **2017**, *2* (4), 876-881.

51. Over, H., Surface chemistry of ruthenium dioxide in heterogeneous catalysis and electrocatalysis: from fundamental to applied research. *Chem. Rev.* **2012**, *112* (6), 3356-3426.

52. Choi, K.-M.; Akita, T.; Mizugaki, T.; Ebitani, K.; Kaneda, K., Highly selective oxidation of allylic alcohols catalysed by monodispersed 8-shell Pd nanoclusters in the presence of molecular oxygen. *New J. Chem.* **2003**, *27* (2), 324-328.

53. Stacchiola, D.; Burkholder, L.; Tysoe, W. T., Enantioselective chemisorption on a chirally modified surface in ultrahigh vacuum: adsorption of propylene oxide on 2-butoxide-covered palladium (111). *J. Am. Chem. Soc.* **2002**, *124* (30), 8984-8989.

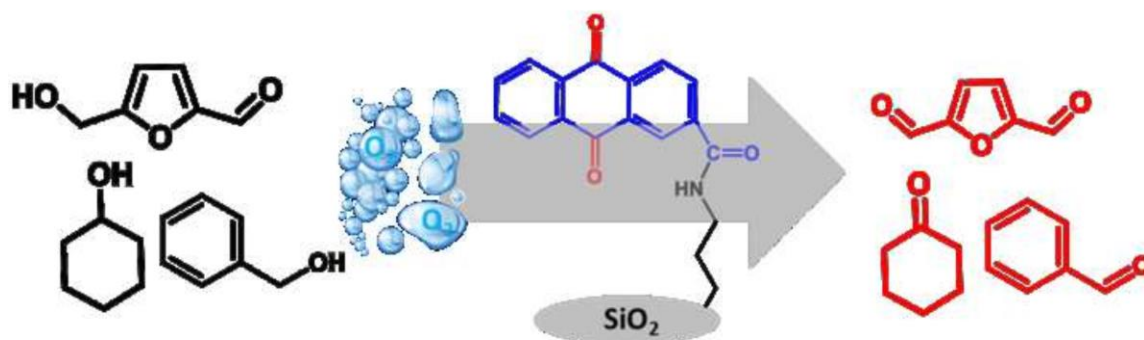
54. Arends, I. W.; Sheldon, R. A.; Wallau, M.; Schuchardt, U., Oxidative transformations of organic compounds mediated by redox molecular sieves. *Angew. Chem. Int. Ed. Engl.* **1997**, *36* (11), 1144-1163.

55. Yang, T.-j.; Lunsford, J. H., Partial oxidation of methanol to formaldehyde over molybdenum oxide on silica. *J. Catal.* **1987**, *103* (1), 55-64.

56. Over, H.; Kim, Y. D.; Seitsonen, A. P.; Wendt, S.; Lundgren, E.; Schmid, M.; Varga, P.; Morgante, A.; Ertl, G., Atomic-Scale Structure and Catalytic Reactivity of the RuO<sub>2</sub>(110) Surface. *Science* **2000**, *287* (5457), 1474-1476.

57. Novio, F.; Monahan, D.; Coppel, Y.; Antorrena, G.; Lecante, P.; Philippot, K.; Chaudret, B., Surface chemistry on small ruthenium nanoparticles: evidence for site selective reactions and influence of ligands. *Chem. Eur. J.* **2014**, *20* (5), 1287-1297.

# CHAPTER 4 Non-metallic Aerobic Oxidation of Alcohols over Anthraquinone Based Compounds



---

## ABSTRACT:

The catalytic performances of substituted anthraquinones were investigated in catalytic oxidation of alcohols like cyclohexanol, benzyl alcohol and 5-hydroxymethylfurfural (HMF) to carbonyl compounds (cyclohexanone, benzyl aldehyde and diformylfuran). The reaction proceeds at relatively mild conditions (130 °C, 10 bar O<sub>2</sub>) with strong effect of oxygen pressure on the activity. The reduction potential of anthraquinone plays the key role in the oxidation reactions. TOF numbers and selectivities to carbonyl compounds pass through the maximum with increase of the reduction potential. The maximum activity and selectivity (>80 %) is observed for sulfonated and carboxylated anthraquinones having intermediate reduction potentials ( $\approx$  0.1-0.2 V vs SHE). Grafted 2-carboxyanthraquinone catalyst has demonstrated comparable catalytic performance to the parent molecule and might be used as heterogeneous catalyst. The oxidation reaction was found to have radical character with transfer of hydrogen from alcohol to anthraquinone and subsequent oxidation of hydrogenated anthraquinone by oxygen.

---

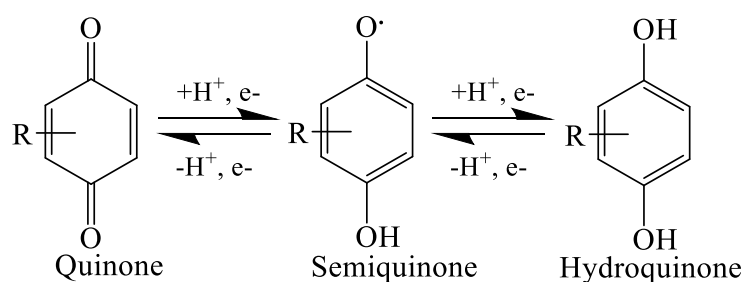
This chapter is based on the following publication:

*J.P. Zhao, D. Wu, W. Y. Hernández, W.J. Zhou, M. Capron\* and V. V. Ordonsky\*,  
Appl. Catal. A-Gen. 2019, doi.org/10.1016/j.apcata.2019.117277*

## 4.1 Introduction

Green and selective oxidation techniques are highly important in the chemical industry, especially in the transformation of alcohols to the carbonyl compounds which can sequentially constitute important intermediates for the production of fine and bulk chemicals like amines, imines, acetals, polymers etc. A large number of oxidants have been reported in the literature and most of them are based on transition metal oxides, such as oxides of chromium and manganese<sup>1</sup> that incidentally creates issues related to handling and disposal. For this purpose, many heterogeneous and homogenous catalysts have been developed on the basis of noble metals such as Pt, Ru, Pd, Au, and Ag for oxidation of alcohols using oxygen and hydrogen peroxide as terminal oxidant<sup>2-6</sup>. Utilization of metallic catalysts creates serious problems related to over oxidation of aldehydes to acids, high cost of metal and its potential leaching<sup>7</sup>.

To achieve more productive processes, researchers have paid a lot of attention to non-metallic systems, mainly including TEMPO and its derivative systems<sup>8</sup> that are efficiently used on industrial scale for dehydrogenation of alcohols selectively to aldehydes and ketones<sup>9</sup>. *In-situ* regeneration of nitroxyl radical is the main challenge for TEMPO application as a catalyst. For example, a system based on TEMPO and  $\text{Mn}(\text{NO}_3)_2\text{-Co}(\text{NO}_3)_2$  was reported<sup>10</sup> to provide oxidation of both aliphatic and aromatic alcohols at mild reaction conditions, however, it requires very diluted alcohol solutions in acetic acid and deactivates in time.



**Scheme 4-1.** Three accessible oxidation states of quinones molecules.

Similar to nitroxyl radicals, quinone molecules provide three readily accessible oxidation states<sup>11</sup>, namely, fully oxidized quinone, one-electron-reduced semiquinone, and two-electron-reduced hydroquinone (**Scheme 4-1**).

Stoichiometric dehydrogenation of alcohols by electron deficient quinone molecules like DDQ (*i.e.* 2,3-Dichloro-5,6-dicyano-1,4-benzoquinone) has been studied in numerous works<sup>12-13</sup>. However, it leads to costly two-step process with

necessary DDQ separation and regeneration. Several alternative strategies have been proposed to avoid it using co-oxidants also known as electron transfer mediators like  $\text{FeCl}_3$  and  $\text{Mn}(\text{OAc})_3$  for re-oxidation of hydrogenated DDQ<sup>14-16</sup>. Thus, it solves the problem of continuous utilization of DDQ as oxidant but produces large amount of waste. Several strategies have been proposed to mediate oxidation of hydroquinones by using heterogeneous or homogeneous co-catalysts such as metal nanoclusters or polyoxometalates<sup>17-19</sup>. The efficient oxidation of activated alcohols has been reported over DDQ using NO and  $\text{tBuNO}_2$  to facilitate hydroquinone regeneration<sup>20-21</sup>. However, all these routes involve presence of aggressive and non-environmentally friendly compounds which restricts the wide application of these processes in industry. Recently they have been used for photooxidation of alcohols to obtain carboxylic acids and aldehydes/ketones in an air atmosphere<sup>22</sup>. However, the productivity of this system was low and accompanied by deactivation of the anthraquinone catalyst.

The advantage of anthraquinones in comparison with DDQ is lower reduction potential which could result in in-situ regeneration of these molecules during oxidation of alcohols. Although a lot of research has been devoted to investigation of different anthraquinones as hydrogen acceptors in electrochemistry<sup>23</sup> or intermediate molecule for hydrogen peroxide synthesis<sup>24</sup> there is no information about anthraquinones as catalytic material in oxidation reactions.

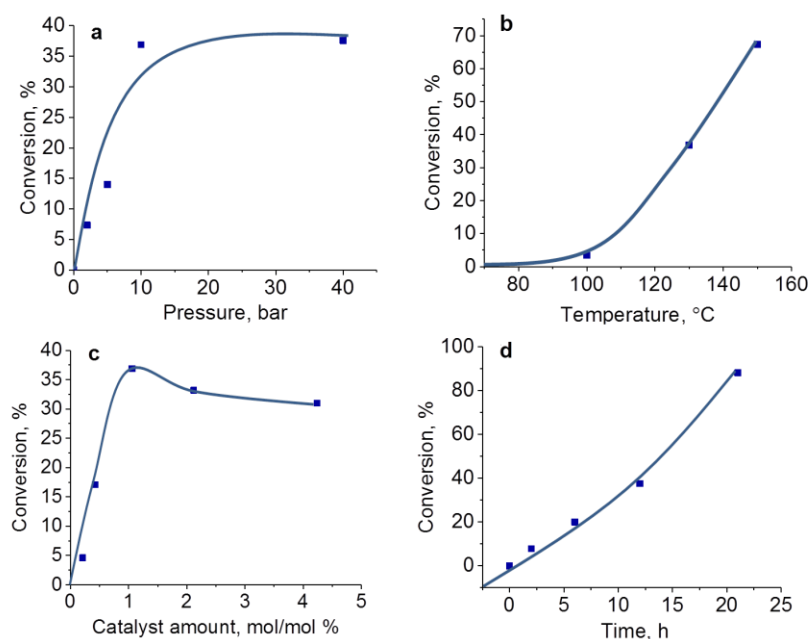
Herein, we demonstrate efficient application of homogeneous and heterogenized non-metallic substituted 9,10-anthraquinones catalyst for selective oxidation of alcohols (*i.e.*, cyclohexanol, benzyl alcohol and HMF). Oxygen is employed as terminal oxidant for oxidative regeneration of quinones, which is cheap and eco-friendly solution for regeneration of catalyst during reaction. Anthraquinone supported catalyst has demonstrated comparable activity and selectivity to the parent homogeneous molecule, which is important for recycling of the material.

## 4.2 Results and discussion

### 4.2.1 Oxidation of alcohols over EQ

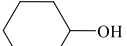
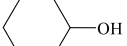
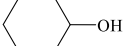
2-ethylanthraquinone (EQ) has been used as a model compound for oxidation of cyclohexanol. **Figure 4-1** shows the results of cyclohexanol oxidation over EQ with variation of the main reaction parameters like catalyst amount, temperature, oxygen

pressure and reaction time. The key role of anthraquinone and oxygen for the cyclohexanol oxidation reaction has been verified by catalytic test with and without EQ and/or oxygen (**Table 4-1**). The reaction did not proceed without oxygen or EQ. GC analysis of EQ after reactions has shown that it does not transform during reaction and might be considered as a catalyst (**Figure 4-2**). Hydrogen peroxide has not been identified in the products of the reaction, which could be the result of its fast decomposition with formation of oxygen and water.



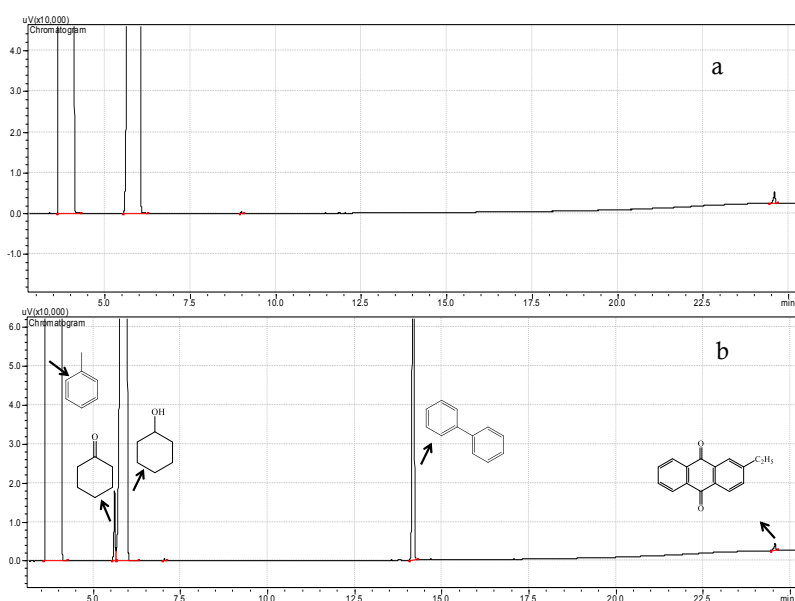
**Figure 4-1.** Cyclohexanol oxidation over EQ with variation of oxygen pressure ( $T=130\text{ }^{\circ}\text{C}$ , 1 mol/mol %, 12 h) (a), temperature (1 mol/mol %, 12 h,  $p(\text{O}_2)=10\text{ bar}$ ) (b), catalyst amount ( $T=130\text{ }^{\circ}\text{C}$ ,  $p(\text{O}_2)=10\text{ bar}$ , 12 h) (c) and time ( $T=130\text{ }^{\circ}\text{C}$ , 1 mol/mol %,  $p(\text{O}_2)=10\text{ bar}$ ) (d)

**Table 4-1.** The role of anthraquinone and oxygen for cyclohexanol oxidation (1 mol/mol % EQ/alcohol, toluene as solvent,  $T=130\text{ }^{\circ}\text{C}$ )

Entry	Substrate	Catalyst	Gas	Time /h	Conv. /%
1		EQ	$\text{N}_2$ , 10 bar	12	0
2		NA	$\text{O}_2$ , 10 bar	12	0
3		EQ	$\text{O}_2$ , 10 bar	12	37

First of all, we have found that the reaction is highly sensitive to oxygen pressure. The catalytic activity increases dramatically with increase of the oxygen pressure up to 10 bar with no changes afterwards (**Figure 4-1a**). Necessity of high pressure of

oxygen might be explained by difficulties in transfer of hydrogen from alcohol to oxygen through EQ molecule. Low pressure of oxygen is not enough to shift the equilibrium of the reaction toward formation of aldehyde and water.



Catalyst	Before reaction/mg	After reaction/mg	Weight losses/%
EQ	52	50.9	<5

**Figure 4-2.** GC Analysis of EQ before (a) and after reaction (b). Reaction conditions: cyclohexanol 2 g, EQ 52 mg and 1 g toluene as solvent, 130 °C, 2 h. Biphenyl as internal standard.

The reaction starts to take place only at the temperatures higher than 100 °C with 67 % conversion of cyclohexanol at 150 °C after 12 h of test (**Figure 4-1b**). The main reaction product was cyclohexanone with selectivity close to 90 % at low conversions (**Figure 4-3**). Increase of the conversion (**Figure 4-1d**) by variation of the reaction time resulted in decrease of the selectivity due to side reactions as cycle opening leading to formation of adipic and hexanoic acid and their esters with cyclohexanol due to esterification reaction. It is interesting to note that increase of the amount of catalyst leads to increase of the activity only till 1 mol/mol % with no further increase of the conversion at higher loading (**Figure 1c**). The maximum conversion about 30 % is similar for variation of oxygen pressure and catalyst loading, which can be explained by poisoning effect of the product cyclohexanone as carbonyl compound on the catalytic activity. Increase of the time of the test results in increase of the conversion but it is mainly due to formation of the products of deeper oxidation.

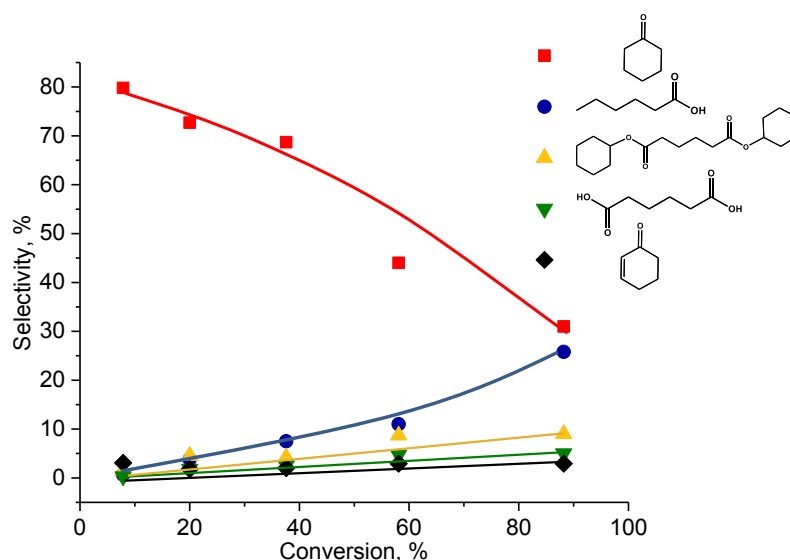


**Figure 4-3.** Selectivities versus conversion in cyclohexanol oxidation over EQ. Reaction condition: 1 mol/mol %,  $T=130$  °C,  $p(O_2)=10$  bar, toluene as solvent.

To verify this hypothesis, we have conducted an experiment with addition of cyclohexanone as an example of carbonyl compound during oxidation of benzyl alcohol (**Table 4-2**). The result showed that benzaldehyde production reduced by half in the presence of 10 wt. % of cyclohexanone, which clearly indicates an inhibition of the alcohol oxidation reaction by other carbonyl compounds. The possible explanation could be in the hindrance of hydrogen abstraction in the presence of another carbonyl group except anthraquinone in the proximity to alcohol.

**Table 4-2.** Selective oxidation of benzyl alcohol in the presence of cyclohexanol (1 mol/mol % EQ/alcohol,  $p(O_2)=10$  bar, 10 wt% cyclohexanone was added in Entry 2)

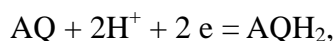
Entry	Substrate	Additive	Time /h	T /°C	Aldehyde yield /%
1		NA	12	150	25
2			12	150	13

Reduction potential of quinone based molecules should play an important role for the reaction of hydrogen transfer as has been demonstrated earlier [11]. The substituted derivatives of quinones with electrophilic and nucleophilic groups with different reduction potentials have been tested in alcohols oxidation hereafter.

#### 4.2.2 Effect of electrochemical potential of quinones on alcohol oxidation

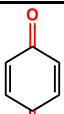
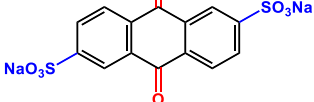
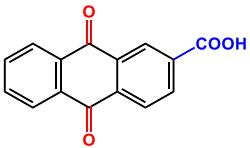
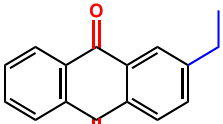
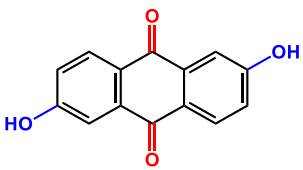
Several commercially available anthraquinones with different groups have been used in this work (**Table 4-3**). 1,4-benzoquinone (BQ) is a simplest quinone containing two carbonyl groups in the ring. Disodium anthraquinone-2,6-disulfonate (SQ) contains two sulfo groups attached to anthraquinone molecules at 2 and 6 carbon atom positions. 2,6-dihydroxyanthraquinone (DAQ) contains hydroxyl groups at the same positions. Anthraquinone-2-carboxylic acid (CQ) contains one carboxylic group at the second position.

The reduction potentials of the molecules vs standard hydrogen electrode (SHE) have been calculated on the basis of Gibbs energy of the reaction:



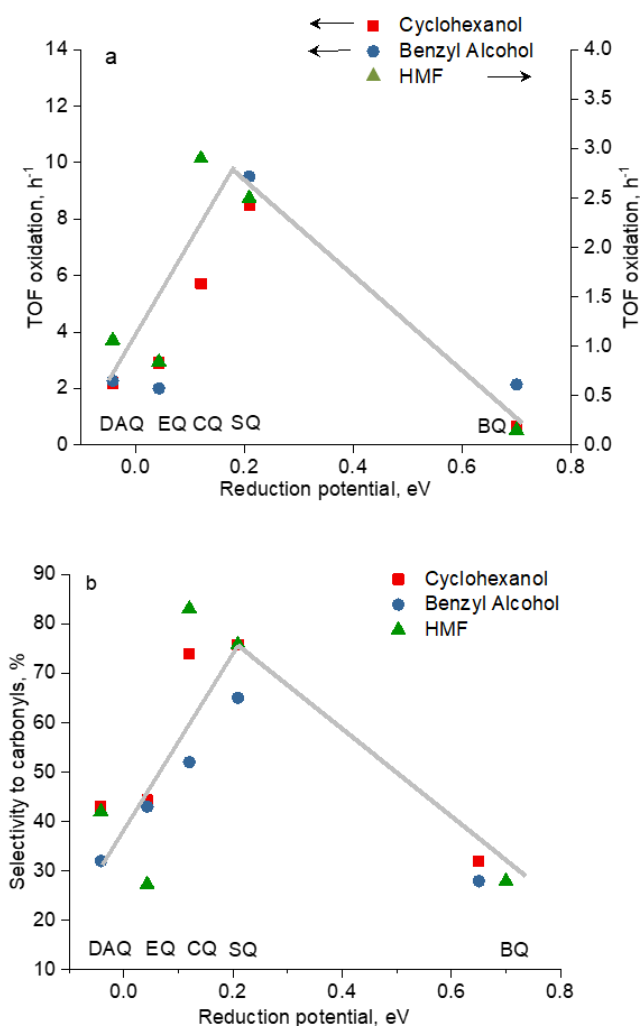
and taking into account  $E_0 = -dG/2F - 4.42\text{ V}$ .

**Table 4-3.** Reduction potential of used quinones

Entry	Quinones	Formula	Reduction potentials / V (vs SHE)
1	BQ		0.65
2	SQ		0.21
3	CQ		0.12
4	EQ		0.043
5	DAQ		-0.042

The results correlate well with experimentally determined numbers for the reduction potentials of known quinones (**Table 4-3**)<sup>25</sup>. BQ has the highest potential

(i.e. 0.65 V) with high stability of formed para-hydroquinone. Presence of electron donating hydroxyl groups leads to decrease of the potential of DAQ to -0.042 V. EQ provides similar reduction potential of 0.043 V. Presence of electrophilic groups for SQ and CQ as expected leads to intermediate reduction potentials between BQ and EQ at 0.21 and 0.12 V, respectively.

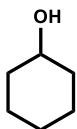
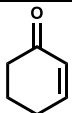
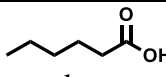
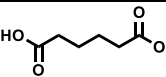
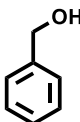
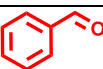
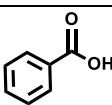
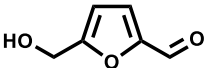
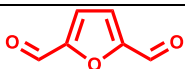
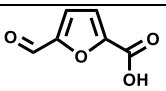


**Figure 4-4.** Correlation between reduction potentials of quinones and TOF numbers of alcohols oxidation (a) and selectivities to carbonyl compounds at comparable conversion 60 % (b). Conditions: cyclohexanol ( $T=130\text{ }^{\circ}\text{C}$ , 1 mol/mol %, 2h), benzyl alcohol ( $T=150\text{ }^{\circ}\text{C}$ , 1 mol/mol %, 2h) and HMF ( $T=130\text{ }^{\circ}\text{C}$ , 1 mol/mol %, 2h), while all  $p(\text{O}_2)$  is 10 bar.

**Figure 4-4** demonstrates the correlation between TOF numbers in cyclohexanol oxidation to cyclohexanone and reduction potentials of quinones (**Table 4-4**). As might be observed the curve has volcano form with the highest activity over anthraquinones containing carboxy (CQ) and sulfo (SQ) groups with intermediate values of reduction potentials around 0.1-0.2 V. Benzoquinone which has the highest reduction potential and highest stability of hydrogenated form has the lowest activity

in the reaction of cyclohexanol oxidation. At the same time, hydrogenated form of EQ has significantly lower stability and is easy to oxidize at room temperature with formation of hydrogen peroxide and initial form of EQ. Efficient oxidation of alcohols according to proposed scheme of the reaction should involve hydrogenation and oxidation of reduced anthraquinone. In this case high efficiency of intermediate reduction potentials for SQ and CQ might be explained by the fact that both reduction and oxidation steps proceed with high rates without limitations<sup>26</sup>

**Table 4-4.** The catalytic results of oxidation of cyclohexanol, benzyl alcohol and HMF over anthraquinone based molecules at the conversion of substrate about 60 %

Substrate	Catalyst	TOF, h <sup>-1</sup>	Selectivity, mol.%			
	<sup>a</sup> <b>BQ</b> <b>SQ<sup>b</sup></b> <b>CQ</b> <b>EQ</b> <b>DAQ</b> <b>CQ/SiO<sub>2</sub></b>	0.6	 32	 57	 and esters 6	 and esters 0
		8.5	75	3	4	7
		5.7	74	2	6	2
		2.9	44	3	33	11
		2.2	43	5	5	25
		6.0	76	3	8	1
			<sup>c</sup> <b>BQ</b> <b>SQ<sup>d</sup></b> <b>CQ</b> <b>EQ</b> <b>DAQ</b> <b>CQ/SiO<sub>2</sub></b>	2.1	 28	 25
9.5	65			2	3	25
13	52			8	13	23
2	43			18	18	6
2.2	32			11	15	26
16	57			3	16	11
	<sup>a</sup> <b>BQ</b> <b>SQ<sup>b</sup></b> <b>CQ</b> <b>EQ</b> <b>DAQ</b> <b>CQ/SiO<sub>2</sub></b>			0.15	 28	 31
		2.5	76	6	0	15
		2.9	83	10	0	4
		0.16	27	28	2	23
		0.11	42	0	0	56
		3.4	88	7	0	4

<sup>a</sup> substrate 2 g, catalyst 50 mg and 1 g toluene as solvent, 130 °C, time 1-24 h

<sup>b</sup> substrate 2 g, catalyst 50 mg and 1 g DMSO and 0.3 g H<sub>2</sub>O as solvent, 130 °C, time 1-24 h

<sup>c</sup> substrate 2 g, catalyst 50 mg and 1 g toluene as solvent, 150 °C, time 1-24 h

<sup>d</sup> substrate 2 g, catalyst 50 mg and 1 g DMSO and 0.3 g H<sub>2</sub>O as solvent, 150 °C, time 1-24 h

**Figure 4-5** presents selectivity of cyclohexanol, benzyl alcohol and HMF oxidation to carbonyl compounds versus conversion over EQ. The selectivity

decreases with increase of alcohol conversion for all alcohols. Depending on the type of alcohol the by-products of the reaction are different (**Table 4-4**). Thus, cyclohexanol during oxidation is accompanied by cycle opening leading to formation of hexanoic acid and adipic acid and subsequent esters formation. These products recall the process of radical synthesis of adipic acid through cycle opening of cyclohexyl peroxide<sup>27</sup>. Besides it, 2-cyclohexenone has been detected as a side product of the reaction with significant amount in the case of BQ as a catalyst. This effect might be explained by deep dehydrogenation of cyclohexanone by BQ possessing high reduction potential. In the case of benzyl alcohol the main side reaction is deep oxidation to benzoic acid and ester formation. Formation of benzyl ether might be explained by coupling of benzyl alcohol radicals. HMF oxidation resulted mainly in stepwise oxidation of carbonyl groups to 2,5-diformylfuran (DFF) and formation of 2,5-furandicarboxylic acid as a final product of the reaction.

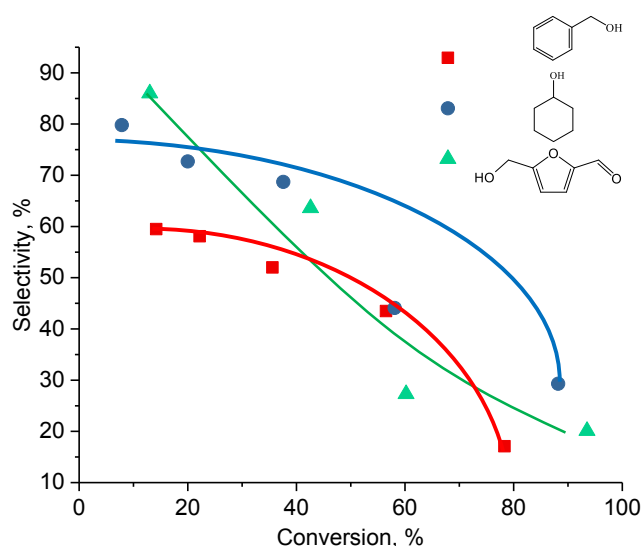


**Figure 4-5.** Selectivity to the target carbonyl compounds during oxidation of corresponding alcohols over EQ. Reaction condition: 1 mol/mol %,  $p(O_2)=10$  bar, toluene as solvent.  $T=130$  °C for cyclohexanol and HMF reaction;  $T=150$  °C for benzyl alcohol reaction.

The selectivity trends for oxidation of alcohols over quinones are similar to those observed for TOF numbers with decrease of the selectivity to carbonyl compounds for high and low reduction potentials (**Figure 4-2**). Thus, selectivity to cyclohexanone, benzaldehyde and DFF reaches 85-90 % during oxidation of corresponding alcohols over CQ and SQ at high conversions. The high selectivity might be explained by high rate of hydrogen transfer from alcohol to anthraquinone and subsequent oxidation of hydrogenated form of anthraquinone. Application of anthraquinones with low or high

reduction potentials should result in the higher residence time of radical form of alcohol or peroxy radical. It should induce deeper oxidation of alcohols, cycle opening and coupling with formation of ether.

### 4.2.3 Supported anthraquinone for oxidation

The heterogeneous catalysts have significant advantages for catalytic application due to easy separation and possibility to use it in continuous flow reactors, which significantly reduce the cost of the process. In order to verify if quinone might be used as supported catalyst in the reaction, we have prepared grafted CQ to amino functionalized silica and tested this catalyst in the reactions of alcohols oxidation. The catalyst has been prepared by treatment of aminopropyl-functionalized silica containing 1 mmol/g of amino groups by CQ to form amide group for grafting of anthraquinone species (**Figure 4-6**). The prepared catalyst has been characterized by solid  $^1\text{H}$  and  $^{13}\text{C}$  NMR, FTIR spectroscopy and TG analysis. Taking into account molecular weight of CQ, the catalyst should contain about 21 wt. % of organic species on the surface (**Figure 4-6**). TG analysis shows several losses of weight at 265, 400 and 560  $^{\circ}\text{C}$  corresponding to decomposition and burning of organic species with a total mass decrease of  $\sim 17$  wt. % which corresponds well to the theoretical content of organic phase.

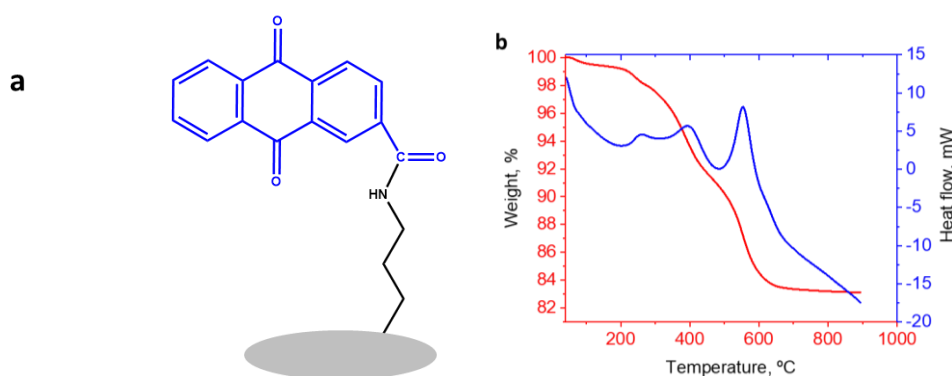


**Figure 4-6.** Structure of grafted CQ (a) and TGA curves of supported CQ/SiO<sub>2</sub> (b)

Solid  $^1\text{H}$  NMR analysis demonstrates presence of a broad peak with several maximums at 7.6, 5.5, 3.7 and 1.1 ppm (**Figure 4-7**). The peaks at highest chemical shift at about 8 ppm can be assigned to protons in aromatic ring of anthraquinone<sup>28</sup>. The strong peak at 5.5 ppm is usually result of the presence of adsorbed water and silanol groups of silica<sup>29</sup>. The protons of aliphatic propyl group should provide

signals in the range from 0 to 3 ppm depending on the distance from Si. The  $^{13}\text{C}$  CPMAS NMR spectrum (**Figure 4-7**) exhibits clearly resolved 3 group of peaks with high (182 and 168 ppm), medium (133 and 126 ppm) and low chemical shifts (9, 22 and 44 ppm). The first group can be assigned to carbon in carbonyl group of anthraquinone and amide. The peaks at about 130 ppm can be attributed to carbon of aromatic rings of anthraquinone. The carbon atoms of aliphatic linker should provide peaks at low chemical shift.

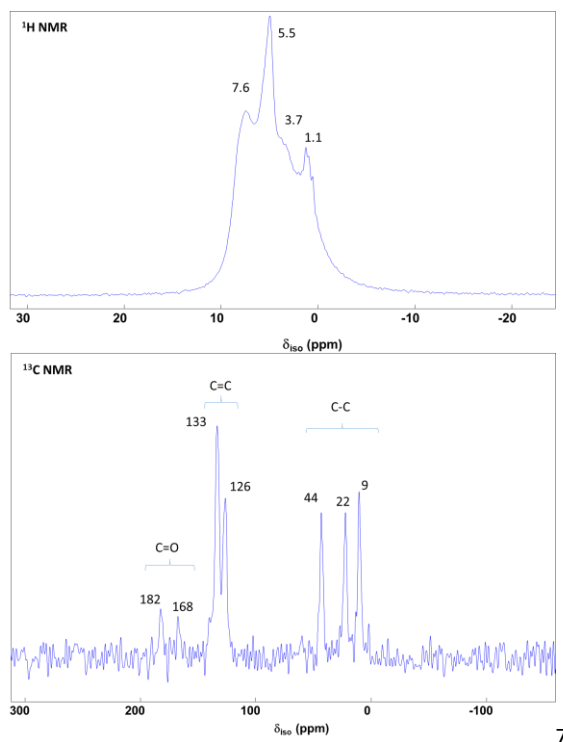


**Figure 4-7.** Solid  $^1\text{H}$  and  $^{13}\text{C}$  CPMAS NMR spectrum of CQ/SiO<sub>2</sub>

The initial CQ has FTIR spectrum (**Figure 4-8**) with the bands corresponding to C=O in carboxylic group and anthraquinone at 1695 and 1675  $\text{cm}^{-1}$ , respectively, with OH deformation bending from carboxylic group at 1432  $\text{cm}^{-1}$ <sup>30</sup>, while the one at 1590  $\text{cm}^{-1}$  might be due to C = C stretching of a quinone ring. The group of bands at 1325, 1273 and 1250  $\text{cm}^{-1}$  can be attributed to C-O stretching and C-H deformation vibrations<sup>31-33</sup>. The prepared material after CQ grafting besides bands related to Si-O modes in silica at 1065 and 797  $\text{cm}^{-1}$  have similar set of bands to CQ at 1675 and 1590  $\text{cm}^{-1}$ . The emerging bands at 1540 and 1640  $\text{cm}^{-1}$  might be attributed to C-N and C=O vibrations in the new amide group<sup>34-35</sup>. The band related to O-H vibration in carboxylic group at 1432  $\text{cm}^{-1}$  disappears after CQ deposition which indicates on formation of amide bond and successful grafting of CQ over aminopropyl-functionalized silica.

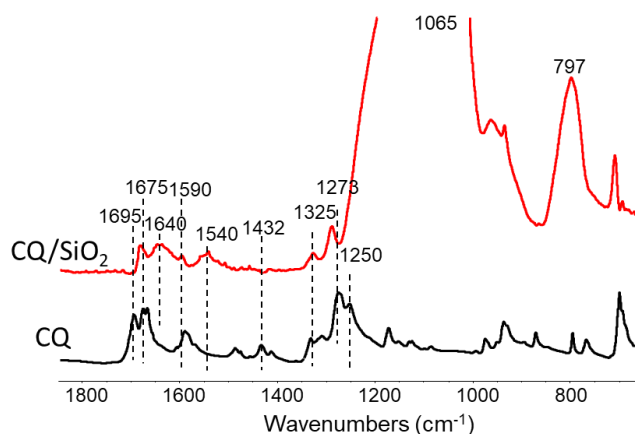


**Figure 4-8.** Scheme of CQ/SiO<sub>2</sub> and FTIR spectroscopy of supported CQ/SiO<sub>2</sub> and CQ

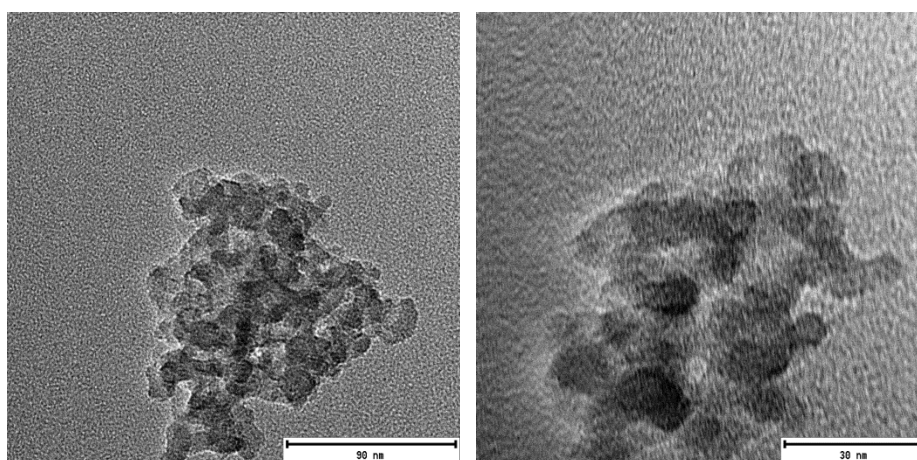


**Figure 4-9.** TEM images of CQ/SiO<sub>2</sub>

The morphology of CQ/SiO<sub>2</sub> catalyst has been studied by TEM (**Figure 4-9**). CQ/SiO<sub>2</sub> is essentially aggregated after grafting and the particles have spherical and uniform shape with a diameter of ~10 nm. The surface modification toward SiO<sub>2</sub> does not destroy the initial structure, which is in agreement with XRD patterns.

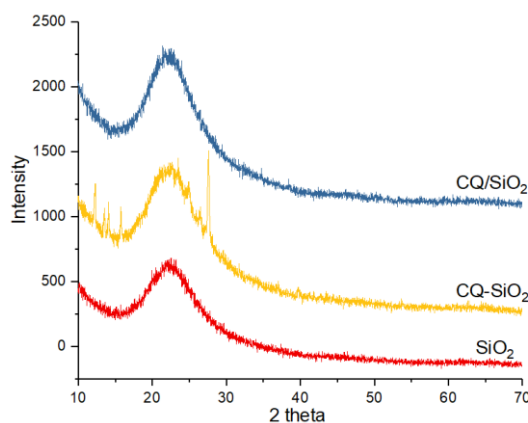


**Figure 4-10.** XRD patterns of grafted CQ/SiO<sub>2</sub>, impregnated CQ-SiO<sub>2</sub> and SiO<sub>2</sub>.

XRD analysis indicates on amorphous nature of prepared catalyst CQ/SiO<sub>2</sub> with uniform distribution of anthraquinone species on the surface of silica (**Figure 4-10**) in comparison with CQ-SiO<sub>2</sub> prepared by simple impregnation method. CQ-SiO<sub>2</sub> exhibits diffraction peaks at 8.7 °, 11.9 °, 15.3 °, 26.8 °, 39.8 ° assigned to CQ<sup>36</sup>.

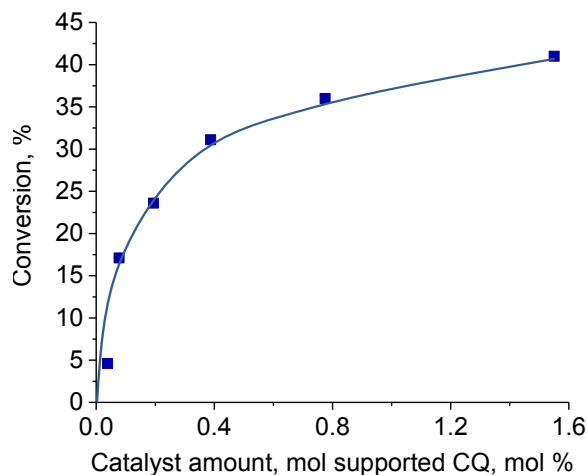


**Figure 4-11.** Cyclohexanol oxidation activity over supported CQ/SiO<sub>2</sub> with variation of catalyst amount ( $T=130\text{ }^{\circ}\text{C}$ ,  $p(\text{O}_2)=10\text{ bar}$ , 12 h).

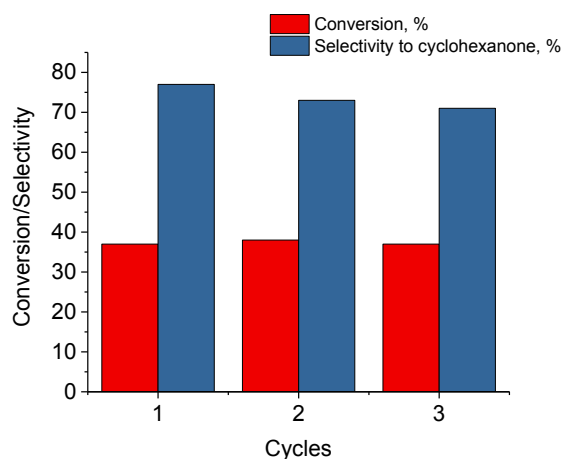


**Figure 4-12.** Catalytic results of cyclohexanol oxidation over CQ/SiO<sub>2</sub> for several cycles with separation of the catalyst by centrifugation ( $T=130\text{ }^{\circ}\text{C}$ , 0.5 mol/mol %,  $p(\text{O}_2)=10\text{ bar}$ , 12h)

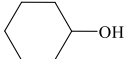
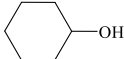
The catalyst with supported CQ demonstrates TOF numbers similar to those of the parent CQ (**Table 4-4**). The calculated reduction potential of grafted CQ (0.087 V) is lower in comparison with parent CQ molecule due to electron donating properties of NH<sub>2</sub>- group. The high activity of supported anthraquinone molecules could be explained by decrease of the poisoning effect of carbonyl groups of isolated anthraquinone molecules on each other over silica surface in comparison with homogeneous counterpart. The increase of the conversion versus amount of the

catalyst supports this assumption (**Figure 4-11**). The selectivities in oxidation of alcohols over CQ/SiO<sub>2</sub> are similar to those over CQ (**Table 4-4**).

The stability of the catalyst has been demonstrated by catalytic tests in 3 cycles with intermediate separation of supported CQ/SiO<sub>2</sub> (**Figure 4-12**). The catalyst shows comparable conversion and selectivity in all cycles. These results demonstrate high potential of application of grafted quinones as selective heterogeneous catalyst in alcohols oxidation.

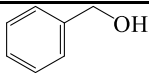
#### 4.2.4 Mechanism of the reaction

**Table 4-5.** Radical scavengers effect in the cyclohexanol oxidation over EQ<sup>a</sup> (1 mol/mol %, p(O<sub>2</sub>)=10 bar, 5 wt% of AgNO<sub>3</sub> or phenol was added in Entry 2 &3)

Entry	Substrate	Additive	Time /h	T /°C	Aldehyde yield /%
1		NA	12	130	29
2		AgNO <sub>3</sub>	12	130	< 5
3		Phenol	12	130	<5

To support that the oxidation mechanism has radical character, a series of experiments were carried out with cyclohexanol as the model compound. The well-known radical scavengers like phenol<sup>37</sup> have been used as additives (**Table 4-5**). The presence of these compounds resulted in almost total suppression of catalytic activity of EQ in oxidation of cyclohexanol. Thus, these results show the key role of radical species forming in the presence of anthraquinones in oxidation of alcohols to carbonyl compounds.

**Table 4-6.** Dehydrogenation of alcohol using SQ (0.2 g SQ, 0.1 g benzyl alcohol, 1 g toluene as solvent)

Entry	Substrate	Catalyst	Time /h	T /°C	Conv / %	Selectivity /%
1		SQ	6	150	5	99

The possible mechanism of the reaction could involve stepwise process with abstraction of hydrogen to hydrogenated form of anthraquinone with subsequent

regeneration of anthraquinone by oxidation with formation of peroxy species decomposing to water and oxygen. In order to verify this assumption we have conducted experiment by treatment of benzyl alcohol in the presence of high amount of SQ in inert atmosphere (**Table 4-6**). The aldehyde was the only product of the reaction and conversion of benzyl alcohol was about 10 % of SQ amount. In comparison with DDQ the reduction potential for anthraquinones is relatively low and hydrogenated form is less stable. In order to shift the equilibrium of the reaction the hydrogenated form has to be continuously oxidized with formation of water. It explains strong effect of oxygen pressure on the catalytic activity (**Figure 4-1**).

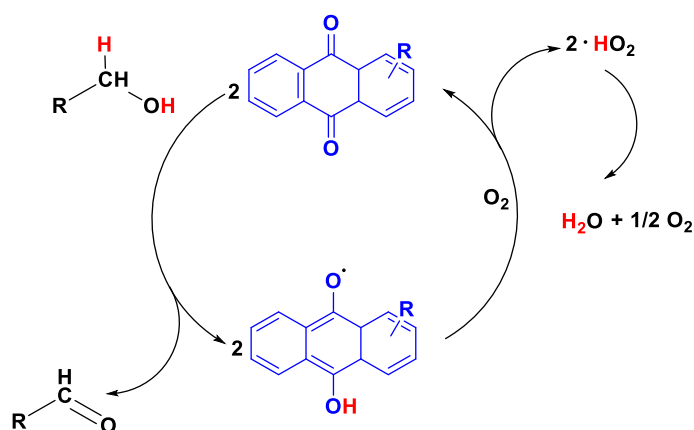


**Figure 4-13.** Scheme of oxidation of alcohol by anthraquinone based compounds.

Based on the above experimental observations, we propose a radical mechanism for the quinone-induced catalytic oxidation of alcohols to carbonyl compounds which is described on the **Figure 4-13**. The mechanism might involve quinone-prompted electron-transfer reaction through activation of C-H and O-H bond over electron-deficient carbonyl group of SQ with subsequent fast oxidation with formation of peroxy-species by oxygen attack.

### 4.3 Conclusion

The substituted anthraquinone molecules have been studied in non-metallic oxidation of alcohols. The oxidation of benzyl alcohol to benzaldehyde, cyclohexanol to cyclohexanone and HMF to DFF proceed with the highest activity and selectivity (>80 %) over sulfonated and carboxylated anthraquinone molecules. This effect has been explained by intermediate reduction potentials, which should provide a well balance hydrogen rate transfer from alcohol to anthraquinone and from anthraquinone to oxygen. The radical mechanism of oxidation over anthraquinones has been

demonstrated in this work by addition of radical scavengers. Finally, grafted anthraquinone has been used as efficient catalyst in oxidation of alcohols.

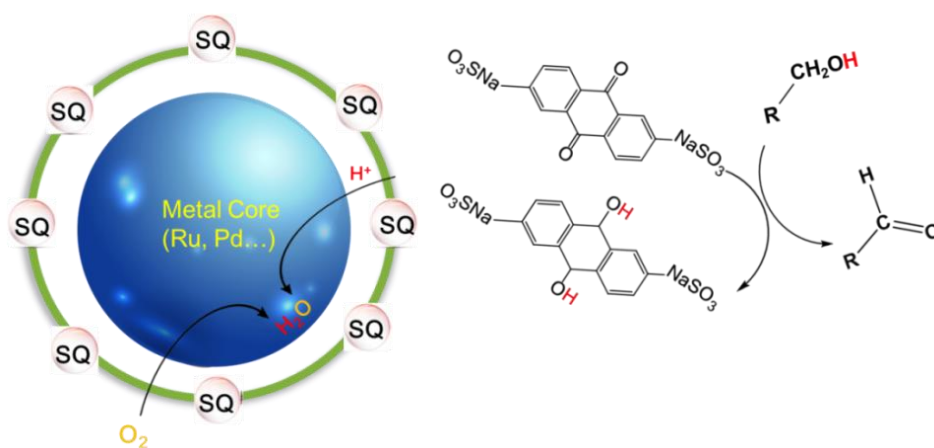
#### 4.4 References

1. Mitchell, S. K.-O., Encyclopedia of Chemical Technology. 4th ed., Wiley-Interscience, New York **1992**, 2, 481-486.
2. Zhai, W.; Xue, S.; Zhu, A.; Luo, Y.; Tian, Y., Plasmon-Driven Selective Oxidation of Aromatic Alcohols to Aldehydes in Water with Recyclable Pt/TiO<sub>2</sub> Nanocomposites. *ChemCatChem*. **2011**, 3 (1), 127-130.
3. Clerick, S.; De Canck, E.; Hendrickx, K.; Van Speybroeck, V.; Van Der Voort, P., Heterogeneous Ru(iii) oxidation catalysts via 'click' bidentate ligands on a periodic mesoporous organosilica support. *Green Chem*. **2016**, 18 (22), 6035-6045.
4. Jensen, D. R.; Schultz, M. J.; Mueller, J. A.; Sigman, M. S., A Well-Defined Complex for Palladium-Catalyzed Aerobic Oxidation of Alcohols: Design, Synthesis, and Mechanistic Considerations. *Angew. Chem. Int. Ed*. **2003**, 115 (32), 3940-3943.
5. Enache, D. I.; Knight, D. W.; Hutchings, G. J., Solvent-free Oxidation of Primary Alcohols to Aldehydes using Supported Gold Catalysts. *Catal. Lett*. **2005**, 103 (1-2), 43-52.
6. Vodyankina, O. V.; Koscheev, S. V.; Yakushko, V. T.; Salanov, A. N.; Boronin, A. I.; Kurina, L. N., Physicochemical investigation of the copper and silver catalysts of the ethylene glycol oxidation. *J. Mol. Catal. A-Chem*. **2000**, 158, 381-387.
7. Aellig, C.; Scholz, D.; Hermans, I., Metal-free aerobic alcohol oxidation: intensification under three-phase flow conditions. *ChemSusChem*. **2012**, 5 (9), 1732-1736.
8. A. E. J. De Nooy; A. C. Besemer; Bekkum, H. v., On the use of stable organic nitroxyl radicals for the oxidation of primary and secondary alcohols. *Synthesis* **1996**, 10, 1153-1176.
9. Sheldon, R. A., Recent advances in green catalytic oxidations of alcohols in aqueous media. *Catal.Today* **2015**, 247, 4-13.
10. A. Cecchetto; F. Fontana; F. Minisci; Recupero, F., Efficient Mn-Cu and Mn-Co-TEMPO-catalysed oxidation of alcohols into aldehydes and ketones by oxygen under mild conditions. *Tetrahedron Lett*. **2001**, 42, 6651-6653.
11. Wendlandt, A. E.; Stahl, S. S., Quinone-Catalyzed Selective Oxidation of Organic Molecules. *Angew. Chem. Int. Ed*. **2015**, 54, 14638 – 14658.
12. Braude, E. A.; Linstead, R. P.; Wooldridge, K. R., Hydrogen transfer. Part IX. The selective dehydrogenation of unsaturated alcohols by high-potential quinones. *J. Am. Chem. Soc*. **1956**, 3070-3075.
13. A. Ohki; T. Nishiguchi; Fukuzumi, K., Transfer hydrogenation and transfer hydrogenolysis—21: Dehydrogenation of alcohols by quinones. *Tetrahedron* **1979**, 35, 1737-1743.
14. C. C. Cosner; P. J. Cabrera; K. M. Byrd; A. M. A. Thomas; Helquist, P., Selective Oxidation of Benzylic and Allylic Alcohols Using Mn(OAc)<sub>3</sub> Catalytic 2,3-Dichloro-5,6-dicyano-1,4-benzoquinone. *Org. Lett*. **2011**, 13, 2072-2075.
15. S.Chandrasekhar; G.Sumithra; J.S.Yadav, Deprotection of mono and dimethoxy phenyl methyl ethers using catalytic amounts of DDQ. *Tetrahedron Lett*. **1996**, 37, 1645-1646.

16. G. V. M.Sharma; B. Lavanya; Mahalingam, A. K.; Krishna, P. R., Mn(OAc)<sub>3</sub>—an efficient oxidant for regeneration of DDQ deprotection of p-methoxy benzyl ethers. *Tetrahedron Lett.* **2000**, *41*, 10323-10326.
17. L. Liu; Floreancig, P. E., 2,3-Dichloro-5,6-dicyano-1,4-benzoquinone-Catalyzed Reactions Employing MnO<sub>2</sub> as a Stoichiometric Oxidant. *Org. Lett.* **2010**, *12*, 4686-4689.
18. Miyamura, H.; Shiramizu, M.; Matsubara, R.; Kobayashi, S., Polymer Incarcerated Gold Catalyzed Aerobic Oxidation of Hydroquinones and Their Derivatives. *Chem. Lett.* **2008**, *37* (3), 360-361.
19. T. Sakamoto; H. Yonehara; Pac, C., Catalytic Activities of CuSO<sub>4</sub>-Al<sub>2</sub>O<sub>3</sub> in Dehydrogenation of Arenes by Dioxygen. *J. Org. Chem.* **1997**, *62*, 3194-3199.
20. Stahl, S. S., Palladium oxidase catalysis: selective oxidation of organic chemicals by direct dioxygen-coupled turnover. *Angew. Chem. Int. Ed.* **2004**, *43* (26), 3400-20.
21. Z. Shen; J. Dai; J. Xiong; X. He; W. Mo; B. Hu; N. Sun; Hua, X., 2,3-Dichloro-5,6-dicyano-1,4-benzoquinone (DDQ)/tert-Butyl Nitrite/Oxygen: A Versatile Catalytic Oxidation System. *Adv. Synth. Catal.* **2011**, *353*, 3031-3038.
22. Y. Xie; W. Mo; D. Xu; Z. Shen; N. Sun; B. Hu; X. Hu, Efficient NO equivalent for activation of molecular oxygen and its applications in transition-metal-free catalytic aerobic alcohol oxidation. *J. Org. Chem.* **2007**, *72*, 4288-4291.
23. Costentin, C., Electrochemical approach to the mechanistic study of proton-coupled electron transfer. *Chem. Rev.* **2008**, *108*, 2145-2179.
24. E.Santacesaria; M.Di Serio; A.Russo; U.Leone; R.Velotti, Kinetic and catalytic aspects in the hydrogen peroxide production via anthraquinone. *Chem. Eng. Sci.* **1999**, *54*, 2799-2806.
25. Adkins, H.; Eloffson, R. M.; Rossow, A. G.; Robinson, C. C., The Oxidation Potentials of Aldehydes and Ketones. *J. Am. Chem. Soc.* **1949**, *71* (11), 3622-3629.
26. Speybroeck, V. v.; Meierb, R. J., A Recent Development in Computational Chemistry: Chemical Reactions from First Principles Molecular Dynamics Simulations *Chem. Soc. Rev.* **2003**, *32*, 151-157.
27. A. Farkas; Passaglia, E., The Decomposition of Cyclohexyl Hydroperoxide and the Peroxide-catalyzed Polymerization of Styrene. *J. Am. Chem. Soc.* **1950**, *72*, 3333-3337.
28. G. W. Francis; Aksnes, D. W., Assignment of the <sup>1</sup>H and <sup>13</sup>C NMR spectra of anthraquinone glycosides from Rhamnus frangula. *Magn. Reson. Chem.* **1998**, *36*, 769-772.
29. R. Lebeda; V. V. Turov; M. Marciniak; A. A. Malygin; Malkov, A. A., Characteristics of the Hydration Layer Structure in Porous Titania-Silica Obtained by the Chemical Vapor Deposition Method. *Langmuir* **1999**, *15*, 8441-8446.
30. S.Bratož; D.Hadži; N.Sheppard, The infra-red absorption bands associated with the COOH and COOD groups in dimeric carboxylic acid—II The region from 3700 to 1500 cm<sup>-1</sup>. *Spectrochimica Acta* **1956**, *8*, 249-261.
31. Helm, D.; Naumann, D., Identification of some bacterial cell components by FT-IR spectroscopy. *FEMS Microbiol. Lett.* **1995**, *126*, 75-80.
32. Singh, M.; Zhou, N.; Paul, D. K.; Klabunde, K. J., IR spectral evidence of aldol condensation: Acetaldehyde adsorption over TiO<sub>2</sub> surface. *J. Catal.* **2008**, *260* (2), 371-379.
33. A. Miki; S. Yeb; Osawa, M., Surface-enhanced IR absorption on platinum nanoparticles: an application to real-time monitoring of electrocatalytic reactions. *Chem. Commun.* **2002**, *14*, 1500-1501.

34. J. L. Bandfield; T.D. Glotch; Christensen, P. R., Identification of some bacterial cell components by FT-IR spectroscopy. *Science* **2003**, *301*, 1084-1087.
35. Ishii, M.; Kawasumi, T.; Igarashi, Y.; Kodama, T.; Minoda, Y., 2-Methylthio-1, 4-naphthoquinone, a New Quinone from an Extremely Thermophilic Hydrogen Bacterium. *Agric. Biol. Chern* **2014**, *47* (1), 165-167.
36. S.Tsai; S. ChuKuo; YangLin, S., Physicochemical characterization of 9, 10-anthraquinone 2-carboxylic acid. *J. Pharm Sci.* **1993**, *82*, 1250-1255.
37. Ahmad, N.; Sharma, S., Green Synthesis of Silver Nanoparticles Using Extracts of Ananas comosus. *Green & Sustain. Chem.* **2012**, *2* (04), 141-148.

# CHAPTER 5 Nanocell Type Ru@quinone Core-shell Catalyst for Selective oxidation of alcohols to carbonyl compounds



---

## ABSTRACT:

Selective aerobic oxidation of alcohols to corresponding carbonyl compounds is one of the most important challenges in the modern chemical industry. The existing metal based heterogeneous catalysts provide low selectivity due to over-oxidation of aldehydes to acids and esters. We have found that coating of Ru nanoparticles by disodium anthraquinone-2,6-disulfonate (SQ) results in selective oxidation of aliphatic, unsaturated and aromatic alcohols to aldehyde. Analysis of core-shell Ru@SQ catalyst shows strong interaction between Ru and SQ species leading to change of the electronic state and structure. In-situ study of alcohol oxidation using FTIR and electrochemistry indicates on hydrogen abstraction by shell quinone species with formation of carbonyl group and hydrogen transfer by quinone to Ru core for water generation. Thus, the catalyst behavior mimics nano-electrocell by separation of oxidation reaction over quinone nano-anode and reduction of oxygen over Ru nano-cathode.

---

This chapter is based on the following publication:

*J.P. Zhao, W.Y. Hernández, W.J. Zhou, Y. Yang, E. I. Vovk, M. J. Wu, N. Naghavi, M. Capron\*, V. Ordonsky\*, 2019, submitted.*

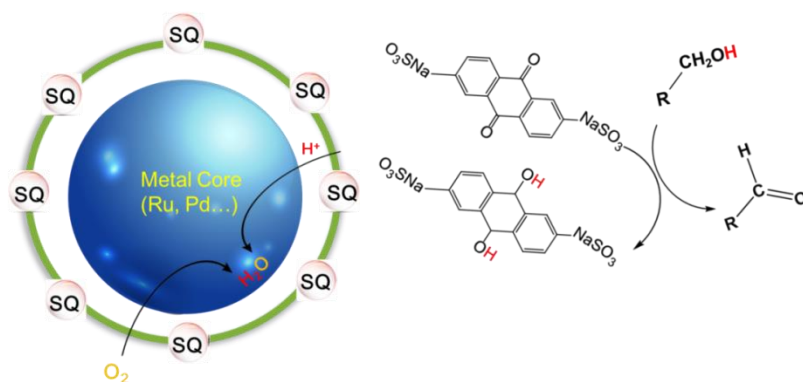
## 5.1 Introduction

The selective oxidation of alcohols to versatile intermediates for the production of chemicals such as aldehydes and ketones remains a challenging task in the industry. It is of special interest the utilization of molecular oxygen (air) as the green oxidant in presence of a heterogeneous catalyst, thus favoring the atom economy of the process in contrast to the use of toxic and expensive stoichiometric oxidants<sup>1-5</sup>.

Metal based catalysts are often used as catalysts for oxidation processes. Different heterogeneous catalytic systems based on Pt<sup>6-8</sup>, Pd<sup>9-10</sup>, Au<sup>11-12</sup> have been reported for oxidation of alcohols. Among metallic catalyst Ru has been shown to be quite efficient in oxidation reactions<sup>13-14</sup>. However, the selectivity to aldehyde or ketone over heterogeneous systems is still challenging problem due to formation of corresponding acids and esters<sup>15</sup>. The oxidation mechanism described for these catalytic systems normally follows an oxidative dehydrogenation pathway, where both abstraction of hydrogen from alcohols and oxygen reduction processes (regeneration of the active site) simultaneously occurs on the metal surface<sup>16</sup>. It triggers further oxidation of aldehydes to acids with decrease of the selectivity and generation of waste products. These catalytic systems are usually efficient in the selective oxidation of aromatic and activated alcohols but less active and selective for oxidation of aliphatic primary alcohols<sup>17-20</sup>.

In the past decade, it has been found that metal-free electron deficient organic compounds like TEMPO and DDQ can be used for dehydrogenation of alcohols with generation of aldehydes and ketones and hydrogenated form of organic compound<sup>21-24</sup>. However, this route requires stoichiometric amount of reagents with difficulties in their separation and regeneration. Recently the new concept has been proposed by in-situ regeneration of these species using oxygen as terminal oxidant. For example, Hu firstly explored an aerobic metal-free alcohol oxidation with a catalyst system consisting of TEMPO/Br<sub>2</sub>/NaNO<sub>2</sub> under air, where the Br<sub>2</sub>/HBr redox pair is used for oxidation of TEMPOH with subsequent regeneration by NO<sub>2</sub> reduction to NO<sup>25</sup>. In 1977, the first DDQ-catalyzed reaction was reported, and showed that the transformation of allylic alcohols to  $\alpha,\beta$ -unsaturated ketones could be achieved by 10 mol% DDQ in the presence of 30 mol% periodic acid under biphasic conditions at room temperature<sup>26</sup>. Helquist subsequently illustrated similar reactivity with Mn(OAc)<sub>3</sub> as the stoichiometric oxidant<sup>27</sup>. By using 20 mol% DDQ and 6.0 equiv

Mn(OAc)<sub>3</sub>, allylic alcohols and benzylic alcohols are observed to be oxidized to the corresponding aldehydes and ketones under mild conditions with good chemoselectivity. However, all these routes are based on homogeneous catalysts and significant amount of toxic transition metal salts leading to problems in separation and environmental pollution.



**Scheme 5-1.** Proposed mechanism of alcohol oxidation by nanocells.

To solve these problems, we propose application of heterogeneous catalyst containing organic hydrogen scavenger (**Scheme 5-1**) for selective alcohols oxidation to carbonyl compounds with metallic core inside able to regenerate organic shell of the catalyst. Hereby, we have studied effect of deposition of quinone species over metal nanoparticles in alcohols oxidation. Deposition of sulfonated anthraquinone over Ru nanoparticles in core-shell catalyst resulted in selective oxidation of alcohols. The alcohol is oxidized over the non-metallic shell sites, with subsequent migration of hydrogen to the metallic core for oxidation to water. This concept provides new opportunity for application of organic/inorganic composite materials for catalytic applications.

## 5.2 Results and Discussion

### 5.2.1 Catalytic performance in oxidation of alcohols

Water-in-oil microemulsions built of water, hexanol, and surfactant cetyltrimethylammonium bromide (CTAB) with RuCl<sub>3</sub> and sodium borohydride have been used for the synthesis of metal nanoparticles. Ru nanoparticles form aggregates and the size of Ru nanoparticles measured by TEM varied in the range 2-3 nm (**Figure 5-1**).

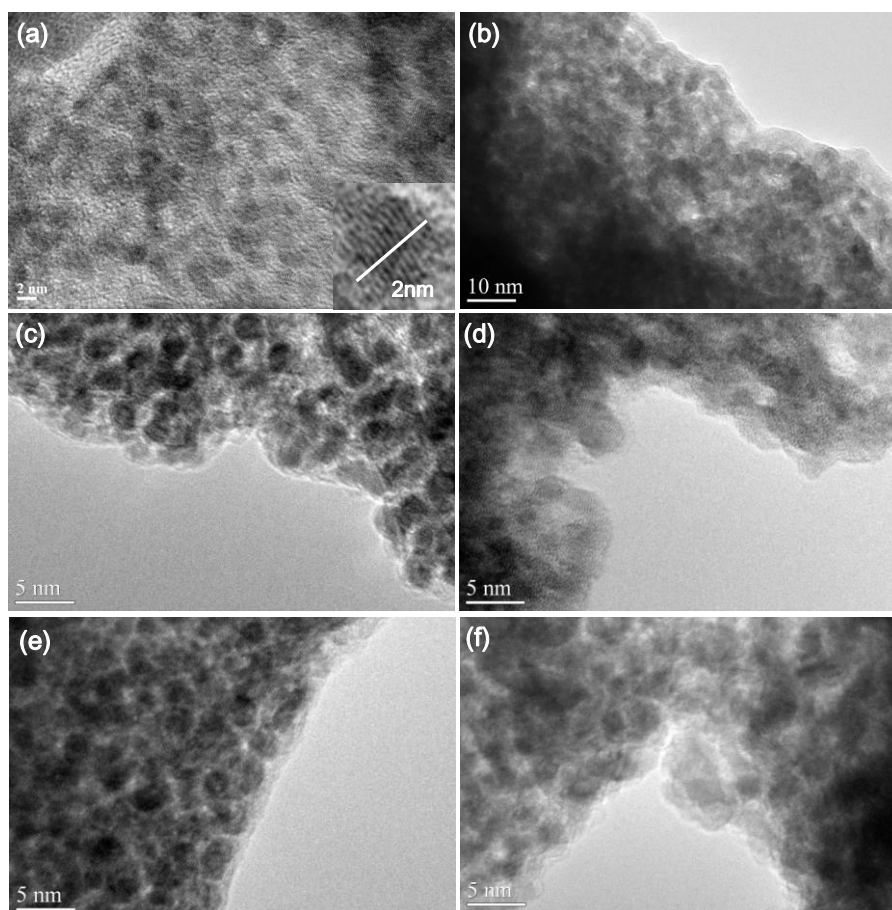


**Figure 5-1.** TEM images of (a) Ru NPs; (b) SQ; (c-f) Ru@SQ-X% catalysts, X=10, 25, 50, 80.

Ru@quinone catalysts with core-shell structure have been prepared using rotary evaporator to deposit quinone over Ru nanoparticles by removal of organic solvent. The received samples are denoted as Ru@quinones-X % (X=10, 25, 50, 80), where X is the weight percentage of quinones in the samples. **Figure 5-1** demonstrates TEM images of Ru nanoparticles coated by different content of disodium anthraquinone-2,6-disulfonate (SQ) in Ru@SQ catalysts. There is a clear contrast between the heavier-atom of Ru in the core and the lighter SQ shell. Increase of the content of SQ phase leads to increase of the thickness of the shell from 1 to 3 nm. The elemental mappings (**Figure 5-2**) further confirm that such core-shell samples are composed of two components, Ru metal in the core and SQ salt in the shell. SQ is uniformly distributed on the surface of Ru nanoparticles.

The catalytic performance of core-shell catalysts with different content of SQ has been compared with reference Ru nanoparticles and pure SQ in selective oxidation of octanol. SQ is almost insoluble in 1-octanol at the reaction conditions and the catalyst can be considered as heterogeneous material. The main products of the reaction

besides aldehyde involve deeper oxidation of aldehyde into octanoic acid, with subsequent esterification to octyl octanoate (**Scheme 5-2**). 1-Octanol in the presence of acid also undergoes etherification reaction, producing dioctyl ether.

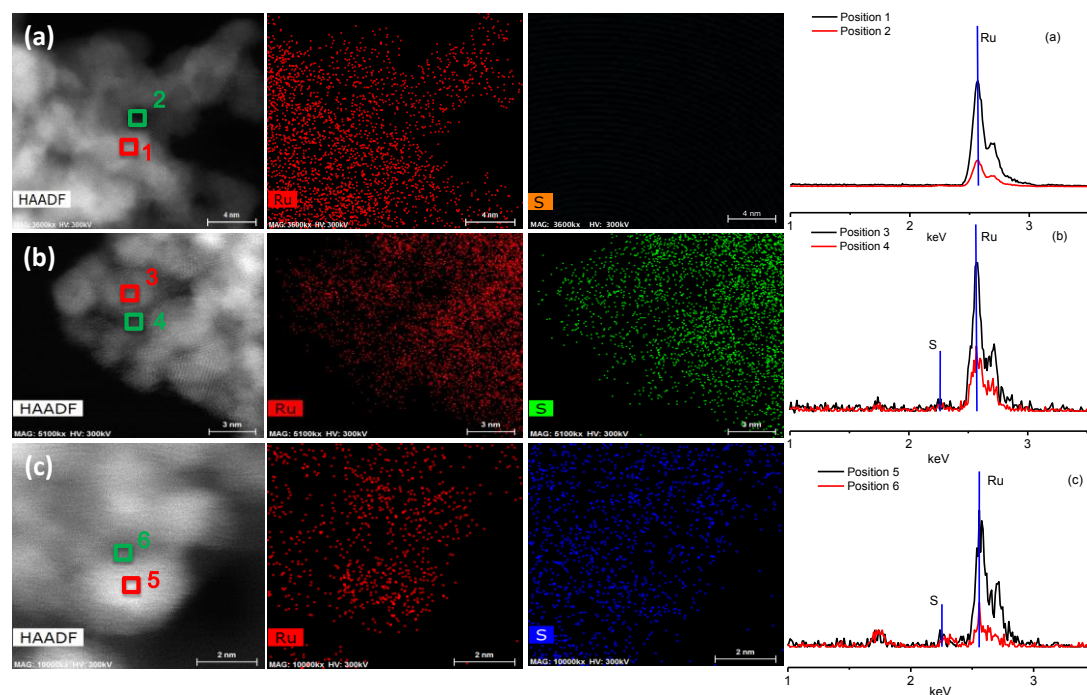
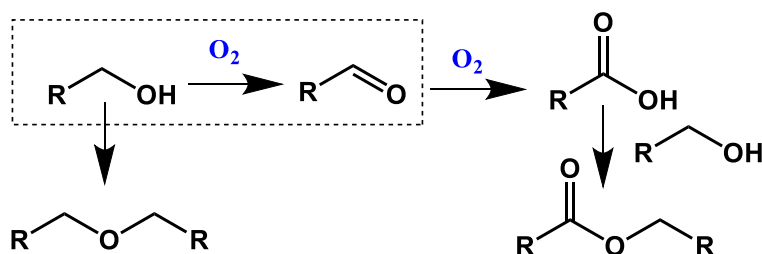
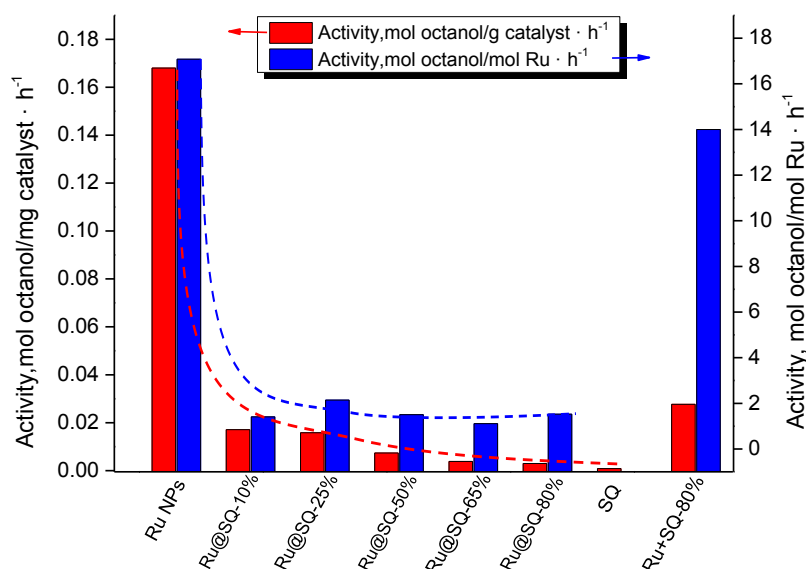


**Figure 5-2.** HRTEM images, spot scan and elemental mappings, EDX for (a) Ru NPs and the representative (b) Ru@SQ-10%, (c) Ru@SQ-50%.

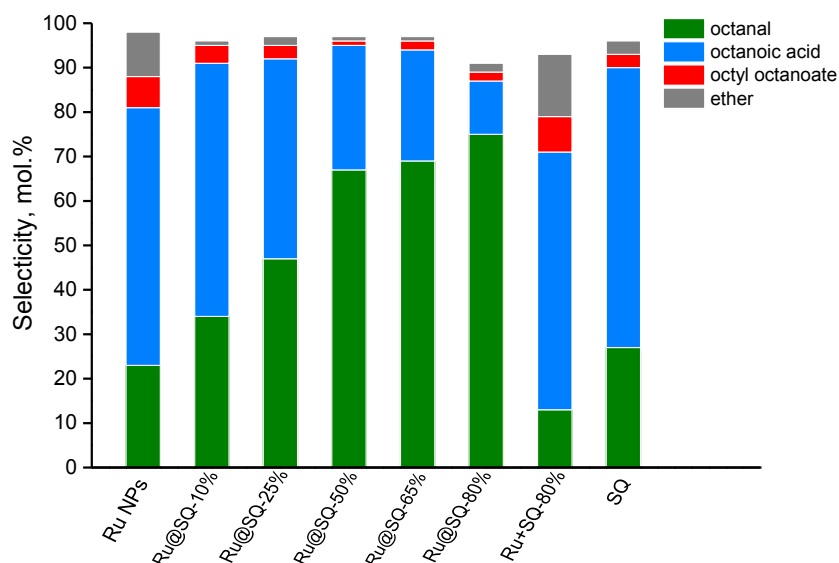


**Scheme 5-2.** The reaction of alcohols oxidation.

The catalytic activity of octanol oxidation is the highest over Ru NPs with decrease of the activity after deposition of SQ (**Figure 5-3**). Higher loading of SQ results in the lower catalytic activity of the catalyst. The lowest activity has been observed over pure SQ. Thus, presence of Ru NPs in the core of the catalyst affects the catalytic activity in alcohols oxidation. Comparison of the catalytic activity of core-shell Ru@SQ-80% with mechanical mixture Ru+SQ-80% demonstrates that the reason of lower activity is the coating of SQ over Ru NPs (**Figure 5-3**). It is interesting to note that activity normalized by Ru is comparable in a series of core-shell Ru@SQ catalysts (**Figure 5-3**).



**Figure 5-3.** The catalytic activity of octanol oxidation by different catalysts. The activity was calculated according to initial conversion (~15%) by the converted moles of 1-octanol (red) per gram of the whole catalyst per hour; (blue) per mol of Ru NPs per hour.

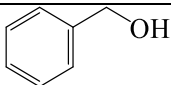
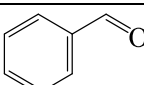
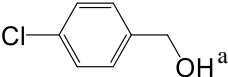
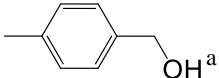
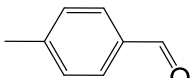
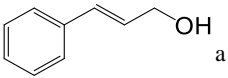
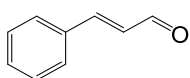
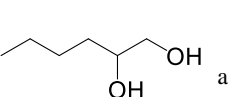
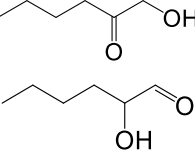
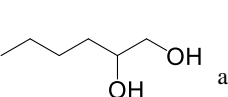
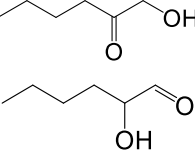
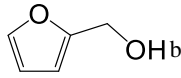
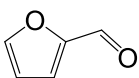
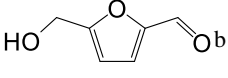
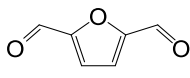
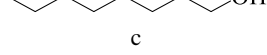
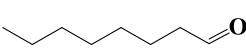
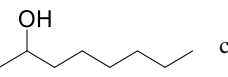
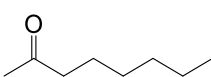
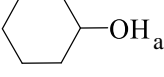
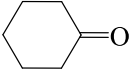


**Figure 5-4.** Shell thickness effects in variation of selectivities versus comparative ~60% conversions in selective oxidation of 1-octanol.

The parent Ru NPs demonstrates (**Figure 5-4**) strong decrease of the selectivity to octanal with increase of the conversion of octanol with formation of acid and ester as side products. **Figure 5-4** shows comparison of the catalytic performance of Ru NPs and the corresponding core-shell Ru@SQ catalysts with different content of SQ at comparable conversions about 60%. At this conversion the selectivity to octanal is only about 20% over Ru NPs. Pure SQ provided even lower selectivity due to

intensive deeper over-oxidation to acid and esters. It is interesting to note that selectivity to octanal was gradually increasing with increase of the content of SQ in the core-shell catalysts from 30 % for Ru@SQ-10% to 74 % for Ru@SQ-80%. Thus, selectivity increases up to 3 times in comparison with pure Ru NPs and SQ. The catalysts with low loading of SQ still could contain accessible Ru surface, which explains low selectivity in this case. Increase of SQ loading leads to increase of the selectivity to aldehydes due to full coverage of Ru surface by SQ.

**Table 5-1.** Substrate scope oxidation by “Nanocell” Ru@SQ-80%.

Alcohols	Alcohols /g	Target Molecule	T /°C	Time /h	Conv. /%	Sele. /%
	1.0		100	6	92	95
	1.0		100	6	95	95
	1.0		100	6	95	95
	1.0		100	18	90	95
	0.5		90	5	46	30
	0.5		90	5	46	22
	0.5		90	3	80	92
	0.4		110	16	69	89
	3.0		100	36	57	74
	1.0		115	60	>90	>90
	1.0		115	60	>90	>90

<sup>a</sup> Reaction conditions: catalyst 50.0 mg, toluene 2.0 g as solvent.

<sup>b</sup> Reaction conditions: catalyst 50.0 mg, toluene 1.0 g + ethanol 1.0 g as solvent.

<sup>c</sup> Reaction conditions: catalyst 50.0 mg, solvent-free.

Usually formation of aldehyde during oxidation of octanol is accompanied by subsequent non-catalytic oxidation, which results in formation of acid and esters. Quinone compounds have been used earlier for suppression of radical non-catalytic route<sup>28</sup>. Thus, the possible role of anthraquinone could be in suppression of radical route of oxidation. In order to verify this concept we have conducted oxidation of octanol using mechanical mixture of Ru NPs with 80 % of SQ (Ru+SQ-80%). It is interesting to note that the selectivity to aldehyde was significantly lower than in the case of core-shell system and comparable with Ru NPs.

Thus, the effect cannot be explained only by the presence of SQ in the reaction mixture with Ru NPs. The significant catalytic effect can be observed only in the case of core-shell Ru@SQ.

The selective oxidation of a wide range of alcohols was studied over Ru@SQ catalysts, in the presence of O<sub>2</sub>. For benzyl alcohol, methyl-substituted and chlorinated benzylic alcohol conversions of 92 %, 95 % and 95 % was achieved within 6 h, respectively (**Table 5-1**). The selectivity to the target products was evaluated to be higher than 95%. Similarly, cinnamyl alcohol was converted to cinnamaldehyde with 95 % selectivity under similar conditions at longer reaction time. In the case of furfuryl alcohol and HMF oxidation the selectivity about 90 % was achieved to furfural and DFF, respectively, at high conversion. Non-activated aliphatic alcohol (1-octanol) and cyclic alcohol (cyclohexanol) over Ru@SQ-80% have been converted to carbonyl compounds with a moderate activity and excellent selectivity. Secondary alcohol 2-octanol can be oxidized with a conversion of >90% and selectivity of 95% to corresponding ketone, which is comparable to the selectivity achieved using TEMPO system<sup>29</sup>. Unfortunately, the selective catalytic oxidation of diols was not successful by using the catalysts studied in this work.

The excellent catalytic activity towards various oxygenate substrates demonstrates that the uniform organic shell around the metal nanoparticles suppressed over-oxidation of aldehydes toward acids. Moreover, the organic shell prevents agglomeration of nanoparticles. Nanocells Ru@SQ exhibit much better catalytic behaviors than conventional Ru/Al<sub>2</sub>O<sub>3</sub><sup>30</sup> at almost the same metal content. Isolation of metal nanoparticles from direct contact with alcohols decreases activity, however, results in significant increase of the selectivity toward carbonyl compounds.

## 5.2.2 Characterization of Ru@quinones Catalysts

The composition and thermal stability of the Ru NPs and Ru@SQ catalysts have been examined by TGA (**Figure 5-5**). The curves show weight losses in roughly two steps. At the range of 25~300 °C, the weight losses determines the total amount of water and organic content 1-hexanol during preparation, especially ~25 wt% for Ru NPs. Above 300 °C, no obvious weight loss was observed for Ru NPs sample. Subsequently, the weight losses of about 45 wt%, 23 wt%, 14 wt% and 9 wt% for Ru@SQ-X% samples (X=80, 50, 25, 10 in sequence) have been observed between 400 °C and 600 °C, which could be presumably ascribed to the combustion of SQ layer and/or its decomposition products.

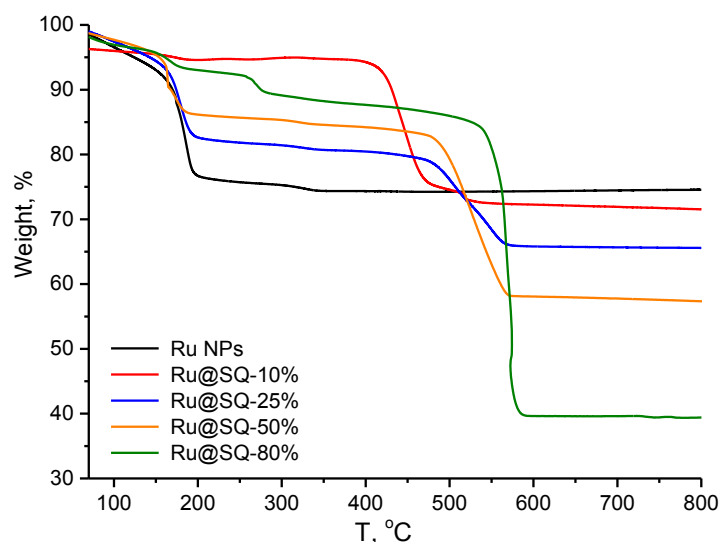


**Figure 5-5.** TGA of Ru@SQ- X% and Ru NPs.

XPS analysis of Ru nanoparticles covered by SQ (monolayer and 80%) in comparison with Ru nanoparticles and pure SQ was performed to investigate the electronic state of the ruthenium species (**Figure 5-6**). Ru 3p core level spectra show the presence of ruthenium in two oxidation states: metallic Ru (Ru 3p<sub>3/2</sub> BE 462.0-463.3 eV) and lower contribution of species with lower electronic density, oxidized Ru<sup>n+</sup> (Ru 3p<sub>3/2</sub> BE 464.6-465.5 eV). This assignment was made according to earlier studies of various Ru compounds including metallic Ru, RuO<sub>2</sub> and Ru(OH)<sub>3</sub> demonstrating different Ru 3p<sub>3/2</sub> BEs<sup>29</sup>.

After deposition of SQ over the surface of Ru NPs, the metallic Ru 3p doublet shifts to lower binding energy value. Additionally, the oxidized Ru related peak appears demonstrating partial oxidation of Ru. With the increase of SQ deposition the intensity of Ru peaks significantly decreases due to the attenuation of Ru signal by SQ

shell. It is notable that with the increase of SQ coating the metal Ru 3p doublet shifts to lower binding energy values from 462.7 eV to 462 eV. This shift can be associated with the effect of electron transfer from SQ to Ru leading to increase of the electronic density over Ru.

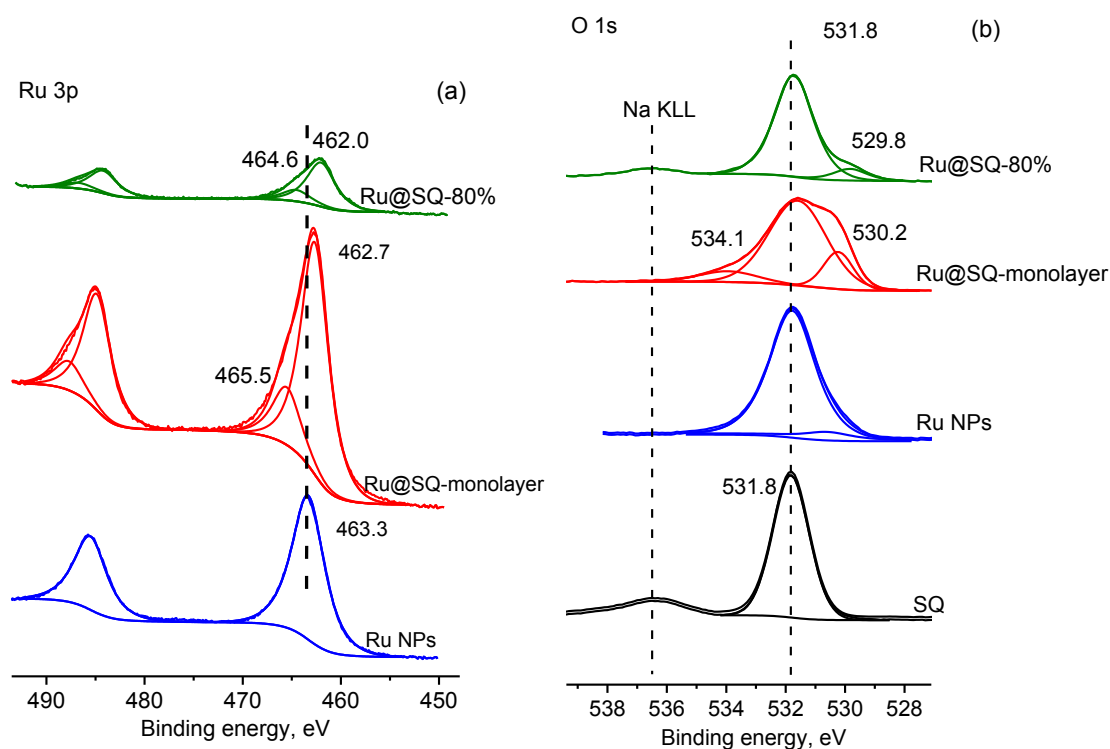


**Figure 5-6.** XPS spectra of Ru NPs, Ru@SQ-monolayer and Ru@SQ-80%. (a) Ru 3p, (b) O 1s core level spectra.

Pure SQ sample demonstrates only one O 1s peak at 531.8 eV while it is expected to have two types of oxygen:  $\text{SO}_3^{2-}$  and C=O. Most probably, it is due to strong interaction and electron transfer between oxygen in  $\text{SO}_3^{2-}$ <sup>30</sup> and oxygen in C=O<sup>31</sup> groups in SQ. Ru NPs demonstrate a similar O 1s peak with 531.8 eV BE which is associated with  $\text{RuO}_3$  or surface  $\text{Ru}(\text{OH})_3$ <sup>32</sup>. SQ coating over Ru NPs leads to appearance of two additional peaks: the broad peak at 534.1 eV which can be assigned to oxygen in sulfo groups<sup>33</sup> and well defined peak at 530.2 eV (529.8 eV after 80% SQ loading). The 530.2 eV peak we associate with bridge Ru-O-SQ species, which appearance indicates strong interaction between SQ and Ru (**Scheme 5-3**). With the increase of SQ loading this peak is attenuated as well as Ru 3p doublet. Pt and Pd nanoparticles do not show a similar strong interaction with SQ (**Figure 5-7**).

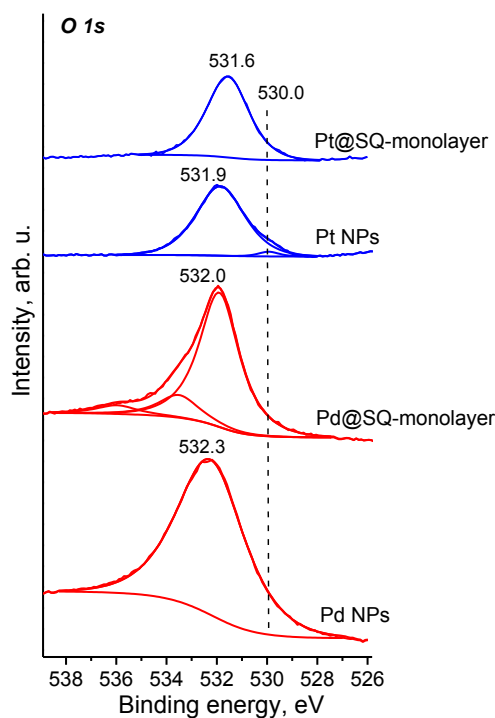
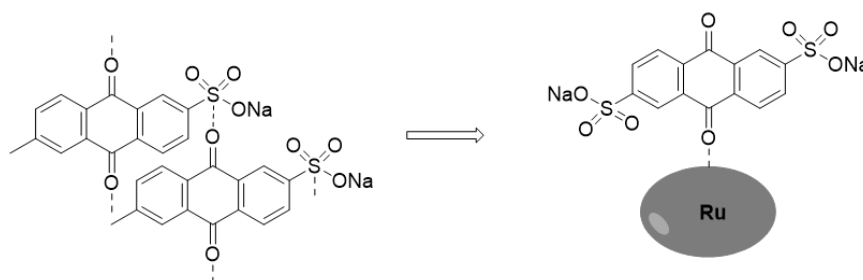


**Figure 5-7.** *O 1s* XPS core level spectra of Pd NPs, Pd@SQ-monolayer and Pt NPs, Pt@SQ-monolayer.



**Scheme 5-3.** *Scheme of interaction between Ru and SQ.*

Pure SQ sample demonstrates only one O 1s peak at 531.8 eV while it was expected to have two types of oxygen:  $\text{SO}_3^{2-}$  and  $\text{C}=\text{O}$ . Most probably O in  $\text{SO}_3^{2-}$ <sup>31</sup> and  $\text{C}=\text{O}$ <sup>32</sup> groups is hard to distinguish in SQ due to strong interaction between these groups. Ru NPs demonstrates the same intense O 1s peak with 531.8 eV BE that was associated with  $\text{RuO}_3$  phase or surface  $\text{Ru}(\text{OH})_3$ <sup>33</sup>. Coating of SQ over Ru NPs leads to appearance of additional peaks at 530.2 eV and 534.1 eV, which could be assigned to oxygen in carbonyl and sulfo groups, respectively<sup>34</sup>. The appearance of these peaks could indicate on strong interaction between  $\text{C}=\text{O}$  and Ru (**Scheme 5-3**), which results in differentiation of O in  $\text{NaSO}_3^-$  and  $\text{C}=\text{O}$ .

### 5.2.3 Structure-catalytic performance relationship

In order to understand the role of SQ and Ru in core-shell catalyst for oxidation of alcohols we have varied type of the metal and quinone. We have used Pd and Pt nanoparticles prepared in the same way for subsequent deposition of SQ to check the effect of metal of the core on the catalytic performance during oxidation of octanol.

**Figure 5-8** demonstrates selectivity-conversion curves for Pd@SQ and Pt@SQ catalysts with different content of SQ in comparison with Pd and Pt nanoparticles. In comparison with Ru catalysts, the deposition of SQ over Pt and Pd leads to low effect in selectivity or significant decrease of the selectivity to aldehyde with increase of the contribution of acid and esters.

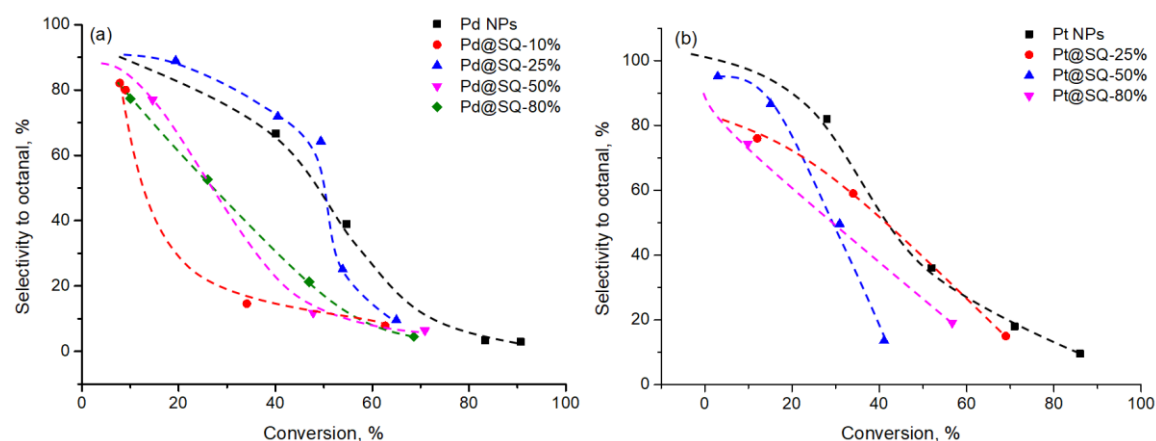


**Figure 5-8.** Shell thickness effects in variation of selectivities versus conversions in selective oxidation of 1-octanol, conditions: 3.0 g 1-octanol, 50 mg catalysts, 10 bar  $O_2$ , 100 °C and solvent-free, time 1-48 h. (a) Pd-based catalysts; (b) Pt-based catalysts.

This effect could be explained by different properties of Ru in comparison with Pt and Pd. Pt and Pd are well known catalysts for hydrogenation/dehydrogenation reactions in comparison with Ru, which is used in hydrogenolysis. The reason is in high oxophilicity of Ru leading to easy adsorption of oxygen on the surface with formation of Ru-O species. In order to confirm it we have examined O 1s XPS spectra. SQ covered Pt and Pd nanoparticles in O 1s spectra do not show peak around 530 eV, which has been associated with Me-O species due to strong interaction between Ru and SQ (**Figure 5-9**). Thus, one can conclude that there is no interaction between Pt, Pd and SQ in contrast to Ru nanoparticles. The small 530 eV peak detected in the spectrum of Pt NPs can be associated with oxidation of a small portion of Pt in the

parent sample. Pd 3d and Pt 4f spectra demonstrate the metallic state of the elements with no changes after SQ loading.

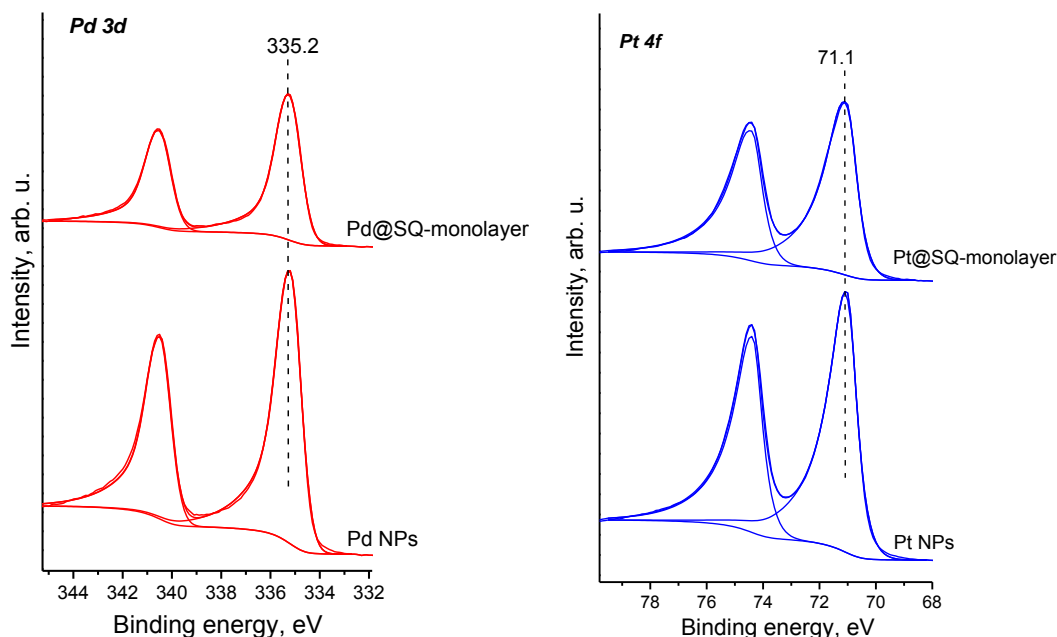


**Figure 5-9.** XPS spectra of Pd 3d in Pd@SQ-monolayer and Pd NPs, Pt 4f in Pt@SQ-monolayer and Pt NPs samples.

**Table 5-2.** Selectivities vs. conversions in selective oxidation of 1-octanol by Ru@quinones-80% at 100 °C.

Catalysts	Time /h	Conversion /%	Selectivity /%			
			octanal	octanoic acid	octyl octanoate	octyl ether
Ru@BQ-80%	24	48	17	32	39	11
Ru@NQ-80%	24	< 5				
Ru@EQ-80%	30	60	13	50	17	18
Ru@CQ-80%	32	54	17	40	29	9

Thus, interaction of Ru with SQ is the key factor of high selectivity during oxidation of alcohols to carbonyl compounds. The mechanism of the reaction has been studied using FTIR and electrochemical methods.

### 5.2.4 Mechanism study

According to our earlier studies oxidation of alcohols over Ru nanoparticles proceed according to Mars-van Krevelen mechanism by interaction of surface RuO<sub>x</sub> species over Ru nanoparticles with alcohol with formation of aldehyde and

subsequent reoxidation of Ru nanoparticles. In order to verify if SQ could be involved in this mechanism of oxidation of alcohols we have performed treatment of the catalyst in octanol in inert atmosphere. The only product of the reaction is octanal. **Figure 5-10** demonstrates the conversion of octanol depending on the content of SQ in the catalyst. The yield of octanal was gradually decreasing from 9 % to 1 % with increase of the content of SQ to 80 %. It indicates on different mechanism of alcohol oxidation in this case and absence of direct contact of octanol with Ru core.

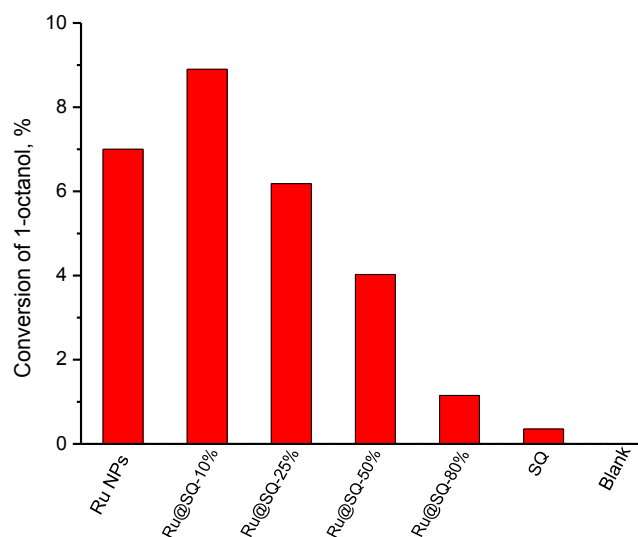


**Figure 5-10.** Oxidation of alcohol by Ru NPs, pure SQ and Ru@SQ-X% catalysts in inert atmosphere. Reaction conditions: the catalysts with normalized amount of Ru, 0.1g octanol, 2.0 g toluene as solvent,  $T=100^{\circ}\text{C}$ , reacted for 3h.

In addition, considering alcohols oxidation to acids as consecutive reaction with intermediate formation of aldehydes the higher selectivity to octanal could be explained by suppression of further aldehyde oxidation over core-shell catalysts. In order to support this assumption we have performed model reaction of oxidation of octanal at mild reaction conditions to avoid autoxidation in **Figure 5-11**. At 60 °C and air instead of oxygen blank experiments without Ru species show almost no conversion of octanal. Ru NPs provide conversion of 26 % of octanal to acid. Increase of the amount of coated SQ leads to suppression of octanal oxidation and correlates with the results of octanol accessibility to Ru core. It proves that SQ shell protects Ru core from interaction with Ru core and suppress over-oxidation, which could be the reason of high selectivity.

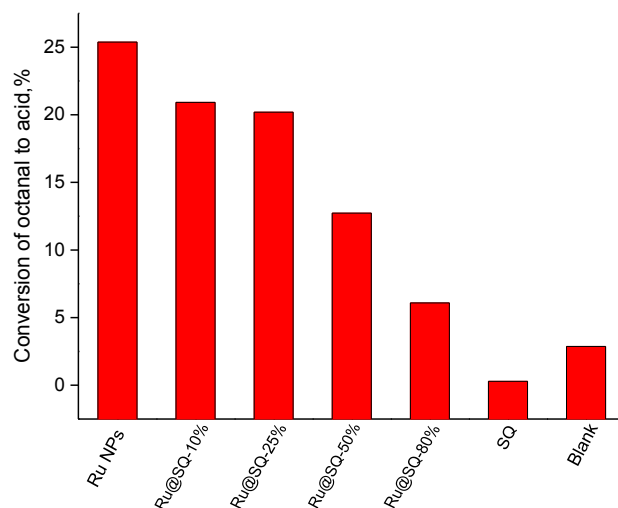


**Figure 5-11.** Oxidation of 1-octanal with different catalysts. Reaction conditions: the catalysts with normalized amount of 5.0 mg Ru, 0.3 g octanal, solvent-free,  $T=60^{\circ}\text{C}$ , and air as oxidant at atmospheric pressure, reacted for 20min.

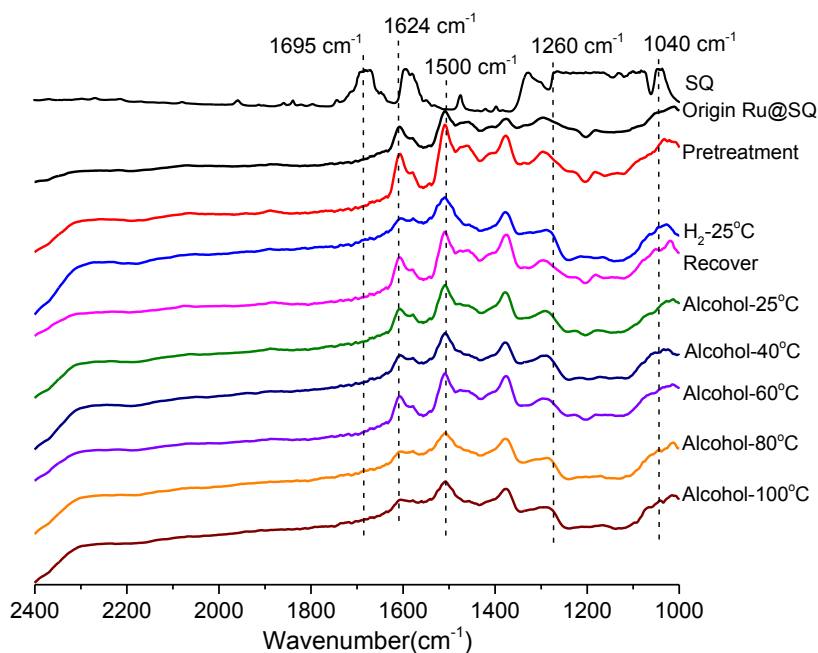


**Figure 5-12.** In-situ IR spectra of Ru@SQ-80% by  $\text{H}_2$  and furfuryl alcohol treatment at diverse temperatures.

The key question in this case is how Ru@SQ catalyst provides oxidative dehydrogenation of alcohols. In-situ FTIR has been used to study the state of SQ during interaction with alcohol. In the FTIR spectrum of parent SQ (**Figure 5-12**), the peaks at  $1220\text{ cm}^{-1}$  and  $1040\text{ cm}^{-1}$  are attributed to the sodium sulfonate substituent groups<sup>31</sup> and the absorptions at  $1500\text{ cm}^{-1}$  is the stretching of aromatic conjugate C=C band<sup>36</sup> strong characteristic peaks at  $1695\text{ cm}^{-1}$  and  $1624\text{ cm}^{-1}$  are respectively assigned to the stretching vibrations of C=O of a non-chelated and a chelated quinone

carbonyl group<sup>37</sup>. And the former disappeared after core-shell structure fabrication, and it could be explained by the interaction between the dissociative quinonyl C=O and Ru NPs, which is totally in accordance with XPS results (**Figure 5-6**). Injection of hydrogen into in-situ IR unit leads to decrease of the intensity of the chelated C=O group at 1624 cm<sup>-1</sup>, which could be recovered after the re-heating treatment at 100 °C, indicating the reduction and oxidation of the C=O groups during cycling. The sodium sulfonate substituent groups have no change, confirming that the sodium sulfonate substituents are thermochemically stable in both catalysts. Prominently, the introduction of furfuryl alcohol vapors in the cell with subsequent incremental temperature from 25 to 100 °C shows disappearance of C=O group at 1624 cm<sup>-1</sup> starting from 80 °C in comparison with no effect for mechanical mixture sample Ru+SQ-80% (**Figure 5-13**). Thus, quinonyl group in our core-shell catalyst can be used for hydrogen transfer abstraction from alcohol with generation of aldehyde and hydrogenated carbonyl group in the shell.

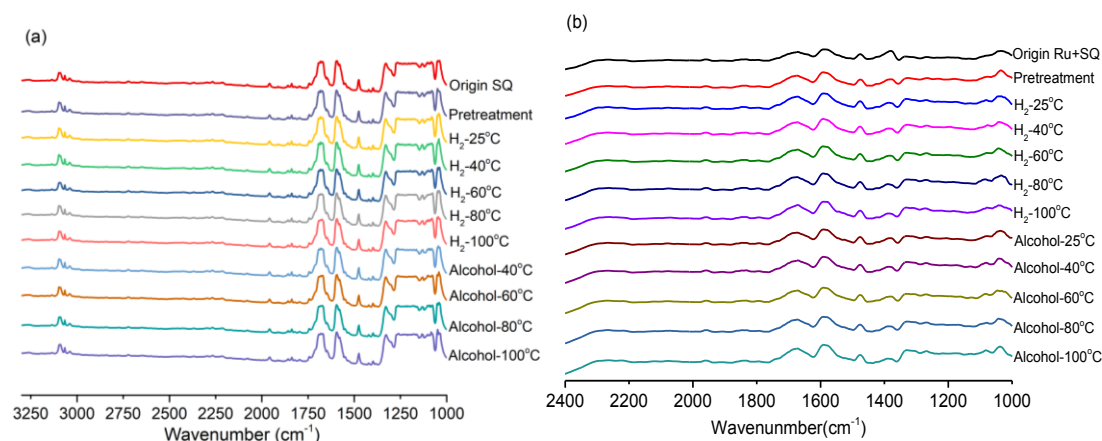


**Figure 5-13.** In-situ IR spectra of (a) pure SQ and (b) mechanical mixture Ru+SQ-80% by H<sub>2</sub> and furfuryl alcohol treatment at diverse temperatures.

In the case of SQ and Ru+SQ-80% catalyst (**Figure 5-13**), addition of hydrogen or alcohol at different temperatures do not lead to the change of the spectra. It means that SQ could not adsorb or chemically react with hydrogen or alcohol in the absence of metal particles in the core.

Electrochemical experiments have been used to further evaluate the state of SQ in the core-shell catalyst. Cyclic voltammograms (CVs) of the bare glassy carbon (GC) electrode, Ru NPs/GC, SQ/GC, and Ru@SQ-80%/GC electrodes in Ar-saturated DMSO solution with 0.1 M LiClO<sub>4</sub> as electrolyte were studied in the presence/absence of 0.1 M furfuryl alcohol (FA). The cyclic voltammetry data for SQ

are characterized by two anodic and cathodic waves, between -1.6 V and -1 V vs  $\text{Ag}/\text{Ag}^+$  as expected corresponding to the two consecutive one-electron reversible transfer process of the oxydo-reduction of anthraquinones to hydroquinone (**Figure 5-14, Table 5-3**). However when 0.1M of furfuryl alcohol (FA) is added a 3<sup>rd</sup> anodic wave occurs at -0.14 V for SQ/FA and at -0.21 V for Ru@SQ-80%-FA corresponding to the oxidation of FA. At the same time, blank Ru NPs/GC and bare GC electrodes have no CVs responses of redox couple that exclude the influence of glassy carbon electrode, as seen in **Figure 5-15**. Moreover, the resulting current density for FA oxidation with the Ru@SQ-80% is higher compared to pure SQ. The negative shift and higher current density of this peak for Ru@SQ-80%, indicates the increase of catalytic activity of Ru@SQ-80% compared to pure SQ for the oxidation of FA. The improved electrocatalytic activity in oxidation of FA could be due to the presence of Ru in the core which accelerates electron transfer via improved conductivity and change of the electronic state of SQ in core-shell catalyst observed by FTIR and XPS.

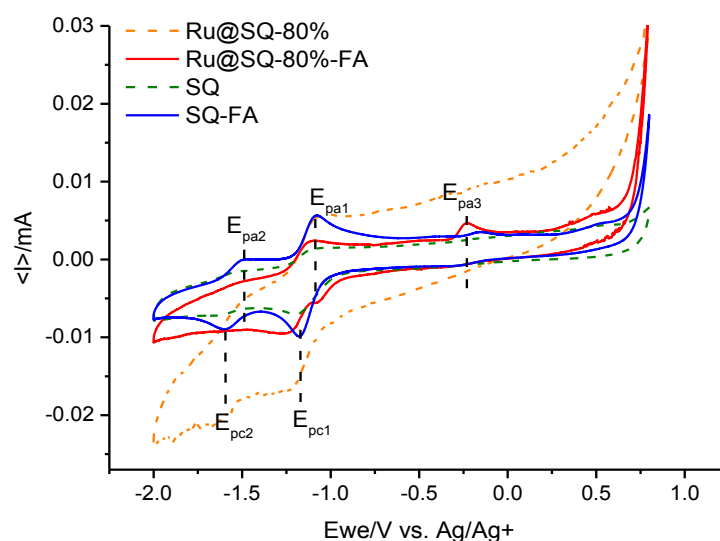


**Figure 5-14.** Cyclic voltammograms of the studied catalysts on a glassy carbon electrode in 0.1 M  $\text{LiClO}_4$  in the DMSO solution with/without 0.1 M furfuryl alcohol (FA) inside in the range of -2.0 to 0.8 V at 100 mV/s scan rate.

It is also interesting to note that the peaks corresponding to the oxydo-reduction of anthraquinone to hydroquinone for pure SQ in the presence of FA presents better pronounced oxy-reduction peaks which could be due to hydrogen transfer from FA.

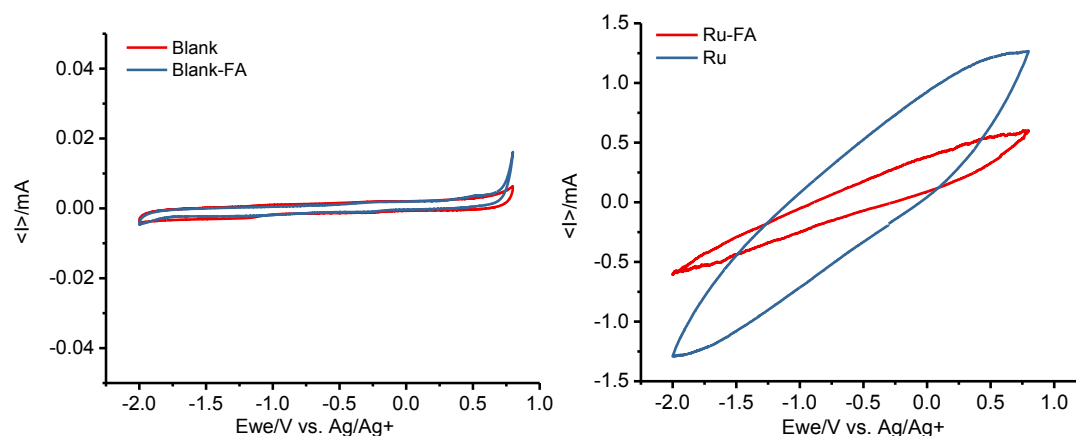


**Figure 5-15.** Cyclic voltammograms of the bare glassy carbon and Ru NPs deposited on electrode in 0.1 M LiClO<sub>4</sub> in the DMSO solution with/without 0.1 M furfuryl alcohol (FA) inside in the range of -2.0 to 0.8 V at 100 mV/s scan rate.

**Table 5-3.** The values of cathodic E<sub>pc</sub> and anodic E<sub>pa</sub> peak potentials in DMSO solution.

	Anodic potential (V vs. Ag/Ag <sup>+</sup> )			Cathodic potential (V vs Ag/Ag <sup>+</sup> )	
	E <sub>pa1</sub>	E <sub>pa2</sub>	E <sub>pa3</sub>	E <sub>pc1</sub>	E <sub>pc2</sub>
SQ	-1.54	-1.13		-1.62	-1.19
SQ-FA	-1.51	-1.08	-0.14	-1.61	-1.18
Ru@SQ-80%	-1.56	-1.06		-1.74	-1.06
Ru@SQ-80%-FA	-1.59	-1.12	-0.21	-1.67	-1.25

### 5.3 Conclusion

In conclusion, we have demonstrated that it is possible to fabricate nanocell with core-shell structure containing Ru nanoparticles in the core and electro-deficient anthraquinones in the shell for selective oxidation of alcohols to carbonyl compounds. XPS analysis shows strong interaction between quinone species and Ru nanoparticles leading to transfer of the electronic density to Ru and easy activation of alcohols over the shell. In-situ mechanism study confirms transfer of hydrogen to carbonyl group of quinone species from alcohol with subsequent transfer to the core for oxygen reduction to water. This concept can be used for other application, where contact of the target product of the reaction with metal results in decrease of the selectivity.

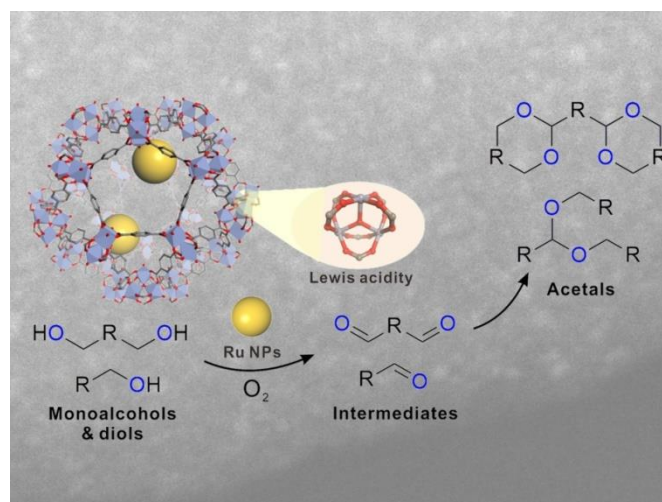
## 5.4 References

1. Steven L. R.; Koteel, C., Activation through impregnation. Permanganate-coated solid supports. *J. Am. Chem. Soc.* **1977**, *99*, 3837-3838.
2. Muzart, J., Chromium-Catalyzed Oxidations in Organic Synthesis. *Chem. Rev.* **1992**, *92*, 113-140.
3. F. M. Perree; Gaudemer, A., Manganese Porphyrin-catalysed Oxidation of Olefins to Ketones by Molecular Oxygen. *J. Chem. Soc. Chem. Commun.* **1981**, 1282, 874-875.
4. Uyanik M. ; K., I., Hypervalent Iodine-mediated Oxidation of Alcohols. *Chem. Commun.* **2009**, *1*, 2086-2099.
5. Satoshi, I.; Koji, K.; Shigeru, I.; Teruaki, M., A New and Facile Method for the Direct Preparation of  $\alpha$ -Hydroxycarboxylic Acid Esters from  $\alpha,\beta$ -Unsaturated Carboxylic Acid Esters with Molecular Oxygen and Phenylsilane. *Chem. Lett.* **1990**, *19*, 1869-1872.
6. Zhai, W.; Xue, S.; Zhu, A.; Luo, Y.; Tian, Y., Plasmon-Driven Selective Oxidation of Aromatic Alcohols to Aldehydes in Water with Recyclable Pt/TiO<sub>2</sub> Nanocomposites. *ChemCatChem.* **2011**, *3* (1), 127-130.
7. Ilyas, M.; Sadiq, M., Liquid-Phase Aerobic Oxidation of Benzyl Alcohol Catalyzed by Pt/ZrO<sub>2</sub>. *Chem. Eng. Technol.* **2007**, *30* (10), 1391-1397.
8. Xie, J.; Huang, B.; Yin, K.; Pham, H. N.; Unocic, R. R.; Datye, A. K.; Davis, R. J., Influence of Dioxygen on the Promotional Effect of Bi during Pt-Catalyzed Oxidation of 1,6-Hexanediol. *ACS Catal.* **2016**, *6* (7), 4206-4217.
9. Hackett, S. F.; Brydson, R. M.; Gass, M. H.; Harvey, I.; Newman, A. D.; Wilson, K.; Lee, A. F., High-activity, single-site mesoporous Pd/Al<sub>2</sub>O<sub>3</sub> catalysts for selective aerobic oxidation of allylic alcohols. *Angew. Chem. Int. Ed.* **2007**, *46* (45), 8593-8596.
10. Parlett, C. M. A.; Bruce, D. W.; Hondow, N. S.; Lee, A. F.; Wilson, K., Support-Enhanced Selective Aerobic Alcohol Oxidation over Pd/Mesoporous Silicas. *ACS Catal.* **2011**, *1* (6), 636-640.
11. Zhao, G.; Ling, M.; Hu, H.; Deng, M.; Xue, Q.; Lu, Y., An excellent Au/meso- $\gamma$ -Al<sub>2</sub>O<sub>3</sub> catalyst for the aerobic selective oxidation of alcohols. *Green Chem.* **2011**, *13* (11), 3088-3092.
12. Tanaka, A.; Hashimoto, K.; Kominami, H., Preparation of Au/CeO<sub>2</sub> exhibiting strong surface plasmon resonance effective for selective or chemoselective oxidation of alcohols to aldehydes or ketones in aqueous suspensions under irradiation by green light. *J. Am. Chem. Soc.* **2012**, *134* (35), 14526-14533.
13. Nie, J.; Xie, J.; Liu, H., Efficient aerobic oxidation of 5-hydroxymethylfurfural to 2,5-diformylfuran on supported Ru catalysts. *J. Catal.* **2013**, *301*, 83-91.
14. Wang, G.; Andreasson, U.; Backval, J. E., Aerobic oxidation of secondary alcohols via ruthenium-catalysed hydrogen transfer involving a new triple catalytic system. *J. Am. Chem. Soc.* **1994**, *4*, 1037-1039.
15. A.C. Schmidt; Stark, C. B. W., TPAP-Catalyzed Direct Oxidation of Primary Alcohols to Carboxylic Acids through Stabilized Aldehyde Hydrates. *Org. Lett.* **2011**, *13*, 4164-4167.
16. Hernandez, W. Y.; Hadjar, A.; Giroir-Fendler, A.; Andy, P.; Princivale, A.; Klotz, M.; Marouf, A.; Guizard, C.; Tardivat, C.; Viazzi, C., Electrochemically-assisted NO<sub>x</sub> storage–reduction catalysts. *Catal. Today* **2015**, *241*, 143-150.

17. Adair, G. R. A.; Williams, J. M. J., Oxidant-free oxidation: ruthenium catalysed dehydrogenation of alcohols. *Tetrahedron Lett.* **2005**, *46* (47), 8233-8235.
18. Deffernez, A.; Hermans, S.; Devillers, M., Bimetallic Bi–Pt, Ru–Pt and Ru–Pd and trimetallic catalysts for the selective oxidation of glyoxal into glyoxalic acid in aqueous phase. *Appl. Catal. A: Gen.* **2005**, *282* (1-2), 303-313.
19. Mori, K.; Hara, T.; Mizugaki, T.; Ebitani, K.; Kaneda, K., Hydroxyapatite-Supported Palladium Nanoclusters: A Highly Active Heterogeneous Catalyst for Selective Oxidation of Alcohols by Use of Molecular Oxygen. *J. Am. Chem. Soc.* **2004**, *126*, 10657-10666.
20. Hosokawa, S.; Hayashi, Y.; Imamura, S.; Wada, K.; Inoue, M., Effect of the Preparation Conditions of Ru/CeO<sub>2</sub> Catalysts for the Liquid Phase Oxidation of Benzyl Alcohol. *Catal. Lett.* **2009**, *129* (3-4), 394-399.
21. Ryland, B. L.; Stahl, S. S., Practical Aerobic Oxidations of Alcohols and Amines with Homogeneous Copper/TEMPO and Related Catalyst Systems. *Angew. Chem. Int. Ed.* **2014**, *53* (34), 8824-8838.
22. Ma, S.; Liu, J.; Li, S.; Chen, B.; Cheng, J.; Kuang, J.; Liu, Y.; Wan, B.; Wang, Y.; Ye, J.; Yu, Q.; Yuan, W.; Yu, S., Development of a General and Practical Iron Nitrate/TEMPO-Catalyzed Aerobic Oxidation of Alcohols to Aldehydes/Ketones: Catalysis with Table Salt. *Adv. Synth. Catal.* **2011**, *353* (6), 1005-1017.
23. Walsh, K.; Sneddon, H. F.; Moody, C. J., Solar photochemical oxidations of benzylic and allylic alcohols using catalytic organo-oxidation with DDQ: Application to lignin models. *Org. Lett.* **2014**, *16* (19), 5224-5227.
24. Hu, Y.; Chen, L.; Li, B., Fe (NO<sub>3</sub>)<sub>3</sub>/2, 3-dichloro-5, 6-dicyano-1, 4-benzoquinone (DDQ): An efficient catalyst system for selective oxidation of alcohols under aerobic conditions. *Catal. Commun.* **2018**, *103*, 42-46.
25. Liu, R.; Liang, X.; Dong, C.; Hu, X., Transition-metal-free: A highly efficient catalytic aerobic alcohol oxidation process. *J. Am. Chem. Soc.* **2004**, *126* (13), 4112-4113.
26. Scott, J. W.; Parrish, D. R.; Bizzarro, F. T., A Rapid and Mild Process for the Oxidation of 2, 3-Dichloro-5, 6-dicyanobenzoquinone (DDQ) from 2, 3-Dichloro-5, 6-dicyanohydroquinone (DDHQ). *Org. Prep. Proced. Int.* **1977**, *9* (2), 91-94.
27. Cosner, C. C.; Cabrera, P. J.; Byrd, K. M.; Thomas, A. M. A.; Helquist, P., Selective Oxidation of Benzylic and Allylic Alcohols Using Mn(OAc)<sub>3</sub>/Catalytic 2, 3-Dichloro-5, 6-dicyano-1, 4-benzoquinone. *Org. Lett.* **2011**, *13* (8), 2071-2073.
28. Gulaboski, R.; Bogeski, I.; Mirčeski, V.; Saul, S.; Pasieka, B.; Haeri, H. H.; Stefova, M.; Stanoeva, J. P.; Mitrev, S.; Hoth, M., Hydroxylated derivatives of dimethoxy-1, 4-benzoquinone as redox switchable earth-alkaline metal ligands and radical scavengers. *Sci. Rep.* **2013**, *3*, 1865.
29. A.Cecchetto; F. Fontana; F. Miniscia; Recuperoa, F., Efficient Mn–Cu and Mn–Co–TEMPO-catalysed oxidation of alcohols into aldehydes and ketones by oxygen under mild conditions. *Tetrahedron Lett.* **2001**, *42*, 6651–6653.
30. Corberán, V. C.; González-Pérez, M. E.; Martínez-González, S.; Gómez-Avilés, A., Green oxidation of fatty alcohols: Challenges and opportunities. *Appl. Catal. A: General* **2014**, *474*, 211-223.
31. Zhao, J.; Yang, J.; Sun, P.; Xu, Y., Sodium sulfonate groups substituted anthraquinone as an organic cathode for potassium batteries. *Electrochem. Commun.* **2018**, *86*, 34-37.
32. Peake, B.; Simpson, J., X-Ray crystal structure determination of some sodium anthraquinone sulfonate derivatives. *Aust. J. Chem.* **1993**, *46* (10), 1595-1604.

33. Ananth, A.; Gandhi, M. S.; Mok, Y. S., A dielectric barrier discharge (DBD) plasma reactor: an efficient tool to prepare novel RuO<sub>2</sub> nanorods. *J. Phy. D.: Appl. Phys.* **2013**, *46* (15), 155202-155210.
34. Lim, Y.; Tan, Y.; Lim, H.; Huang, N.; Tan, W.; Yarmo, M. A.; Yin, C.-Y., Potentiostatically deposited polypyrrole/graphene decorated nano-manganese oxide ternary film for supercapacitors. *Ceram. Int.* **2014**, *40* (3), 3855-3864.
35. Wendlandt, A. E.; Stahl, S. S., Quinone-Catalyzed Selective Oxidation of Organic Molecules. *Angew. Chem. Int. Ed.* **2015**, *54*, 14638 – 14658.
36. Wang, Y.; He, T.; Liu, M.; Ji, J.; Dai, Y.; Liu, Y.; Luo, L.; Liu, X.; Qin, J., Fast and efficient oil-water separation under harsh conditions of the flexible polyimide aerogel containing benzimidazole structure. *Colloid Surf. A* **2019**, *581*, 123809.
37. Demagos, G. P.; Baltus, W.; Höfle, G., New anthraquinones and anthraquinone glycosides from *Morinda lucida*. *Zeitschrift für Naturforschung B* **1981**, *36* (9), 1180-1184.

# CHAPTER 6 Direct Aerobic Oxidation of Mono-alcohols and Diols to Acetals Using Tandem Ru@MOF Catalysts



---

## ABSTRACT:

The aerobic oxidation of monoalcohols and diols to acetals is an important academic and industrial challenge for the production of fine chemicals and intermediates. The existing methods usually rely on a two-step process in which alcohols are first oxidized to aldehydes over metal catalysts (Ru, Pt, Pd) and then acetalized using acids. Due to the instability of aldehydes, how to avoid over-oxidation to their respective carboxylic acids and esters is a long-standing challenge. For this reason, certain non-conjugated dialdehydes have never been successfully produced from diol oxidation. Hereby we report a Ru@MOF tandem catalyst containing ultra-fine Ru nanoparticles (< 2 nm) for direct alcohol to acetal conversion of monoalcohols and diols with no formation of carboxylic acids. Mechanistic study reveals that the presence of Lewis acid sites in the MOF work in concert with Ru active sites to promptly convert aldehydes to acetals thereby effectively suppressing the formation of over-oxidation byproducts.

This chapter is based on the following publication:

---

*S. Zhang, J. P.H. Li, J.P. Zhao, D. Wu, B. Yuan, V. Ordomsky\*, T. Li\*, Nano Research, 2019. submitted.*

## 6.1 Instruction

Acetals are an important class of industrial products that can be used as precursors for polymer synthesis (e.g. polyacetal resins)<sup>1</sup>, stable organic intermediates for fine chemicals production<sup>2-4</sup> and even gasoline and diesel additives<sup>5</sup>. In organic synthesis, acetalization is a common way to stabilize and protect reactive carbonyl groups for subsequent transformation of complex organic compounds<sup>6</sup>. Current methods to produce acetals rely on a two-step process: oxidation of alcohol to aldehyde/ketone<sup>7</sup> followed by acetalization using a Brønsted or Lewis acid catalyst<sup>8</sup>. The oxidation of alcohol is a challenging task in its own right because aldehydes tend to over-oxidize and form by-products such as carboxylic acids and esters thereby reducing the yield and increasing the difficulty during product isolation<sup>9</sup>. On the other hand, traditional acetalization processes commonly involve the use of strong corrosive homogeneous acids as the catalysts which are not only unrecyclable but also detrimental to the environment<sup>10-11</sup>.

Direct alcohols to acetals conversion (DAAC) can eliminate the concern for aldehyde over-oxidation and minimize the reaction steps at the same time. Although DAAC of activated aromatic alcohols such as benzyl alcohol is common in literature<sup>12-15</sup>, DAAC of aliphatic alcohols is rare and usually requires sophisticated metal based homogeneous catalysts and, in certain cases, with acid additives<sup>16-18</sup>. Such a homogeneous system results in complex separation procedures, corrosion of the equipment and formation of waste products.

Therefore, the development of heterogeneous catalysts for DAAC is of significant industrial interest. To the best of our knowledge, there have only been three reports regarding the direct conversion of aliphatic monoalcohols to their relative acetals using heterogeneous photocatalysts<sup>19-21</sup>. Traditional heterogeneous catalysts, although desired, remain unavailable. In particular, DAAC of polyols has never been achieved due to reaction complexity.

The design of an efficient heterogeneous catalyst for DAAC should involve a combination of a metallic functional moiety for alcohol oxidation and an acidic functional moiety for acetalization. Much effort has been devoted to developing efficient aerobic oxidation methods for alcohols using readily available metal supported heterogeneous catalysts<sup>22</sup>, among which, Ru stands out as a highly efficient oxidation catalyst<sup>23</sup>. However, its high tendency of over-oxidizing aldehydes to acids

and esters is a key bottleneck to its wide use.

Over the past decade, metal-organic frameworks (MOFs) have drawn tremendous attention as heterogeneous supports for ultrafine catalytic metal and metal oxide nanoparticles due to their high surface area, the ability to stabilize NPs through physical confinement and the ability of fine tuning catalytic local environment around the metal catalysts <sup>24-31</sup>.

Recently, the inherent acidity of certain MOFs has been utilized as solid acids for various acid catalyzed reactions including Friedel-Crafts acylation <sup>32-33</sup>, esterification <sup>34</sup>, olefin isomerization <sup>35</sup> and, of course, acetalization of aldehydes <sup>15, 36-39</sup>. Compared to other solid acids such as zeolites and metal oxides, MOFs provide a far richer platform allowing for fine tuning of acidity and local environment owing to their modular synthesis <sup>40-41</sup>. We reason that by bringing ultrafine Ru nanoparticles in close proximity to the Lewis acidic sites in the MOF, the resultant tandem catalyst can suppress over-oxidation of aldehydes through a rapid acetalization process thereby achieving DAAC with high selectivity.

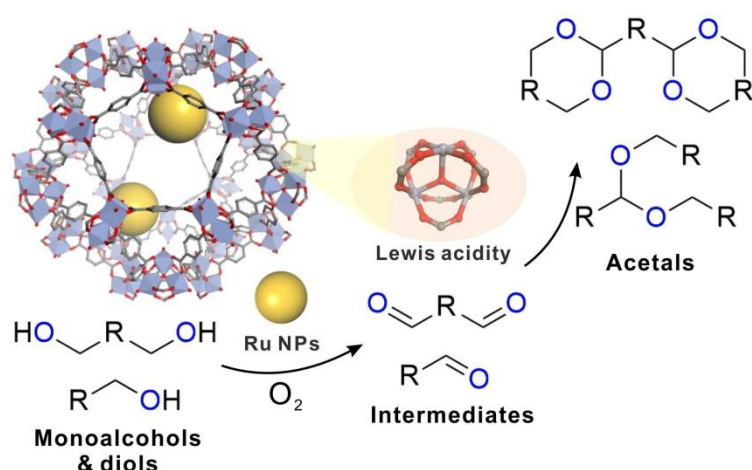


**Figure 6-1.** Graphic illustration of the tandem catalytic process of alcohols to acetals in Ru@MOF.

Herein, we report a series of tandem Ru@MOF catalysts for DAAC of aliphatic alcohols, diols, and biomass (**Figure 6-1**). Through a double-solvent approach, ultrafine Ru NPs < 2.0 nm were evenly distributed in the MOF matrices. Owing to a cooperative effect of Ru NPs and Lewis acidic sites within the MOFs, butanol, ethylene glycol and 1,3-propanediol were successfully converted to their respective acetals through aerobic oxidation under solvent-free conditions. Mechanistic study showed that strong acidity is critical for the efficient acetalization of aldehyde thereby preventing over-oxidation and ensuring high selectivity towards desired products.

## 6.2 Results and Discussion

### 6.2.1 Synthesis and characterization of the catalysts

MIL-101(Cr) was synthesized according to a previously reported method<sup>42</sup>. The reason to select MIL-101(Cr) as the MOF support is largely because of its excellent chemical and mechanical stability. Meanwhile, its relatively large aperture size ( $1.2 \times 1.2$  nm &  $1.6 \times 1.4$  nm)<sup>43</sup> would allow passage of bulky molecules such as acetals. Moreover, the  $\text{Cr}_3(-\text{COO})_6(\text{OH})_3$  secondary building unit (SBU) can provide moderate acidity that are capable of achieving many acid catalyzed conversions including cyanosilylation of benzaldehyde<sup>44</sup> and oxidation of anthracene to 9,10-anthraquinone<sup>45</sup> *etc.* The scanning electron microscopy (SEM) images (**Figure 6-2**) show monodispersed octahedral crystals of MIL-101(Cr) with an average particle size of  $225 \pm 75$  nm.

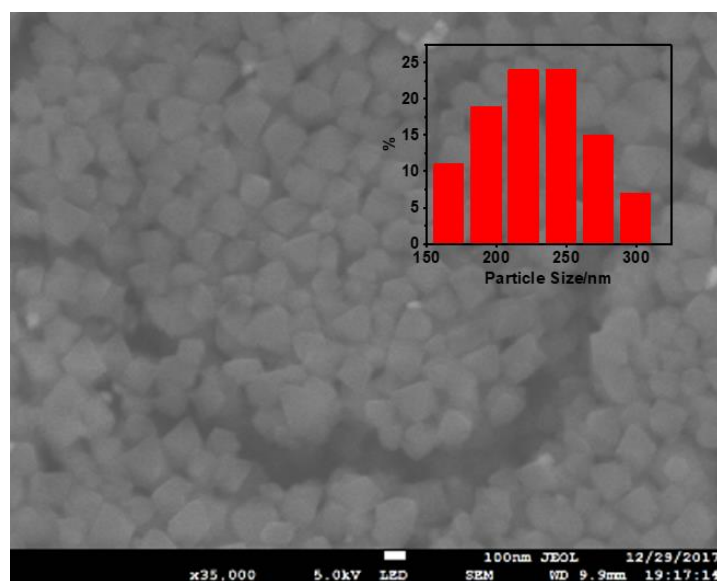


**Figure 6-2.** The SEM image of MIL-101(Cr) particles. Inset shows the size distribution of MIL-101(Cr).

The crystallinity of the MOF was further confirmed by its powder X-ray diffraction (PXRD) pattern (**Figure 6-3C**). To load the MOF cavities with Ru NPs, a modified double-solvent approach was adopted<sup>46</sup>. Specifically,  $\text{RuCl}_3$  was dissolved in a small amount of ethanol/water mixture and then mixed with MIL-101(Cr). After introducing excess petroleum ether as the secondary solvent, ethanol was gradually drawn out from the water phase therefore subsequently pushing  $\text{RuCl}_3$  and  $\text{H}_2\text{O}$  into the hydrophilic cavities within the MOF. After reducing  $\text{Ru}^{3+}$  in a hydrogen atmosphere at  $200\text{ }^\circ\text{C}$ ,  $\text{Ru@MIL-101(Cr)}$  was obtained as the final product with 5.4

wt% of Ru as quantified by inductively coupled plasma optical emission spectrometry (ICP-OES) (**Table 6-1**).

**Table 6-1.** ICP-OES results

MOF	Ru	Cr	Al	Zr	Loading/%
Ru@MIL-101(Cr)	1	3.456			5.4
Ru@MIL-100(Al)	1		1.540		7.6
Ru@MOF-808(Zr)	1			4.914	7.5
MIL-101(Cr)@Ru	1	2.73			6.8

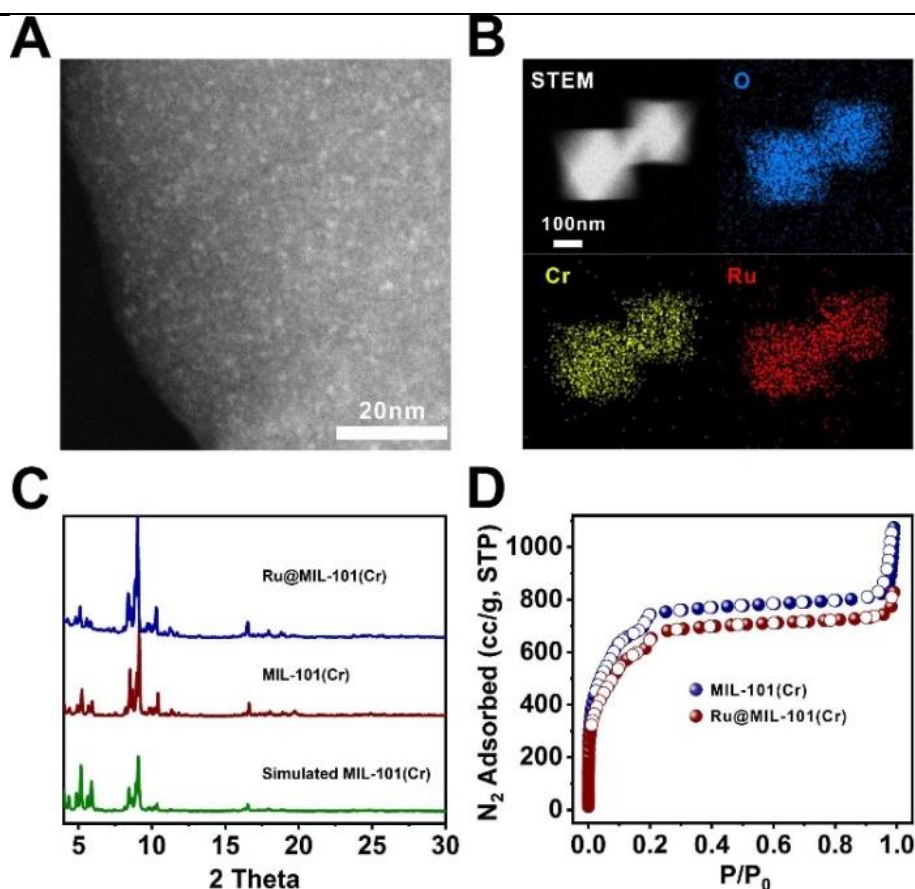


**Figure 6-3.** Characterization of Ru@MIL-101(Cr) catalyst by TEM analysis (A) DF-TEM image; (B) STEM-EDS elemental mapping; (C) PXRD and (D)  $N_2$  sorption isotherms of MIL-101(Cr) (navy) and Ru@MIL-101(Cr) (red) at 77K.

The high-angle annular dark-field scanning transmission electron microscopy (HAADF-STEM) image along with energy dispersion X-ray spectroscopy (EDS) elemental mapping results shows that Ru NPs with an average size of  $\sim 1.1$  nm was evenly distributed across the whole crystallite (**Figure 6-3A&B**). Macroscopically, the original green color of the MIL-101(Cr) powder turned greyish as a result of Ru NPs incorporation (**Figure 6-4**). The nitrogen adsorption isotherm of

Ru@MIL-101(Cr) at 77 K shows an uptake capacity of 828 cc/g at 0.95 P/P<sub>0</sub> and a BET surface area of 2140 m<sup>2</sup>/g. These values are only slightly lower than that of the neat MIL-101(Cr) (1073.9 cc/g and 2509.3 m<sup>2</sup>/g) suggesting that the porosity of the MOF was largely unaffected by the incorporation of Ru NPs which is essential for rapid molecular diffusion during catalysis (**Figure 6-3D**).

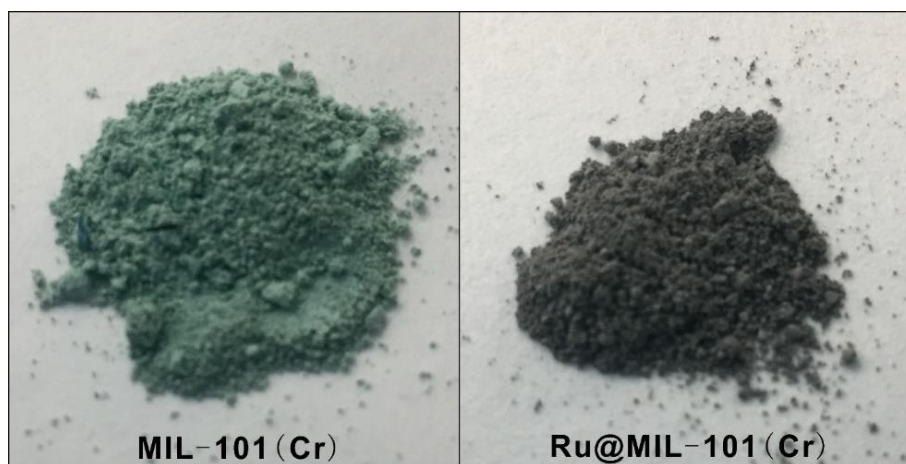


**Figure 6-4.** Photographs of the MIL-101(Cr) and Ru@MIL-101(Cr).

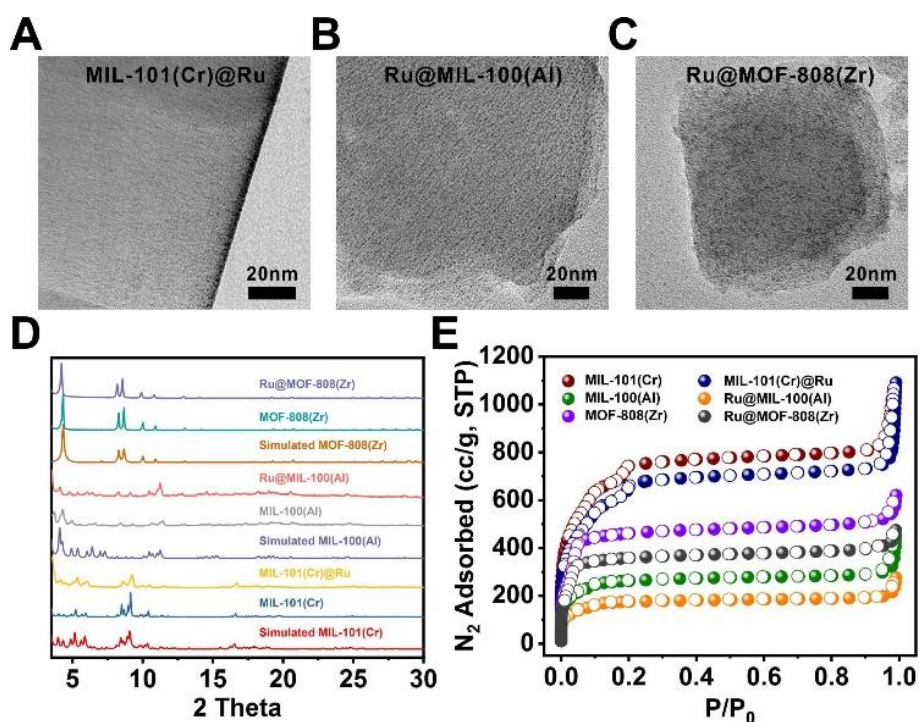


**Figure 6-5.** TEM images of MIL-101(Cr)@Ru (A), Ru@MIL-100(Al) (B), Ru@MOF-808(Zr) (C), their PXRD patterns compared to neat MOF and simulated MOF (D) and N<sub>2</sub> sorption isotherms at 77K (E).

MIL-100(Al)<sup>47</sup> and MOF-808(Zr)<sup>33</sup> are representative examples of an aluminum MOF and a zirconium MOF. By switching Cr(III) SBU to that of Al(III)

and Zr(IV), we aim to modulate the acidity of the MOFs thereby investigating the role of acidity in the DAAC process. The crystallinity of these two MOFs was confirmed by their respective PXRD patterns with sizes of crystals similar to those of MIL-101(Cr) (**Figure 6-5D** and **Figure 6-6**).

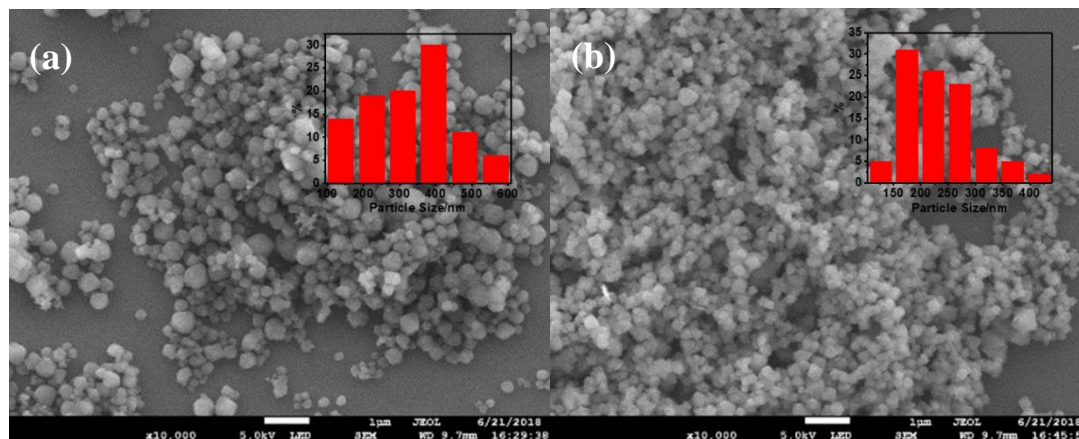


**Figure 6-6.** The SEM image of: (a) MIL-100(Al) particles. Inset shows the size distribution of MIL-100(Al); (b) MOF-808(Zr) particles. Inset shows the size distribution of MOF-808(Zr).

After Ru NPs incorporation, two catalysts, Ru@MIL-100(Al) and Ru@MOF-808(Zr) were obtained. The Ru loadings were determined to be 7.6 and 7.5 wt% respectively by ICP-OES (**Table 6-1**). The PXRD patterns show no loss of crystallinity after Ru impregnation (**Figure 6-5D**). The sizes of the Ru NPs in Ru@MIL-100(Al) and Ru@MOF-808(Zr) were determined to be  $1.0 \pm 0.3$  nm and  $1.2 \pm 0.2$  nm, respectively, by TEM (**Figure 6-5B, 5C**). Meanwhile, they are evenly distributed throughout the MOF particles similar to that of Ru@MIL-101(Cr) (**Figure 6-3A**). N<sub>2</sub> adsorption experiments at 77 K were performed to quantify the retention of porosity after Ru impregnation (**Figure 6-5E**). Compared to their neat MOF counterparts, Ru@MIL-100(Al) and Ru@MOF-808(Zr) show 34% and 22% decrease of total N<sub>2</sub> uptake after Ru NPs inclusion due to the reduction of MOF weight percent as well as partially occupied pore volume.

## 6.2.2 Direct Alcohol to Acetal Conversion

To demonstrate that Ru-MOFs can be used for tandem catalysis, we first selected 1-butanol as an example to synthesize 1,1-dibutoxybutane (DBB) through DAAC (**Table 6-2, Figure 6-7**).

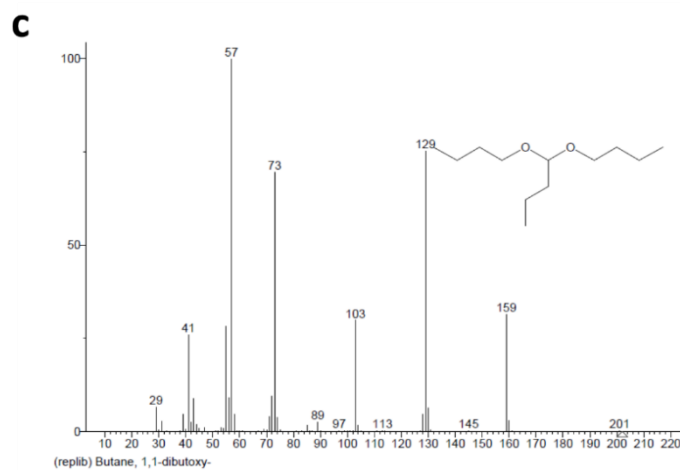
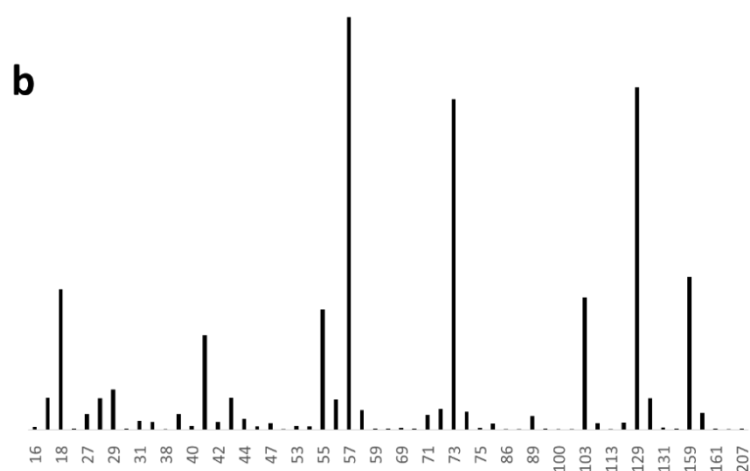
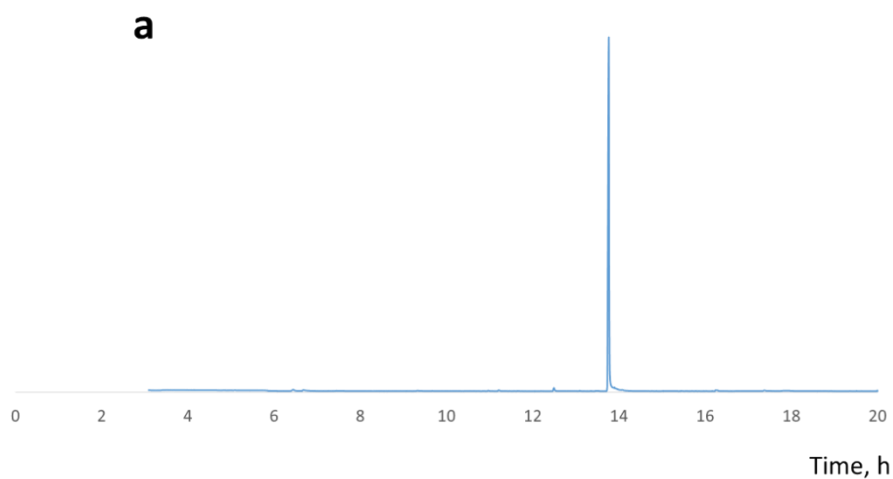
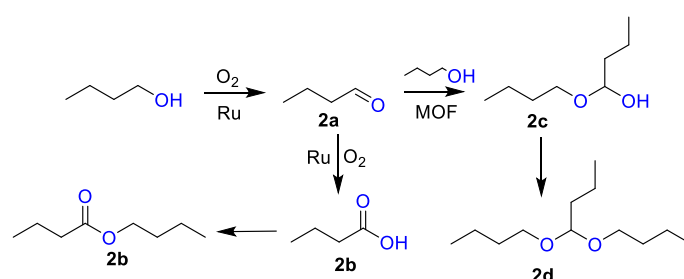


**Figure 6-7.** GC-MS analysis of the products of butanol oxidation over Ru@MIL-101(Cr) (a) with MS spectrum of the main product at 14 min (b) and spectrum from NIST library 1,1-dibutoxybutane (c). The distribution of the fragments for this product is similar to those for the product at 14 min.

The reaction condition was solvent free which, although challenging, is desirable for industrial manufacturing. After 16 h of reaction at 100 °C, 60% 1-butanol was

converted by Ru@MIL-101(Cr). The product analysis reveals that 92% of the product was 1,1-dibutoxybutane (2d) whereas only ~8% was butyraldehyde. Interestingly, no carboxylic acid was observed in the product mixture suggesting that aldehyde over-oxidation was effectively suppressed (**Table 6-2**). In contrast, commercial Ru on carbon (Ru/C) catalyst (Johnson Matthey, 5%Ru/C, FT02RU0006) exhibited high reactivity towards butanol oxidation with an overall conversion of 81 %. However, no DBB was found in the product due to the absence of proper acid sites. Meanwhile, it is worth noting that 33% of the product was butyric acid suggesting severe over-oxidation, which totally correlates with previous reports<sup>23</sup>.

**Table 6-2.** Oxidation of 1-butanol over Ru@MOF catalysts in comparison with



reference Ru/C (3 g of 1-butanol, catalysts (100 mg), 16 h, 100 °C, 10 bar O<sub>2</sub>)

Catalysts	Conversion (%)	Selectivity (%)			
		2a	2b	2c	2d
Ru@MIL-101(Cr)	60	8	0	0	92
MIL-101(Cr)@Ru	36	32	22	0	41
Ru@MOF-808(Zr) <sup>[a]</sup>	17	8	0	44	48
Ru@MIL-100(Al)	28	14	0	1	85
Ru/C + MIL-101(Cr) <sup>[b]</sup>	23	21	1	0	68
Ru/C	81	52	33	0	0
MIL-101(Cr)	0	0	0	0	0
MIL-100(Al)	0	0	0	0	0
MOF-808(Zr)	0	0	0	0	0

<sup>a</sup>The main by-product is 1-butoxybutan-1-ol. <sup>b</sup>Mechanical mixture of 100 mg 5% Ru/C and 100 mg MIL-101(Cr) as catalysts.

To elucidate the effect of Ru spatial distribution on DAAC efficiency, a control catalyst, MIL-101(Cr)@Ru, was prepared in which Ru NPs were purposefully deposited at the MOF skin layer through a conventional wet impregnation and

solution reduction method (**Figure 6-5A**).

The TEM image shows that Ru NPs were exclusively located in the 10 nm thin layer on the MOF surface with a total Ru loading of 6.8 wt% (**Figure 6-5A**). MIL-101(Cr)@Ru exhibits lower overall conversion (36%) compared to Ru@MIL-101(Cr). However, nearly 22% of the product was butyric acid and ester due to over-oxidation. This is because after the alcohol oxidation process by the external Ru NPs, the aldehyde product molecules conveniently diffuse outward before acetalization could occur. The accumulation of aldehyde eventually led to the formation of over-oxidation products. In another scenario, 5%Ru/C was physically mixed with MIL-101(Cr) particles.

Although no acid products were observed, only ~23% of alcohol conversion was achieved with low selectivity (68%) to acetal products. This is likely because the interaction between the ultra-fine Ru NPs located in the MOF cavities with the MOF ligand molecules preserves unique active sites for highly efficient alcohol oxidation. We investigate and discuss the possible active sites on the Ru@MIL-101(Cr) catalyst using in situ Fourier transform infrared spectroscopy (FTIR) in the later part of the paper (vide infra). As a control experiment, neat MIL-101(Cr), MIL-100(Al) and MOF-808(Zr) exhibits no catalytic activity towards alcohol oxidation (**Table 6-2**).

It is apparent that the participation of MIL-101(Cr) to the catalytic process not only achieved one-step synthesis of acetal but also effectively suppressed the formation of over-oxidized by-products. This achievement can be attributed to the cooperative effect of the Lewis acidic sites in the MOF framework and the Ru nanoparticles in close proximity.

To elucidate the relationship between MOF acidity and DAAC efficiency, Ru@MIL-100(Al) and Ru@MOF-808(Zr) were tested for DAAC of 1-butanol. Ru@MOF-808(Zr) only showed a conversion of 17% after 16 h of reaction. Interestingly, the selectivity for the fully acetalized product 2d was only 48% (Table 1), considerably lower than that of Ru(@MIL-101(Cr). Apart from butyraldehyde, the main by product is hemiacetal indicating that the acidity of MOF-808(Zr) is insufficient for complete acetalization. Ru@MIL-100(Al), on the other hand, achieved a conversion of 28% which is still lower than that of Ru@MIL-101(Cr) but higher than that of Ru@MOF-808(Zr). The selectivity for product 2d is 85% with only 1% hemiacetal byproduct formation (**Table 6-2**).

To quantitatively understand the nature of the acidity,  $\text{NH}_3$  temperature-programmed desorption ( $\text{NH}_3$ -TPD) was performed (**Figure 6-8B**).

$\text{NH}_3$ -TPD Detailed calculation as follows:

$$n_{\text{NH}_3} = 1 \text{ g} * \text{Quantity mmol/g}$$

$$n_{\text{metal}} = (1 \text{ g} * N_{\text{metal}}) / (M_{\text{MOF}} \text{ g/mol})$$

$$\text{Rate} = n_{\text{NH}_3} : n_{\text{metal}}$$

Here, quantity is the data which we get from  $\text{NH}_3$  adsorption (from 50 °C to 300 °C),  $M_{\text{MOF}}$  -the molecular formula of MOFs, show in **Table 6-3**,  $N_{\text{metal}}$  -the number of metal in molecular formula [MIL-101(Cr):  $\text{Cr}_3(\text{H}_2\text{O})_3\text{O}[(\text{O}_2\text{C})\text{C}_6\text{H}_4(\text{CO}_2)]_3$ , MIL-100(Al):  $\text{Al}_3\text{O}(\text{OH})(\text{H}_2\text{O})_2[\text{C}_6\text{H}_3(\text{CO}_2)_3]_2$ , MOF-808(Zr):  $\text{Zr}_6\text{O}_4(\text{OH})_4[\text{C}_6\text{H}_3(\text{CO}_2)_3]_2(\text{HCOO})_6$  ].

**Table 6-3.**  $\text{NH}_3$ -TPD results.

The type of MOF	Quantity (mmol/g)	$\text{NH}_3$ /(mg/g)	Metal/(mg/g)	$\text{NH}_3$ :Metal (mol:mol)
MIL-101(Cr)	3.088	52.6	200	1:1.24
MIL-100(Al)	1.979	33.6	128	1:1.53
MOF-808(Zr)	1.524	25.9	401	1:1.42

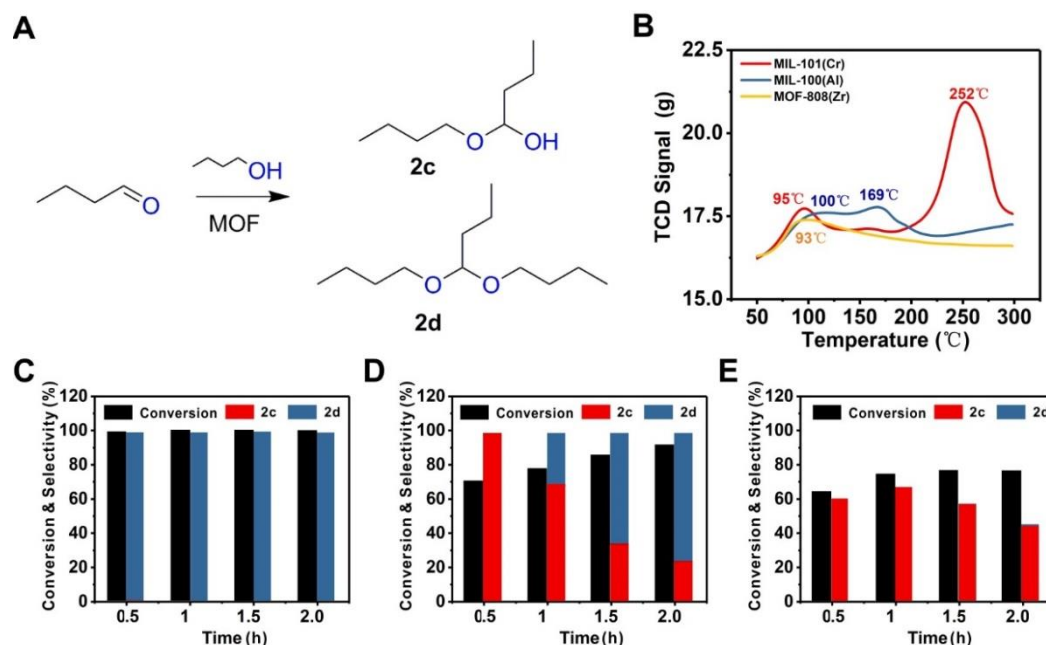


**Figure 6-8.** (A) Schematic illustration of the acetalization of butyraldehyde with butanol. (B)  $\text{NH}_3$ -TPD curves of MIL-101(Cr) (red), MIL-100(Al) (blue), and MOF-808(Zr) (orange). Acetalization kinetics of butyraldehyde with butanol using MIL-101(Cr) (C), MIL-100(Al) (D), and MOF-808(Zr) (E) as catalysts.

MOF-808(Zr) shows a NH<sub>3</sub> desorption peak at ~93 °C whereas MIL-100(Al) exhibits two NH<sub>3</sub> desorption peaks at ~100 °C and ~169 °C respectively. Interestingly, MIL-101(Cr) shows two distinctive NH<sub>3</sub> desorption peaks at ~95 °C and ~252 °C respectively. Since the temperature required for NH<sub>3</sub> desorption directly correlates to the acid strength of the catalysts, the acidity trend of these three MOFs is in the following order: MIL-101(Cr) > MIL-100(Al) > MOF-808(Zr). Moreover, by inspecting the integrated peak area, it is not difficult to conclude that MIL-101(Cr) contains the highest content of acidic sites per unit mass (**Figure 6-8B**).

**Table 6-4.** Oxidation of diol to dialdehyde and acetal by Ru@MIL-101(Cr) under 10 bar O<sub>2</sub> atmosphere (3 g of diol, catalysts (100 mg), 16 h, 130 °C, 10 bar).

The reaction scheme shows two reactions. The first reaction starts with ethylene glycol (HO-CH<sub>2</sub>-CH<sub>2</sub>-OH) reacting with O<sub>2</sub> in the presence of Ru@MIL-101(Cr) to produce ethylene glycol acetal (3a) and ethylene glycol dialdehyde (3b). The second reaction starts with 1,3-propanediol (HO-CH<sub>2</sub>-CH<sub>2</sub>-CH<sub>2</sub>-OH) reacting with O<sub>2</sub> in the presence of Ru@MIL-101(Cr) to produce 1,3-propanediol hemiacetal (3c) and 1,3-propanediol acetal (3d).

Substrates	Conversion (%)	Selectivity (%)			
		3a	3b	3c	3d
Ethylene glycol (EG)	11	7	93	-	-
1,3-Propanediol (PD)	65	-	-	12	88

Next, we investigated the acetalization kinetics of different MOFs for the acetalization of butyraldehyde with 1-butanol. The reaction was carried out with stoichiometric ratio of butanol and butyraldehyde (2:1). For MIL-101(Cr), butanol conversion reached 100% after merely 0.5 h of reaction. Moreover, the product was exclusively acetal (2d) with no hemiacetal product (2c) detected. MOF-808(Zr), on the other hand, only achieved 78% butanol conversion after 2 h reaction with hemiacetal 2c as the main product. Although, small amount of 2d was also observed.

The acetalization efficiency of MIL-100(Al) falls in between MIL-101(Cr) and MOF-808 with a conversion of 90% at 2 h and 75% selectivity for 2d. This trend is consistent with the acidity trend measured by NH<sub>3</sub>-TPD and our catalytic results for 1-butanol oxidation which also suggests that high Lewis acidity is required for the rapid acetalization of aldehydes to their respective acetals. In this case, MIL-101(Cr) is the best catalyst.

Finally, Ru@MIL-101(Cr) was used for the DAAC of diols (**Table 6-4**). It is well known that the industrial production of glyoxal is achieved by gas-phase catalytic oxidation of ethylene glycol (EG)<sup>48</sup>. 1,3-propanediol (PD), however, cannot be directly oxidized to their dialdehydes because of the high tendency of over-oxidation as well as the inherent instability of malondialdehyde<sup>49</sup>. New enzymatic methods have been proposed recently for oxidation of diols, however, the productivity is still low for broad application<sup>50</sup>. EG and PD are capable of forming five and six-member 1,3-dioxane ring after acetalization which are thermodynamically favored products. Therefore, we reason that the alcohol oxidation and acetalization steps can be achieved without addition of a secondary alcohol thereby reducing the possibility of additional byproducts formation.

The results show that DAAC using Ru@MIL-101(Cr) is indeed applicable for diols. After 16 h reaction, 11% and 65% conversion were achieved for EG and PD respectively. The selectivity for the fully acetalized product 3b is 93% and 3d is 88%, respectively (**Table 6-4**). We suspect that the slow reaction of EG is largely due to the difficulty of the oxidation step rather than acetalization step since EG can form a thermodynamically stable five-member ring after acetalization therefore commonly used as an acetalization reagent for aldehyde group protection. Taking the advantage of this feature, we further propose that it is possible to use EG as the acetalization agent for the asymmetric DAAC of a bi-component system.

### 6.2.3 Mechanism study

To understand the high reactivity of the Ru@MOF catalyst, *in situ* Fourier transform infrared spectroscopy (FT-IR) experiments were performed on Ru@MIL-101(Cr) and MIL-101(Cr) to probe the interface between Ru NPs and MOF (**Figure 6-9**). Most IR features from these two samples are identical and could be assigned to features from the 1,4-dicarboxybenzene ligand. Two vibrational peaks at

1890  $\text{cm}^{-1}$  and 1704  $\text{cm}^{-1}$ , however, only appeared on Ru@MIL-101(Cr) suggesting that they are Ru induced. For simplicity we assign these Ru induced features as  $\alpha$  and  $\beta$  peaks. Compared to the neat MOF sample, there is no reactant replacement in  $\alpha$  peak neighboring region. These suggest that the  $\alpha$  peak corresponds to surface adsorbed organic residues (e.g. C=O bond) on the Ru surface that are independent of the MOF support. The  $\beta$  peak, 1704  $\text{cm}^{-1}$ , appears to be a partial band shift from 1666  $\text{cm}^{-1}$  of the MIL-101(Cr) sample, as the original peak on MOF diminished to a shoulder. Therefore, it is likely that the  $\beta$  peak is related to species at Ru/MIL-101(Cr) interface (e.g. O-C=O from the MOF ligand). The MIL-101(Cr) assignments themselves are consistent with that found in the literature<sup>51-52</sup>. Because of the limited information, all these assignments are only tentative here.

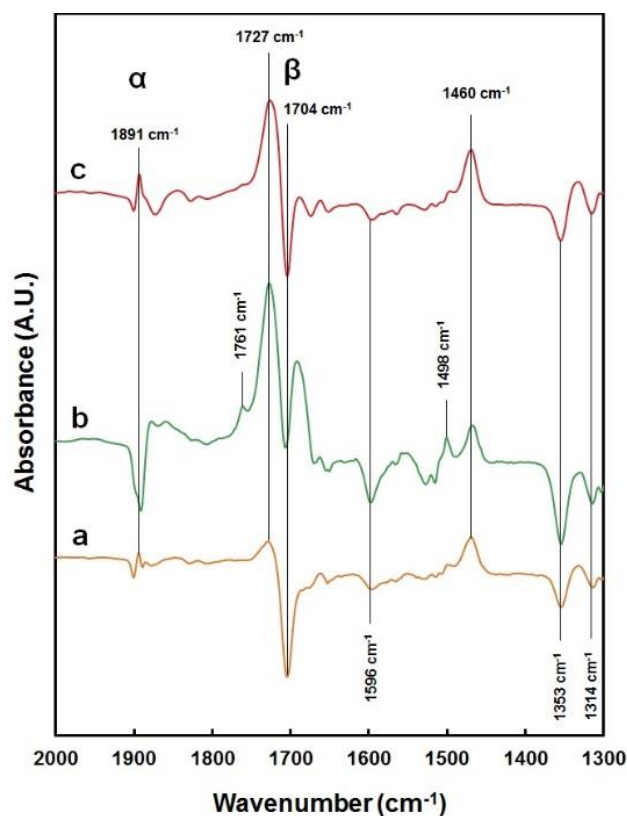


**Figure 6-9.** FTIR spectra for the a) MIL-101(Cr) and b) Ru@MIL-101(Cr) and samples using Ar background. The figure shows the region from 2000 – 1300  $\text{cm}^{-1}$ .

Adsorption of butanal and butanol has been used to identify the role of these sites. Fig. 6 shows the IR structure obtained after the first 1 h of different reactant treatments over 3 independent Ru@MIL-101(Cr) samples. The appearance of C-H stretching bands at 2962, 2931, 2898, and 2874  $\text{cm}^{-1}$  (**Figure 6-10**) and vibration band at 1460  $\text{cm}^{-1}$  indicates the adsorption of reactants in Ru@MIL-101(Cr)<sup>53-56</sup>.

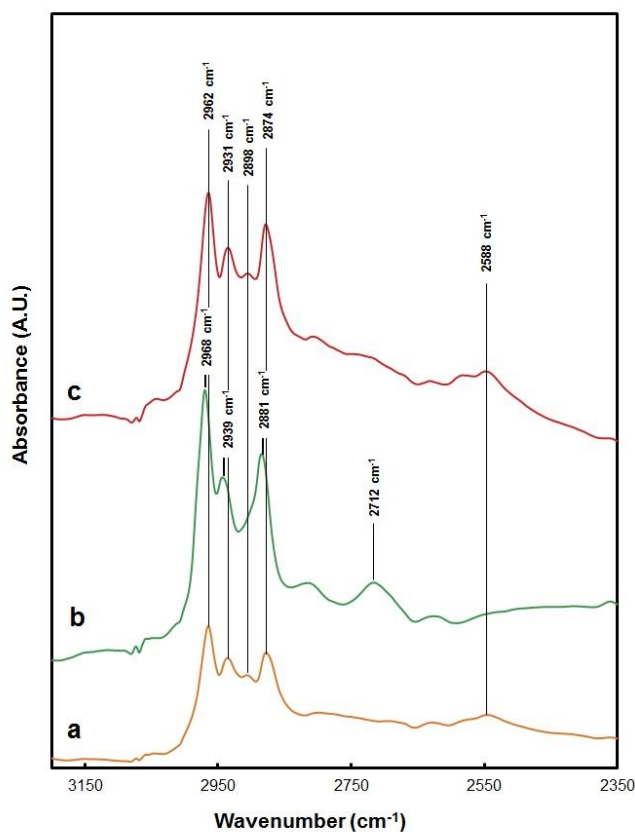


**Figure 6-10.** Stacked plot of the FTIR spectra after 1 h for the a) BuOH adsorbed, b) butanal adsorbed, and c) the 2:1 BuOH/butanal reaction mixture flow (Ru@MIL-101(Cr) sample background), each at 100 °C. The figure shows the region from 3100 – 2350  $\text{cm}^{-1}$ .

Meanwhile, negative bands that align with the aforementioned  $\alpha$  or  $\beta$  peaks start to emerge. This feature can be attributed to the displacement of adsorbed species on the Ru NP surface by adsorbate molecules. At the same time, it also suggests that Ru interaction with MIL-101(Cr) framework induced new active sites for the reactants in this catalyst system. Further analysis reveals that BuOH adsorption only replaced the  $\beta$  peak whereas butanal adsorption led to the replacements of both  $\alpha$  and  $\beta$  peaks (**Figure 6-11**). This suggests that the  $\beta$  adsorption site associated with the Ru/MOF interface is strongly related to the activation of butanol and subsequently the DAAC reactivity. When a 2:1 BuOH/butanal mixture was introduced to the Ru@MIL-101(Cr) catalyst, a mixture of BuOH and butanal features is observed. The results strongly support that the new one step acetal synthesis reaction reported in this paper is due to the unique catalysis design of Ru@MIL-101(Cr) structure. At present, no further analysis was made as this is beyond the scope of the work. Further assignments of the above adsorption process including kinetics details and a more specialized time resolved IR transient study transients will be discussed in the follow up work.

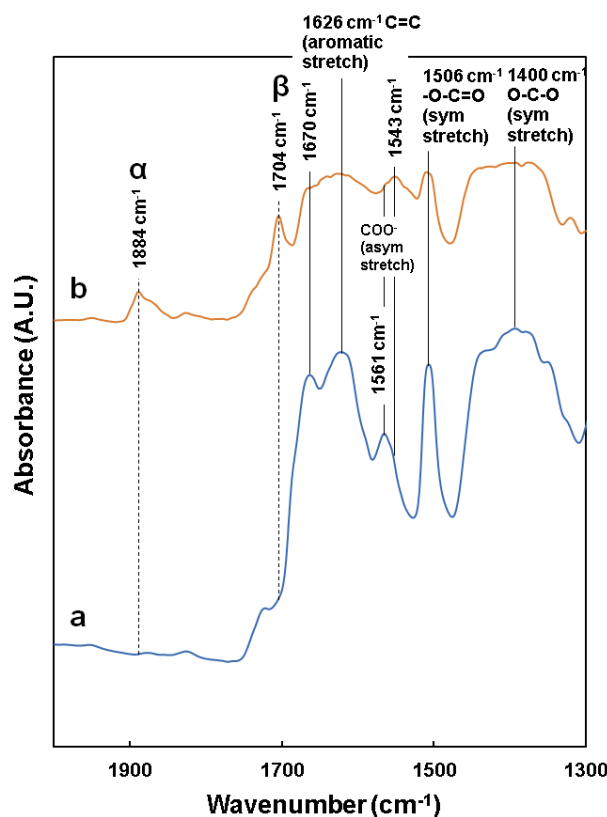


**Figure 6-11.** Stacked plot of the FTIR spectra after 1 h for the a) BuOH adsorbed, b) butanal adsorbed, and c) the 2:1 BuOH/butanal reaction mixture flow (Ru@MIL-101(Cr) sample background), each at 100 °C. The figure shows the region from 2000 – 1300  $\text{cm}^{-1}$ .

### 6.3 Conclusion

To conclude, the presence of Ru NPs inside a MOF structure enables direct alcohol to acetal catalytic conversion. This conversion is accomplished by a tandem catalytic process where the alcohol to aldehyde oxidation occurs over Ru NPs and the acetalization process occurs over the acid sites in the MOFs. The catalytic activity and selectivity to acetals increases from Ru@MOF-808(Zr) to Ru@MIL-100(Al) to Ru@MIL-101(Cr). This trend correlates with the increase of Lewis acidity sites in the MOF structure. One key factor for an efficient catalyst is the close proximity of Ru nanoparticles to Lewis acidic sites which allows on-site removal of the reaction intermediate, aldehyde, by a rapid acetalization process thus preventing over-oxidation. Through in situ FTIR study, we unveiled that the unique MOF pore environment provides new active sites on Ru NPs that is responsible for the activation of butanol. As a result, Ru@MIL-101(Cr) provides high DAAC activity for monoalcohol (1-butanol), diols (EG, PD) with selectivity up to 90%.

## 6.4 References

1. Kumbar, S.; Laurencin, C.; Deng, M., *Natural and synthetic biomedical polymers*. Elsevier: Oxford: 2014.
2. Zhao, Y.-J.; Loh, T.-P., Bioinspired Polyene Cyclization Promoted by Intermolecular Chiral Acetal-SnCl<sub>4</sub> or Chiral N-Acetal-TiCl<sub>4</sub>: Investigation of the Mechanism and Identification of the Key Intermediates. *J. Am. Chem. Soc.* **2008**, *130* (30), 10024-10029.
3. Inoue, M., Convergent syntheses of polycyclic ethers. Illustrations of the utility of acetal-linked intermediates. *Org. Biomol. Chem.* **2004**, *2* (13), 1811-1817.
4. Inoue, M.; Yamashita, S.; Ishihara, Y.; HIRAMA, M., Two convergent routes to the left-wing fragment of ciguatoxin CTX3C using O, S-acetals as key intermediates. *Org. Lett.* **2006**, *8* (25), 5805-5808.
5. Garcia, E.; Laca, M.; Pérez, E.; Garrido, A.; Peinado, J., New class of acetal derived from glycerin as a biodiesel fuel component. *Energy Fuels.* **2008**, *22* (6), 4274-4280.
6. Sartori, G.; Ballini, R.; Bigi, F.; Bosica, G.; Maggi, R.; Righi, P., Protection (and deprotection) of functional groups in organic synthesis by heterogeneous catalysis. *Chem. Rev.* **2004**, *104* (1), 199-250.
7. D. I. Enache; J. K. Edwards; P. Landon; B. S. Espriu; A. F. Carley; A. A. Herzing; M. Watanabe; C. J. Kiely; D. W. Knight; Hutchings, G. J., Solvent-Free Oxidation of Primary Alcohols to Aldehydes Using Au-Pd/TiO<sub>2</sub> Catalysts. *Science* **2006**, *311* (5759), 362-365.
8. Kanai, S.; Nagahara, I.; Kita, Y.; Kamata, K.; Hara, M., A bifunctional cerium phosphate catalyst for chemoselective acetalization. *Chem. Sci.* **2017**, *8* (4), 3146-3153.
9. Parmeggiani, C.; Cardona, F., Transition metal based catalysts in the aerobic oxidation of alcohols. *Green. Chem.* **2012**, *14* (3), 547-564.
10. Dong, J.-L.; Yu, L.-S.-H.; Xie, J.-W., A Simple and Versatile Method for the Formation of Acetals/Ketals Using Trace Conventional Acids. *ACS Omega* **2018**, *3* (5), 4974-4985.
11. Gregg, B. T.; Golden, K. C.; Quinn, J. F., Indium (III) trifluoromethanesulfonate as an efficient catalyst for the deprotection of acetals and ketals. *J. Org. Chem.* **2007**, *72* (15), 5890-5893.
12. Li, X.; Goh, T. W.; Li, L.; Xiao, C.; Guo, Z.; Zeng, X. C.; Huang, W., Controlling catalytic properties of Pd nanoclusters through their chemical environment at the atomic level using isorecticular metal-organic frameworks. *ACS Catal.* **2016**, *6* (6), 3461-3468.
13. Li, X.; Guo, Z.; Xiao, C.; Goh, T. W.; Tesfagaber, D.; Huang, W., Tandem catalysis by palladium nanoclusters encapsulated in metal-organic frameworks. *ACS Catal.* **2014**, *4* (10), 3490-3497.
14. Vohra, M. I.; Li, D.-J.; Gu, Z.-G.; Zhang, J., Insight into the epitaxial encapsulation of Pd catalysts in an oriented metalloporphyrin network thin film for tandem catalysis. *Nanoscale* **2017**, *9* (23), 7734-7738.
15. Firmino, A. D.; Mendes, R. F.; Antunes, M. M.; Barbosa, P. C.; Vilela, S. r. M.; Valente, A. A.; Figueiredo, F. M.; Tomé, J. o. P.; Paz, F. A. A., Robust Multifunctional Yttrium-Based Metal-Organic Frameworks with Breathing Effect. *Inorg. Chem.* **2017**, *56* (3), 1193-1208.
16. Gunanathan, C.; Shimon, L. J.; Milstein, D., Direct conversion of alcohols to

- acetals and H<sub>2</sub> catalyzed by an acridine-based ruthenium pincer complex. *J. Am. Chem. Soc.* **2009**, *131* (9), 3146-3147.
17. Bueno, A. C.; Gonçalves, J. A.; Gusevskaya, E. V., Palladium-catalyzed oxidation of primary alcohols: Highly selective direct synthesis of acetals. *Appl. Catal., A-Gen* **2007**, *329*, 1-6.
  18. Sahoo, A. R.; Jiang, F.; Bruneau, C.; Sharma, G.; Suresh, S.; Achard, M., Acetals from primary alcohols with the use of tridentate proton responsive phosphinepyridonate iridium catalysts. *RSC Adv.* **2016**, *6* (102), 100554-100558.
  19. Zhang, H.; Zhu, Z.; Wu, Y.; Zhao, T.; Li, L., TiO<sub>2</sub>-photocatalytic acceptorless dehydrogenation coupling of primary alkyl alcohols into acetals. *Green Chem.* **2014**, *16* (9), 4076-4080.
  20. Zhang, H.; Wu, Y.; Li, L.; Zhu, Z., Photocatalytic Direct Conversion of Ethanol to 1, 1-Diethoxyethane over Noble-Metal-Loaded TiO<sub>2</sub> Nanotubes and Nanorods. *ChemSusChem* **2015**, *8* (7), 1226-1231.
  21. Zhang, H.; Zhang, W.; Zhao, M.; Yang, P.; Zhu, Z., A site-holding effect of TiO<sub>2</sub> surface hydroxyl in the photocatalytic direct synthesis of 1, 1-diethoxyethane from ethanol. *Chem. Commun.* **2017**, *53* (9), 1518-1521.
  22. Mallat, T.; Baiker, A., Oxidation of alcohols with molecular oxygen on solid catalysts. *Chem. Rev.* **2004**, *104* (6), 3037-3058.
  23. Mori, S.; Takubo, M.; Makida, K.; Yanase, T.; Aoyagi, S.; Maegawa, T.; Monguchi, Y.; Sajiki, H., A simple and efficient oxidation of alcohols with ruthenium on carbon. *Chem. Commun.* **2009**, (34), 5159-5161.
  24. Yang, Q.; Xu, Q.; Jiang, H.-L., Metal-organic frameworks meet metal nanoparticles: synergistic effect for enhanced catalysis. *Chem. Soc. Rev.* **2017**, *46* (15), 4774-4808.
  25. Chen, Y.-Z.; Zhou, Y.-X.; Wang, H.; Lu, J.; Uchida, T.; Xu, Q.; Yu, S.-H.; Jiang, H.-L., Multifunctional PdAg@ MIL-101 for one-pot cascade reactions: combination of host-guest cooperation and bimetallic synergy in catalysis. *ACS Catal.* **2015**, *5* (4), 2062-2069.
  26. Rungtaweeworanit, B.; Baek, J.; Araujo, J. R.; Archanjo, B. S.; Choi, K. M.; Yaghi, O. M.; Somorjai, G. A., Copper nanocrystals encapsulated in Zr-based metal-organic frameworks for highly selective CO<sub>2</sub> hydrogenation to methanol. *Nano Lett.* **2016**, *16* (12), 7645-7649.
  27. Hu, P.; Morabito, J. V.; Tsung, C.-K., Core-shell catalysts of metal nanoparticle core and metal-organic framework shell. *ACS Catal.* **2014**, *4* (12), 4409-4419.
  28. Lu, G.; Li, S.; Guo, Z.; Farha, O. K.; Hauser, B. G.; Qi, X.; Wang, Y.; Wang, X.; Han, S.; Liu, X., Imparting functionality to a metal-organic framework material by controlled nanoparticle encapsulation. *Nat. Chem.* **2012**, *4* (4), 310.
  29. Falcaro, P.; Ricco, R.; Yazdi, A.; Imaz, I.; Furukawa, S.; Maspoth, D.; Ameloot, R.; Evans, J. D.; Doonan, C. J., Application of metal and metal oxide nanoparticles@ MOFs. *Coord. Chem. Rev.* **2016**, *307*, 237-254.
  30. Evans, J. D.; Sumbly, C. J.; Doonan, C. J., Post-synthetic metalation of metal-organic frameworks. *Chem. Soc. Rev.* **2014**, *43* (16), 5933-5951.
  31. Zhao, M.; Yuan, K.; Wang, Y.; Li, G.; Guo, J.; Gu, L.; Hu, W.; Zhao, H.; Tang, Z., Metal-organic frameworks as selectivity regulators for hydrogenation reactions. *Nature* **2016**, *539* (7627), 76.
  32. Calleja, G.; Sanz, R.; Orcajo, G.; Briones, D.; Leo, P.; Martínez, F., Copper-based MOF-74 material as effective acid catalyst in Friedel-Crafts acylation of anisole. *Catal. Today* **2014**, *227*, 130-137.
  33. Jiang, J.; Gándara, F.; Zhang, Y.-B.; Na, K.; Yaghi, O. M.; Klemperer, W. G.,

- Superacidity in sulfated metal–organic framework-808. *J. Am. Chem. Soc.* **2014**, *136* (37), 12844-12847.
34. Caratelli, C.; Hajek, J.; Cirujano, F. G.; Waroquier, M.; i Xamena, F. X. L.; Van Speybroeck, V., Nature of active sites on UiO-66 and beneficial influence of water in the catalysis of Fischer esterification. *J. Catal.* **2017**, *352*, 401-414.
35. Chołuj, A.; Zieliński, A.; Grela, K.; Chmielewski, M. J., Metathesis@ MOF: simple and robust immobilization of olefin metathesis catalysts inside (Al) MIL-101-NH<sub>2</sub>. *ACS Catal.* **2016**, *6* (10), 6343-6349.
36. Dhakshinamoorthy, A.; Alvaro, M.; Garcia, H., Metal organic frameworks as solid acid catalysts for acetalization of aldehydes with methanol. *Adv. Synth. Catal.* **2010**, *352* (17), 3022-3030.
37. Gao, H.; Luan, Y.; Chaikittikul, K.; Dong, W.; Li, J.; Zhang, X.; Jia, D.; Yang, M.; Wang, G., A Facile in Situ Self-Assembly Strategy for Large-Scale Fabrication of CHS@ MOF Yolk/Shell Structure and Its Catalytic Application in a Flow System. *ACS Appl. Mater. Interfaces* **2015**, *7* (8), 4667-4674.
38. Arrozi, U. S.; Wijaya, H. W.; Patah, A.; Permana, Y., Efficient acetalization of benzaldehydes using UiO-66 and UiO-67: Substrates accessibility or Lewis acidity of zirconium. *Appl. Catal., A-Gen* **2015**, *506*, 77-84.
39. Hou, J.; Luan, Y.; Huang, X.; Gao, H.; Yang, M.; Lu, Y., Facile synthesis of Cu<sub>3</sub>(BTC)<sub>2</sub>/cellulose acetate mixed matrix membranes and their catalytic applications in continuous flow process. *New J. Chem.* **2017**, *41* (17), 9123-9129.
40. Jiang, J.; Yaghi, O. M., Brønsted acidity in metal–organic frameworks. *Chem. Rev.* **2015**, *115* (14), 6966-6997.
41. Ma, L.; Abney, C.; Lin, W., Enantioselective catalysis with homochiral metal–organic frameworks. *Chem. Soc. Rev.* **2009**, *38* (5), 1248-1256.
42. Bromberg, L.; Diao, Y.; Wu, H.; Speakman, S. A.; Hatton, T. A., Chromium (III) terephthalate metal organic framework (MIL-101): HF-free synthesis, structure, polyoxometalate composites, and catalytic properties. *Chem. Mater.* **2012**, *24* (9), 1664-1675.
43. Férey, G.; Mellot-Draznieks, C.; Serre, C.; Millange, F.; Dutour, J.; Surblé S.; Margiolaki, I., A chromium terephthalate-based solid with unusually large pore volumes and surface area. *Science* **2005**, *309* (5743), 2040-2042.
44. Henschel, A.; Gedrich, K.; Kraehnert, R.; Kaskel, S., Catalytic properties of MIL-101. *Chem. Commun.* **2008**, (35), 4192-4194.
45. Kholdeeva, O. A.; Skobelev, I. Y.; Ivanchikova, I. D.; Kovalenko, K. A.; Fedin, V. P.; Sorokin, A. B., Hydrocarbon oxidation over Fe-and Cr-containing metal-organic frameworks MIL-100 and MIL-101—a comparative study. *Catal. Today* **2014**, *238*, 54-61.
46. Aijaz, A.; Karkamkar, A.; Choi, Y. J.; Tsumori, N.; Rönnebro, E.; Autrey, T.; Shioyama, H.; Xu, Q., Immobilizing highly catalytically active Pt nanoparticles inside the pores of metal–organic framework: a double solvents approach. *J. Am. Chem. Soc.* **2012**, *134* (34), 13926-13929.
47. Yang, J.; Wang, J.; Deng, S.; Li, J., Improved synthesis of trigone trimer cluster metal organic framework MIL-100Al by a later entry of methyl groups. *Chem. Commun.* **2016**, *52* (4), 725-728.
48. Kurina, L.; Azarenko, E.; Vodyankina, O., Coking during ethylene glycol oxidation to glyoxal on a silver catalyst. *React. Kinet. Catal. Lett.* **1998**, *63* (2), 355-358.
49. Mohammad, M.; Nishimura, S.; Ebitani, K. In *Selective aerobic oxidation of 1, 3-propanediol to 3-hydroxypropanoic acid using hydrotalcite supported bimetallic*

- gold nanoparticle catalyst in water*, AIP Conf. Proc., AIP: 2015; pp 58-66.
50. Isobe, K.; Nishise, H., Enzymatic production of glyoxal from ethylene glycol using alcohol oxidase from methanol yeast. *Biosci. Biotechnol. Biochem.* **1994**, *58* (1), 170-173.
51. Maksimchuk, N.; Timofeeva, M.; Melgunov, M.; Shmakov, A.; Chesalov, Y. A.; Dybtsev, D.; Fedin, V.; Kholdeeva, O., Heterogeneous selective oxidation catalysts based on coordination polymer MIL-101 and transition metal-substituted polyoxometalates. *J. Catal.* **2008**, *257* (2), 315-323.
52. Ravichandran, S. A.; Rajan, V. P.; Aravind, P. V.; Seenivasan, A.; Prakash, D. G.; Ramakrishnan, K. In *Characterization of Terephthalic Acid Monomer Recycled from Post-Consumer PET Polymer Bottles*, Macromol. Symp., Wiley Online Library: 2016; pp 30-33.
53. Guertin, D. L.; Wiberley, S. E.; Bauer, W. H.; Goldenson, J., The infrared spectra of three aluminum alkoxides. *J Phys. Chem.* **1956**, *60* (7), 1018-1019.
54. Knözinger, H.; Bühl, H.; Röss, E., The dehydration of alcohols over alumina: VII. The dependence of reaction direction on the substrate structure. *J. Catal.* **1968**, *12* (2), 121-128.
55. Mo, C.; Yuan, Z.; Zhang, L.; Xie, C., Infrared absorption spectra of nano-alumina. *Nanostruct. Mater.* **1993**, *2* (1), 47-54.
56. Liu, X., DRIFTS study of surface of  $\gamma$ -alumina and its dehydroxylation. *J. Phys. Chem. C.* **2008**, *112* (13), 5066-5073.

# Chapter 7 General Conclusion and Perspectives

## 7.1 General Conclusion

Selective synthesis of carbonyl compounds is one of the key reactions in the utilization of alcohols. Selectivity and stability control is the biggest challenges in industrial production. Recently, many efforts have been made to develop novel catalysts with high selectivity and stability. The understanding of key factor determining the activity and selectivity is crucial for the rational design of efficient catalysts. The main research content of this thesis is to explore the high selective and stable metal catalysts in catalytic selective oxidation of alcohols. The main conclusions are as follows:

### 7.1.1 Selective conversion of alcohols to aldehydes/ketones over small Ru NPs

Effect of the size of Ru nanoparticles for alcohols oxidation has been studied. Non-supported Ru NPs with sizes in the range 2 to 10 nm have been synthesized using microemulsion method with variation of aqueous phase content and used for oxidation of alcohols to aldehydes or ketones with O<sub>2</sub> as the oxidant.

The highest selectivity to aldehyde has been observed over small non supported size Ru NPs. This catalytic performance can be attributed to high content Ru-O species on the surface of small size Ru nanoparticles, which undergo reduction with formation of water and aldehyde and easy oxidation cycles during the reaction according to the Mars–van Krevelen mechanism. The presence of surface oxide layer over small size Ru nanoparticles suppresses over-oxidation of aldehydes to acids.

To conclude, the dimension of the metal particle can greatly influence the catalytic performance in oxidation reactions. The excellent selectivity and yield to aldehydes can be achieved using small size Ru NPs.

### 7.1.2 Oxidation of alcohols based on non-metal anthraquinone-based catalysts

Application of homogeneous and heterogenized non-metallic substituted 9,10-anthraquinones catalyst for catalytic oxidation of alcohols has been demonstrated with O<sub>2</sub> as terminal oxidant. The plausible mechanism could involve stepwise process with abstraction of hydrogen to hydrogenated form of anthraquinone with subsequent regeneration of anthraquinone by oxidation with formation of peroxy species decomposing to water and oxygen.

Carboxylated and sulfonated electrophilic anthraquinones with medium reduction potentials around 0.1~0.2 V showed a volcano curve with the highest activity and selectivity to carbonyl compounds. It might be stated that both reduction and oxidation steps proceed without limitations. Anthraquinones with lower or higher reduction potentials should lead to the longer residence time of alcohol radical form or peroxy radical leading to over-oxidation of alcohols.

Besides, anthraquinone supported catalyst has demonstrated comparable activity and selectivity to the parent molecule. Solid state <sup>1</sup>H NMR and FTIR spectra indicate on successful formation of amide bond and grafting of CQ over aminopropyl-functionalized silica, which suggests the feasibility of the grafted quinones with high potential as selective heterogeneous catalyst in alcohols oxidation.

### 7.1.3 Design nanocells Ru@SQ catalyst with core-shell structure

Finally, Ru NPs and disodium anthraquinone-2,6-disulfonate (SQ) have been used for the synthesis of core-shell nanocell catalyst containing SQ as a shell and metal as a core.

Coating of small size Ru NPs significantly improves the selectivity to aldehydes in oxidation of alcohols in comparison with pure SQ or Ru NPs. Coating of Ru nanoparticles by SQ results in selective oxidation (>90 %) of aliphatic, unsaturated and aromatic alcohols to aldehyde. Analysis of core-shell Ru@SQ catalyst results in strong interaction between Ru and SQ species through C=O leading to change of the electronic state and structure. *In-situ* study of alcohol oxidation using FTIR and

electrochemistry indicates on hydrogen abstraction by shell quinone species with formation of carbonyl group and hydrogen transfer by quinone to Ru core for water generation. Thus, the catalyst behavior mimics nano-electrocell by separation of oxidation reaction over quinone nano-anode and reduction of oxygen over Ru nano-cathode.

The nanocell catalysts provide the tool to perform selective catalytic oxidation over non-metallic organic species in heterogeneous state in comparison with existing homogeneous electrophilic agents (TEMPO, DDQ).

#### **7.1.4 Oxidation of monoalcohols and polyols to acetals by Ru@MOF catalyst**

The presence of Ru NPs inside a MOF structure enables direct alcohol to acetal catalytic conversion. This conversion is accomplished by a tandem catalytic process where the alcohol to aldehyde oxidation occurs over Ru NPs and the acetalization process occurs over the acid sites in the MOFs. One key factor for an efficient catalyst is the close proximity of Ru nanoparticles to Lewis acidic sites which allows on-site removal of the reaction intermediate, aldehyde, by a rapid acetalization process thus preventing over-oxidation. Through *in situ* FTIR study, we revealed that the unique MOF pore environment provides new active sites on Ru NPs that is responsible for the activation of butanol.

## **7.2 Perspectives**

### **7.2.1 Synthesis of subnanometric nanoparticles for selective oxidation of alcohols**

The effect of significant increase of the selectivity for small size Ru nanoparticles could be further improved by decrease of Ru species to subnanometric scale (< 1 nm). It should significantly improve the selectivity further for the synthesis of aldehydes. According to *in-situ* characterization of the mechanism of the reaction, we have proposed that effect is related to surface Ru-O species. This layer oxidizes alcohol to aldehyde according to Mars-van Krevelen mechanism with fast

regeneration by oxygen. Thus, synthesis of small size nanoparticles with stable Ru oxide layer on the surface could be used as efficient inorganic material for oxidation of alcohols. Subnanometric nanoparticles could be synthesized using template technique.

The effect of support for oxidation of alcohols is another important aspect of this work. We have found that alumina support has negative effect for selective oxidation to aldehydes but the reason is not clear. Thus, it could be interesting to study effect of support for oxidation of alcohols and use it for deposition of subnanometric Ru nanoparticles.

### **7.2.2 Stable core-shell materials for oxidation of alcohols**

The main limitation for developed core-shell materials with anthraquinone coated over Ru nanoparticles is in dissolution of organic shell during reaction due to water formation. It limits the effect of the catalyst structure on the selectivity to aldehyde. Thus, synthesis of stable organic shell on the surface of Ru nanoparticles is the main challenge for further development of the catalyst. The possible solution of this problem could be polymerization of anthraquinone units on the surface of Ru nanoparticles. It should significantly improve stability of the coating toward dissolution and improve selectivity and recyclability of the catalyst.

### **7.2.3 Use of organic shell based on nitroxyl radicals**

Stable nitroxyl radicals like TEMPO is perspective material for stoichiometric dehydrogenation of alcohols. In-situ regeneration of hydrogenated form (=N-OH) can be performed by transition metal salts in the presence of air. Coating of polymeric form of nitroxyl radicals over Ru nanoparticles could be interesting alternative to quinone species for oxidation of alcohols to aldehydes.

# Author Introduction

**Jingpeng ZHAO** was born in August 1989 in Shandong, China. He obtained his bachelor's degree in materials chemistry from Qingdao University of Science and Technology in 2008. After that, he continued his studies in physical chemistry at Shanghai University under the guidance of Dr. Xin Feng. In 2016, he was sponsored by CIFRE for his PhD joint program at Unit é de catalyse et de chimie du solide (UCCS), Université de Lille, France and E2P2L Lab in Solvay, China. The PhD thesis was supervised by Dr. Vitaly V. Ordomsky and Dr. Mickael Capron. The research, described in this thesis, focuses on designing efficient catalysts with high selectivity and stability in selective oxidation of alcohols to corresponding aldehydes or ketones.

## List of Published Papers

- (1) **J.P. Zhao**, W.Y. Hernández, W.J. Zhou, Y. Yang, E. I. Vovk, M. Capron\*, V. Ordomsky\*. Selective Oxidation of Alcohols to Carbonyl Compounds over Small Size Colloidal Ru Nanoparticles, *ChemCatChem*, **2019**, doi.org/10.1002/cctc.201901249
- (2) **J.P. Zhao**, D. Wu, W.Y. Hernández, W. J. Zhou, M. Capron\*, V. Ordomsky\*. Non-metallic Aerobic Oxidation of Alcohols over Anthraquinone Based Compounds. *Appl. Catal., A.-Gen*, **2019**, doi.org/10.1016/j.apcata.2019.117277
- (3) **J.P. Zhao**, W.Y. Hernández, W.J. Zhou, Y. Yang, E. I. Vovk, M. J. Wu, N. Naghavi, M. Capron\*, V. Ordomsky\*, Nanocell Type Ru@quinone Core-shell Catalyst for Selective oxidation of alcohols to carbonyl compounds. *submitted*, **2019**.
- (4) **J.P. Zhao**, W.Y. Hernández, W.J. Zhou, M. Capron\*, V. Ordomsky\*. Non-metallic Epoxidation of Alkenes over Anthraquinone Based Compounds. *submitted*, **2019**.
- (5) G. Liang, Y. Zhou, **J.P. Zhao**, Andrei Y. Khodakova\* Vitaly V. Ordomsky\*.

Structure-Sensitive and Insensitive Reactions in Alcohol Amination over Nonsupported Ru Nanoparticles. *ACS Catalysis*, **2018**, 8, 11226-11234.

- (6) S. Zhang, J. P.H. Li, **J.P. Zhao**, D. Wu, B. Yuan, W.J. Zhou, V. Ordonsky\*, T. Li\*. Direct Aerobic Oxidation of Mono-alcohols and Diols to Acetals Using Tandem Ru@MOF Catalysts. 2019, *Nano Research*, submitted.

## List of Patents

- (1) **J.P. Zhao**, W.Y. Hernández, S. Streiff, W.J. Zhou, M. Capron, V. Ordonsky. Method for the oxidation of alcohol, 2018.
- (2) **J.P. Zhao**, W.Y. Hernández, S. Streiff, W.J. Zhou, M. Capron, V. Ordonsky. Selective oxidation of alcohols, 2018.

## Conference

- (1) **J.P. Zhao**, M. Capron\*, V. Ordonsky\*, Metallic Ru Size Effect in Selective Oxidation of Alcohols to Carbonyl Compounds, *French Conference on Catalysis, Frejus, 2019*, poster presentation
- (2) **J.P. Zhao**, M. Capron\*, V. Ordonsky\*, Non-metallic Aerobic Oxidation of Alcohols over Anthraquinone Based Compounds., *2017 Solvay China Conference - Effective Catalysis, a key driver for Sustainable chemistry, Shanghai, 2017*, poster presentation

# Acknowledgement

First and foremost, I am gratefully thankful to my supervisors, Dr. Vitaly V. Ordonsky and Dr. Mickael Capron. They are such distinctive gentleman, one crazy and dedicated Russian and the other enthusiastic and optimistic French. It is that their encouragement, guidance and full support enabled me to finalize my PhD thesis.

Many thanks to Olivier Gardoll, Laurence Burylo, Pardis Simon and Martine Frère, Maya Marinova, Bertrand Doumert, Stephane Chambrey for help with TPR, XRD, XPS, TEM, solid NMR measurements and experimental realization in Lille University. And other technical supports from the project partners, Li Tao and Yang Yong groups in Shanghai Tech. University deserve my thanks and respects. In addition, I would also like to gratitude Solvay's staff and colleagues, especially Stephane Streiff, Zhen Yan, Wenjuan Zhou, Yesid Enciso, Mengjia Wu and Tina Shen who offer lots of academic advices and security protection.

Thanks to CNRS and Solvay Company to financially support my PhD thesis.

I also appreciate to all my dear group members: Dr. Carmen Ciotonea, Dr. Juliana Aparicio, Dr. Claudia Tavera, Dr. Bang Gu, Dr. Xiang Yu, Dr. Shaohua Xie, Dr. Sara Navarro-jaen, Dr. Feng Niu, Dr. Jin Sha, Dan Wu, Qiyan Wang, Li Gao, Gongming Peng, D'èora Strossi, Melissa de la Rocha.

Finally, thanks for the care and understanding of my families during my Phd period. They give me a spirit of strength and help me tide over difficulties! All the best to my family and all friends a healthy and well-being life!